Lithium, Magnetic Resonance and the Human Brain

2011

LITHIUM, MAGNETIC RESONANCE AND THE HUMAN BRAIN

David Andrew Cousins

Thesis submitted to meet the requirements for entry to the degree of Doctor of Philosophy

June 2011

Institute of Neuroscience
Faculty of Medical Sciences
Newcastle University
Newcastle upon Tyne
UK

For Zac and Theo

Abstract

This thesis explores the effects of lithium on the human brain using structural, functional and spectroscopic magnetic resonance techniques. Contemporary issues surrounding the pharmacological effects of lithium are investigated and aspects of its pharmacokinetics examined.

Bipolar disorder is known to be associated with dysfunction of the monoaminergic neurotransmitter systems of the brain. It is proposed that the antimanic properties of lithium derive from its attenuation of the actions of dopamine. In a randomised, placebo-controlled study of lithium involving 24 healthy men, mania was modelled by the administration of methamphetamine. Sustained attention, known to be disturbed in mania, was assessed during functional magnetic resonance imaging. Within the lithium group, response times were slowed and the effects of methamphetamine on functional magnetic resonance imaging contrast diminished. These findings are discussed in the context of current theories and contrasted with existent data.

Lithium has been reported to increase the volume of grey matter in the brain in numerous magnetic resonance imaging studies. This observation was replicated in a longitudinal, voxel-based morphometry study of 31 healthy men. Combining quantitative imaging with various structural analysis techniques, it is argued that the grey matter change may be better accounted for by lithium altering the relaxation characteristics of protons; that is to say, signal change not true volume expansion. The biophysical basis of this theory is discussed, together with its implications.

The pharmacokinetic properties of lithium in man are incompletely characterised, in particular its distribution in various tissues of the brain. The development of a magnetic resonance spectroscopy tool is described; its purpose was to determine the concentration of lithium in grey and white matter in a time-scale suited to clinical practice. Lithium was found to be evenly distributed in the brain regions examined, with total acquisition times constrained to less than 20 minutes. The applications and future developments of *in vivo* lithium spectroscopy are considered.

It is concluded that various magnetic resonance techniques may be usefully applied to the investigation of the interactions between lithium and the human brain.

ACKNOWLEDGEMENTS

It has been a privilege to write this thesis and I have been honoured by the company and support of many fine folk – certain souls warrant specific mention.

I am greatly indebted to my two supervisors: Professor Andrew Blamire for his patient guidance, enthusiasm and encouragement throughout the process culminating in this thesis; Professor Nicol Ferrier, simply for inspiring me for nearly two decades (though the funding of late was also greatly appreciated).

My thanks are offered to Professor John O'Brien and Dr Pete Thelwall, the internal assessors for this PhD. They happily put me through my paces and in doing so, strengthened the study methodology as well as my resolve.

At the Newcastle Magnetic Resonance Centre, Pete Thelwall taught me how to build a coil, construct a phantom and finesse a figure – but not how to tidy a workshop. Benjamin Aribisala wrote the software package that enabled me to perform relaxometry analysis with ease, for which he has my thanks and admiration. Fiona Smith was central to the lithium MRS work described in this thesis – she analysed the spectra, generated the models, prepared the figures for the spectroscopy chapter and, reassuringly, looked as bemused as I felt during the developmental process.

Thanks are due to Carol Smith and Louise Morris, highly talented and tolerant radiographers both. Nicola Purdy worked extremely hard to secure the drugs used in this project; the help of the Pharmacy Department was indispensable.

In terms of scientific development, Peter Gallagher assisted with the RVIP task development, Dr Michael Firbank guided the fMRI project and Dr Richard McQuade advised on all things dopamine. Professor Steve Williams, of the Institute of Psychiatry, presented a training opportunity which brought me into contact with Mitul Mehta and Matthew Kempton – the generous chaps who introduced me to the complexities of automated image analysis. I am grateful to the Medical Research Council who, through a Clinical Research Training Fellowship, funded the work conducted.

It gives me the greatest pleasure to acknowledge the love and enduring support of those dearest to me: my family, ever-present in the wings; my boys, Zac and Theo – bright stars and comedy geniuses both; finally, my wife Sarah…for everything.

ACRONYMS & INITIALISMS

AA	·	arachidonic acid
AC	·	adenylate cyclase
ACC	·	anterior cingulate cortex
AFP	·	adiabatic full-passage
AHP	·	adiabatic half-passage
AKT	·	Ak transforming (Ak being a strain of mouse)
AUC	·	area under curve
bcl-2	·	B-cell lymphoma 2
BDNF	·	brain derived neurotrophic factor
BET	·	brain extraction tool
BOLD	·	blood oxygen level dependent
cAMP	·	cyclic adenosine monophosphate
CANTAB	·	Cambridge neuropsychological test automated battery
COMT	·	catechol-*o*-methyl transferase
COX	·	cyclo-oxygenase
CSF	·	cerebrospinal fluid
CSI	·	chemical shift imaging
DARPP-32	·	dopamine and cAMP regulated phosphoprotein of 32 kDa
DAT	·	dopamine transporter
DLPFC	·	dorsolateral prefrontal cortex
DOTP	·	dioctyl terephthalate
DTPA	·	diethylene triamine pentaacetic acid
ECT	·	electroconvulsive therapy
EEG	·	electroencephalogram
EM	·	electromagnetic
EPI	·	echo planar imaging
FDR	·	false detection rate
FID	·	free-induction decay
FLIRT	·	FSL non-linear registration tool

fMRI · functional magnetic resonance imaging

FMRIB · fMRI of the brain (oxford centre thereof)

FOV · field of view

FSL · FMRIB software library

FWE · family-wise error

FWHM · full-width half-maximum

GPCR · G-protein coupled receptor

GSK-3β · glycogen synthase kinase 3β

GUI · graphical user interface

HAM_D · Hamilton depression rating scale

HRF · haemodynamic response function

HVA · homovanillic acid

ICBM · International Consortium for Brain Mapping

ICV · intracerebral volume

IGF · insulin-like growth factor

ISIS · image selected in vivo spectroscopy

LISERS · lithium side-effects rating scale

MARSBAR · Marseille boîte à région d'intérêt

MAO · monoamine oxidase

mM · millimolar

MNI · Montreal Neurological Institute

MR · magnetic resonance

MRC · Medical Research Council

MRC-LAMP · lithium amphetamine study

MRC-LISP · lithium spectroscopy study

MRC-LITE · lithium T_1 effect study

LREC · local ethics research committee

LTS · long-term support

MRI · magnetic resonance imaging

MRS · magnetic resonance spectroscopy

NAA · N-acetylaspartate

NMR · nuclear magnetic resonance

NMV · net magnetisation vector

PBVC · percentage brain volume change

PET · positron emission tomography

PFC · prefrontal cortex

PI-cycle · phosphatidylinositol cycle

PIP2 · phosphatidylinositol bisphosphate

PKA · protein kinase A

PKC · protein kinase C

PP1 · protein phosphatase 1

PP2A · protein phosphatase 2A

PPM · parts per million

PVE · partial volume effect

RF · radiofrequency

ROI · region of interest

RVIP · rapid visual information processing

SDT · signal detection theory

SGPFC · subgenual prefrontal cortex

SI · spectroscopic imaging

SIENA · structural image evaluation using normalisation of atrophy

SPM · statistical parametric mapping

SPSS · statistical package for the social sciences

TBV · total brain volume

TE · echo time

TTHA · triethyltetraminehexaacetic acid

TR · repetition time

VBM · voxel-based morphometry

VMAT2 · vesicular monoamine transporter 2

VTA · ventral tegmental area

SYMBOLS

A'	·	sensitivity index
B''	·	response bias
B_0	·	external magnetic field
B_1	·	RF transmitter magnetic field
f	·	fraction of false positives
γ	·	gyromagnetic ratio
h	·	fraction of correct responses
I	·	a quantum spin number
M	·	net magnetisation vector
m	·	a quantum number denoting spin energy level
μ	·	nuclear magnetic moment
T	·	Tesla
T_1	·	spin-lattice relaxation (longitudinal)
T_2	·	spin-spin relaxation (transverse)
t	·	time
τ	·	an arbitrary time period
V	·	voltage
ν	·	rotational frequency in Hertz
ω	·	rotational frequency in $\text{rad}\cdot\text{s}^{-1}$

Contents

List of Figures

List of Tables

1 INTRODUCTION

Lithium is beguiling. The simplest of drugs with the most complex effects, its discovery fundamentally altered the treatment of the recurrent depressive disorders but the manner by which it confers therapeutic advantage remains unclear. This introductory chapter describes the properties of lithium as both ion and drug, considering its principal indications in psychiatry and outlining the pertinent explanations of its effects. It should be acknowledged that our understanding of lithium is inextricably linked to the ailments for which it is prescribed, and vice versa to some extent. Thus, by first considering lithium's principal indications, the scene can be set for the pharmacodynamic theories. Given the breadth and depth of the field this introduction is brief – in the chapters that follow, a more detailed appraisal of the literature relevant to the each hypothesis is presented.

1.1 PHYSICAL PROPERTIES OF LITHIUM

Classified as an alkali metal and being the least dense of the solid elements, lithium has both typical and anomalous properties within its group. Lithium easily yields its single valence electron to form a cation and is highly reactive, not being found naturally in its elemental form. Having a small ionic radius and a large field density at its surface, lithium behaves anomalously in aqueous solution compared to sodium and potassium (Stern and Amis, 1959). This is most likely the consequence of a disproportionately large hydration shell which restricts its ionic mobility, in physiological terms resulting in properties such as low lipid solubility. If comparisons to the behaviour of other ions in biology are to be drawn, then magnesium and calcium would be suitable choices (Birch, 1976) – the so called diagonal relationship.

Even its name speaks of anomaly, originally lithion (Greek: *lithos*, stone), so named because unlike other members of its group it was discovered in non-plant material. Ironically petalite, its mineral ore, was named for its leaf-like qualities.

Lithium has five isotopes, only two of which are sufficiently stable to be of any relevance to biological sciences – ^{7}Li and ^{6}Li, with respective natural abundances of approximately 93% and 7% (Brevard, 1981). In terms of human and animal physiology, it is not clear how much of a distinction need be made between the two isotopes;

physically and chemically, the difference can be crucial. ^{6}Li absorbs neutrons, a property that can be used to chart its distribution in tissues (Thellier et al., 1976), whilst ^{7}Li possesses net-spin and has favourable magnetic resonance (MR) characteristics (Komoroski, 2000).

1.2 CLINICAL USE OF LITHIUM

The most common contemporary medicinal use of lithium is in the management of recurrent mood disorders, bipolar disorder in particular. Of its many other indications, its potential role in the treatment of neurodegenerative conditions is most pertinent to this thesis.

1.2.1 Historical perspective

Essentially… from panacea to poison and back again; repeatedly. Its current place is a matter of perspective.

As early as 1843, the aptly named physician Alexander Ure proposed that lithium carbonate should be used as a treatment for urinary calculi, based largely on its affinity for uric acid (Ure A. 1860). Subsequently advocated for topical application to gouty joints – gout being associated with high uric acid levels – lithium soon found favour in related conditions (Garrod, 1859). Its virtues were extolled for the myriad ailments considered to be a consequence of the uric acid diathesis, including psychiatric maladies such as melancholia and *folie* (somewhat similar to mania). Thus, within 100 years of its discovery by man, eminent psychiatrists such as the Lange brothers were in a position to systematically examine lithium's efficacy in depression, concluding in its favour (Shorter, 2009).

Around that time – the turn of the 19th century – there developed something of a fervour for bottled *Lithium Waters*, which fuelled spa resorts, entrepreneurs and round-the-world cyclists (Johnson, 1984). In truth, such waters contained minuscule quantities of lithium; their use, together with the uric acid diathesis, soon fell into disrepute. The proprietary solution was to add lithium in more substantial quantities to tonics and carbonated soft drinks such as 7·UP, but public opinion was against it and their popularity declined.

A further 50 years down the line, two near simultaneous publications dictated the future course of lithium prescription. The Australian psychiatrist John Cade found it to be effective in mania (Cade, 1949), whilst Corcoran et al. (1949) reported on its toxicity as a table salt substitute in those with cardiac disease. The American Food and Drugs Administration decreed it to be too toxic for use, imposing a 15 year ban. Some European psychiatrists championed its cause, others opposed it; their counterparts in North America were unable to do either directly (Lieberman, 2006). The pioneering work on lithium continued through this conflict, comprising some of the first systematic trials of any treatment in psychiatry (Schou et al., 1954). Clinical practice followed at a pace once monitoring and safety parameters had been established. Lithium is now accepted world-wide as a core treatment for the recurrent mood disorders (Grunze et al., 2009, 2010).

Once more, the passage of half a century has brought a change in the perception of lithium, widening the breadth of indications. Stemming from theoretical reasoning and preclinical experiments (Wada, 2009), the current outlook is optimistic and the diathesis that of neuroplasticity – a matter which is considered later in this thesis.

1.2.2 Clinical indications

The principal clinical application of lithium is in the management of recurrent mood disorders (outlined in the textbox on page 6). These common conditions present a huge burden to the sufferer and to society, accounting for a substantial proportion of morbidity and mortality worldwide (Lopez et al., 2006). The importance, therefore, of any intervention that can lessen their detriment should not be underestimated.

Guidelines and algorithms vary in their positioning of lithium within the hierarchy of antimanic drugs, acknowledgement of its antidepressant properties and role in maintenance treatment… thus, in almost every respect.

BIPOLAR DISORDER

All recent guidelines for the pharmacological management of bipolar disorder have advocated the use of lithium, though with variable emphasis on its role in different phases of the illness (Grunze et al., 2004, 2009, 2010). Despite recent pharmacological advances, it remains a core treatment of this condition (Cousins and Young, 2007).

Manic episodes Approximately two thirds of patients with mania respond to lithium, nearly twice the placebo rate (Poolsup et al., 2000). Response evolves over days to weeks, treatment ideally continuing for at least three months after remission is secured in order to prevent relapse.

Depressive episodes Lithium is now rarely initiated solely to treat acute bipolar depression, though it can be effective in this capacity (Nolen and Bloemkolk, 2000). In those already taking lithium, their dose should be optimised – additional or alternative medications may be considered if this proves ineffective.

Mixed presentations Although some benefit may be conferred, lithium is not as effective in mixed states as it is in mania (Swann et al., 1997).

Prophylaxis Lithium can be the mainstay of maintenance treatment, either alone or in combination with other medications. It reduces the risk of both depressive and manic relapses, but analysis of all but the most recent studies suggests it is most efficacious in preventing the latter (relative risk reductions of 28% and 38% for depression and mania respectively; Geddes et al., 2004).

Suicide prevention For reasons not entirely accounted for by its amelioration of episode frequency and severity – nor entirely understood – lithium reduces the risk of completing suicide whilst it is being taken (Cipriani et al., 2005).

There is a discrepancy between the efficacy and effectiveness of lithium, naturalistic studies indicating poorer outcomes than the controlled trials. This in itself is not unusual, but with lithium there are two specific caveats: patients tend to stop taking lithium (Maj et al., 1998) and rapid cessation may hasten relapse (Baldessarini et al., 1999). It has been argued that if lithium is stopped suddenly – especially after a short treatment period – the increased risk of relapse may counterbalance the prophylactic gains and overall, lithium may be detrimental (Goodwin, 1994).

Acute depression Lithium is superior to placebo in the treatment of episodes of major depression (Adli et al., 1998), though it is now rarely used in this capacity. As with most antidepressant drugs, about two thirds of patients respond, entering remission after several weeks (Baron et al., 1975). It can also be effective in the prevention of relapse in unipolar disorder (Cipriani et al., 2006), but the nature of the empirical data makes it difficult to establish the magnitude of this effect in comparison to traditional antidepressants.

Augmentation In those with a depression refractory to treatment, lithium can be used to good effect as an augmenting agent (Crossley and Bauer, 2007). Approximately half of those so treated can be expected to respond (Price et al., 1986), a not inconsiderable effect given the severity and intractability of the depressive states for which augmentation is indicated. A small proportion of cases improve within 48 hours, the majority take 4–6 weeks (Bauer et al., 2003). Swift responses most likely have a basis in the enhancement of serotonergic functioning whilst late responses may be due to lithium fostering neuronal resilience and recovery.

Augmentation is a strategy wherein an agent is added to an antidepressant regime in order to enhance its effects. If the augmenter has its own antidepressant properties, the combination should be synergistic.

1.2.3 Therapeutic levels

In establishing the correct dose of lithium, clinicians usually rely on a combination of experience and regular serum monitoring, the therapeutic window of lithium being narrow. In acute mania, serum concentrations of 0.8–1.2 mM are typically required, with levels at the lower end of this range the usual target in the treatment of depression. The optimum serum concentration for prophylaxis is still a matter for debate – some advocate reducing the level to 0.6–0.8 mM whilst others council the continuation of the dose which resolved the acute episode. At the heart of this debate is the fear that patients are either inadequately protected or unnecessarily poisoned. To further compound matters, there are no indices which robustly predict response to treatment or predict relapse, adherence to treatment aside.

With lithium, blood tests guide rather than guarantee the outcome.

Regrettably there is insufficient data, observational or experimental, to resolve this matter with certainty.

MOOD DISORDERS

These common psychiatric disorders are syndromal diagnoses, arising from a complex interplay of genetic, environmental and psychosocial factors. They are considered the result of stress on predisposed individuals in both psychological and biological models.

UNIPOLAR DISORDER

Also known as *Major Depressive Disorder*, the lifetime risk of developing this condition is about 10%. It most commonly affects women but spans race, class and age (though onset is typically in the fourth decade). It has a propensity to recur. Episodes generally last for several months, considered 'chronic' once unresolved for more than two years.

The core symptoms of depression are a pervasive lowering of mood and/or a loss of interest or pleasure. These are associated with changes in sleep, appetite and libido, together with impaired concentration and psychomotor retardation. Thoughts are dominated by pessimism, guilt, worthlessness and hopelessness, often culminating in suicidal ideation. Delusions and hallucinations may develop in severe cases, most often mood-congruent.

Treatment comprises antidepressants, various psychological interventions or a combination of the two. Recovery can be expected in the majority of cases, as can recurrence. Chronic illness is common and about one in ten cases become refractory to treatment.

BIPOLAR DISORDER

Formally known as *Manic Depressive Disorder*, this highly recurrent condition is less common than unipolar disorder, having a prevalence of 1–2%. It affects men and women equally, most frequently emerging in the late teens to early twenties. Bipolar depressive and manic episodes span weeks to months, hypomania is generally shorter lived.

Bipolar disorder can be subclassified: BD-I — episodes mania with or without depression; BD-II — episodes of hypomania *and* depression; BD-III — induced by electroconvulsive therapy (ECT) or antidepressants.

Mania comprises an abnormally and persistently elevated, expansive or irritable mood together with increased psychomotor activity, excessive optimism, grandiosity, social disinhibition and unrestrained hedonism; psychosis may occur. Hypomania is similar but less severe. Bipolar depression is akin to unipolar disorder, but retardation and excessive sleep can predominate. In mixed episodes, features of depression and mania co-occur.

Mania usually responds to lithium, sodium valproate, antipsychotics or benzodiazepines, alone or in combination. The optimal approach to bipolar depression is unclear, as the antidepressants may trigger mania and worsen the course of the illness; second-generation antipsychotics and lamotrigine are proving effective without this risk. Maintenance treatment is commonly required — often involving the continuation of lithium and/or sodium valproate, latterly the second-generation antipsychotics have come to the fore.

1.2.4 Safety considerations

Lithium can be rightly viewed as a harmful substance, for an excess can lead to serious adverse consequences – careful monitoring is thus required during initiation and throughout long-term administration. Toxicity must, however, be distinguished from the more common and less harmful side-effects which frequently accompany its use. The safe use of lithium has been reviewed by Berghofer et al. (2006).

SIDE-EFFECTS

Lithium has the potential to induce a wide range of side-effects, many of which appear shortly after initiation and subside within a matter of weeks. The most frequent of these – nausea, abdominal pain, diarrhoea, increased thirst and urination, fine tremor – are usually well tolerated. Very often, the most troublesome side-effects are in the neuropsychiatric domain and principally comprise fatigue, impaired concentration and poor memory; these can be difficult to separate from the symptoms of the illnesses for which lithium is prescribed.

Vigilance for progressive or late side-effects of lithium is also required. Weight gain can be considerable and is probably multifactorial. Kidney function must be monitored as renal impairment is an uncommon but serious consequence of lithium treatment. Endocrine dysfunction, especially goitre and hypothyroidism, should be enquired about and investigated regularly. The development of acne and the exacerbation of psoriasis can occur at any point during treatment, the latter being a relative contraindication.

INTOXICATION

Lithium intoxication is a serious matter, over-shadowing much of its use. Overt intoxication presents with the symptoms listed below and commonly has an identifiable cause – impaired renal function, dehydration and the co-administration of certain drugs for example. A substantial risk may be posed by undetected 'subthreshold' intoxication, whereby symptoms are not marked but tissue damage accrues.

- *Mild:* nausea · loose stools · polyuria · thirst · impaired concentration · marked fine tremor
- *Moderate:* nausea · vomiting · diarrhoea · excessive thirst · coarse tremor · slurred speech · incoordination · disorientation · drowsiness
- *Severe:* vomiting · incontinence · excessive thirst · ataxia · parkinsonism · myoclonus · seizures · apathy · somnolence · coma

Toxicity would be expected at levels of 1.5 mM and above, though it can occur with serum levels in the standard therapeutic range. The reasons for this are incompletely understood, but a plausible explanation would be that some individuals have a higher tissue concentration of lithium for a given serum level.

1.3 PHARMACOKINETICS OF LITHIUM

1.3.1 Absorption

Lithium is readily absorbed from the gastrointestinal tract, reaching peak plasma levels between one and three hours. Its absorption is unaffected by food and following a standard dose is usually complete within six to eight hours (Alda, 2006).

1.3.2 Distribution

The distribution of lithium is both wide and swift. Lithium is thought not to be bound to plasma proteins to any significant degree and enters tissues readily, the tissue concentration generally being lower than that of the serum (Komoroski, 2000). It enters and exits cells by a variety of mechanisms including: Na-K ATPase, Na-K co-transport, anion exchange, leakage and Na-Li exchange (Duhm, 1992). The balance of these mechanisms determine its intracellular concentration. Cellular and subcellular concentrations are difficult to establish, but are again thought to be lower than serum levels (Riddell et al., 1990).

Our knowledge of the distribution of lithium in tissues comes largely from preclinical studies. The scarcity of data from human subjects is mainly due to the logistical and technical challenges in assaying it.

1.3.3 Elimination

Lithium is almost exclusively eliminated by the kidneys, described by first-order kinetics and determined primarily by the glomerular filtration rate. The serum half-life of elimination is typically 18–24 hours, but this can increase with age by as much as a factor of two (Alda, 2006). Tissue elimination half-life may be longer still (Thornhill and Field, 1982). Medications such as non-steroidal anti-inflammatory drugs (NSAID) and certain diuretics delay elimination and risk toxicity if concurrently prescribed with lithium (Shalmi and Thomsen, 1991).

1.4 PHARMACODYNAMICS OF LITHIUM

1.4.1 Conceptual frameworks

In short, the matter of how lithium works is unresolved – in reality, its actions and effects are highly contextual. In this thesis, we refer to the *effects* of lithium as the apparent changes it brings about, be they subjective, neuropsychological, physiological, cellular, therapeutic or otherwise; we reserve the term *actions* for the direct influence the lithium ion exerts on its surroundings in order to bring about its effects. By making this distinction we can clarify some aspects of the research into the workings of this drug. Much of our understanding of lithium is nested within the constructs of mood disorders, which in turn have been dominated by psychopharmacologically derived – or driven – theories. The actions of lithium may be unchanging, but the investigation and interpretation of its effects are vulnerable to contextual trends.

Lithium induces many effects, but may actually have few actions. Plurality within theories can thus be embraced or avoided.

CANDIDATE SYSTEMS

The major mood disorders have been said to be due to a functional derangement of the serotonergic, noradrenergic and dopaminergic neurotransmitter systems of the brain – the *monoamine hypothesis*. In depression there is a deficit of effective monoaminergic transmission; in mania an excess.

This clearly limited view was neither destined nor intended to completely explain the fragility of the human condition; it provided a valuable framework for discussion and research.

The monoaminergic neurotransmitter systems of the central nervous system (CNS) are well defined and share common characteristics. Serotonin, dopamine and noradrenaline – the neurotransmitters in question – are synthesised in specific neurones from amino-acid precursors, determined and driven by key enzymes. Synthesis takes place in the cytosol and whilst a portion of the transmitters remain in this cellular compartment, most are stored in vesicles, increasing the efficiency of release. Upon neuronal firing, transmitter release occurs by vesicular merger with the presynaptic membrane. Once in the synapse, the monoamines bind to specific receptors to bring about changes in cellular functioning, either in the postsynaptic neurone or their neurone of origin via autoreceptor activation. Typifying G-protein coupled receptor (GPCR) slow-neurotransmission, their effects manifest over milliseconds to minutes (Greengard, 2001b). Termination of action occurs by reuptake and/or molecular breakdown with the dominant mode of termination varying by brain region and transmitter. All of the monoamine neurotransmitters can be degraded by monoamine oxidase (MAO), though additional enzyme pathways are well recognised.

The monoaminergic neurones arise from cell bodies in distinct, closely approximated brainstem nuclei and project to discrete, widely distributed regions in spinal, cerebellar, striatal, limbic and cortical areas. They modulate a vast array of functions including, but by no means limited to, mood, cognition, movement, sensory-gating and vegetative processes. Understandably, these systems are the target for numerous psychotropic medications.

THE POSITION OF LITHIUM

Lithium has always been something of a cuckoo in the monoamine nest, its effects not confined to neurotransmitter release and receptor activation. Indeed many of its effects occur downstream of receptors, involving the modulation of complex cellular transduction pathways in the postsynaptic neurone (Beaulieu and Caron, 2008). Of late, these effects have been interpreted in terms of neuronal viability in addition to signal transduction (Quiroz et al., 2010).

1.4.2 Lithium and the monoamines

SEROTONERGIC NEUROTRANSMISSION

Emotional processing circuits are richly innervated by serotonin (5-HT) and it is considered central to mood modulation, with a dominant role in the mediation of anxiety (Stein and Stahl, 2000). Lithium is thought to enhance serotonergic functioning, preclinical studies indicating that it achieves this enhancement through a variety of effects. The uptake of tryptophan is increased with short term administration (Aragon et al., 1987), and more 5-HT is presumably synthesised with an abundance of precursor. The release of 5-HT is enhanced by acute and chronic lithium treatment (Gottberg et al., 1989), with a reduction in the density of 5-HT receptors in the hippocampus more so than other brain regions (Subhash et al., 1999), receptor density reduction reflecting increased presynaptic 5-HT activity. Lithium also induces changes in 5-HT_{1A} receptors, again localising to the hippocampus (Treiser et al., 1981).

The tryptamine serotonin is synthesised from the essential amino-acid tryptophan, the steps catalysed by tryptophan hydroxylase and amino acid decarboxylase. Monoamine oxidase governs its metabolism to 5-HIAA.

In healthy humans the prolactin response to L-tryptophan administration is increased by acute and chronic treatment with lithium, indicating an enhancement of serotonergic activity (Price et al., 1989). In depression, the prolactin response to L-tryptophan is diminished and lithium corrects this in the short-term, though it is not clear whether this is sustained (Deakin et al., 1990; Price et al., 1990). These effects may be due to enhanced synthesis and release rather than receptor changes; short-term lithium administration does not appear to alter the sensitivity of key receptors in man, as it fails to attenuate the effects of the 5-HT_{1A} receptor agonist gepirone (Walsh et al., 1991). In patients with affective disorders stabilised by lithium, tryptophan depletion fails to alter mood (Hughes et al., 2000; Johnson et al., 2001), such that lithium may protect against transient reductions in serotonergic function.

The rate limiting step in serotonin synthesis is not enzyme activity but precursor abundance. Depleting dietary tryptophan lowers mood in those with a history of depression whilst L-tryptophan administration can be an effective antidepressant augmentation strategy.

DOPAMINERGIC NEUROTRANSMISSION

In addition to its established roles in working memory, attentional processes and bodily movement, dopamine modulates mood systems, crucially contributing to drive and pleasure seeking (Greengard, 2001a). Evidence for an interaction between

Dopaminergic interpretations of bipolar disorder are returning to the fore, dragging lithium in their wake.

lithium and dopamine is most consistently found in its ability to attenuate the effects of stimulants. Preclinical behavioural models in the rat support an attenuation of dopaminergic transmission by lithium, evidenced by a reduction in spontaneous exploration of new environments (Gray et al., 1976; Bloom et al., 1983; Hines and Poling, 1984) and a diminution of the effects of amphetamines after acute and chronic administration (Flemenbaum, 1975; Borison et al., 1978; Berggren et al., 1978, 1981; Berggren, 1985; Lerer et al., 1984; Gould et al., 2001). There are, however, negative findings from comparable studies (Ebstein et al., 1980; Fessler et al., 1982; Pittman et al., 1984; Arriaga et al., 1988; Cappeliez and Moore, 1990) The neurobiological correlates of the effects are unclear – after chronic administration of lithium to rats, the synthesis and release of dopamine has been shown to decrease (Rastogi and Singhal, 1977; Baptista et al., 1993), increase (Berggren, 1985) or remain unaltered (Reches et al., 1984). Studies of dopamine metabolites are similarly mixed (Hesketh et al., 1978; Gottberg et al., 1989). Inactivation of dopamine through cellular uptake is increased *in vivo* in the rat brain following chronic lithium administration (Ahluwalia and Singhal, 1981). The application of lithium to cells *in vitro* provides support to this observation (Dunigan and Shamoo, 1995) and the elevation in the dopamine transporter (DAT) binding of [^{125}I]RT-121 alludes to the mechanism (Carli et al., 1997). Lithium also has an effect on dopamine receptor expression, preventing neuroleptic-induced postsynaptic supersensitivity but not reversing it (Bloom et al., 1983; Bunney and Garland, 1983). Comparable studies have been conducted in man, the findings of which are considered in *Chapter 4*.

NORADRENERGIC NEUROTRANSMISSION

Underpinning vigilance and motivation in healthy subjects, disturbing the noradrenergic systems impairs such functions and also generates anxiety and irritability. The evidence that lithium modifies this system is somewhat inconsistent and so a consensus on its effects is difficult to establish (Juckel and Mavrogiorgou, 2006). Studies in rodents yield a mixed picture, suggesting that the manner in which lithium affects noradrenergic systems may be sensitive to the dose, duration and region examined.

Soon after lithium injection, noradrenaline concentrations in the mediobasal hypothalamus fall (Otero Losada and Rubio, 1992); after an hour, levels are elevated in the visual cortex (Gottberg et al., 1988). Iontophoretic application of lithium to the prefrontal cortex attenuates noradrenergic modulation of firing rates (Kovacs and Hernadi, 2002). Peripheral assays of the turnover of the transmitter in healthy subjects have shown that whilst lithium does not alter noradrenergic functioning after treatment periods of 1–3 weeks (Rudorfer et al., 1985; Grof et al., 1986), longer term administration appears to increase its release (Manji et al., 1991). In mania, lithium may reduce noradrenaline excretion but in depression the reverse can occur (Greenspan et al., 1970; Beckmann et al., 1975; Bowers and Heninger, 1977). The effects of lithium on the release of noradrenaline may be driven by it altering the sensitivity of α_2-autoreceptors (Brambilla et al., 1988); its prevention of β-adrenergic supersensitivity may be important in chronic treatment (Risby et al., 1991; Lenox et al., 1998)

1.4.3 Signal transduction pathways

Monoaminergic neurotransmitters can bring about long term changes in postsynaptic cells, receptor activation triggering a cascade of intracellular signalling systems which may modify cellular functions by altering gene expression and protein transcription (Greengard, 2001b). In addition to modifying neurotransmitter activity, lithium affects these second-messenger systems in various ways.

The inositol depletion hypothesis is the most established in this field (Berridge et al., 1989). In brief, lithium alters the balance of the phosphatidylinositol cycle (PI-cycle) by inhibiting inositol monophosphatase, increasing inositol monophosphate and decreasing free myoinositol concentrations in the brain. It it thought that in reducing free myoinositol, intracellular processes that depend on it are slowed and signal transduction altered. Moreover, the effects may be more marked in cells where the PI-cycle is functioning in such a way that free myoinositol levels are high (Gani et al., 1993) – an abnormality purported to occur in mania. The functioning of the

PI-cycle is dependent upon the presence of ionic co-factors such as calcium and magnesium. Lithium, with its diagonal relationship to these ions, may inhibit inositol monophosphatase by displacing or altering the concentration of its co-factors.

The actions of second-messenger systems are not restricted to cellular transduction as they interact with molecular pathways governing cellular integrity and survival. That lithium may alter the balance of activity in these systems, and so cellular viability, is attracting much interest.

1.4.4 Neuroplasticity

Lithium has been found to limit the damage caused to neurones by a variety of insults. Often described as neuroprotective or neurotrophic, there is an emerging consensus that an *effect on neuroplasticity* is the preferred expression. It is thought that lithium's enhancement of neuronal viability and resilience is not simply a consequence of its therapeutic effect, but central to it. This topic has been extensively reviewed, (with the reviews synthesised by Wada, 2009). The key points are summarised below.

The neuroplastic effects of lithium are increasingly well defined in preclininal studies; whether these effects can be demonstrated in the human brain *in vivo* is uncertain.

LITHIUM AND APOPTOSIS

A wealth of data from neuronal cell cultures and rodent brain studies demonstrates or supports the neuroprotective effects of lithium, mediated through a variety of mechanisms but principally by the modulation of apoptotic pathways. Central in this regard is glycogen synthase kinase-3β (*GSK-3β*), a serine/threonine kinase ubiquitously expressed in tissues and extensively in the brain. This protein kinase is constitutionally active and by phosphorylating its substrates, leads to their inactivation or degradation. Expression of *GSK-3β* is tightly regulated as when activated or inactivated, numerous cellular processes come to pass that are generally pro- or anti-apoptotic respectively; inactivation thus favours neuroprotection. Inhibition of *GSK-3β* usually comes about through the actions of AKT (Ak transforming), another serine/threonine kinase whose activity is increased by various growth factors including brain-derived neurotrophic factor (BDNF) and the insulin-like growth factors (IGF).

APOPTOSIS: the process of programmed cell death. Its prevention is the microscopic embodiment of lithium's antisuicidal properties.

Lithium inhibits *GSK-3β*, the consequences of which are pertinent to is psychopharmacological profile. The mechanism of this inhibition is largely unresolved, but may occur directly though lithium competing with the cofactor magnesium and indirectly via the facilitation of AKT. Amongst other things, inhibition of *GSK-3β* by lithium brings about an accumulation of β-catenin, facilitating the processes of down-stream pathways. The products of the Wnt/β-catenin pathway include BDNF and IGF-I and IGF-II. Receiving much attention for its putative role in the development and maintenance of the mood disorders as well as their treatment, BDNF levels are lowered in episodes, improve with recovery, and are increased by lithium and antidepressants.

Other components of the neuroprotective pathways are affected by lithium, notably *bcl-2*. Shown to encode cytoprotective protein in cells of human neuronal origin, *bcl-2* has been found to foster the regeneration of CNS axons. Lithium appears to up-regulate *bcl-2*, enriching hippocampal neurogenesis in the dentate gyrus of mice.

1.5 AIMS OF THIS THESIS

The literature on lithium is vast, but on appraising the field three topics attracted our attention, variously begging confirmation, explanation or exploration. First, the disorders for which lithium is prescribed have long been associated with abnormalities of the monoaminergic neurotransmission and of late there has been a resurgence of interest in the role of dopamine in bipolar disorder. Driven most recently by the clear antimanic properties of dopaminergic antagonists, it is of interest to examine whether lithium's therapeutic effect may in part be due to a modulation of dopaminergic neurotransmission. The following hypothesis was therefore proposed:

> *Lithium carbonate will lessen the effects of methamphetamine by attenuating dopaminergic neurotransmission in healthy men, gauged by subjective ratings, performance on a task of sustained attention and fMRI signal change; these effects will be evident at serum levels advocated for the treatment of mania and not with a lower dose schedule.*

Second, the proposal that lithium has neuroprotective properties is gaining a great deal of attention and widespread acceptance. The extensive and consistent preclinical evidence has begun to influence clinical research, with investigators examining the potential role of lithium in various neurodegenerative conditions. Neuroprotective effects of lithium have not, however, been convincingly demonstrated in man. The mechanism underlying the most commonly cited supporting evidence, the observation of increases in grey matter volume on MRI scanning, has yet to be explained. In this thesis it is proposed that the imaging findings are better accounted for by an alteration in MRI contrast, more specifically:

> *The increase in grey matter volume following lithium treatment is artefactual, arising from a misclassification of tissue types during intensity-based image analysis, in turn due to lithium reducing the T_1 relaxation time of protons.*

Third, there is still relatively little known about the relationship between serum and brain concentrations of lithium in man. The feasibility of detecting lithium using MRS was established two decades ago but progress has been slow, the field restricted to a few specialist centres. Whilst quantitative spectroscopic and imaging-based techniques have been developed, comparison of the concentration of lithium in grey and white matter has not been achieved. Furthermore, the reported signal resolutions remain too low and the scan times too long for this technique to have clinical utility. As part of this thesis, the development of lithium MRS equipment and techniques was undertaken, setting the following targets:

> *A lithium MRS technique should be developed for use on a clinical scanner, with the aim of enabling the concentration of lithium in the human brain to be quantified in vivo. Acquisition times should be short enough that the technique could be used clinically, with a resolution such that signal derived from grey and white matter can be discriminated.*

2 MAGNETIC RESONANCE

The field of magnetic resonance (MR) is attractive to neuroscientists and clinicians alike, enabling the structure, function and composition of the human brain to be probed *in vivo*. As a complete account of the MR phenomenon is beyond the scope of this thesis, the aim of this chapter is to provide an overview that is sufficient to permit the critical appraisal of the techniques used. Following an outline of the fundamental principles, the acquisition and analysis of structural and functional data is reviewed before moving on to magnetic resonance spectroscopy (MRS).

2.1 FUNDAMENTAL PRINCIPLES

2.1.1 Nuclear properties

Certain atomic nuclei possess *net-spin*, a property central to MR that arises from the inherent *spin* of subatomic particles. Spin is intrinsic and although it does not derive from a rotational motion, it is said to have a direction. The spins of paired particles are in opposite directions and so balanced; if a nucleus has an uneven sum of protons and neutrons, imbalance exists and net-spin emerges. The angular momentum associated with spin gives rise to a *magnetic moment* (μ) which characterises the microscopic magnetic field surrounding the nucleus (figure 2.1 on page 20). At equilibrium in the absence of a macroscopic magnetic field, the individual nuclear magnetic moments are randomly orientated and cancel out, resulting in *zero net magnetisation*.

The situation changes in the presence of an external magnetic field and aspects of the interaction can be manipulated by the application of electromagnetic (EM) waves in the radiofrequency (RF) range. In magnetic resonance imaging (MRI), the interaction is restricted to hydrogen nuclei (hereafter referred to as *protons*, since a single proton comprises the nucleus of ^{1}H). Protons have well characterised spin properties which will be used to outline the principles of MR; spectroscopy and multinuclear detection is considered later in this chapter.

2.1.2 *Nuclear behaviour in a magnetic field*

INDIVIDUAL NUCLEI

When exposed to a static magnetic field (B_0), the magnetic moment of a nucleus is said to align with respect to that field (itself traditionally orientated along the z-axis). Quantum mechanics tells us that this alignment can be in any direction but that its z-axis component is restricted to a number of states, characterised by the quantum number m. This m can take $2I + 1$ values running from $-I$ to $+I$ in unit steps, in which I is the spin quantum number of the nucleus. Protons have two possible energy states ($I = ½$; $m = +½$ and $m = -½$); in the $m = +½$ state the z-axis component of μ is parallel to B_0 whilst in the $m = -½$ state it is antiparallel (figure 2.1 on page 20). Excited-state and ground-state are synonymous with antiparallel and parallel. Opposing B_0, antiparallel is often described as the higher energy level.

Particles with spin have angular momentum and an associated magnetic moment; both are vectors, the angular momentum vector being referred to as the *spin polarization axis*. For protons, μ and the spin polarization axis are aligned and in the same direction. When exposed to an external magnetic field these vectors move around it, describing a circular path in the plane perpendicular to the axis of B_0. This is called *precession* (figures 2.1 and 2.2 on page 20), classically analogous to the motion of an angled gyroscope. The rotating mass of a gyroscope gives it an angular momentum parallel to its axis – when the axis deviates from the vertical, the net angle between it and the force of gravity results in a torque which causes the whole gyroscope to precess. Within the *vector model*, the external magnetic field is analogous to gravity and the nucleus to the gyroscope.

The frequency of precession – *Larmor frequency* – is dependent upon the direction and strength of the applied magnetic field, as well as the properties of the nucleus itself. This is expressed formally in equation 2.1, where ω_0 is the angular frequency of the precession (in rad·s^{-1}), γ is the gyromagnetic ratio of the nucleus and B_0 is the strength of the applied magnetic field (in Tesla). The sign in the formula indicates the direction of the precessional rotation; negative in the case of protons.

$$\omega_0 = -\gamma B_0 \tag{2.1}$$

The Larmor frequency can also be expressed in Hertz, requiring the simple transformation apparent in equation 2.2 and a change of notation (ν_0).

$$\nu_0 = -\frac{1}{2\pi}\,\gamma B_0 \tag{2.2}$$

MULTIPLE NUCLEI

Individual protons are not observed in MR experiments but rather great swathes of them. A group of protons which are experiencing the same magnetic field is called a *spin packet*, their behaviour usually explained using classical theory and the principles of the vector model. At equilibrium in an applied magnetic field the magnetic moments of the protons in a spin packet are not randomly aligned but *anisotropically* distributed – fractionally more are in the ground-state (figure 2.2 on the next page). When they are summed they do not fully cancel out and so a magnetic field emerges, each spin packet vector subsequently contributing to the *net magnetisation vector* of the whole sample. At equilibrium, the net magnetisation vector emerges parallel to the applied field because fractionally more protons are in the ground-state. The behaviour and manipulation of this vector is central to the magnetic resonance technique.

2.1.3 Signal preparation

The net magnetisation vector can induce a voltage difference in a conducting array as it sweeps round its precessional path – the basis of signal detection. At equilibrium, however, the vector evades detection for two reasons: first, being small and in the z-axis, it is subsumed into the B_0 field; second, it is static and so does not meet the criteria for magnetic induction. This situation would alter were the net magnetisation vector temporarily shifted into the x-y plane. This can be achieved by the application of an RF pulse though a *transmitter coil*.

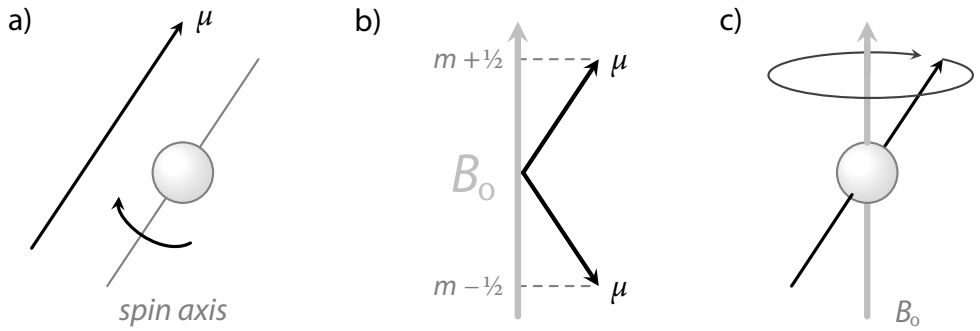

Figure 2.1: a) Spin of an individual proton generates a magnetic moment μ, aligned with the spin polarisation axis; b) In the presence of an external magnetic field B_0 applied along the *z*-axis, there are two possible quantum energy states that describe the alignment of the *z*-axis component of μ for an $I = ½$ spin; c) Precession of an individual proton's μ about the axis of the applied magnetic field – at equilibrium the path is circular because the angle subtended to B_0 is constant for that proton.

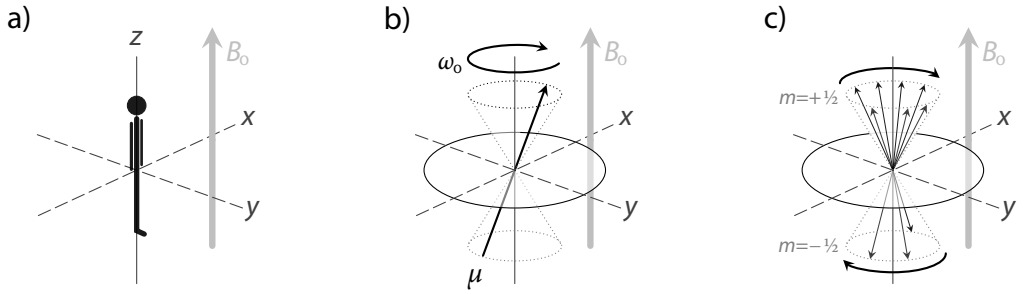

Figure 2.2: Precession in a B_0 field – a) Right-handed axis diagram indicating the alignment of the applied magnetic field B_0 and the typical placement of a subject; b) Precessional path of μ about the *z*-axis for a single proton, the direction indicating its negative Larmor frequency; c) Multiple phase-incoherent vectors precessing with the same direction and frequency, their position above and below the *x*-*y* plane indicative of their parallel and antiparallel spin state respectively.

Pulse application The RF pulse is an EM wave and by arranging the angle at which it is applied, an additional magnetic field (B_1) arises, perpendicular to B_0 and rotating at the frequency of the EM wave. If the rotation matches the Larmor frequency, *phase cohesion* is induced and *vector tipping* occurs. The net magnetisation vector experiences a combined magnetic field, angled to the z-axis and rotating around it. This new field generates a new torque on M, rotating it towards the x-y plane.

Vector path It is important to consider how the path of the net magnetisation vector can be visualised. Viewed as a fixed observer in a space external to the nucleus, the so-called *laboratory frame*, the net magnetisation vector would rotate down towards the x-y plane with the tip of its axis describing a spiral within a sphere. This complicated trajectory can be simplified by adopting the *rotating frame of reference*, in which the x and y axes themselves rotate at the Larmor frequency. Travelling with the precessing vector enables one to describe the path as a simple arc (figure 2.3 on page 24). In the diagrams which follow, we consider the behaviour of the net magnetisation vectors of several spin packets at once. As these can be made to precess at different frequencies, the rotating frame is more correctly described as moving with the B_1 field.

PRECESSIONAL PHASE

The net magnetisation vector undergoes precession. When fully aligned with the B_0 field, the angle subtended by the net magnetisation vector in the 'precession cone' is zero but when it is shifted toward the x-y plane, the familiar situation of precession as a sweeping arc of motion is encountered. The net magnetisation vector is a composite of all the vectors in the spin packets; at equilibrium, these vectors do not precess in phase and at any given point in time they are randomly distributed around the circular precessional path. They will, however, be rotating at largely the same frequency. If the B_1 field created by the RF pulse rotates synchronously with the precessing vectors, then their frequencies are matched and the vectors are brought into phase (figure 2.4 on page 24). As phase cohesion is a requirement for realigning the net magnetisation vector, the RF pulse needs to be circularly polarized at the Larmor frequency.

TRANSVERSE MAGNETISATION

It takes energy to create a sizeable transverse component to the net magnetisation vector and this is delivered by making use of the phenomenon of *resonance*. For our purpose, this can be much simplified (figure 2.4 on page 24).

Resonance When an object it is exposed to an oscillation which matches its natural frequency, it gains a great deal of energy from that oscillating force. Essentially, an RF pulse of Larmor frequency will resonate with the protons in the spin packet, delivering energy which elevates a proportion to a higher state. The ratio of protons in the ground-state and excited-state equalises, progressively depleting the longitudinal magnetization at the expense of which a transverse component arises.

Tipping As the transverse component emerges, the net magnetisation vector moves away from the z-axis, with the angle subtended to this axis usually denoted by θ. A *tip angle* of 90° means that the net magnetisation vector has been fully shifted from the longitudinal plane into the transverse; 180° sees it realigned with the z-axis but in the opposite direction. Precession occurs all the while.

Strictly, θ is the angle difference between the net magnetisation vector before and after the RF excitation pulse. This becomes important in multiple pulse sequences. Note that tip angle is synonymous with flip angle and nutation angle.

2.1.4 *Signal detection*

When the net magnetisation vector is precessing in the transverse plane, it is capable of inducing an electrical voltage in a conductor and thereby generating a current (figure 2.5 on page 26). An RF *receiver coil* can now be used to detect and convey this signal. Coils come in many forms; some systems use separate coils for transmitting and receiving signals, other use *transceiver coils* to do both.

CHARACTERISTICS OF THE SIGNAL

The current induced in the RF coil is small and requires amplification before it can be processed further. In its purest form it should be a periodic oscillation at the Larmor frequency but, for reasons we will discuss later, other 'off-resonance' frequencies are also detected. Following a simple 90° tip, the signal is of maximal amplitude just after

the excitatory RF pulse is removed – this being the point when the net magnetisation vector is wholly in the transverse plane. This position is not sustained and with time, the longitudinal magnetisation returns and phase cohesion is lost.

The spin packet regains its equilibrium through *relaxation* processes, described by the time-constants T_1 and T_2. These two relaxation processes are important in MRI image creation, providing different information on tissue characteristics and disease states. Both types of relaxation occur concurrently for all protons, but T_1 relaxation takes longer than T_2. The construction of the RF pulse sequence dictates which process dominates in the signal detected (see §2.1.5 on page 25).

LONGITUDINAL RELAXATION (T_1)

When protons regain equilibrium, the energy they absorbed from the RF pulse is dissipated into their surroundings. This is called longitudinal, T_1 or *spin-lattice relaxation*, the term lattice harking back to the origins of the field in the analysis of crystal structures. Longitudinal relaxation represents the recovery of the longitudinal component of the net magnetisation vector, which occurs in an exponential manner. The time-constant T_1 is the time taken for the longitudinal component to return to 63% of its equilibrium value, and is heavily dependent on the strength of the applied magnetic field.

TRANSVERSE RELAXATION (T_2)

Transverse, T_2 or *spin-spin relaxation* derives from the interactions of the protons with each other and not the lattice. In this form of signal decay it is the transverse component of the magnetisation vector which diminishes. There is no actual energy dissipation from the tissue with T_2 relaxation, but rather a redistribution amongst spins as they lose phase coherence. Such *dephasing* can be thought of as reducing how much of the transverse signal can be detected rather than how much is actually present. The transverse magnetisation decays in an exponential manner with the time-constant T_2 being the time taken for it to lose 63% of its original value. T_2 times are relatively independent of the strength of the applied magnetic field.

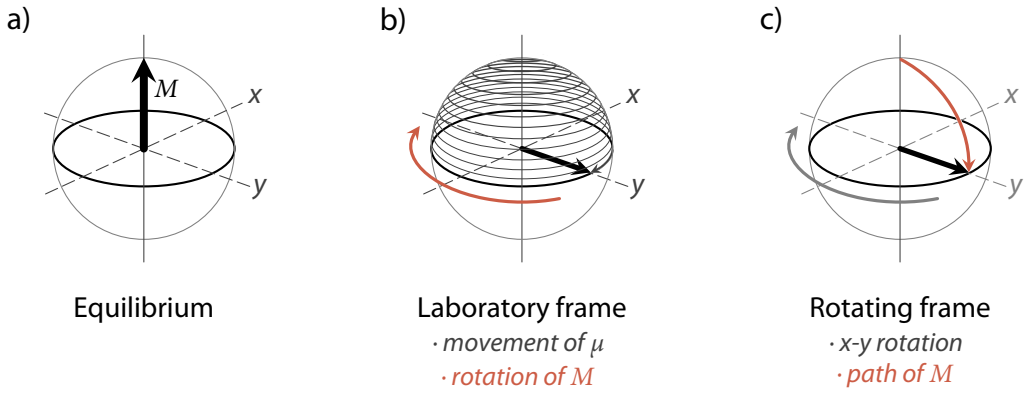

Figure 2.3: The net magnetisation vector M at equilibrium (a) and following a 90° radiofrequency pulse (b and c). In the *laboratory frame*, each μ spirals towards the *x*-*y* plane, the $m = +½$ spins moving top-down and the $m = -½$ spins bottom-up (not depicted). M follows suit, rotating about the *z*-axis at the Larmor frequency. In the *rotating frame*, the *x*-*y* plane turns with a frequency equal to ω_0 so that from the perspective of M, the 90° tip is a simple arc.

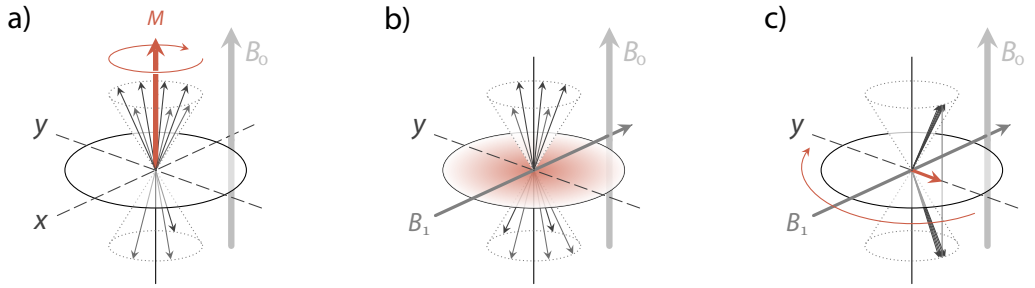

Figure 2.4: Application of a B_1 field – a) at equilibrium there are more spins in the ground state and so M, the net magnetisation vector, emerges parallel to the B_0 field. The spins, however, are not in phase; b) a radiofrequency pulse generates a B_1 field along the *x*-axis, elevating a proportion of the spins to the excited state and diminishing the longitudinal component of M. The resultant transverse component of M is diffusely distributed because of spin phase incoherence; c) when the radiofrequency pulse is circularly polarized at the Larmor frequency, the B_1 field draws the precessing spins into phase and a coherent transverse component of M emerges.

2.1.5 *Signal manipulation*

The most basic of MR investigations is the application of an RF pulse and the collection of whatever signal emerges – the *pulse-acquire* experiment. The data so produced is of interest in spectroscopy, but of limited use in structural or functional imaging. In order to produce images, the transverse magnetisation is manipulated in such a way as to emphasise specific relaxation processes in the signal and encode that information spatially. This can be achieved by running sequences of RF pulses to create *echoes*, often in conjunction with the application of additional magnetic fields. Note that the time interval between successive pulse sequences applied to the same slice is known as the *repetition time* (TR). In addition to the basic signal collection, two of the most important components of such sequences will be considered, namely the *spin-echo* and the *gradient echo*.

PULSE-ACQUIRE

Following a single RF pulse, the signal returned progressively diminishes over time (figure 2.6 on the following page). This sort of signal profile is called a *free-induction decay*, having the characteristics of a damped sinusoid. The oscillations are at the Larmor frequency and the time-constant $T_2^\star$ describes the decay of the observed transverse magnetisation. $T_2^\star$ decay is not a pure process but rather an admixture of relaxation mechanisms and the effects of magnetic field inhomogeneities, which together result in a rapid loss of signal.

In a perfectly uniform magnetic field, protons dephase though spin-spin interactions whilst maintaining precession at the Larmor frequency. With clinical scanners, B_0 is ever so slightly inhomogeneous as local tissue conditions cause small perturbations in the magnetic field and as a consequence, adjacent spin packets precess at slightly different rates. At an arbitrary time after an RF pulse ($t = \tau$), the transverse magnetisation will be composed of lead-vectors and lag-vectors from spin packets in stronger and weaker field areas with faster and slower frequencies of precession respectively. It will have dephased to a greater extent than that predicted by its T_2 time.

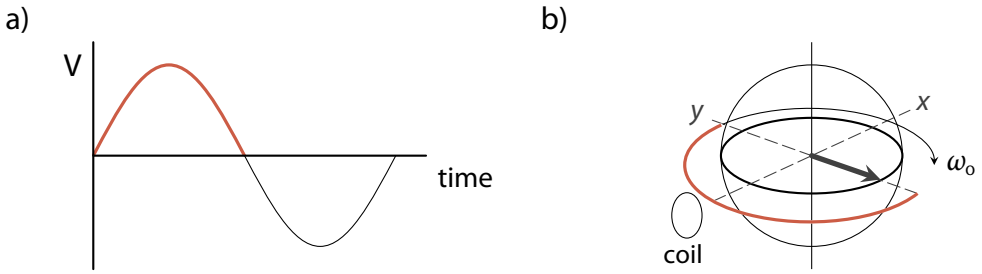

Figure 2.5: MR signal detection – a) the signal is time-varying (voltage × time); b) a voltage difference is induced as the transverse magnetisation sweeps past the radiofrequency coil, the highlighted 180° arc matching the coloured portion of the sine wave.

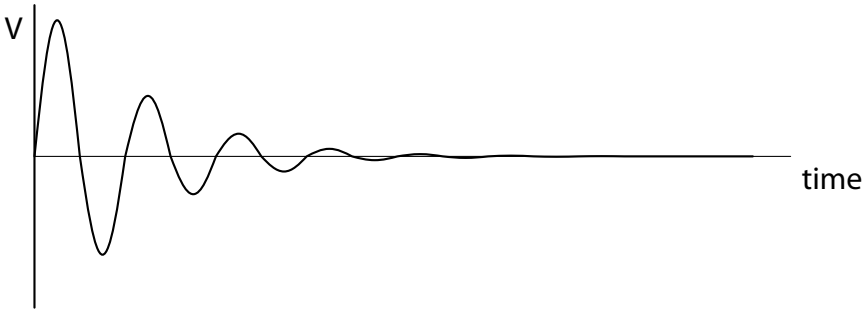

Figure 2.6: Simulated profile of a free-induction decay – after a radiofrequency pulse the voltage amplitude (V) of the signal diminishes over time, decaying by the function T_2^*.

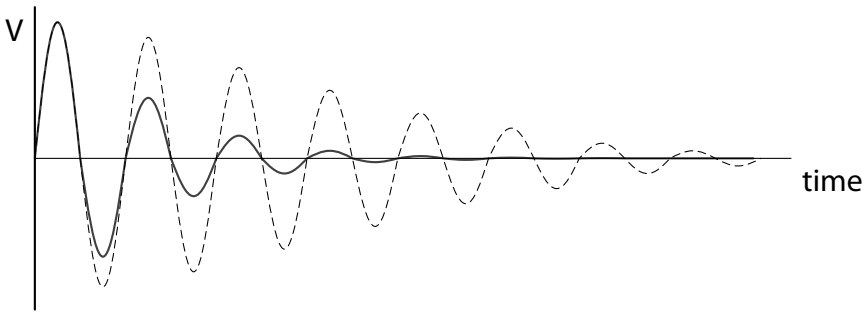

Figure 2.7: Simulated profiles for T_2^* (solid line) and T_2 (broken line) in a free-induction decay. The decay of signal occurs more swiftly than predicted from the T_2 of the subject matter because of the effects of local field inhomogeneities.

Consequently, $T_2^\star$ is always shorter than T_2 and rarely follows a simple exponential function (figure 2.7 on the previous page). To isolate T_2 relaxation from the corrupting effects of field inhomogeneities, a spin-echo is created.

SPIN-ECHO SEQUENCE

Consider a partially dephased transverse magnetisation at $t = \tau$ following a 90° tip (figure 2.8 on page 30). If a 180° tip is performed at $t = \tau$, the vectors will be flipped into mirror-image positions; lead-vectors now lag behind but they continue to precess at a greater frequency. If a second time period equal to τ is allowed to pass, the fastest precessing spins will have caught up with the slower ones and the transverse magnetisation will be as one. This *refocussing* occurs at a time $t = 2\tau$. All the while, a decay of the transverse magnetisation due to dephasing occurs. Thus, when the transverse magnetisation at $t = 2\tau$ has returned to its original position it will be of lesser magnitude. If this magnitude has reduced to 63% of its original value, then $t = 2\tau$ is equal to the T_2 of that sample. The time taken from the application of the first RF pulse to the peak of the echo is called the *echo-time* (TE), equal to $t = 2\tau$ in the sequence described. The TE is a determinant of image contrast and scan acquisition time. Spin-echoes are used in many pulse sequences, but are particularly valuable in creating T_2 contrast.

GRADIENT-ECHO SEQUENCE

If spin-echo sequences negate the effects of variable rates of precession, then gradient-echoes can be said to capitalise upon them. Following an RF pulse, a transverse magnetisation will emerge and precess at the Larmor frequency. If an external magnetic gradient is deliberately applied across the sample, some spin packets will experience a greater field strength than others and consequently precess at a higher frequency. Dephasing is thus exaggerated. When that gradient is removed and an opposing one applied, the modification to the precessional frequencies is reversed. Importantly, the direction of precession is also reversed so that the vectors rephase and an echo signal can be obtained.

As a gradient-echo can be obtained with a single RF pulse which need not be a full 90° tip, acquisition times are shorter than spin-echo techniques. The TE is determined by the application of the gradients, and is typically short. As a 180° rephasing pulse is not applied, the effects of local field inhomogeneities are upheld and the signal is effectively a free induction decay (FID) governed by $T_2^\star$ relaxation. With careful selection of timing parameters and tip angles, good T_1 contrast can be generated whilst maintaining short acquisition times. Gradient-echo sequences are therefore the mainstay of structural imaging techniques, but also find application in fMRI.

2.1.6 Image generation

The signals thus far described would, if processed as images, produce a single point whose intensity would reflect the signal returned from the whole field of view of the coil. In order to produce an image, this space must be parcellated and the signal acquired in a way that denotes its spatial location. Since the voltage induced by the transverse magnetisation is what we have to work with, spatial encoding is largely achieved by altering the frequency and phase of the vector precession through the application of additional magnetic gradients. It is now common practice to directly acquire 3D volumetric images, but the concepts underpinning spatial location are more easily understood by considering earlier 2D volumetric techniques. Here, the specimen volume is divided into slices and each slice into a matrix before reconstruction of the data points as a 3D image. Each spatial location is rendered as a volume element or *voxel* (volumetric pixel).

SLICE SELECTION

Acquiring a signal from a designated 2D slice simply involves making the spin packets in that space precess at a specific frequency whilst setting the receiver coil to detect that – and *only* that – frequency. Recalling equation 2.1 on page 19, the frequency of precession is proportional to the magnitude of the applied magnetic field and so largely determined by the strength of the scanner. Subtle but predictable shifts in the Larmor frequency can be brought about by changing the field strength, typically

through the application of magnetic gradients. Applying restricted frequency RF pulses will excite spin packets at specific points on this gradient, with the width of the slice determined by the breadth of the frequency composition of the RF pulse and the slope of the gradient. The orientation of the gradient governs the plane of the slice, broadly considered as axial, sagittal or coronal but often with a degree of angulation.

ENCODING LOCATION

When the slice selection RF pulse is applied, the spin packets in that slice precess in phase and at the same frequency but those in neighbouring slices do not. However, there is no localisation *within* the slice. Consider the selected slice as a square with vertical and horizontal axes. With two axes come two modes of manipulation. If a magnetic gradient is applied along the horizontal axis, a series of columns can be envisaged in which each spin packet precesses at a progressively higher frequency. One dimension is thus encoded. If a second gradient is briefly applied along the vertical axis, the phase of the spins is altered. Spins in the strongest part of the gradient will be phase advanced compared to those in the weakest, emerging as a series of rows with designated phase positions. Acquisition can be timed to each phase position and location encoded. A matrix can thus be created in which spin packets have a determined phase and frequency of precession (figure 2.9 on the following page). For each slice, the *phase-encoding gradient* is applied just after slice-encoding (t = zero) and the *frequency-encoding gradient* during signal acquisition (t = TE). The procedure is repeated many times for each slice, with progressively steeper phase-encoding gradients, the number of which determines the matrix resolution.

DECODING THE SIGNAL

The received signal is a mixture of oscillating signals at different frequencies which must be analysed to determine which components are present. This is done mathematically using the Fourier transform.

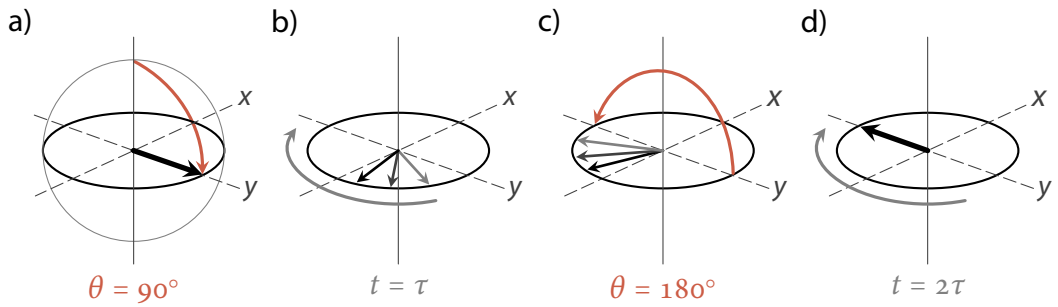

Figure 2.8: Spin echo sequence – a) a 90° radiofrequency pulse is used to create the transverse magnetisation; b) as this precesses in the *x-y* plane, field inhomogeneities contribute to the dephasing of the vectors and some spins precess faster than others; c) at $t = \tau$, a 180° pulse flips the vectors over in the *x-y* plane and precession continues at the same rate for each spin; d) the faster spins therefore catch up with the slower ones, such that at $t = 2\tau$ the transverse magnetisation is rephased.

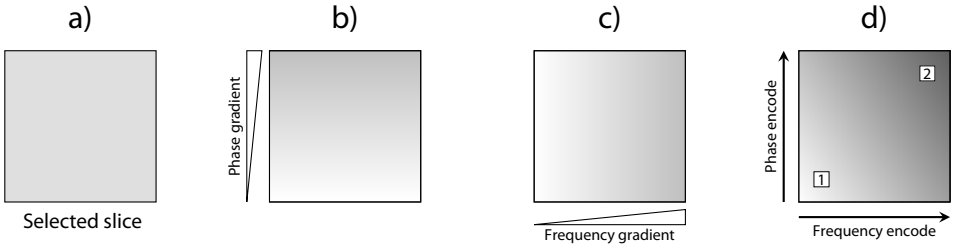

Figure 2.9: Spatial encoding – a) the frequency and phase of precession throughout the selected slice is uniform; b) phase encoding gradient at $t = 0$, the spin packets at the top are phase-advanced; c) frequency encoding gradient at $t = \text{TE}$, the spin packets on the right precess more rapidly; d) with combined encoding, pixel 1 will be both at a lower frequency and less phase advanced than pixel 2.

2.2 STRUCTURAL IMAGING

Anatomical images are a necessary part of most magnetic resonance studies and the experiments described in this thesis are no exception. In addition to our investigation of the effects of lithium on assessments of brain structure, we make use of anatomical images when processing both our functional and spectroscopic data. An appreciation of the nature of signal contrast, tissue characterisation and image analysis techniques will aid the appraisal of our methods.

2.2.1 Signal contrast

On a typical T_1-weighted anatomical image the CSF appears dark and, conveniently, white matter is white and grey matter grey. The grey-scale intensity of each pixel in the image reflects the intensity of the signal arising from its sister voxel. The magnitude of this signal is proportional to the size of the transverse component of the net magnetisation vector at the time of acquisition, which in turn is dependent upon a number of factors. Some of these are inherent to the tissue, others related to the acquisition parameters. It follows that tissue contrast is largely determined by the pulse sequence applied.

2.2.2 Tissue characterisation

Were the brain homogeneous, all areas would have the same magnetization and behave identically, so the returning signal would be uniform throughout – we can be thankful because this is not the case. The absorption of RF energy is greatest in the areas with the highest density of spins and so it follows that overall, CSF is capable of returning more signal than brain tissue. This form of *intrinsic contrast* can be thought of as determining the absolute amount of signal available, but further contrast can be achieved by utilising variations in the rate of signal return. In other words, the contrasting T_1 and T_2 times of the different tissues come into play and we can choose which relaxation mechanism to emphasize. Contrast in anatomical images is most commonly weighted towards T_1 relaxation, which occurs when the energy delivered

by an RF pulse is absorbed by the lattice and the longitudinal component of the net magnetisation vector restored (see §2.1.4; text on page 23). T_1 relaxation is governed by a number of different tissue properties, which for brain tissues are outlined in table 2.1 below.

TISSUE	LIPID CONTENT	TUMBLING	T_1 TIME	SIGNAL
White matter	High	$= \omega_0$	Short	High
Grey matter	Low	$< \omega_0$	Long	Medium
Cerebrospinal fluid	Negligible	$> \omega_0$	Very long	Low

Table 2.1: Tissue characteristics determining T_1 and signal intensity

Energy transfer to the lattice – in this case tissue – is most efficient if the tumbling rate of its molecules closely matches the Larmor frequency of the spins. This is the situation for white matter, explaining its short T_1 and high signal intensity on anatomical images. Grey matter molecular tumbling rates are less than the Larmor frequency, giving a long T_1 time. For CSF the tumbling rate is much higher than the Larmor frequency, but as this results in inefficient energy transfer its T_1 is much longer than that of brain tissue.

The T_1 times of brain tissues can be measured by charting the signal returned at various time points and fitting these values to an exponential function. This, however, is *not* the basis of tissue differentiation in structural imaging. In T_1-weighted imaging, data is collected at a single time point on the relaxation curve. In essence, tissues with a short T_1 will have recovered more of their longitudinal component of the net magnetisation vector than tissues with a long T_1. Contrast is therefore relative and the timing of data acquisition crucial (figure 2.10 on page 34). In practice, each voxel contains a proportion of different tissue types with varying rates of recovery. The longitudinal vector therefore comprises swiftly and slowly relaxing elements, the ratios of which can be used to decipher the dominant tissue type.

2.2.3 *Image acquisition*

The magnitude of the signal detected by the coil array is proportional to the transverse component of the net magnetisation vector, but the longitudinal component is that which defines T_1 relaxation. As this aligns with the B_0 field it cannot be detected. T_1-weighted sequences must therefore contain a second RF pulse which brings the recovering longitudinal component into the transverse plane. The signal detected immediately after this second pulse is proportional to the T_1 recovery (figure 2.11). High resolution images can be obtained relatively swiftly by using gradient-echo techniques and low flip angles, but sufficient time must be allowed for T_1 relaxation to occur, otherwise contrast will be inadequate. As T_1 is proportional to B_0, structural scans take longer to perform on stronger magnet systems.

2.3 STRUCTURAL IMAGE ANALYSIS

It is a basic tenet of image analysis that the dimensions of a voxel genuinely represent a volume of tissue in space. Thus, the volume of a structure or tissue can be calculated by summating the voxels its image contains. All that is required is a technique for selecting the correct voxels. Later in this thesis, attention is directed to a number of MRI studies in which brain grey matter volumes are reported. Strictly, grey matter is a tissue class rather than a macroscopically distinct structure. It can be measured in a variety of ways, broadly classifiable into manual, semi-automated and fully automated techniques; the most commonly used methods are outlined below.

2.3.1 *Manual techniques*

REGION OF INTEREST

Selecting a brain structure and defining it on an image is a strategy with a long history spanning numerous technological advances. Currently, a fairly standard approach involves an investigator viewing the images on a computer screen, identifying the relevant structure and manually outlining it using a mouse or similar device. The

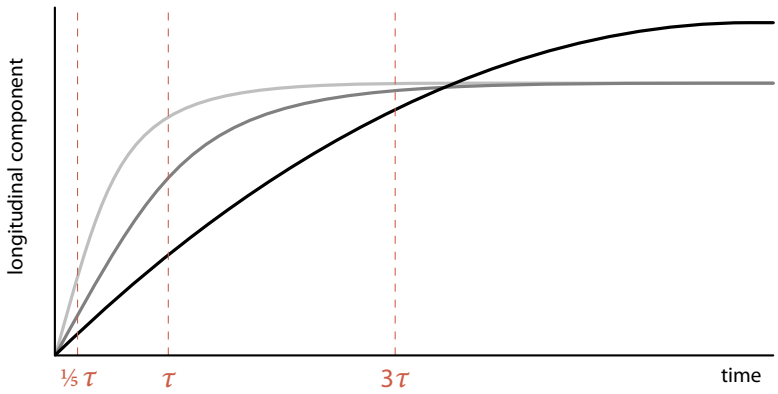

Figure 2.10: Simulated T_1 recovery for brain tissues. The longitudinal component of the net magnetisation vector recovers more swiftly in white matter (■) compared to grey matter (■) and CSF (■). Its signal is therefore relatively greater and contrast can be established. The timing of data acquisition determines the contrast: at time = τ, good contrast is achieved; at shorter and long acquisition times, contrast is inadequate. Overall, the greater spin-density of cerebrospinal fluid means that is is able to return more signal than brain matter.

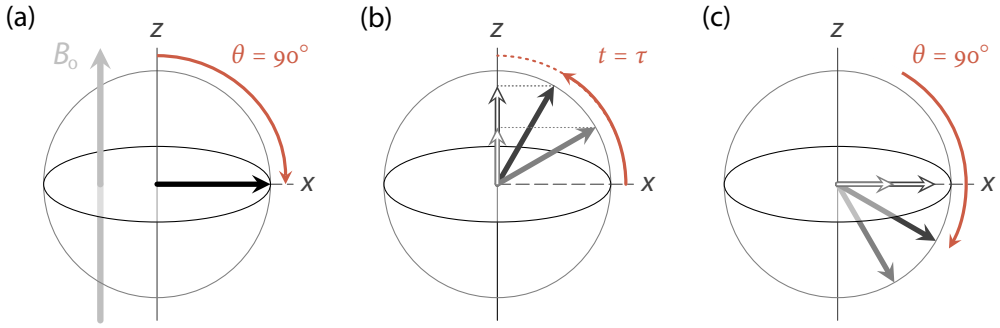

Figure 2.11: T_1-weighted imaging – (a) following the application of a 90° radiofrequency pulse, the net magnetisation vector is fully in the transverse plane; (b) spin packets in tissues with a short T_1 recover more swiftly than their counterparts in tissues with a long T_1. At $t = \tau$, the longitudinal component of their magnetisation vectors will have recovered to a greater extent; (c) in order to be detected, the longitudinal components of the vectors must be tipped into the transverse plane by a second 90° radiofrequency pulse. The time period τ is a determinant of tissue contrast.

number of voxels in the region are summed and a volume derived. To perform a region of interest (ROI) analysis well, the software package does not need to be sophisticated but the operator's knowledge of neuroanatomy should be. The pro's and con's of this approach are linked; investigators are able to draw on their experience to gauge the boundaries of a structure, but with that judgement comes subjectivity. Estimates of the reliability of the measurement within and between investigators are therefore important, but these values are influenced by the complexity of the ROI. More recently, ROI studies have made use of standardised imaging atlases in which key anatomical areas have been defined. In applying these regions, the subject's scan must be normalised to the brain template or the ROI morphed to the individuals image.

2.3.2 *Semi-automated techniques*

THRESHOLDING

When viewed on a computer screen, images are typically presented in grey-scale. Since grey matter is of intermediate intensity between white matter and CSF, it can be delineated by setting upper and lower intensity thresholds. Such thresholds may be set manually on each image slice, which results in a bounding box that encapsulates the grey matter. Additional editing may be required to remove extraneous areas. The sum of the voxels that lie between these threshold values is the grey matter volume; those beneath the lower summate to the CSF volume and those above the upper to the white matter volume. Thresholding is effectively a large scale, semi-automated ROI analysis and so open to subjectivity, though reliabilities are usually very good.

An important limitation of this technique is the loss of intensity information along the data path. At the point of encoding, voxels are 16-bit which gives 2^{16} intensity values (65,536). A standard monitor presents 8-bits, giving 2^8 shades (256). The human eye, however, can probably discern about 85 shades of grey. Automated techniques can scrutinise the intensity profile of the each voxel at its original resolution, potentially offering a more powerful analysis but not resolving the delineation of specific anatomical structures.

Intensities could be rendered in True-colour, but such a strategy brings its own problems, not least of which is the standardisation of the palette.

2.3.3 Automated techniques

VOXEL-BASED MORPHOMETRY

In this fully automated technique, specific brain structures need not be nominated as the entire brain is surveyed for global and regional differences in tissue volumes. The voxel-by-voxel approach means that the amounts of grey matter, white matter and CSF are compared between subject groups for each individual voxel. Images pass though a number of preprocessing stages before the voxel-wise statistical analysis, performed using computer software packages such as statistical parametric mapping (SPM).

Normalisation When using voxel-based morphometry (VBM) to compare groups of subjects, the brain structures of one individual need to be in alignment with the corresponding structures of the other subjects; voxel-by-voxel should be like-with-like. Clearly this will not be the case with the raw images as the size and shape of the brain differs considerably between individuals. What is required then, is that each image occupies a standard space, that each brain structure generally occupies the same co-ordinates in this space, and that these co-ordinates have some anatomical meaning. The normalisation process aims to achieve this.

- *Templates:* The ICBM152, an average of 152 normal MRI scans created by the Montreal Neurological Institute (MNI), is the current standard template for image analysis; a common alternative is to generate a study-specific template.
- *Transformations:* first, a 12 parameter linear affine transformation is applied (translation, rotation, scaling and skew in the x, y and z axes); second, a non-linear deformation process finalises the matching of the image to the template. Transformed images are said to be in *standard space*.
- *Co-ordinates:* the MNI standard space approximates to the Talairach stereotactic co-ordinate system, but the matching is not exact. Although conversion algorithms exist, co-ordinates should be cross-referenced to an appropriate atlas and interpretation of the results guided by neuroanatomical knowledge.

Segmentation Individual images are divided by tissue class, typically into three compartments – grey matter, white matter and CSF. The result for each subject is three discrete 3D-images in standard space; one for each tissue compartment. Segmentation is achieved by examining the *intensity* of each voxel, matching its characteristics to the established profiles of each tissue class. The chance of allocating a voxel to a particular tissue class is adjusted according its location in standard space using *a priori probability images*, as well as considering the classification of its *neighbours*.

Modulation Transforming an image in the way described approximates its volume to that of standard space. Early VBM studies would therefore discuss tissue densities or concentration differences rather than volumes. Addressing this problem led to the development of *optimized VBM*, with subsequent incorporation into the algorithms of recent versions of SPM (SPM8). Selecting *'normalisation with modulation'* retains the transformation parameters and applies them to the individual segmented standard space images, weighting the 'density' of the tissue in each voxel by the deformation it underwent. This is often described as multiplication by Jacobian determinants. When the transformed voxels are compared, intensity differences can be considered to reflect changes in volume.

The stages of normalisation, segmentation and modulation are described as individual processes but in practice they are launched by a single SPM script and cycled through until the criteria are met.

Smoothing The final stage of preprocessing is spatial smoothing, in which the segmented images are convolved with an isotropic Gaussian kernel. In essence, each voxel becomes the weighted average of itself and its surrounding voxels. This process reduces the small scale differences between each subject, corrects for inaccuracies in normalisation, improves the signal-to-noise ratio and renders the data more normally distributed. Gaussian distributed data is a requirement for the parametric statistics of SPM to be valid. The upshot is an improved chance of detecting a difference when multiple parametric statistical comparisons are made. However, spatial resolution is dramatically reduced and the choice of kernel size can have a marked effect on the results. Most commonly the filter size matches the expected effect size, equating to a kernel of full-width half-maximum (FWHM) between 8 and 14 mm.

Statistical analysis In a typical experiment, the smoothed images of one group of subjects are compared to another, with the results expressed as a map of voxel intensities which represent the volume of the tissue in question. Regional volume differences are determined by the application of t or F contrast conditions, ranked by cluster size and degree of significance, and depicted in the *glass brain* view. The standard threshold for a significant difference for each measurement is set at $p < 0.05$, but as millions of t-tests are performed the problem of *false positive* results is sizeable. The conservative technique of Bonferroni correction is generally considered excessively strict and probably inappropriate, given that it assumes each measurement is entirely independent of the others. The intensity of a voxel, however, is not independent of its neighbours – recall that this characteristic was used to aid segmentation. Smoothing the images improves the predictability of these voxel intensity correlations and allows the more lenient *Gaussian Random Field Theory* to be used in calculating the corrected p values. It is commonplace to perform a family-wise error correction.

SIENA ALGORITHM

The SIENA algorithm (structural image evaluation, using normalisation, of atrophy) is a fully automated analysis tool from the FMRIB group, permitting the longitudinal estimation of changes in brain structure – atrophy or loss of volume in particular. Two structural images of the head of a single subject, taken at different time points, are submitted to the program; the output is an estimate of percentage brain volume change (PBVC) and an image depicting the change. To achieve this, SIENA segments brain from non-brain in each image using the brain extraction tool (BET) in FSL, estimating the external surface of the skull in each case. The two brain images are registered using FLIRT, a linear registration tool in which the skull images are applied to constrain scaling and skew, correcting for changes in imaging geometry over time. Using the registered brain images, internal and external brain surface points are determined and the surface motion estimated on the basis of these points. The PBVC is estimated from the mean perpendicular edge motion across the entire brain surface. Accuracy of the technique is approximately 0.2% brain volume change error.

With VBM techniques, volumes are derived by counting the number of voxels allocated to each tissue class following segmentation; estimates rely on the classification being correct and consistent. The SIENA algorithm calculates volumes by determining the edges of tissues, scrutinising intensity gradients at the subvoxel level to derive surface points. Within a given tissue class, changes in intensity are small and gradients shallow but between classes the gradient will be steep. Encountering a sharp change in intensity values within or between voxels leads SIENA to denote the presence of a tissue boundary. Specifying a two-compartment model – brain and CSF – robustly and accurately detects tangible changes in the volume of the brain, relatively independent of interscan fluctuations in voxel intensity that can hinder tissue classification.

2.4 RELAXOMETRY

In T_1-weighted imaging, contrast is relative. This suffices for most situations but in some circumstances it may be desirable to quantify the actual T_1 times of the tissues under investigation. If signal is acquired from a sample at various points in the relaxation process and the intensities charted as a function of time, the rate of longitudinal relaxation may be determined. T_1 times can be accurately measured in this way using the *inversion recovery* technique. Here, a 180° pulse inverts the longitudinal component of the net magnetisation vector, after which it recovers to its equilibrium position passing though a null en route. The extent of the recovery is sampled by the application of a 90° pulse at selected time points. Only a single 90° pulse is permitted after an inversion – the sample must then be allowed to relax fully before the process is repeated with a new acquisition time. Several runs are performed over a range of sampling times, with a plot of signal intensity against the TR allowing the T_1 to be derived.

The inversion recovery technique is inefficient as equilibrium must be restored for the collection of each data point. As full relaxation takes three to four times the T_1 of the sample, a substantial amount of time can be spent acquiring the necessary data – multiply this by the number of voxels sampled and scan durations become

prohibitive if anything other than the crudest resolution is desired. The problem has been overcome by the development of T_1-reordering sequences.

QUANTITATIVE T_1 MAPPING

Consider a sample divided into four voxels (*A*, *B*, *C* and *D*), each containing tissue whose T_1 needs to be determined. If data is acquired at four time points for each voxel in turn, and equilibrium restored by leaving a gap of four-fold T_1 between inversions, the total scan duration will be 64 times the longest T_1 in the sample. Efficiency is increased by applying the inversion pulse to all four voxels simultaneously, but subjecting each voxel to the 90° sampling pulse at different times. Starting in order, scant relaxation will have occurred when voxel *A* is sampled but by the time the fourth 90° pulse is applied, the tissues in voxel *D* will be near-fully relaxed. On the next run the acquisition begins with voxel *B*, then progressing in order so that this time it is voxel *A* that is near-fully relaxed. Once four runs have been completed, data at the necessary times points will have been acquired from all voxels – the data is then rearranged, plotting the signals from each voxel as a function of the time between the 180° and 90° pulses rather than the order in which they were acquired. Scaling up the complexity in terms of sampling times, voxels and slices, high resolution images may be constructed in which voxel intensity denotes actual T_1 time – a T_1 map.

2.5 FUNCTIONAL IMAGING

Using MRI, inferences can be made about changes in brain activity, often in the context of a presented stimulus or whilst a task is performed. The most commonly used form of fMRI relies on the association between metabolic demand, local blood flow and oxygen consumption, the oxygenation level of blood influencing the relaxation behaviour of tissue water and so signal strength. The contrast in signal strength that arises from this relationship is referred to as blood oxygen level dependent, hence the term BOLD fMRI. As such functional imaging indirectly assesses brain activity, the physiological basis of BOLD contrast will be described before moving on to the analysis process.

2.5.1 Brain activity and blood flow

Blood is delivered throughout the body in a pulsatile manner, reaching the cerebrum through the bilateral carotid and vertebral arteries. Descending the arterial tree, pulsatility is smoothed out by the elastic walls of the vessels so that blood flow is relatively steady at the capillary level. Here, nutrients and metabolites are exchanged across the blood brain barrier and oxygen is absorbed. Venous blood therefore has a proportion of deoxyhaemoglobin, in contrast to the fully saturated arterial blood.

NEUROVASCULAR COUPLING

When neurones are transmitting signals their metabolic activity increases and their oxygen requirements rise; local blood flow follows suit, a phenomenon known as neurovascular coupling. Regional increases in blood flow develop slowly compared to neuronal activity and resolve more gradually still (Blamire et al., 1992), being described by the haemodynamic response function (HRF) depicted in figure 2.12 on page 42. The mechanisms linking neuronal activity to such increases in blood flow are incompletely understood, with theories variously focussing on oxygen consumption, energy demands and synaptic processes as the principal drives. Still the topic of debate, a consensus view of neurovascular coupling is emerging that links blood flow to synaptic activity more strongly than to the energy requirements of the cell.

The energy requirements of a signalling neurone are largely directed to restoring ion concentrations after postsynaptic depolarisation (Attwell and Iadecola, 2002). In primates, increased BOLD contrast more closely correlates with local field potentials than multi-unit activity (Logothetis, 2002). Local field potentials are thought to reflect the summation of postsynaptic potentials and so the input to a neuronal population; multi-unit activity most likely reflects the outgoing action potentials. The BOLD contrast, therefore, may be a composite measure of the input and intrinsic processing of a neuronal population rather than that population's output. The dominant factors under-pinning the BOLD signal change may not be the energy consuming ones.

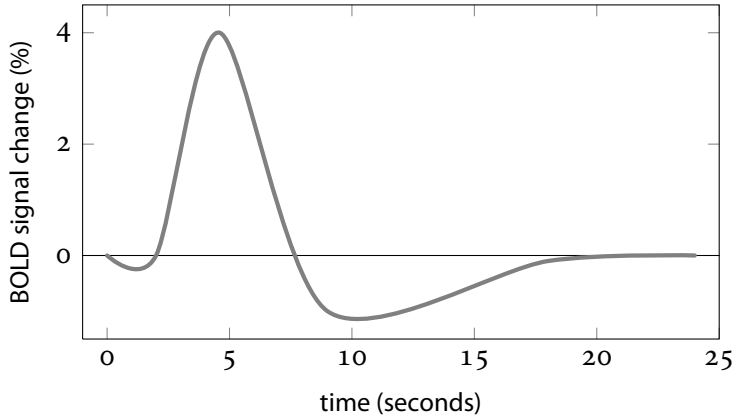

Figure 2.12: Depiction of the haemodynamic response function.

Classical neurotransmission involves the release of effector molecules from the presynpatic terminal which, on binding to postsynaptic receptors, trigger depolarisation and so signal conveyance. Many neurotransmitters are vasoactive and so are causally implicated in neurovascular coupling. Glutamate, an excitatory neurotransmitter, has received much attention, with a feed-forward system of controlling blood flow proposed (Attwell and Iadecola, 2002). On binding neuronal NMDA receptors, glutamate causes an influx of calcium which activates nitric oxide synthase, the product of which diffuses out of the cell to relax arteriolar smooth muscles and so increase local blood flow. Glutamate-triggered intracellular cascades through phospholipase A2 (PLA2) and arachidonic acid (AA) pathways in astrocytes increase concentrations of the vasodilator cyclo-oxygenase (COX) (Zonta and Carmignoto, 2003).

SUPERABUNDANT PERFUSION

In terms of magnitude, the increase in regional cerebral blood flow is not tightly coupled to the increase in cerebral oxygen requirements, with perfusion outstripping demand. The looseness of the coupling is paramount to BOLD fMRI. Although more oxygen is extracted into the tissues, neuronal activation results in a surplus of oxyhaemoglobin in the local capillary bed such that the proportion of deoxyhaemoglobin in the venous blood decreases. The oxygenation status of haemoglobin influences its magnetic properties, in turn altering its effects on the relaxation times of protons. Transverse decay is particularly susceptible in this regard, so functional imaging sequences are usually $T_2^\star$-weighted.

2.5.2 BOLD contrast

Oxyhaemoglobin is diamagnetic and has little effect on the relaxation rates of neighbouring spins; deoxyhaemoglobin is paramagnetic and its effects are marked. Paramagnetic substances induce dephasing and shorten the $T_2^\star$ of water, decreasing the strength of the signal when they are present. The decrease in the proportion of deoxyhaemoglobin that occurs with neuronal activation diminishes this effect, lengthening the $T_2^\star$ and increasing the signal intensity. This intensity change is the basis of contrast in BOLD fMRI, the increased signal of the active state being compared with the decreased signal either at rest, or in a less demanding condition. The magnitude of the signal change is dependent on many factors, including but not limited to: subject's age, blood pressure and vascular structure; magnetic field strength, echo time and voxel size; task characteristics, difficulty and duration. Overall, the percentage change in signal rarely enters double figures.

UTILISING THE CONTRAST

The BOLD contrast is qualitative and because of its complex basis, there are limits to what can be said about the actual levels of activation between subjects, across sessions and to some extent within scans. The profile of the HRF means that the maximal signal

intensity change will always be offset from the neuronal activation that triggered it, though the offset and profile are considered to be sufficiently predictable that they may be modelled during the analysis of images. Anatomical, physiological and medical factors may, however, affect the characteristics of the haemodynamic response. The transient nature of the HRF, and so the BOLD contrast, limits the range of experiments suited to fMRI.

SIGNAL CHANGE

The relative nature of the BOLD contrast means that signal change is paramount, whilst statements about absolute levels of brain activity are inappropriate. Changes in BOLD signal intensity that occur after the presentation of a stimulus, for example, can of course be quantified but the derived values are necessarily described with respect to a specified or defined condition. Conditions such as neutral stimuli or periods in which the subject is instructed to rest are commonly used. Signal intensities in excess of the specified baseline are termed *activations*, whilst reductions are described as *deactivations*.

Given the flow of events from neuronal signalling to increased blood flow and so greater signal intensity on fMRI, it makes intuitive sense to describe the contrast change as an activation. The notion that deactivations reflect a reduction in neuronal firing is conceptually more challenging and in terms of neurovascular physiology, incompletely established. The significance of BOLD deactivations will be considered in greater detail later in this thesis.

2.5.3 Image acquisition

In order to detect BOLD contrast, a fast sequence sensitive to changes in $T_2^\star$ relaxation is required. Echo planar imaging (EPI) is most commonly used, with which complete slices can be be acquired swiftly and whole brains imaged in seconds. Images acquired using EPI sequences are prone to susceptibility artefacts which manifest as regions of signal dropout. Magnetic field gradients are generated when tissues or substances with different magnetic susceptibilities are situated close together and these gradients

cause distortions which give rise to the image artefacts. The orientation and nature of the boundary determines the distortion, with air-tissue regions being most affected, particularly the frontal and paranasal sinuses. Signal from orbitofrontal regions especially may be absent or warped. Such artefacts are generally more marked at higher field strengths, offsetting to some degree the gains in BOLD contrast sensitivity that also come with more powerful magnet systems.

2.5.4 Image analysis

The data acquired during an fMRI session can be analysed in numerous ways, with several different sorts of output objectives. Frequently, the goal is to generate a statistical parametric map of voxel resolution, from which regional increases and decreases in BOLD contrast can be discerned. In creating such maps, the time series of a subject's image are commonly processed through realignment, motion correction, transformation into standard-space followed by smoothing. A study specific design matrix specifying the task parameters provides the framework in which the General Linear Model (GLM) is applied in first and second level analyses. Activations and deactivations in BOLD signal are calculated by statistical inference methods using Gaussian random field theory.

PREPROCESSING

Images must be processed before statistical analysis can begin. Software packages such as SPM and FSL can be used throughout, but it is important that a consistent approach is adopted. The first stage of any fMRI analysis is to ensure that the problem of T_1 saturation has been addressed. Echo planar image intensity takes several seconds to stabilise so a 'run in period' is required. This can be achieved by deliberately acquiring a number of dummy scans before data collection begins in earnest, or simply excluding the first few images from the time series.

Realignment Movement of a subject's head is a frequent occurrence during functional imaging, due to the long scan times and motor responses required. This is

generally minimised by the judicious use of head restraints, but even then needs addressing in the first stages of analysis. Realignment of the images typically involves taking the first scan dynamic and adjusting each subsequent image in the time series so that they match its position. A mean image and a log file of the realignment are generated for use in subsequent analysis stages.

Spatial normalisation Akin to the stage in VBM (detailed in §2.3.3 on page 36), the principal difference is the choice of templates to which the EPI images of the subject may be normalised. In addition to standard T_1-weighted templates, EPI equivalents are available to which the EPI data for subjects in a study can be normalised directly and swiftly. A degree of caution must be advised – as signal dropout is sensitive to field strength, the quality of normalisation may be compromised in studies using stronger or weaker magnet systems than the one used to generate the template. Alternatively, individual T_1-weighted images may be normalised to the ICBM152 template, yielding a subject-specific transformation matrix; if the EPI data is in coregistration with the structural scans, the transformation matrix may be applied to complete the normalisation to standard-space.

The EPI template supplied with SPM8 is the smoothed, segmented, normalised average of the mean fMRI images of 13 subjects, acquired on a 2T machine.

Smoothing The rationale for smoothing is similar to the situation for VBM. Inter-subject variability is reduced, SNR is increased and statistical requirements are met. It is generally the case that kernel sizes are smaller, tending toward 8 mm.

STATISTICAL ANALYSIS

In fMRI studies involving the presentation of stimuli or the performance of tasks, analysis aims to establish whether or not fluctuations in BOLD signal intensity are related to the experimental conditions applied. Consider a simple blocked design study in which a group of subjects view either a flashing checkerboard or a fixation cross, presentations lasting 20 seconds and alternating over time. It could reasonably be envisaged that neural activity would increase when the visually intense stimulus was presented, leading to the hypothesis that the BOLD signal would be greater during

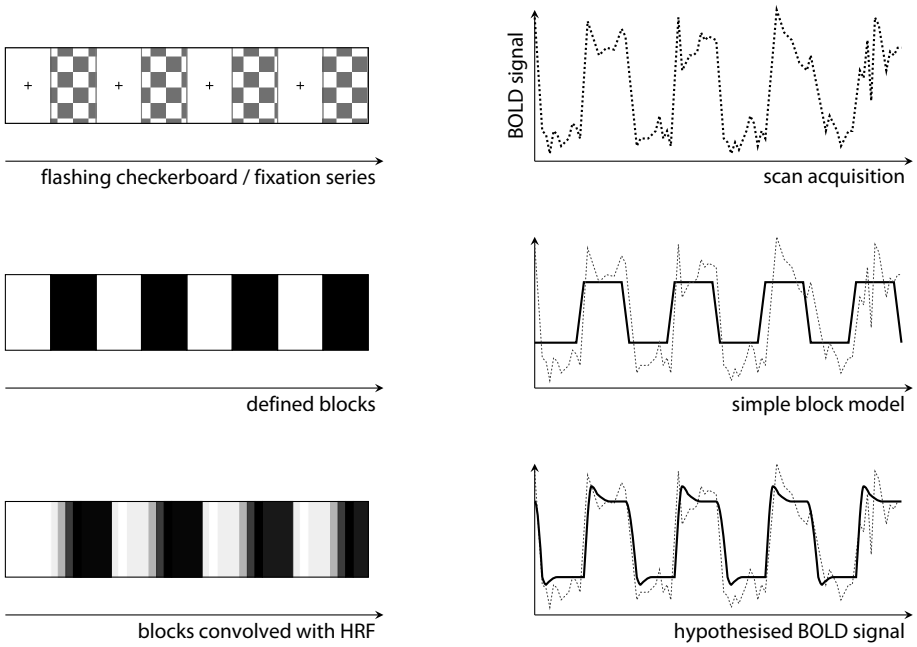

Figure 2.13: Convolution model of the BOLD response for a simple blocked task.

such blocks compared to the ones in which the fixation cross appeared. Two stages of analysis are required: the description and modelling of events (figure 2.13) followed by the comparison of derived conditions.

First-level analysis Information about the onset and duration of each block is submitted to a model which is then applied to the preprocessed EPI time series. Neuronal activity should closely match the stimuli but given the nature of the haemodynamic response, BOLD signal change will be offset. This matter is addressed by convolving the specified design with the HRF, the result of which is a hypothesised pattern of BOLD signal for the experiment conducted. A modified *t*-test is applied to every voxel in each image of the time series, individually for all subjects studies, examining how closely its intensity correlates with the hypothesised BOLD signal. The result is a *t*-map image for each subject, each voxel in the map having an associated uncorrected *p* value. The conditions specified in the model applied are labelled and a contrast-vector defined, these first-level contrasts being suitable for submission to higher level analyses.

In this example, a model-driven approach would be appropriate. Other methods can be applied to the analysis of fMRI data, including model-free analyses which make no assumptions about the observed signal.

Second-level analysis In many respects, data emerging from the first-level analysis is handled in the same way as any other empirical observation made on a subject; the peculiarities arise from the subtle nature of the signal change combined with the sheer volume of the data and the number of comparisons that must be made. For studies involving numerous subjects, consideration must be given to how data from individuals will be combined. It is now common practice to perform a *random-effects analysis*, accounting for condition-to-condition variations within-subjects and between-subjects, thus permitting inferences to be made about population effects. The alternative *fixed-effects analysis* does not take the inter-subject variability into account and with small groups, it is prone to bias if strong areas of signal change occur in individuals. Contrasts compiled in either manner can be analysed using statistics such as *t*-tests, analysis of variance or correlations – all based on the GLM.

Statistical inference Within the GLM, responses are assumed to have a linear relationship to the stimulus or task intensity. Statistical scores derived from these analyses indicate the degree of matching between the signal intensity of a voxel and that predicted in the hypothesised model. This matching can be gauged by testing one's hypothesis against the null hypothesis, with the probability of obtaining the experimental result by chance denoted by the *p* value, itself an indicator of the reliability of the conclusion. Voxels are said to show activation only if the statistical score and the *p* value cross a specified threshold. Active voxels fall into clusters; the expected number of clusters, and voxels within a cluster (k), can be calculated using Gaussian random field theory, accounting for the effects of spatial smoothing. Comparing the observed and expected clusters allows statements to be made about the significance of the findings. The analysis of fMRI data involves multiple comparisons, the effects of which must be controlled. As with voxel-based morphometry (§2.3.3; text on page 38), Bonferonni correction is considered too harsh and largely inappropriate. Family-wise error correction is commonly adopted, though less conservative strategies such as false detection rate corrections may be applied. Regardless, the technique and threshold should be stipulated *a priori*.

The null hypothesis in such a setting would state that no relationship exists between the voxel intensity observed and the presence of the stimulus or the performance of a task.

2.6 MAGNETIC RESONANCE SPECTROSCOPY

As the principles and practice of MRI are derived from those of nuclear magnetic resonance spectroscopy, this section does not present a new set of basic concepts, simply the process of analysing the signal on the basis of subtle differences in resonance frequencies of spins. This introduction is restricted to the most rudimentary form of MRS: the acquisition of data from the free induction decay. Here, the basic premise is that within the MRS signal, spins have discernibly different frequencies which are specific to certain compounds and whose signal-magnitude reflects the concentration of the substance that gave rise to the signal. The nature of MRS is outlined using examples from proton spectroscopy, later moving to the basics of multinuclear work.

MRI can actually be considered as a special form of MRS in which the proton singlet from water is isolated and manipulated.

2.6.1 *Free induction decay*

The FID has previously been presented as an oscillating signal of mixed frequencies whose magnitude diminishes over time, decaying by the function T_2^*. In the simulated example provided (figure 2.6 on page 26), Fourier transformation would yield a spectral singlet of a height and width respectively determined by the amplitude and decay of the time-domain FID. If an FID were to be derived from a sample containing spins with distinct Larmor frequencies, numerous peaks would be apparent after transformation (figure 2.14 on page 50). The profile of peaks is the magnetic resonance spectra of the sample, the area under each peak being the concentration of specific spins.

2.6.2 *Resonance frequencies*

The Larmor frequency of a spin is directly proportional to the magnitude of the applied external magnetic field, but spins are not exposed to B_0 only, nor to that field in its entirety. Nuclei with spin – even simple ones such as the proton of hydrogen – have electron shells which possess both charge and movement, so generating their own magnetic moments. The magnetic field experienced by a nucleus during magnetic resonance investigations must therefore include that induced by its electrons. The

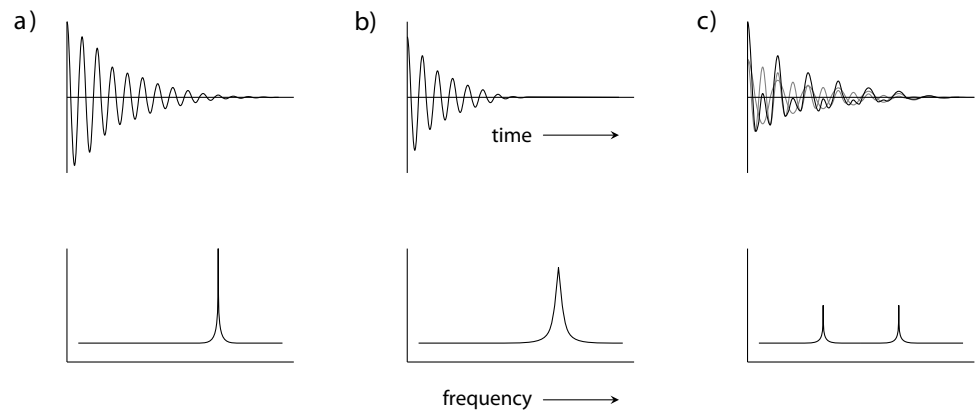

Figure 2.14: Fourier transformation of the free induction decay, a mathematical process by which the function of time is converted into the function of frequency – a) decay of a single nuclear species gives rise to one narrow peak; b) with a rapid decay of the signal the spectral singlet is wide but the integral of the peak, reflecting the concentration of spins, is constant; c) spins with different Larmor frequencies contribute to a more complex FID, resolving to two spectral peaks.

local environment and molecular bonding of a nucleus determines the behaviour of its electrons, and so the magnitude of their magnetic moments. The magnetic moments of an electron may effectively shield the nucleus, thus determining total field to which the nucleus is exposed when the B_0 field is applied. These influences manifest as a range of resonance frequencies for kindred spins in complex samples, a phenomenon termed *chemical shift*. Although the magnitude of the shift may be small, it is detectable and underpins much clinical MRS work. Unlike MRI, the relaxation properties of the spins are not the primary concern but can be of some importance.

SPECTRAL FORM

Within complex molecules, chemical shift for protons is largely determined by the geometry of their bonds to other atoms. For the metabolic compounds typically encountered *in vivo*, proton bonding configurations are sufficiently consistent and characteristic that the associated chemical shifts may be used to identify them, metabolites having a spectral 'signature' as it were. To capture such signatures the RF pulse must be sufficiently hard to excite spins across a range of frequencies, with the receive profile of the coil comparably broad. With these provisos in place, a simple pulse-acquire sequence with collection of the FID will often suffice.

The spectral signature of a metabolite emerges as a peak localised to a specific position relative to the 'on-resonance' signal of water. The size of each peak in the frequency spectrum is proportional to the amount of metabolite present – concentrations of compounds may therefore be derived by integrating the area under the peak at a specified resonance.

SPECTRAL ANALYSIS

The analysis of proton MRS spectra from tissues such as the brain can be a challenge. Whilst abundant compounds may be easily identified, those of a lesser concentration may be difficult to discern from noise. Further, some metabolites generate sufficiently similar chemical shifts that their peaks can barely be distinguished. There exist numerous techniques to extract, delineate and integrate the data from an FID, but these are beyond the scope of this introduction.

2.6.3 Calibration

The signal intensity – and so the area under a peak – is also a function of the tip angle induced by the RF pulse. Although maximum signal intensity arises with a 90° tip, whatever nutation is chosen its profile across the sample must be known if meaningful concentrations are to be derived. It is therefore standard practice to calibrate the pulse sequence at the outset of an experimental series.

For on-resonance hard pulses, tip angle is related to RF exposure and signal intensity is a sinusoidal function of the tip angle achieved. A series of pulse-acquire experiments in which the duration of the RF pulse is progressively increased will yield a range of signal intensities, as depicted in figure 2.15 on page 52. Whilst the maximum signal can be demonstrated empirically in this way, it is easier to identify the null signal from a 180° tip – halving the duration of that pulse will result in a 90° tip.

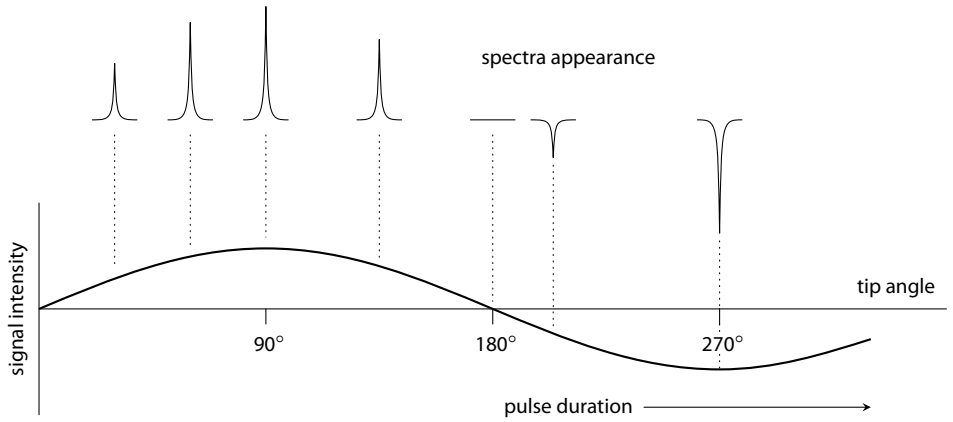

Figure 2.15: Pulse calibration. With hard pulses, increasing the energy delivered increases the tip angle induced. Signal intensity varies sinusoidally – spectra collected after various pulse durations will fit this pattern. The maximum signal represents a 90° tip, the null point is 180° after which the signal becomes negative (Replicated from lecture notes by James Keeler, University of Cambridge).

2.6.4 Quantification strategies

Remaining with the example of proton spectroscopy, the concentration of one metabolite relative to others in the spectra can be established by deriving the ratio of each to an easily recognisable and universally present metabolite such as N-acetylaspartate (NAA) or creatine. In principle, MRS may also enable the concentration to be measured in absolute terms; in practice this proves difficult – although the area under the peak is proportional to the metabolite concentration, other factors also affect the results.

REFERENCE COMPOUNDS

For absolute quantification, the signal acquired from the sample must be calibrated against one derived from a reference substance of known concentration. Suitable reference compounds may either be internal to the subject (a stable metabolite, for example) or external (a solution placed within the sampling volume of the coil). In either situation there will be differences between the sample and the reference compound which will have a bearing on the magnitude and quality of the spectra, independent of their respective concentrations. The position of the samples within the coil, the temperature of the calibration compound, differences in the relaxation properties of the various substances and many more factors require consideration if

For the studies conducted in this thesis, external references were the only option as lithium is not found naturally to an appreciable degree *in vivo*.

absolute quantification is to be achieved. Of these, the most pertinent to our thesis are the occurrence of partial saturation of the MR signal and the related effects of B_1 field inhomogeneities that characterise surface coils.

Other factors such as diffusion, MR visibility, nuclear Overhauser effects, differences in the localised sampling volume and T_2 losses have less of a bearing on simple pulse-acquire experiments.

PARTIAL SATURATION

If spins are not permitted to return to their original state between applied pulses, the longitudinal component of their net magnetisation vector will adopt a new steady-state equilibrium of diminished magnitude (equation 2.3 below). When a 90° pulse is applied to a spin packet that has not achieved full longitudinal relaxation, the resultant signal will be smaller than the original. This effect is called *partial saturation* and occurs if the pulse repetition time is less than three to four times the T_1 of the sample.

$$M_z = M_0 \frac{(1 - e^{-TR/T_1})sin\theta}{1 - cos\theta e^{-TR/T_1}} \tag{2.3}$$

If the sample and reference compound have different T_1 values, there exists the possibility that partial saturation may occur in one but not the other, or in both to a different degree. There are many reasons why differences in T_1 times should exist – the characteristics of the tissue and reference compound rarely match and if tissue pathology is present, its distribution may be uneven. If the magnitude of the partial saturation effect is known, the reduction in signal amplitude can be systematically corrected using equation 2.3, at least for simple pulse-acquire experiments. This, however, requires precise knowledge of the T_1 relaxation time for the sample and reference compound.

Such corrections are unnecessary if partial saturation is avoided – achieved by setting the TR to greater than at least three times the T_1 of the most slowly relaxing sample under investigation. With this approach, T_1 data is still required but its accuracy is less of a concern than with correction techniques, especially if estimates err on the side of caution. The duration of experiments may be greater, but so is one's certainty in the validity of the data.

Proton MRS studies of man often use volume coils, advantageous because of the even B_1 field they provide. In some situations – multinuclear MRS for example – surface coils may confer certain benefits, principally better signal-to-noise ratios (SNR). A standard pulse delivered by a surface coil generates an inhomogeneous B_1 field and so a range of tip angles will arise across the sample for a given excitation. Consequently, signal strength will be low in areas with a tip less than 90° and partial saturation a possibility in regions where spins are recovering from tips of greater magnitude. The field inhomogeneities of surface coils may be overcome by the application of adiabatic pulse sequences.

2.6.5 Determining T_1

In order for spectroscopic quantification to be valid, the relaxation times of the samples must be understood. For simple pulse-acquire experiments, knowledge of the T_1 suffices and T_2 times need not be considered. The T_1 time of a sample can be measured in several ways, most commonly using inversion-recovery or saturation-recovery methods.

Inversion-recovery The inversion recovery techniques applied in MRS are identical to those using the field of imaging (described in §2.4). Determining the T_1 time of a sample using inversion recovery is not time efficient. With multinuclear MRS, the experiments can be very lengthy as the longitudinal relaxation of some nuclear species is substantially longer than that of protons.

Saturation-recovery This technique allows T_1 times to be estimated swiftly, being more efficient in the acquisition of data early in the relaxation process. In essence, two or more 90° pulses are applied in succession with the FID signal acquired immediately after the final excitation. The magnitude of recovery of the longitudinal magnetisation is related to the interval between the pulses and it is the extent of this recovery that is detected after the second tip.

2.6.6 *Multinuclear* MRS

Magnetic resonance spectroscopy is not restricted to probing protons and of the numerous nuclei that can detected, several are suited to investigation *in vivo* (table 2.2 on page 56). It is a requirement that the spins have gyromagnetic ratios that, at clinical field strengths, equate to Larmor frequencies excitable by RF waves. Detection is simply a matter of retuning the scanner to the appropriate frequency; generating a useful signal is somewhat more challenging. The properties of the spins detectable with MRS dictate the SNR that can be achieved and thus the feasibility of *in vivo* studies in man. In terms of the spin, the major determinants of SNR are its sensitivity, relaxation properties and concentration, each of which will be considered in turn.

SENSITIVITY

Sensitivity is a measure of the number of spins detectable, usually expressed relative to that of protons. Recall that the magnetic moments of spins are anisotropically distributed and that the signal arises from a change in the proportions of parallel and antiparallel spins (§2.1.2; page 18). The MR sensitivity is related to the ratio of spins in the ground and excited states, together with their propensity to move from the former to the latter following the application of RF waves. Sensitivity thus increases with field-strength, though its relative value remains unchanged. For protons in the field strengths typical of clinical scanners, the asymmetry at equilibrium is of the order of a few spins per million and so the signal is derived from a tiny fraction of the whole. All of the isotopes commonly used in clinical multinuclear MRS investigations have low sensitivities, such that high field strength scanners are generally a requirement.

MRI and MRS can be described as low sensitivity techniques. This should not be confused with their sensitivity as diagnostic tools, which can be impressive.

RELAXATION

If the T_1 of a sample is short, spins may evade detection; if it is long, the duration of experiments may become prohibitive. As T_1 is proportional to field strength, scans lengthen as B_0 increases, offsetting the gains in sensitivity to an extent. Transverse relaxation determines the spectral profile; spins with long T_2 times yield narrow lines.

ISOTOPE	SPIN (I)	ABUNDANCE (%)	γ ($\times 10^7$)	SENSITIVITY
^{1}H	½	99.985	26.7510	1.00
^{7}Li	⅜	92.4	10.3964	0.29
^{13}C	½	1.10	6.7263	0.0159
^{23}Na	⅜	100	7.0761	0.0925
^{31}P	½	100	10.8289	0.0663

Table 2.2: Properties of various nuclear species that are amenable to detection with MRS. The gyromagnetic ratio (γ) is expressed in rad $T^{-1}s^{-1}$ (reproduced from Ramaprasad (2005)).

For nuclei which are not spin-half, relaxation may not fit a simple exponential decay. The nuclear quantum spin number I defines the number of energy states a nucleus can adopt (§2.1.2; page 18); four in the case of ⅜ spins. In such quadrupolar nuclei the z component of the net magnetisation vector can align along one of two axes, typically resulting in biexponential relaxation behaviour. These profiles must be characterised lest fast and slow components be confused.

CONCENTRATION

As the magnitude of the spectral peak is related to the number of spins in the sampled volume, higher concentrations are easier to discern from noise. It is generally the case with multinuclear MRS that spin concentration is not open to manipulation. Absolute concentrations are constrained by physiology often reduced to undetectable levels by the presence pathology. There are two obvious exceptions to this scenario. First, if the favourable isotope of an element has a low natural abundance, as with ^{13}C, its concentrations can be enriched by exogenous administration without altering physiological systems or total spin number. Second, if the substance is being administered anyway, ^{7}Li for example, concentrations can be maximised within safe limits.

3 FMRI TASK PREPARATION

In the psychological laboratory setting, researchers have innumerable tasks at their disposal; a proportion of these are suited to fMRI experimentation but almost all require modification prior to application. Specifically, fMRI tasks must be logistically possible in the scanner environment with stimulus presentations or task onsets predictably linked to the acquisition of images. With BOLD fMRI, the physiological basis of the contrast places constraints on the duration of the task and the frequency of stimulus presentation. When fMRI is combined with a pharmacological intervention, task brevity and repeatability often become important considerations. In anticipation of the fMRI study described presently, this chapter introduces the principal task and outlines the modifications made to ensure that it was fit for purpose. Two pilot studies were performed to this effect: one established the block parameters whilst the other gauged our adaptations. The methodological developments are the focus of this chapter, the pertinence of the task is considered later in this thesis.

3.1 NEUROPSYCHOLOGICAL TESTING

This thesis examines whether lithium attenuates the effects of methamphetamine, a stimulant which acts to increase synaptic dopamine concentrations. Dopamine modulates numerous brain functions including attention, working memory, drive and various aspects of emotional processing (Greengard, 2001a) and patients with bipolar disorder may have impairments across these domains. Sustained attention has been found to be disturbed in various phases of the illness. Continuous performance tasks (CPT) engage sustained attention and are known to be sensitive to the manipulation of dopaminergic systems (McTavish et al., 2001; Hearn et al., 2004) as well as being suited to functional imaging work (Coull et al., 1996; Lawrence et al., 2003). Building on local experience, the *Rapid Visual Information Processing* task (RVIP) was selected for use (see §3.2) and through collaboration, a blocked version suitable for BOLD fMRI was prepared.

Continuous performance tasks often involve the subject attending to a series of stimuli for several minutes. In partitioning tasks into a blocked format, their difficulty and/or nature may be fundamentally altered. Validation of the RVIP task in blocked format was therefore necessary. Before addressing this matter, the logistics of task presentation and performance rating require consideration.

3.1.1 Task presentation

When performing the RVIP task, subjects view numbers set against a plain background screen – black on white in most settings (see figure 3.1 on page 62). Sans serif letterforms in yellow or white against a blue background provide good visual contrast, with the advantage that after-image effects are negated. This format was used in all the experiments in this thesis, be they developmental, practice or proper.

Development and training In the RVIP task validation series and study training sessions, subjects performed the tasks on a laptop computer. Responses were recorded by a single keystroke using the index finger of the dominant hand, the subject seated a comfortable distance from the screen.

Laptop computer ERGO MICROLITE™ 12.1″ XGA LCD screen 1024 × 768 resolution.

fMRI presentation Images were back-projected onto a screen at the foot of the scanner bed and viewed through a front-silvered mirror angled at 45° to the supine subject. The arrangement was such that the arc subtended by the letterforms and the extent of the visual field occupied by the background matched those on the personal computer. Responses were recorded through a hand-held optical-fibre device, subjects using the thumb of the dominant hand for reasons of comfort.

Projector CANON XEED SX6; max resolution 1400 × 1050, contrast ratio 1000:1, uniformity 88%, 3500 lumens.

Software systems The RVIP task was prepared for presentation using proprietary software (E-prime® Psychology Software Tools, www.pstnet.com) on a personal computer running the Windows® XP operating system (Microsoft® Corporation). During fMRI conditions, each block was triggered by the scanner to ensure that the image acquisitions matched the task presentations, and so the specified analysis model.

3.1.2 Task performance

In the continuous performance tasks, subjects typically view sequential stimuli with the aim of responding in the affirmative when certain conditions are met. The time taken to respond is recorded and the appropriateness of the response determined by cross-reference to the stimulus order. From these values, the rates of correct and incorrect responses can be calculated, together with the performance indices derived from the principles of *Signal Detection Theory* (SDT; Grier, 1971) – see the textbox on page 60. According to SDT, decisions are based on the acquisition of information and the application of rules. If one focusses on acquisition, most targets are identified but false responses are likely; attending to the rules reduces errors but at the expense of target detection. A subject's strategy can be gleaned from the calculated parameters of *sensitivity index* (A') and *response bias* (B'').

3.2 RAPID VISUAL INFORMATION PROCESSING TASK

3.2.1 Task description

The RVIP task taxes both attention and memory, but the burden on memory is slight. The target strings are short and displayed on the screen whilst the task runs.

This simple continuous performance task requires a substantial degree of attention (Wesnes and Warburton, 1983a). Subjects view a series of single integers from the range 2 to 9 displayed in quick succession, typically 100 per minute. As these digits flow past, subjects attend to the order of presentation and respond if they spot one of a number of prespecified patterns. The target sequences span three digit presentations, being discretely grouped runs of odd or even integers of increasing numerical value. Suitable groupings are 246, 468, 357 and 579. Target strings are nested in a pseuo-random series of digits and appear several times per minute, the gap between target sequences varying so that subjects are unable to predict the occurrence of the next presentation. A subject's response is valid for up to three digit presentations inclusive of the last digit in the target sequence, with responses at other times deemed false (see figure 3.2 on page 62). Very short response latencies are typically excluded, deemed chance occurrences or preemptive strikes – a lower threshold of 125 ms is standard.

MEASURES OF TASK PERFORMANCE

In the complex field of performance assessment, the simplest measurements are often the most informative. The time taken to respond to a target stimulus (*response latency*) exemplifies this. Categorising a response is also straightforward: correct responses are *hits*; failures to respond are *misses*; responses in the absence of a target are *false alarms*. Matters are more complicated for the rates and patterns of response.

	Response present	*Response absent*
Target present	Hit	Miss
Target absent	False alarm	Correct rejection

ACCURACY & ERRORS

If a subject responded correctly to all sequences and incorrectly to none, they would return a result of 1.0 for the *fraction of correct responses* (h; equation 3.1). Such a score could also be achieved simply by pressing the button after every single digit – the lack of selectivity would be evidenced as a high *fraction of false responses* (f; equation 3.2). Clearly, h is of limited use in isolation and the interpretation needs to factor in the number of mistakes made; derived from SDT, A' and B'' serve this purpose.

$$h = \frac{\text{correct responses}}{\text{total number of target digits}} \tag{3.1}$$

$$f = \frac{\text{false alarms}}{\text{total number of non-target digits}} \tag{3.2}$$

SENSITIVITY INDEX (A')

The sensitivity index reflects the selectivity of a subject and is denoted by A' (equation 3.3). It shows the sensitivity to errors regardless of error tendency, and is calculated from the fraction of correct and false responses (range 0 to 1; poor to good).

$$A' = 0.5 + \frac{(h - f) + (h + f)^2}{4h(1 - f)} \tag{3.3}$$

RESPONSE BIAS (B'')

A' can be identical for different response patterns. For example, a cautious but accurate responder ($h = 0.6$; $f = 0.001$) and a 'trigger-happy' subject ($h = 0.8$; $f = 0.13$) would both have an A' of 0.9. Here, the response bias, B'' (equation 3.4), comes into play. Values of 0.992 and 0.171 are returned for our example subjects. Note that with perfect score ($h = 1$; $f = 0$), B'' is indeterminable as the denominator is zero.

$$B'' = \frac{(h - h^2) - (f - f^2)}{(h - h^2) + (f - f^2)} \tag{3.4}$$

The control task condition is similar in structure to the RVIP task condition but places fewer demands on attention. Here, a similar series of digits are presented and subjects respond when they spot a prespecified single target digit. The timings and target frequencies match those of the RVIP task condition. In the standard clinical laboratory RVIP task condition (Cambridge Neuropsychological Test Automated Battery, CANTAB), digits are presented every 600 ms for about seven minutes. Targets occur on average eight times per minute, separated by a variable gap of 8 to 15 digits. The control task condition lasts around two minutes and is usually performed after the RVIP task condition. Given the stimulus duration used in these tasks, responses are permissible within 1800 ms of the onset of the target presentation.

3.2.2 Task performance and the effects of methamphetamine

DETERMINING PERFORMANCE

Whilst subjects differ in their aptitude and performance, fluctuations in a given individual's response latency and accuracy are thought to reflect changes in their level of attention. Performance, and to some extent strategy, may be dictated by the construction of the RVIP task. Modulating the number of target sequences to attend to, the rate of digit presentation and the frequency of target or false-start sequences alters its difficulty and nature. In setting or altering these parameters, consideration must be given to the population studied as well as the envisaged effects of any intervention.

ANTICIPATED EFFECTS OF METHAMPHETAMINE

Task performance Following methamphetamine, subjects would be expected to react more swiftly and to be more attentive, but with the potential for an impairment in the inhibition of false responses – the response latency should shorten whilst h and f most likely rise, increasing A' but decreasing B'' scores. Given the anticipated increase in h, the version of the RVIP task employed had to be sufficiently taxing lest a ceiling effect be encountered. A baseline accuracy of 50–75% was considered suitable, permitting the detection of change without making the task too demoralising.

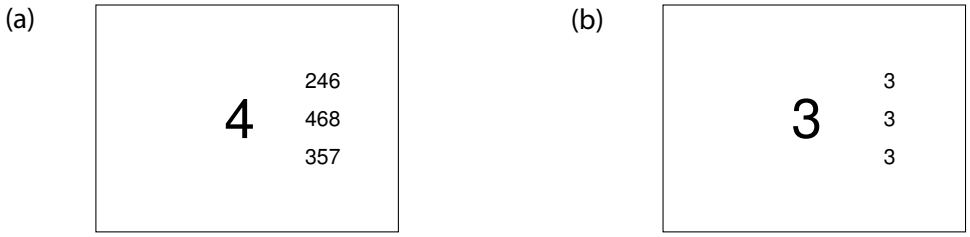

Figure 3.1: Presentation format of the RVIP task condition (a) and the control task condition (b). In both situations the central digit changes whilst the subject tries to spot the sequences on the right of the screen. For the control condition, the digit 3 is shown on multiple lines so that the visual field occupancy largely matches that of the RVIP task proper.

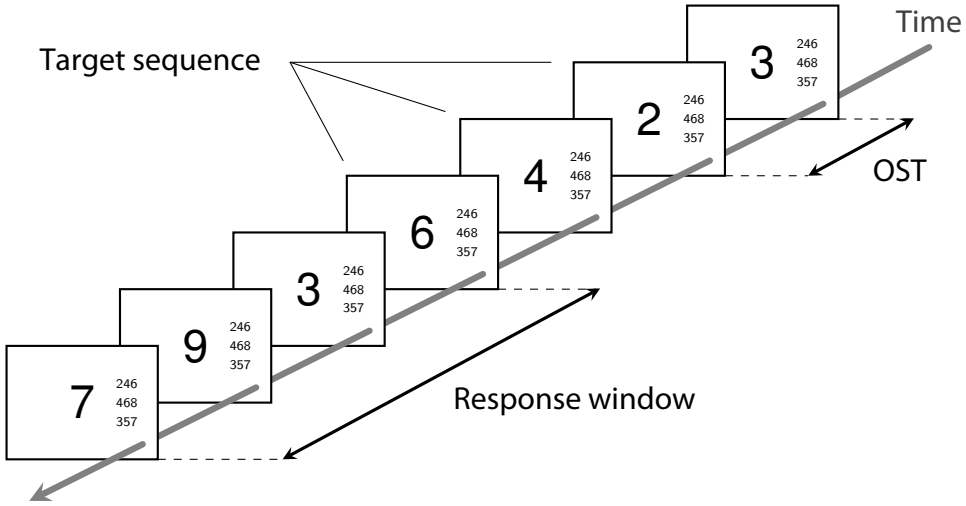

Figure 3.2: An excerpt from the sequence presentation for the RVIP task condition. Each digit is displayed for a specified period, *on screen time* (OST), before being replaced by the next digit. There is no interstimulus interval in the RVIP task. The run of digits depicted contains the target sequence 246. On spotting the sequence, subjects have a period equal to 3 × OST in which to respond.

Task format With an unbroken task in the absence of stimulant medication, a subject's performance would be expected to worsen over the run because their attention will most likely wane (assuming practice effects have been overcome). Hits, false responses and reaction times are usually averaged over the entire run, so this decline may not be described. In reporting that methamphetamine increases the hit rate, for example, reliance on averaged values leaves two potential patterns of effect unresolved: target detection rates may have genuinely risen or the deterioration over time may have been prevented (figure 3.3; page 64). In theory, the latter may go undetected in a blocked version of a task if average scores for the whole run are relied upon.

The principal issue with a blocked task is the pattern of deterioration in performance with time. If attention were to wane steadily over the entire run of blocks, the nuances of methamphetamine's effects are of no consequence. Should a subject's level of attention return to baseline at the start of each block, there is cause for concern; blocks may be too short to detect a pure 'prevention of the deterioration in attention' action of methamphetamine (see figure 3.4 on the following page). Alternating the RVIP task condition with the easier control task condition may permit a period of rest and foster such a recovery to baseline.

Existing empirical data enabled an exploration of this issue (Hearn et al., 2005). From this blinded cross-over study of methamphetamine and hydrocortisone, data from eight male subjects (mean age in years ± sd: 24.3 ± 7.5) was extracted and re-analysed. Each subject completed a CANTAB version of the RVIP task on two occasions, punctuated by a week in which they took placebo tablets daily; methamphetamine preceded the second session (0.15 $mgkg^{-1}$ i.v.), a placebo injection the first. As a standard version of the RVIP task was used, performance over time was investigated by dividing the data into seven periods of 60 seconds. Methamphetamine was found to increase the hit rate and A' scores over the entire task period, with a similar pattern for reductions in response latency time (figure 3.5 on the next page). On the basis of this finding, the effects of methamphetamine should be detectable using a blocked version of the RVIP task.

The help and support of Peter Gallagher, who made this data available for analysis, is gratefully acknowledged.

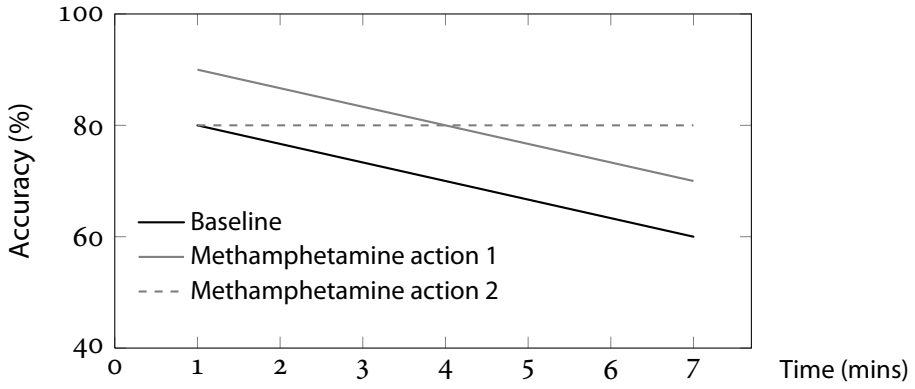

Figure 3.3: Simulation of a standard RVIP task during which performance wanes. The mean baseline accuracy is 70% and in this example, methamphetamine increases accuracy by 10%, either by elevating target detection (1) or reducing fatigue (2).

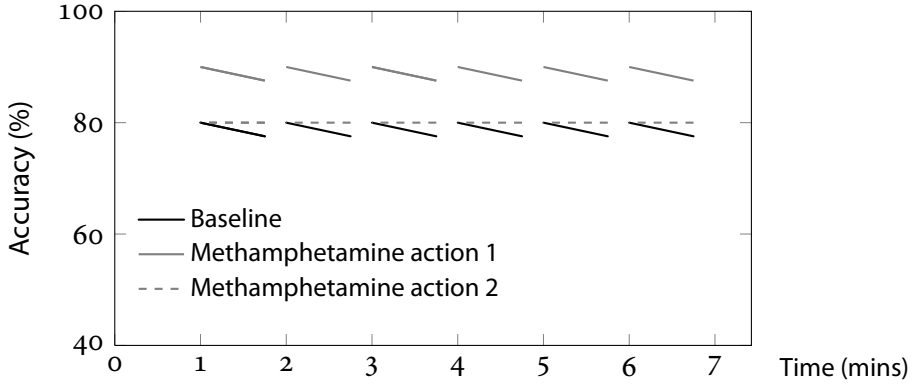

Figure 3.4: Simulated data modelling blocks of 42 seconds in which it is assumed that attention is refocused with each new block. In theory, the effects of methamphetamine would only be detected in a blocked RVIP if it were to demonstrate *action 1*.

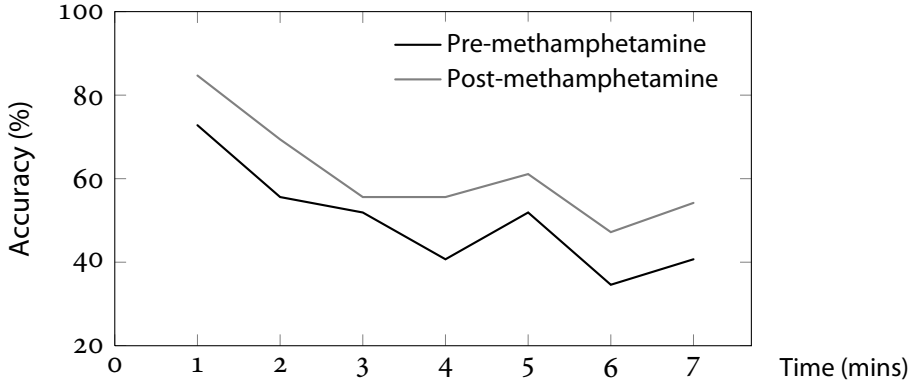

Figure 3.5: Empirically derived data from a standard RVIP task before and after methamphetamine, with accuracy scores determined for each minute of the task. The pattern of scores suggests that the postulated *action 1* predominates.

3.2.3 Adapting the RVIP task

The pilot studies examined two versions of the RVIP task: a standard one running without interruption and another comprised of shorter bursts – the *'continuous'* and *'blocked'* designs (RVIP-C and RVIP-B respectively). For reasons which will become apparent, each developmental version attracted an additional identifier, that of the duration of stimulus presentation. Thus, RVIP-C600 refers to a sedate, uninterrupted version in which the stimuli are on-screen for 600 ms, whilst the RVIP-B400 was pacier and in blocked format.

CONTINUOUS DESIGN

The index format – RVIP-C600 – comprised exposure to seven minutes of the RVIP task condition followed by two minutes of the control condition. Three target sequences were used in the RVIP task condition (246 · 468 · 357); a single digit (3) in the control condition. Digits were drawn from a programmed list of numbers, the order of presentation fixed by trial and identical for all subjects. On this list were 700 digits in pseudo-random order, with target sequences interspersed throughout. At the rate of presentation of 100 digits per minute (on-screen time 600 ms, no interstimulus interval), targets appeared at an average frequency of eight per minute. The interval between targets varied from 8 to 15 digits.

This design replicated the standard CANTAB version of the RVIP

Thanks are due to Matthew Kempton, who graciously divulged his method and lists.

BLOCKED DESIGN

The RVIP-B600 was based on the work of Kempton (2006), its content adapted to match our continuous design. Blocks lasted 40 seconds, separated by an interval of two seconds during which instructions appeared indicating the nature of the task to follow. The blocks were presented in pseuo-random order, no more than two blocks of the same type appearing consecutively. For each condition, six blocks were contrived by partitioning RVIP-C600 digit-list (without repetition or overlap). Comparing the RVIP-C600 with the RVIP-B600, the total duration of the RVIP task condition was shorter, and the control condition longer, in the blocked version.

Kempton used four targets in the RVIP condition, zero as the control target and included a 'fixation-cross' block. In this thesis, three RVIP task targets were used (emphasising attention by lessening the memory load), '3' replaced zero (it being too easily recognised) and the 'fixation-only' task was omitted.

3.2.4 Pilot study I — Continuous versus blocked

METHODS

Subjects Five subjects were recruited – friends and colleagues who had not previously undergone neuropsychological testing. All were healthy right-handed men (mean age in years ± sd: 31 ± 3.1) with a high level of education (mean duration in years ± sd: 20 ± 1) and no history of psychiatric illness.

Task delivery Subjects completed the tasks in a quiet room during the morning, the RVIP-C600 preceding the RVIP-B600. An interval of 30 minutes separated the sessions, during which time other tasks in development were completed.

Analysis Hit rates, false alarm rates, response latencies, A' and B'' were derived from the raw E-prime® data using spreadsheet functions, analysed using SPSS (*v.*17, SPSS inc., USA). Responses occurring less than 125 ms after stimulus presentation were excluded, these representing either guesses or chance occurrences. Given the likely distribution of the data, median response latencies were analysed. All measured and derived variables were treated as continuous, with group values reported as the mean ± sd. The small sample size favoured the use of nonparametric statistical tests; the Mann-Whitney *U* test was applied as the observations were considered unpaired.

RESULTS (RVIP-600)

Continuous versus blocked design Compared to the continuous design, the hit rate appeared higher in the blocked version of the RVIP task condition but the difference did not reach significance; no difference was observed when the different designs of control task condition were contrasted (table 3.1, page 67). False alarm rates were low and did not differ according to design. Sensitivity index scores demonstrated the same pattern of results as the hit rates, not differing on formal comparison. As some subjects committed no false alarms, the group mean B'' could not be calculated. Subjects responded more swiftly in the blocked versions of the tasks, significant at trend level for the RVIP task condition but not the control task condition.

	TASK PERFORMANCE		MANN-WHITNEY *U*		
	RVIP-C600	RVIP-B600	ranks	Z	*p*
RVIP TASK CONDITION					
Hit rate (%)	77 ± 19	94 ± 10	10	− 1.51	.131
False alarm rate (%)	0.62 ± 0.9	0.65 ± 0.7	10	− .108	.914
Sensitivity index (A')	0.95 ± 0.04	0.98 ± 0.02	10	− 1.52	.129
Median response latency (ms)	362 ± 22	336 ± 26	10	− 1.78	.076
CONTROL CONDITION					
Hit rate (%)	99 ± 3	98 ± 2	10	− .837	.403
False alarm rate (%)	0.22 ± 0.3	0.11 ± 0.2	10	− .904	.366
Sensitivity index (A')	0.99 ± 0.01	0.99 ± 0.00	10	− .837	.403
Median response latency (ms)	465 ± 38	489 ± 17	10	− .943	.421

Table 3.1: Continuous versus blocked version of the RVIP (stimulus duration 600 ms, n = 5), in which the rate of presentation of digits was 100 per minute. Group values are reported as the mean ± sd. Statistical scores and significance levels refer to the comparison of the continuous and blocked versions for each measure. The statistical statements for the comparison of the RVIP task and control task conditions are presented in the body of the text.

RVIP condition versus control condition The hit rate was higher in the control task condition compared to the RVIP task condition for the continuous version (77 ± 19 versus 99 ± 3; 10 ranks, Z −2.12, $p = 0.034$) but not the blocked version (94 ± 10 versus 98 ± 2; 10 ranks, Z −0.11, $p = 0.910$). False alarm rates did not differ between the conditions in either the continuous or blocked versions. Subjects took longer to respond in the control task condition during the continuous version (control task versus RVIP task, median response latency: 465 ± 38 versus 362 ± 22; 10 ranks, Z −2.61, $p = 0.009$) and the blocked version (control task versus RVIP task, median response latency: 489 ± 17 versus 336 ± 26; 10 ranks, Z −2.62, $p = 0.009$).

INTERPRETATION

Comparison of tasks As expected, the control task was easier; in this scenario the swifter responses in the RVIP task condition reflect the anticipation of sequence completion rather than difficulty. Performance was superior on the blocked design compared to the continuous design of the RVIP task.

Overall performance Subjects performed extremely well on the RVIP-B600 task, with accuracies close to the ceiling for that level of difficulty. Thus, in order to detect the proposed effects of methamphetamine the task needed to be more taxing.

Within-task performance In restructuring the RVIP task, the major concern was that its nature and/or difficulty could be altered. Continuous tasks may be more sensitive to the effects of a fixed strategy, fatigue and wandering attention whilst the brief interludes in a blocked task permit the refocussing of attention and adjustment of strategies. This possibility was explored by dividing the data from the RVIP-C600 into pseudo-blocks of 40 seconds, contrasting the pattern of scores and response times with those of the RVIP-B600. No deterioration in performance with time was observed for either design (data not shown). Subjects simply performed better on the blocked version. The difference in performance by task design was therefore most likely due to a practice effect, all subjects having completed the blocked design after first performing the continuous version.

3.2.5 Modifying the RVIP task

The demand placed on a subject's attention during the RVIP task can be raised either by introducing a fourth target sequence or by increasing the rate of presentation of digits. Introducing an additional target sequence alters both the attentional demand and the memory load of the task, with the limiting disadvantage that only four target sequences can be derived from the available integers. Increasing the rate of presentation of digits offers a parametric, unrestricted variation in the level of difficulty and was the preferred option.

Revisions: The stimulus duration was reduced from 600 to 400 ms, resulting in a rate of presentation of 150 digits per minute. To retain the block duration, the number of presentations – and targets – was increased. Targets thus appeared at a frequency of approximately 12 per minute in both the task and control conditions.

3.2.6 *Pilot study II — Evaluating the modified task*

METHODS

Subjects Five volunteers were recruited from amongst colleagues who had not taken part in the first pilot study. All subjects were right-handed men (age 37.6 ± 3.7) with a high level of education (years in education 21 ± 2). Subjects were healthy, had no history of psychiatric illness and were not regularly taking medication.

Task presentation The tasks were conducted in the same manner as the first pilot study, the continuous design followed by the modified blocked design task. Unlike the first pilot study there was only a short interval between the sessions.

RESULTS (RVIP-400)

Continuous versus blocked design Between task designs, no difference in hit rate, sensitivity index or median response latency was observed (see table 3.2 below). In the control task condition, false alarm rates were higher in the blocked version.

	TASK PERFORMANCE		MANN-WHITNEY *U*		
	RVIP-C400	RVIP-B400	ranks	Z	*p*
RVIP TASK CONDITION					
Hit rate (%)	52 ± 22	59 ± 12	10	− .314	.753
False alarm rate (%)	0.19 ± 0.2	0.26 ± 0.3	10	− .321	.748
Sensitivity index (A')	0.88 ± 0.06	0.90 ± 0.03	10	− .530	.596
Median response latency (ms)	450 ± 59	395 ± 51	10	− 1.36	.175
CONTROL CONDITION					
Hit rate (%)	88 ± 4	91 ± 4	10	− .862	.389
False alarm rate (%)	0.00 ± 0.0	0.25 ± 0.3	10	− 2.39	.017
Sensitivity index (A')	0.97 ± 0.01	0.98 ± 0.01	10	− 1.12	.262
Median response latency (ms)	431 ± 45	445 ± 41	10	− .838	.402

Table 3.2: Continuous versus blocked version of the RVIP (stimulus duration 400 ms, n = 5), in which the rate of presentation of digits was 150 per minute. Group values are reported as the mean ± sd. Statistical scores and significance levels refer to the comparison of the continuous and blocked versions for each measure. The statistical statements for the comparison of the RVIP task and control task conditions are presented in the body of the text.

RVIP condition versus control condition With the revised timings, hit rates were higher in the control task condition than the RVIP task condition in the continuous (88 ± 4 versus 52 ± 22; 10 ranks, Z −2.65, $p = 0.008$) and blocked versions (91 ± 4 versus 59 ± 12; 10 ranks, Z −2.62, $p = 0.009$). More false responses were made during the RVIP task condition for the continuous version only (false alarm rate, RVIP task condition versus control condition: 0.19 ± 0.2 versus 0.00 ± 0.00). Sensitivity scores mirrored the pattern for hit rates. Subjects responded more slowly in the control condition, most notably on the RVIP-B400 version.

Comparing presentation rates Performance on the blocked RVIP task conditions was compared (RVIP-B400 versus RVIP-B600). Those subjects undertaking the more rapid version had lower hit rates (59 ± 12 versus 94 ± 10; 10 ranks, Z −2.64, $p < 0.01$), and A' scores (0.90 ± 0.03 versus 0.98 ± 0.02; 10 ranks, Z −2.65, $p < 0.01$), together with slower response times (395 ± 51 versus 336 ± 26; 10 ranks, Z −1.98, $p < 0.05$). False alarm rates did not differ. Comparing the blocked control task conditions (RVIP-B400 versus RVIP-B600), those exposed to the swifter rate of presentation similarly had lower hit rates (91 ± 4 versus 98 ± 2; 10 ranks, Z −2.65, $p < 0.01$) and A' scores (0.98 ± 0.01 versus 0.99 ± 0.00; 10 ranks, Z −1.47, $p = 0.017$), but did not differ in response times or false alarm rates when compared to the subjects in the first pilot study.

INTERPRETATION

Hastening the rate of presentation of digits in the RVIP task ostensibly increased its difficulty, subjects making fewer correct detections and reacting less swiftly. The resultant baseline scores are better suited to our stimulant model in which an improvement in performance is anticipated.

4 LITHIUM & BRAIN FUNCTION

Dysfunction of the various monoamine neurotransmitter systems has long been implicated in the conditions for which which lithium is commonly prescribed; it follows that lithium may act on such neuronal pathways. In this chapter, the proposal that lithium attenuates dopaminergic neurotransmission in man is examined, principally though the use of a stimulant model of mania. By way of introduction, the role of dopamine in the brain is outlined and its relevance to bipolar disorder and lithium use explored. The assessment tools are then justified, before moving to a description of the study proper – a randomised, single-blind, placebo-controlled investigation of lithium's effects on methamphetamine administration, gauged by measuring performance on a task of sustained attention together with signal change on BOLD fMRI.

4.1 BACKGROUND

4.1.1 Dopamine in the central nervous system

Four major dopaminergic pathways have been identified in the human brain (Seamans and Yang, 2004). The *tuberoinfundibular pathway* is constrained to the hypothalamus and regulates some functions of the anterior pituitary through the release of dopamine into the portal vessels. The *nigrostriatal pathway* originates in the substantia nigra pars compacta and terminates in the dorsal striatum, modulating the functions of motor systems. The *mesolimbic pathway* arises in the ventral tegmental area (VTA) and projects to the ventral striatum, bed-nucleus of the stria terminalis, hippocampus and septum. Although the neuronal cell bodies of the *mesocortical pathway* are located in the VTA, they may be distinguished from those of the mesolimbic pathway and project more widely to the frontal and temporal cortical regions. These distributed pathways modulate domains such as attention, impulsivity, reward seeking, emotional processing, working memory and executive functions (Adler et al., 2006).

SYNTHESIS AND BREAKDOWN

The metabolic pathways of dopamine are well defined (Westerink, 1985) and only certain points merit attention. First, once tyrosine has crossed the blood-brain barrier and entered neurones, the rate of its conversion to dopamine via L-dopa is limited by the activity of tyrosine hydroxylase; the metabolic pathway is usually saturated so increasing precursor concentrations does not affect production. Second, the actions of dopamine can be terminated by a number of processes: simple diffusion away from receptor sites; enzymatic breakdown by catechol *o*-methyl transferase (COMT) and monoamine oxidase (MAO) to produce homovanillic acid (HVA); active cellular reuptake mechanisms involving various transporters. The dominant mechanism varies with brain site – whilst the DAT is active in the striatum, its absence in the prefrontal cortex (PFC) means that COMT activity and uptake into noradrenergic cells are the major determinants in cortical regions. Third, as both the *de novo* synthesised and recycled dopamine are rapidly broken-down by intraneuronal MAO, vesicular storage is necessary if large quantities are to be released; concentration into vesicles is determined by the monoamine transporters (VMAT2). Finally, dopamine neurones exhibit tonic and phasic patterns of firing, governed in part by COMT allele polymorphisms and the actions of DAT. High-activity COMT allele status results in low tonic levels overall, with low levels of dopamine in the PFC and high levels subcortically after phasic release; the reverse with low-activity COMT status (Tunbridge et al., 2004).

SIGNAL TRANSMISSION

Dopamine is a slow-acting neurotransmitter, its mode of action distinct from the processes of fast neurotransmission in which sub-millisecond response times permit the very rapid conveyance of signal between brain regions (Greengard, 2001b). Dopamine, on binding to a receptor, invokes the actions of second messengers, protein kinases and protein phosphatases to bring about its effects; these manifest over hundreds of milliseconds to minutes (Greengard, 2001a). Slow-acting neurotransmitters act to modulate the efficiency of fast neurotransmission systems, both inhibitory (GABA) and excitatory (glutamate).

The vesicular release of dopamine is calcium-dependent and is usually triggered by incoming depolarisation (Westerink, 2006). The rate and pattern of neuronal firing, together with the occupation and activity of presynaptic dopamine autoreceptors, determines the extent of dopamine release. Dopamine receptors have been grouped into two families: D1-type and D2-type (Kebabian and Calne, 1979). The D1-type receptors (D1 and D5) are mostly coupled to stimulatory subunits of G-proteins (G_{as}) and increase the production of the second messenger cAMP by activating adenylate cyclase (AC). The resulting cascade through protein kinase A (PKA), protein phosphatase 1 (PP1) and DARPP-32 (dopamine and cAMP regulated phosphoprotein of 32 kDa) achieves their cellular effect. The D2-type receptors (D2, D3, and D4) are coupled to inhibitory subunits (G_{ai}) and deactivate AC, reducing the production of cAMP and its effects on downstream pathways (Greengard, 2001a). Protein kinases such as DARP-32 are also inhibited by increased intracellular calcium concentrations, such as that which occurs as a consequence of glutamate receptor occupation (Lindskog et al., 2006).

Dopaminergic GPCR signalling is thought to conclude within around 30 minutes of transmitter release, terminated by receptor internalisation and desensitisation. Desensitisation is achieved by β-arrestin proteins decoupling the receptors from the G-proteins, but this in itself does not appear to mark the end of dopaminergic signalling (Beaulieu et al., 2004). On binding internalised D2-type receptors and PP2A, β-arrestin inactivates AKT and so reduces the inhibition of the constitutionally active *GSK-3β* (Beaulieu et al., 2007). This signalling pathway has a slower response time compared to those traditionally associated with GPCR transmission; it is also a putative site of action of lithium (Beaulieu and Caron, 2008).

4.1.2 Dopamine and bipolar disorder

The role of dopamine and the importance of brain network dysfunction in bipolar disorder have recently been reviewed (Cousins et al., 2009; Palaniyappan and Cousins, 2010), the key points being summarised below. Much of the available evidence pertains to mania, long-argued to be a hyperdopaminergic state (Silverstone, 1985).

Conceptual frameworks Dopamine governs reward-seeking behaviour, potentially mediating impulsivity and risk-taking in mania (Seamans and Yang, 2004). Through modulating activity in frontal regions, dopamine could be central to the well recognised alterations in cognition that may accompany bipolar disorder (Adler et al., 2006; Robinson and Ferrier, 2006). Although striatal systems are less clearly implicated in mania, patients with bipolar disorders demonstrate an excess of soft neurological signs (Goswami et al., 2006) and more commonly develop extrapyramidal side effects with antipsychotics than other diagnostic groups (Hamra et al., 1983; Gao et al., 2008).

Drug challenges Psychostimulants which increase dopaminergic activity in the brain can mimic or induce manic presentations (Jacobs and Silverstone, 1986). Mania can also be triggered by L-dopa, dopaminergic agonists and dopamine reuptake inhibitors (van Praag and Korf, 1975; Gerner et al., 1976; Silverstone, 1984). Reducing the synthesis of catecholamines improves the symptoms of mania in those already receiving standard treatment (McTavish et al., 1999, 2001; Scarnà et al., 2003).

Neurotransmitter metabolites The concentration of HVA in the cerebrospinal fluid (CSF) is usually, but not invariably, found to be increased during mania (Gerner et al., 1984); likewise urinary dopamine (Koslow et al., 1983).

Presynaptic imaging Investigated using the [^{18}F]6-fluoro-L-dopa positron emission tomography (PET) ligand, the rate of synthesis of dopamine appears to be normal in mania (Yatham et al., 2002b); vesicular storage and release has not been similarly investigated. The VMAT2 can be visualised with PET, [^{11}C]DTBZ ligand binding linearly reflecting the density of monoaminergic synaptic projections in the brain (Vanderborght et al., 1995). In euthymic patients with bipolar disorder, [^{11}C]DTBZ binding is greater than normal in the thalamus and ventral midbrain, the binding potentials correlating with impaired performance on tests of verbal learning and executive function, though not with ratings of mood (Zubieta et al., 2001).

Receptor imaging In patients with bipolar disorder, D1-receptor binding, assessed by [^{11}C]SCH23390 PET, is reduced in the frontal cortex but not in the striatum (Suhara et al., 1992). Striatal D2-receptor density is normal in mania, as gauged by [^{11}C]raclopride binding (Yatham et al., 2002a). Whilst D2-receptor density is unrelated to mood symptoms, the presence of psychosis in mania is associated with increased binding (Pearlson et al., 1995). Euthymic patients do not differ from healthy subjects in the amphetamine displacement of [^{123}I]IZBM binding, suggesting normal striatal D2 and D3-receptor expression in this phase of the illness (Anand et al., 2000).

Second-messenger systems Concentrations of PKA regulatory subunits are reduced in the cytosolic fractions of the cortex in patients with bipolar disorder examined post-mortem (Rahman et al., 1997), potentially reflecting disrupted dopaminergic signalling through cAMP and PP1 pathways. Located downstream of D2-receptors, platelet phosphatidylinositol bisphosphate (PIP2) concentrations are elevated in mania (Brown et al., 1993); levels of inositol within the frontal and occipital cortex are lowered in bipolar disorder (Silverstone et al., 2005) whilst protein kinase C (PKC) activity is enhanced in frontal brain regions (Wang and Friedman, 1996).

DEPRESSIVE STATES

Historically, dopaminergic models of bipolar disorder are presented as dichotomous, with depression considered to be a hypodopaminergic state. Simply stated, there are notable conflicts between theory and observation. Lowering of mood can occur with drugs that deplete dopamine (Schatzberg and Nemeroff, 1998) or antagonise its receptors (Willner, 1983), but antidepressant effects have also been ascribed to such medications (Davies and Shepherd, 1955; Mulholland and Cooper, 2000; Berk et al., 2007). In Parkinson's disease (the prototypical hypodopaminergic state) depression commonly occurs (Lieberman, 2006), especially in those with degeneration of the VTA (Torack and Morris, 1988); the association, however, is highly inconsistent (Lieberman, 2006), non-specific (Gotham et al., 1986), not related to illness duration (Brown, 1995) nor invariably resolved with dopamine replacement strategies. Metabolite

studies generally support a reduction in dopamine turnover in bipolar depression (Subrahmanyam, 1975; Gerner et al., 1984), but the assessments are confounded by the level of physical activity and the presence of psychosis; for that matter, the reality of psychotic depression means that theories purporting a global reduction in dopaminergic functioning in depression are most likely an oversimplification.

4.1.3 Bipolar disorder and lithium

Lithium is an established treatment for bipolar disorder (see §1.2.2 on page 3), with evidence to support its use in all phases of the illness. There is a widespread consensus that its greatest efficacy is observed whilst managing acute mania. As a maintenance treatment, it may be more effective in preventing relapse into mania than into depression (Geddes et al., 2004; Nivoli et al., 2010), but this asymmetry in efficacy may balance out as new data is entered into meta-analysis. Lithium confers protection against completing suicide, but this effect is lost on withdrawal (Cipriani et al., 2005).

Treatment with lithium is not effective in all cases and much work has focussed on identifying the profile of those who respond. Characterised on clinical grounds, the best response is seen in those with episodic presentations resolving to normal functioning, euphoric symptoms whilst manic, a family history of bipolar disorder in first-degree relatives and the absence of a personality disorder (Maj, 1992). Despite numerous endeavours, no biological markers that consistently identify lithium responders have been found (Grof, 2006).

4.1.4 Lithium and dopamine

If mania is a hyperdopaminergic state and lithium an effective antimanic agent, it may follow that lithium acts to attenuate dopaminergic neurotransmission. In accepting this conclusion, caution must be advised. Mania is not purely driven by dopaminergic dysfunction and lithium has numerous, wide-ranging effects; the explorations of its effects on dopaminergic systems may have been skewed by the observation that is more effective in mania than depression, leading to a degree of circularity.

EFFECTS ON COGNITION

The influence of lithium on cognitive functioning has been investigated in various subject groups; its effects are subtle and the interpretation of studies hindered by such matters as illness state, treatment duration and serum level achieved. Nevertheless, consistent findings have emerged from reviews of the field (Pachet and Wisniewski, 2003; Wingo et al., 2009). Lithium impairs performance on tasks assessing verbal memory and psychomotor speed, whilst attention, visual memory and constructional ability appear to be largely unaffected. By inference, modulation of dopaminergic functioning could be proposed to underlie these effects.

NEUROENDOCRINE MEASURES

Serum prolactin levels are determined in large part by the activity of the tuberoinfundibular pathway, dopamine acting to inhibit the release of the hormone. Thus, an elevated prolactin level may reflect a reduction in dopaminergic activity, at least in this pathway. Lithium has been associated with increases in prolactin (Joffe et al., 1986), but negative and opposite findings abound (Lanng Nielsen et al., 1977; Baptista et al., 2000; Basturk et al., 2001). Prolactin release is governed by various systems including serotonergic ones, sensitive to the effects of stress and illness as well as many of the commonly prescribed psychotropic medications. It is not a particularly specific outcome measure.

PHARMACOLOGICAL MODELS

Lithium has been shown to attenuate the effects of amphetamines in some, but not all, rodent studies (see §1.4.2 on pages 11–12). In patients with affective disorders, the euphoria, arousal and sense of activation that follows amphetamine administration are diminished by lithium (Vankammen and Murphy, 1975); a similar effect is seen in recreational users (Flemenbaum, 1975). Application of a stimulant model of mania forms the basis of the study described in this chapter, the rationale for which is considered in the sections that follow.

4.2 MODELS & MEASURES

Mania is a severe condition that presents a challenge to ethical research because it is frequently associated with impaired judgement and loss of insight. Interventions are therefore often investigated using healthy subjects in which the illness is partially replicated. Amphetamine administration to healthy subjects has been extensively used as a model of mania (Jacobs and Silverstone, 1986). Illness models have certain merits in research: specific aspects of syndromal presentations may be isolated or emphasised, pharmacological interventions can be investigated in a focussed manner and the preclinical to clinical gap bridged. Logistical difficulties arising from florid presentations – consent, polypharmacy, timing, containment – are also bypassed.

Models of illness, however, are never fully accurate and their specific limitations must be recognised. In addition to ensuring a model replicates the pertinent clinical features and proposed neurochemical derangements, the assessments undertaken are of some importance. Whilst a model of mania may consistently induce hyperactivity, for example, quantifying such changes may be challenging and problematic in some research settings, not least imaging studies. Drawing from the extensive battery of neuropsychological tasks, cognitive and emotional processing can be assessed easily and reliably in various environments; consequently, dysfunction in these domains has been investigated in studies of mania and in models of mania. In the study described in this thesis, subjects completed a task which required their sustained attention before and after receiving methamphetamine.

4.2.1 Amphetamine models of mania

Amphetamines act to increase the synaptic concentrations of monoamines (principally the catecholamines) and to a lesser extent the excitatory neurotransmitter glutamate (Sulzer et al., 2005). Administration to healthy human subjects consistently elevates mood, alertness and arousal, with increases in energy and mental speed reported; appetite is generally reduced, as is the need for sleep (Jacobs and Silverstone, 1986). These subjective and behavioural effects mirror some of the key features of mania.

MODE OF ACTION

Whilst it is clear that many of the effects of the amphetamines are driven through the elevation of extracellular concentration of dopamine and noradrenaline, the mechanisms of their actions remain incompletely defined – for a comprehensive review of the topic, see Sulzer et al. (2005). Amphetamines are dopamine-releasing agents, with scant affinity for dopamine receptors. In effect, they reverse the direction of passage of dopamine across key membranes. Extracellular amphetamine at a low concentration is readily exchanged for cytosolic dopamine via the DAT; at higher concentrations the drug enters neurones by diffusion and releases dopamine from its intracellular binding sites, resulting in an outpouring of dopamine into the synapse through reverse transport involving the DAT. Release by efflux may occur though a rapid, channel-like route and a slower exchange process. The channel-like route resembles vesicular release and so likely mediates the psychoactive effects of amphetamines.

Amphetamines, by increasing the activity of PKC, also modify the functional status of the DAT by phosphorylation and internalisation. Activation of presynaptic PKC has several consequences, including the downregulation of the DAT with a subsequent reduction in the reuptake of dopamine, and the induction of dopamine efflux. An increase in the cytosolic concentrations of dopamine may also be brought about by changes in vesicular storage. Amphetamines cause a redistribution of the VMAT2 protein, reducing the uptake of dopamine into vesicles. Furthermore, when the drug accumulates in vesicles, its weak base properties disrupt the proton electrochemical gradients that encourage monoamine storage, increasing the fraction of dopamine in the cytosol with subsequent efflux by the mechanisms previously described.

DIFFERENTIAL EFFECTS OF AMPHETAMINE DERIVATIVES

It is commonly thought that dextroamphetamine (D-amphetamine) and its principal derivative methamphetamine have different effects, at least subjectively. Methamphetamine is often touted as the more potent, addictive and CNS specific of the two stimulants; these claims generally do not stand up to scrutiny (Shoblock et al., 2003a), the two compounds having similar pharmacokinetic properties with a substantial

overlap in subjective effects (Sevak et al., 2009). Both drugs increase synaptic noradrenaline, dopamine and glutamate, but the regional effects (Shoblock et al., 2003b) and ratios of the transmitters released may vary subtly. Striatal dopamine release underpins at least part of the model of mania, as the reduction in [^{11}C]raclopride binding that follows D-amphetamine administration correlates inversely with ratings of euphoria in healthy subjects (Drevets et al., 2001).

REGIONAL EFFECTS

Functional imaging studies have favoured D-amphetamine as the intervention, though the doses used have been quite wide ranging. The findings have been somewhat mixed and inconclusive. Assessed using [^{18}F]-fluorodeoxyglucose PET, very high oral doses of D-amphetamine induce a global increase in cerebral glucose metabolism (Vollenweider et al., 1998). In healthy subjects, regional changes in cerebral blood flow and glucose metabolism occur in brain areas innervated by dopamine, with increases (Devous et al., 2001) and decreases (Mathew and Wilson, 1985; Wolkin et al., 1987; Kahn et al., 1989) observed. Some fMRI studies have found D-amphetamine to increase BOLD signal in task-specific regions during sensory, motor and working memory paradigms (Mattay et al., 2000; Uftring et al., 2001); others have reported decreases in similar experimental conditions (Howard et al., 1996; Willson et al., 2004).

PRACTICAL CONSIDERATIONS

When D-amphetamine is administered in clinical studies, it is most often given orally. This results in a delayed onset of action which peaks, on average, at about 75 minutes after administration (Jacobs and Silverstone, 1986; Silverstone et al., 2004). Absorption of amphetamines can be affected by concurrent medications and physiological factors, making timing of the peak effect difficult to predict. Methamphetamine may be administered intravenously to humans, bypassing first-pass metabolism and resulting in near immediate effects. This predictability, combined with local expertise (Hearn et al., 2004), made methamphetamine the more desirable derivative for the study undertaken in this thesis.

4.2.2 Sustained attention

Impairments in cognition are now well recognised in bipolar disorder, delineated in numerous studies and synthesised by meta-analysis (Robinson et al., 2006). Several cognitive domains are affected during acute episodes and the abnormalities remain detectable in euthymia (Ferrier et al., 1999), even when medications are considered (Goswami et al., 2009; Balanzá-Martínez et al., 2010). Sustained attention is one such domain. Whilst manic, patients perform poorly on tasks requiring sustained attention (Sax et al., 1999; Clark et al., 2001), including the RVIP task. This disruption to attention is particularly marked in patients who are psychotic (Quraishi and Frangou, 2002). Once euthymic, attentional deficits are demonstrable in some (El-Badri et al., 2001; Wilder-Willis et al., 2001; Harmer et al., 2002; Liu et al., 2002; Clark et al., 2002, 2005) but not all tasks (Addington and Addington, 1997). The impairments in attention are not the most striking abnormality evident in patients with bipolar disorder, being gauged as of moderate effect size (Kurtz and Gerraty, 2009).

Engaging and sustaining attention is necessary for the completion of most tasks, be they formal neuropsychological tests or mundane matters of day to day life. Disturbances in attention can have wide ranging consequences for social and occupational functioning, influencing or masquerading as impairments over a number of cognitive domains. Investigation of attention in its own right is therefore of importance. Attention has long been conceptualised as a tripartite system comprising alerting, orienting and executive functions (Miller and Cohen, 2001). Each component may be considered in its own regard and, for the purposes of investigation, emphasised in the construction of individual tasks. In this way, neuronal networks have separately been identified that serve to obtain the alert state (*alerting* – Coull et al., 1996), enhance the processing of target information (*orienting* – Corbetta et al., 2000) and resolve the conflict in whether or not to respond (*executive* – Botvinick et al., 1999). Using the single, sophisticated Attentional Network Task (ANT), Posner's group have demonstrated that whilst all three networks are engaged with attention, each may be dissociated by varying the demands of the task (Fan et al., 2005).

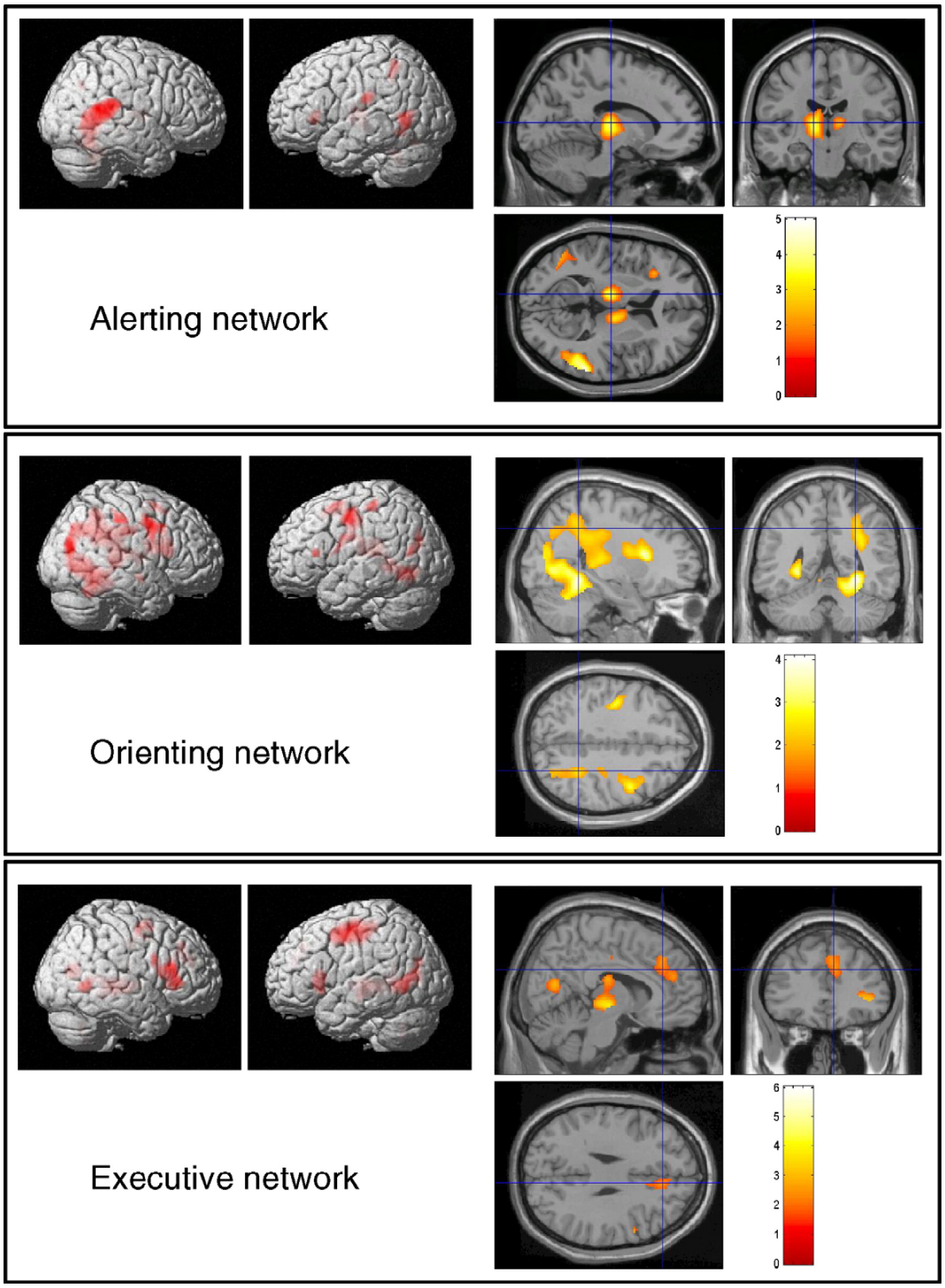

Figure 4.1: Attentional networks demonstrated using BOLD fMRI. The three networks – alerting, orienting, executive – demonstrate independence, but are all engaged by tasks requiring sustained attention. The images above were acquired whilst the Attention Network Task was performed by healthy subjects (figure reproduced from Fan et al., 2005).

The alerting network comprises the thalamus together with anterior and posterior cortical regions; in orienting to visual stimuli, the frontal eye fields and parietal areas are engaged whilst the anterior cingulate cortex is dominant in conflict resolution (figure 4.1 on page 82). Alerting is sensitive to manipulations of noradrenergic neurotransmission (Marrocco and Davidson, 1998; Coull et al., 2000, 2001) whilst the executive network is modulated by dopaminergic systems (MacDonald et al., 2000).

THE RAPID VISUAL INFORMATION PROCESSING TASK

Tasks which require sustained attention can be simply constructed and are well suited to functional imaging investigations. The principal requirements of the task used in this thesis were that it should invoke changes in brain activity detectable with BOLD fMRI, be sensitive to methamphetamine and be of relevance to – or disturbed by – the presence of mania. The RVIP task was considered suitable for these purposes (see *Chapter 3* for a description of the task).

Regional effects In performing the RVIP, healthy subjects engage alerting and orienting networks as well as prefrontal regions, evidenced by an increase in cerebral blood flow using PET (Coull et al., 1996). The pattern of activation demonstrated by PET (figure 4.2 on the following page) has since been replicated in an fMRI investigation, validating the use of a blocked design (Lawrence et al., 2003). Regional deactivations that arise when subjects engage with the RVIP task condition are seen in anterior and posterior medial cortical regions as well as the precuneus.

Deactivations occur in these regions regardless of the task in hand. The significance of this observation is considered in greater detail later in this chapter.

Sensitivity to stimulants Performance on the RVIP task is modified by stimulants (Wesnes and Warburton, 1983b), with methamphetamine consistently shortening the response latency (McTavish et al., 2001; Hearn et al., 2004). Some studies have found it to increase sensitivity index scores (Hearn et al., 2004) whilst others report a tendency for impulsive responding (McTavish et al., 2001). Methamphetamine may influence all attentional networks, but the executive component is implicated by its effects on response bias, effects prevented by tyrosine depletion (McTavish et al., 2001).

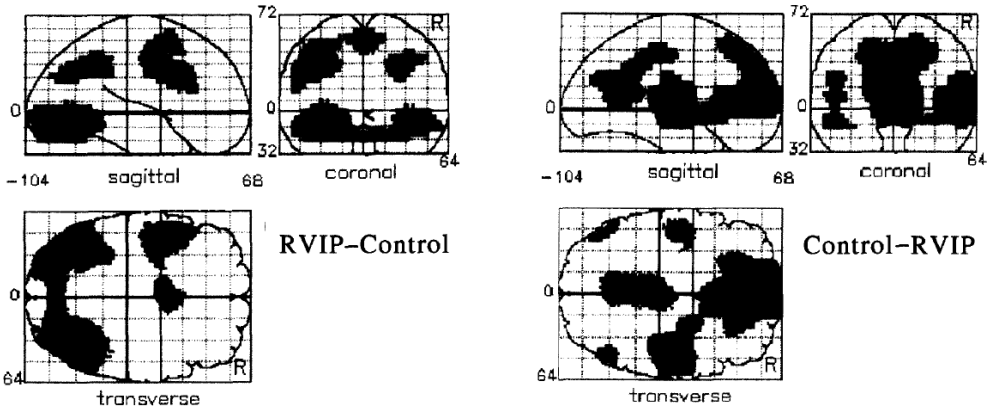

Figure 4.2: Regional cerebral blood flow by PET during the RVIP task. The RVIP–Control contrast demonstrates increased blood flow on performing the RVIP task condition; the Control–RVIP contrast shows regional reductions in blood flow (figure reproduced from Coull et al., 1996.)

Dysfunction in bipolar disorder Mania is associated with abnormal performance on the RVIP task (Clark et al., 2001), principally a lower response sensitivity and with a tendency to respond impulsively, reflected in lower A' and B'' values respectively. Response latency times are disrupted in mania and slowed in euthymic patients compared to control subjects and healthy first-degree relatives (Clark et al., 2005). Imaging studies of bipolar disorder utilising the RVIP task have yet to be reported.

4.2.3 Existing studies

Silverstone's group extended the amphetamine model into the fMRI field, their experiments culminating in a study of the attenuating effects of the medications used in mania. The effects of D-amphetamine on BOLD fMRI were examined using motor, verbal memory and spatial attention paradigms (Willson et al., 2004). Signal intensity in the regions of activation was compared before and after D-amphetamine. In the tasks of cognitive function, D-amphetamine reduced BOLD signal intensity. The regions of interest identified in the Willson et al. (2004) study were applied in the analysis of a second study (Bell et al., 2005a) – the tasks and the D-amphetamine intervention were unchanged, but subjects had been randomised to receive either lithium, valproate or placebo prior to the sessions. Lithium attenuated the effects of D-amphetamine on signal change in the spatial attention task, but not the memory or motor task.

4.3 STUDY OBJECTIVES

There is evidence that mania can be considered a hyperdopaminergic state and that lithium may act to reduce neuronal activity in dopaminergic pathways. Tasks that require sustained attention engage brain regions innervated by monoaminergic systems and are sensitive to manipulations of dopamine synthesis and release. By combining tasks, fMRI assessment and amphetamine administration, the monoaminergic systems of the brain may be probed *in vivo* in man. Within this framework, lithium has been shown to modify the effects of D-amphetamine on regional activation during attentional processing. A more predictable onset of action can be achieved by giving intravenous methamphetamine in preference to oral D-amphetamine, and methodological strength may be gained by the use of a longitudinal design with examination of dose related effects. On the basis of these assertions and in light of the evidence presented, the following hypothesis was proposed:

> *Lithium carbonate will lessen the effects of methamphetamine by attenuating dopaminergic neurotransmission in healthy men, gauged by subjective ratings, performance on a task of sustained attention and BOLD fMRI signal change; the effects will be evident at serum levels advocated for the treatment of mania and not with a lower dose schedule.*

4.4 STUDY METHODOLOGY

4.4.1 Study design

The experiment, hereafter referred to as the MRC-LAMP study, was a randomised, single-blind, placebo-controlled study of healthy male subjects in which the effects of lithium on a stimulant model of mania were investigated. In brief, all subjects underwent fMRI investigation on two occasions, separated by a period in which they received either lithium or placebo tablets for 11 days. Subjects were randomly allocated to one of three groups: high dose lithium, low dose lithium, placebo. During each fMRI session the subjects completed the blocked RVIP task twice, the second occasion immediately preceded by an intravenous dose of methamphetamine.

The study duration derived from the pharmacokinetics of lithium and its anticipated acute effects (see §1.3).

The study was funded by the Medical Research Council (MRC) and approved by a Local Research Ethics Committee (LREC) for the Newcastle upon Tyne region.

4.4.2 Subject recruitment

Healthy male subjects were recruited from the population of Newcastle upon Tyne, attracted by advertisements placed in various sites around the University campus, local recreation centres and business parks. The advertisements alluded to the nature of the research, directing interested parties to a study-specific website where a detailed account of the study was provided, together with instructions on how to contact the research team. All subjects were recruited by this route, it being inappropriate to enlist friends or colleagues into this sort of study. The suitability of volunteers was first checked by way of a phone call or email, with eligible candidates invited to a full screening assessment at the Newcastle Magnetic Resonance Centre.

4.4.3 Screening session

The purpose of the screening visit was threefold: enrolment, assessment and training. A full screening visit typically lasted 2–3 hours, with all assessments undertaken during morning hours.

ELIGIBILITY & CONSENT

Individuals were eligible for the study if they were male, 18–45 years of age, right-handed, in good health and naïve to prescribed or illicit stimulants. Volunteers with any history of psychiatric illness were excluded, as were those with medical conditions deemed to have a bearing on the study investigations or the safety of medication administration. Individuals were assessed with the Structured Clinical Interview for the Diagnostic and Statistical Manual of Mental Disorders (4^{th} edition, Non-Patient version, SCID_NP; **?**), and a medical history was elicited by systematic enquiry. Suitable volunteers were invited to participate, all of whom provided written and informed consent.

BASELINE ASSESSMENTS

Subjects underwent a physical examination during which height, weight, pulse rate and blood pressure were recorded. A urine sample was tested on-site for the presence of illicit drugs and those testing positively for stimulants were excluded from further participation. Breath analysis for alcohol was performed, with a negative reading required for continuation. A venous blood sample was taken for the measurement of urea and electrolytes, liver function, thyroid function and a full blood count.

Substance use was gauged by direct questioning, specifically the units of alcohol imbibed per week and the number of cigarettes smoked per day (or equivalent nicotine replacement measures). The average daily consumption of caffeinated drinks was also noted. Past and present illicit drug use was recorded and whilst cannabis use was not an absolute exclusion criterion, those judged to be heavy users were considered inappropriate for further participation.

Subjects then completed a visual analogue scale (VAS) assessing 16 domains known to be sensitive to the effects of psychotropic medications (Bond and Lader, 1974). This familiarised them with the tool prior to the series of assessments spanning methamphetamine administration. Those attending the screening session considered themselves right-handed, but this was formally assessed using the standard Edinburgh Handedness Inventory (Oldfield, 1971).

As aptitude determines performance on various neuropsychological tests, the duration of education for each subject was recorded, together with their highest qualification. Intelligence was more formally gauged by having subjects complete the National Adult Reading Test (NART – Bright et al., 2002).

NEUROPSYCHOLOGICAL TASK TRAINING

During the screening visit, subjects completed the RVIP task on two occasions; a third training run was performed at the beginning of scan day one, subjects having slept in the intervening period. In these sessions, subjects became familiar with the task and through practice their performance was expected to improve to a plateau level. Training to the level of automatic functioning was not the goal, rather the reaching of a stable baseline against which drug interventions could be compared. The structure and delivery of the task, both inside and out of the magnet, has previously been described (see §3.1.1 on page 58).

4.4.4 Assessment sessions

As noted, subjects underwent fMRI investigation twice. The sessions were very similar in structure, though subjects were more familiar with the scanner environment and the effects of methamphetamine on the second occasion. On the second assessment day, subjects also completed the Lithium Side-Effects Rating Scale (LISERS) and gave a blood sample immediately before entering the scanner – this was used to measure the serum lithium concentration, but was taken from all subjects to maintain blinding. On both occasions the assessment sessions took much of a day, the shared features of which are described in the sections that follow.

PREPARATION

On arrival in the morning, subjects were greeted and reminded of the schedule for the day. Consent was checked and the researcher reassured themselves that each subject had a full understanding of the nature of the project and proposed interventions. The MRI-specific safety questions were posed by one of the duty radiographers, all of

whom were familiar with the study protocol. Alcohol breath testing was performed and a fresh urine sample taken to exclude recent stimulant use. Cardiovascular vital signs were recorded, a VAS completed and an intravenous cannula inserted for the purposes of venous sampling and methamphetamine administration. Once subjects were comfortable, they were invited to enter the scan room.

MAGNETIC RESONANCE IMAGE ACQUISITION

Data was acquired from all participants using the same 3T whole body Philips Achieva System using an 8-channel SENSE head coil. After the acquisition of a T_1-weighted image (3D T1_FFE sequence: TR = 9.6 ms, TE = 4.6 ms; flip angle = 8°, FOV = 240 × 180 × 240 mm, contiguous isometric voxel size 1 mm), the fMRI series began (gradient echo EPI sequence: TR = 3 s, TE = 30 ms; flip angle = 90°, FOV = 240 × 240 × 240 mm, matrix 80 × 80, 30 slices, slice thickness = 5 mm). On each assessment day, subjects completed the blocked RVIP protocol twice (presentation and equipment described in §3.1.1); the well-being of the subjects was enquired after at regular intervals and subjects were able to indicate discomfort or distress throughout the session.

RVIP FUNCTIONAL SERIES

The format of the task was identical on each occasion, though the actual sequence of digits varied between sessions. Each functional run comprised ten presentation blocks, five each for the RVIP task condition and control task condition. Blocks were presented in a pseudo-random order (R·C·R·R·C·R·C·C·R·C, where R is the RVIP condition and C is the control condition). The block duration was 40 seconds, each block preceded by instructions appearing on screen for 5 seconds. Inclusive of two dummy scans, the total length of each functional series was 7.6 minutes (152 dynamics of TR = 3 s).

Being tiresome to repeatedly describe fMRI sessions as 'pre-methamphetamine and after the course of lithium or placebo' for example, shorthand forms were adopted. The assessment days before and after the course of tablets were denoted by the numbers 1 and 2; pre- and post-methamphetamine status by the letters A and B respectively.

METHAMPHETAMINE ADMINISTRATION

On completing the first functional RVIP task series, subjects were instructed to remain still whilst they were moved out of the scanner bore. The principal investigator then entered the scan room, checked their well-being and their willingness to continue before recording their pulse rate. Methamphetamine was given intravenously (0.15 mg/kg diluted with normal saline, Martindale Pharmaceuticals™ injection BP) as a slow push over 30 seconds. Subjects were replaced in the scanner, the second functional series conducted immediately thereafter.

RECOVERY

Once out of the scanner, the post-methamphetamine assessments were performed. These comprised a VAS series, cardiovascular vital signs and a review of well-being at 45 minute intervals. Once the assessments were complete and the subject comfortable, they were allowed to go home. Subjects received a card stating that they had taken methamphetamine as part of a clinical study, with contact details in case of emergency.

4.4.5 Lithium/Placebo administration

LITHIUM

Lithium was administered as Priadel™ tablets in all instances, with the lowest denominator of 200 mg selected to permit flexibility of dosing whilst retaining consistency of appearance. Tablets were repackaged by pharmacy, bottles labelled as containing 'MRC-LAMP study medication' with instructions to take a specified number at night. The dose was calculated using the method described by Chiu et al. (2007): after converting serum creatinine levels to mg/dl (equation 4.1) and estimating the creatinine clearance (equation 4.2; age in years, weight in kg), a target serum level of either 0.5 or 0.9 was entered into equation 4.3 and the daily dose of lithium calculated. The tablets were given for 11 days, reflecting the four days typically required for lithium to reach steady-state (§1.3) followed by a full week at the target level. A consistent duration was favoured over repeated cycles of checking serum levels and modifying doses.

$$\text{Serum creatinine in mg/dl (SCR)} = \frac{\text{serum creatinine in mmol/l}}{88.4} \tag{4.1}$$

$$\text{Creatinine clearance (CRCL)} = \frac{(140 - \text{age}) \times \text{weight}}{(72 \times \text{SCR})} \tag{4.2}$$

$$\text{Lithium dose in mg} = \frac{\text{weight} \times 20 \times \text{CRCL}}{100} \times \text{target level} \tag{4.3}$$

PLACEBO TABLETS

As this study was a single-blind investigation without a run-in period or cross-over phase, the placebo tablets did not have to be identical to the Priadel™ in all respects. They simply had to be convincingly medication-like, yet pharmacologically inert. Plain lactose tablets were sourced from a reputable homeopathic company, certified as free from active ingredients (no matter how low the concentration). The lactose tablets were small, round and white; not dissimilar to many medications. Conforming to European production standards and passing UK pharmacy quality control tests, the placebo tablets were repackaged into generic containers and labelled in the same manner as the lithium prescription. The number of tablets prescribed was determined by calculating the dose of Priadel™ that the subject would have received had they been randomised to the low-dose lithium group.

4.4.6 Analysis

CLINICAL MEASURES & RATINGS

Using SPSS (*v.*17, SPSS inc., USA), histograms of clinical measures and VAS scores were examined and the data tested for normality of distribution (Shapiro-Wilk test). For the three groups, normally distributed data was compared using an ANOVA test, controlling for multiple comparisons during *post-hoc* analysis. With the nonparametric equivalent Friedman test, *post-hoc* comparisons were adjusted using the Bonferroni technique.

SUSTAINED ATTENTION

Raw data was extracted from E-prime® and entered into a spreadsheet template constructed to calculate hit rates, false alarm rates, response latencies and the derived sensitivity index (A') and response bias (B'') for the individuals and groups. Responses occurring within 125 ms of a stimulus presentation were excluded from analysis (see §3.2.1). The measured and derived variables were treated as continuous and tested for normality as previously described; use of non-parametric statistics was anticipated for the analysis of response latency, a Gaussian distribution being unlikely given the propensity for extreme upper values and the application of a lower threshold.

IMAGE ANALYSIS

Preparation Data was exported from the scanner in proprietary PAR-REC format to a personal computer running a Linux operating system (Ubuntu 8.04 LTS), on which all subsequent processing was conducted. Images were converted into ANALYZE format using MRICRO and subsequently inspected for quality using the same program. Orientation by the radiological convention was maintained as conversion to the neurological orientation is a default process within the statistical parametric mapping program used. Prior to preprocessing, the 4D EPI data was converted to 3D format using the `'fslsplit'` command-line function in FSL. All further analysis stages were completed using SPM8.

Preprocessing For each subject and each session, the dummy scans necessary to overcome T_1 saturation effects were rejected before the 3D functional images were realigned to the first image in the respective time-series, thus correcting for movement effects. Sampling errors were not adjusted as head movement may have been related to the task conditions. Realignment preserved the 3D format of the data whilst generating a mean image for time series, applied during the normalisation process. Each subject's mean EPI file was coregistered to their T_1-weighted image (acquired at the outset of the relevant session) and resliced using a trilinear interpolation, without a mask and with no wrap applied. The T_1-weighted image was then normalised to the

ICBM152 T_1 template and the parameters applied to each image in the 3D realigned EPI series. Source images were smoothed with an 8 mm FWHM Gaussian kernel to ensure adequate matching and when writing normalised images, the default setting for trilinear interpolation was maintained along with a voxel size of $2 \times 2 \times 2$ mm and the template bounding-box. The normalised images so created were spatially smoothed with an 8 mm FWHM Gaussian kernel.

First-level analysis To prevent errors in the definition of parameters, model specification was performed using the batch mode of SPM8. A template .mat file was created in which the onset and duration of each RVIP task and control condition block was defined, interspersed by the instruction slides. A box-car model convolved with a Canonical haemodynamic response function was specified; parametric modulation, temporal derivatives and interactions between trials not being required. The rotational and translational movement parameters generated by the realignment procedure for each subject were considered nuisance covariates and entered as regressors in the design. In keeping with current opinion, global signal intensity was left unscaled and a high pass filter of 128 seconds was applied, the haemodynamic response function serving as a low pass filter. A batch with 96 modules was prepared, one for each session and subject, into which the relevant smoothed 3D images from the preprocessing stages were entered. Model specification and estimation followed, resulting in an SPM.mat file for each module. Contrasts were then defined using the SPM8 GUI 'contrast manager' (RVIP task condition, control task condition, RVIP task condition minus control task condition) and applied to all SPM .mat files (figure 4.3).

Second-level analysis A random effects analysis was applied to investigate the main effect of the task, the differences between sessions determined at the group level. Using the contrasts generated in the first-level analysis, the main effect of the RVIP task was demonstrated with a one-sample *t*-test, with a paired *t*-test used to investigate the effects of methamphetamine on all subjects during the first assessment day. A full-factorial analysis ($2 \times 2 \times 2$) was constructed to investigate the interaction between

lithium, placebo and stimulant (group × methamphetamine × assessment day). Only the RVIP-minus-control contrast (activation) was submitted to this design; multiplying the matrix by − 1 generated the control-minus-RVIP (deactivation) contrast.

Describing contrasts as activations or deactivations is a useful short-hand. With multilevel comparisons, the terms can become misleading. In such instances, a full description supported by diagrams are favoured.

Statistical inference Contrast differences emerging from the comparisons made were primarily assessed at the cluster-level, deemed to be significant at $p < 0.05$ following family-wise-error (FWE) correction. A less conservative threshold was applied in the exploratory analyses ($p < 0.001$ uncorrected); results thereby derived were considered informative, but not acceptable as evidence for the refutation of the null hypothesis. Cluster localisation by MNI coordinates in mm was maintained, with a description of the anatomical positioning favoured over conversion to Talairach coordinates. When given in text or tables, coordinates are invariably in the order *x*, *y* and *z*.

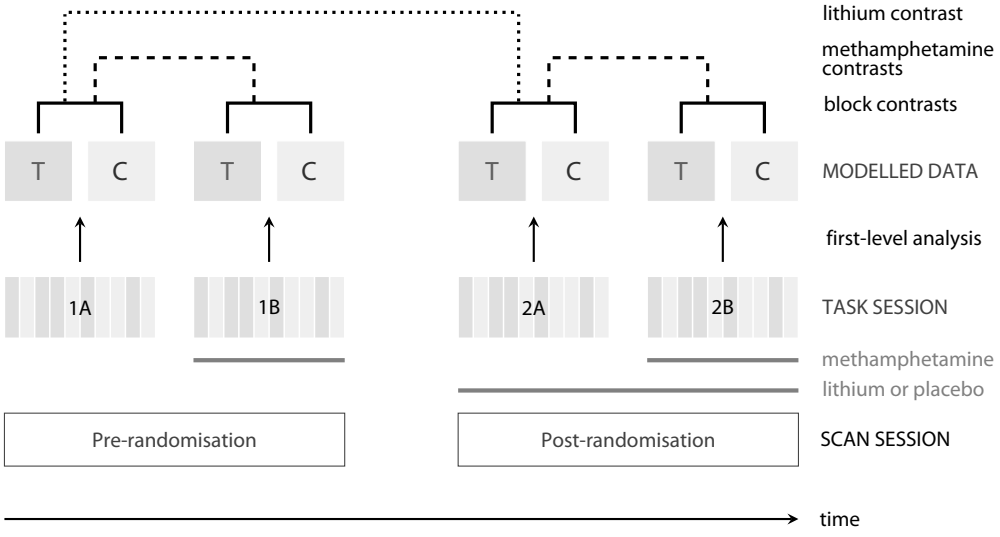

Figure 4.3: Schematic representation of the levels of contrasts in the MRC LAMP study. Subjects underwent investigation on two days (1 and 2; before and after lithium or placebo), each comprising a functional series pre- and post-methamphetamine (A and B). First level analysis modelled the order of presentation of blocks, allowing RVIP task condition (T) and control task (C) conditions to be specified. Subtraction contrasts T–C (RVIP–Control) were entered into the second level analysis, in which the effects of medication across the various sessions were examined.

4.5 RESULTS – CLINICAL VARIABLES

4.5.1 Subject characteristics

Twenty four subjects were enrolled into the study, 18 of whom received lithium and 6 placebo. The characteristics of those completing the study are given in table 4.1 (page 96), with the flow of subjects shown in the CONSORT diagram below (figure 4.4). The subjects in the placebo and lithium groups did not differ in age, handedness, body mass index, or estimates of intelligence (NART score). As the majority of subjects were university or college students, the average duration of education was long; the groups differed in this respect (one-way ANOVA between the three groups: 2 df, $F = 3.56$, $p = 0.047$), *post-hoc* comparison demonstrating a difference between the placebo and lower dose lithium group (18.0 ± 2.4 versus 15.2 ± 2.4, Tukey's HSD $p = 0.044$).

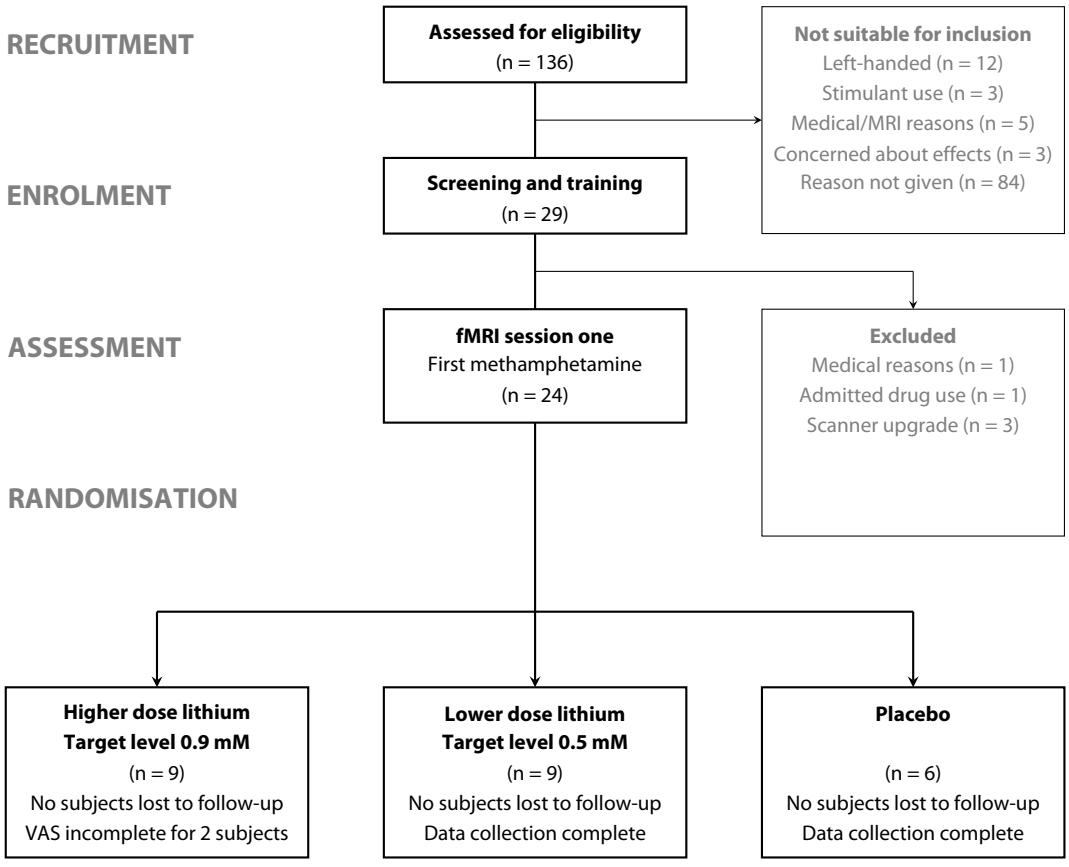

Figure 4.4: CONSORT diagram for the MRC-LAMP study.

	PLACEBO GROUP	LITHIUM GROUPS	
		LOWER DOSE	HIGHER DOSE
CHARACTERISTICS			
Age (years)	25.4 ± 4.0	23.3 ± 5.5	21.2 ± 1.8
Body mass index (kg/m^2)	24.3 ± 2.1	24.4 ± 2.1	24.6 ± 2.3
Handedness (right centile)	88.3 ± 15.1	80.0 ± 12.5	81.7 ± 12.5
Length of education (years)	18.0 ± 2.4	15.2 ± 2.4	15.8 ± 1.3
National Adult Reading Test	32.5 ± 5.0	35.2 ± 6.5	35.8 ± 3.6
Alcohol (units per week)	18.3 ± 9.1	17.4 ± 9.6	19.1 ± 14.8
Caffeine (cups per day)	1.5 ± 1.1	1.2 ± 0.8	1.6 ± 1.8
Cigarettes (per day)	0.0 ± 0.0	0.6 ± 1.7	1.3 ± 1.9
TREATMENT DETAILS			
Duration of treatment (days)	10.2 ± 1.5	10.4 ± 1.6	10.2 ± 1.6
Side effects (LISERS score)	1.3 ± 1.5	2.0 ± 2.2	5.4 ± 5.7
Priadel™ dose (mg per day)	—	911 ± 226	1511 ± 203
Serum lithium level (mM)	—	0.44 ± 0.18	0.85 ± 0.25

Table 4.1: Descriptive statistics (mean ± sd) according to group, for the subject characteristics and medication administered in the MRC-LAMP study. Formal statistical comparisons are presented in the body of the text. Lithium group: higher dose (n = 9), lower dose (n = 9); placebo group (n = 6).

4.5.2 Medication regimes

By self-report, subjects took their tablets on the majority of days, with no individual missing more than one dose. The mean duration of the course of tablets was 10.3 ± 1.5 days (all subjects, n = 24), with no difference between the groups. In those who received lithium, this resulted in a mean serum level of 0.65 ± 0.3 mM (all subjects on lithium, n = 18). Those randomised to receive a higher dose of lithium had greater serum concentrations of lithium than the lower dose group (high dose group 0.85 ± 0.25 versus low dose group 0.44 ± 0.18 mM ; 2-sample t-test : 16 df, t 3.93, $p < 0.001$).

Side effects from the lithium/placebo tablets were few and rarely more than mild on the LISERS. A one-way between-group ANOVA of the LISERS scores showed a trend-level difference (2 df, F = 3.56, $p = 0.091$), ratings numerically greatest in the higher dose lithium group. On no occasion were side effects sufficient to prevent a subject from completing their course, and no serious adverse events were reported. All subjects tolerated the methamphetamine injections, with no adverse events observed.

4.6 RESULTS – NEUROPSYCHOLOGICAL

4.6.1 Sustained attention – practice effects

A complete series of results from the three training sessions was available for 23 of the 24 subjects, one not completing the second practice due to personal time constraints. For all measures, data from at least one session did not conform to a Gaussian distribution; for ease and uniformity, nonparametric tests were applied in all instances.

	PRACTICE SESSIONS			FMRI
	P1	P2	P3	1A
RVIP TASK CONDITION				
Hit rate (%)	67 ± 13	71 ± 16	78 ± 13	82 ± 14
False alarm rate (%)	0.50 ± 0.7	0.84 ± 1.4	0.55 ± 0.7	0.32 ± 0.4
Sensitivity index (A')	0.91 ± 0.04	0.92 ± 0.06	0.94 ± 0.04	0.95 ± 0.04
Median response latency (ms)	398 ± 67	379 ± 49	358 ± 50	347 ± 46
CONTROL CONDITION				
Hit rate (%)	87 ± 6	87 ± 6	84 ± 7	90 ± 5
False alarm rate (%)	0.10 ± 0.2	0.10 ± 0.2	0.13 ± 0.2	0.10 ± 0.2
Sensitivity index (A')	0.97 ± 0.02	0.97 ± 0.02	0.96 ± 0.02	0.98 ± 0.01
Median response latency (ms)	416 ± 35	424 ± 40	426 ± 40	426 ± 43

Table 4.2: Descriptive analysis of performance in those completing all practice sessions (n = 23).

WITHIN-SUBJECT COMPARISONS

Summarising the analyses presented in this section, performance improved over the course of the three training sessions, stabilising by the time subjects entered the fMRI study proper (see table 4.2 above). For the control condition, performance was generally stable with only minor fluctuations in the measures during training. Thus, manipulation of performance on the tasks with methamphetamine was considered to reflect a change from a stable baseline. For the within-subject comparisons reported here, the Friedman repeated measures analysis entailed six comparisons; to maintain an overall alpha level of 0.05, significance was ascribed at $z \geqslant 2.63$ (2-sided), $p < 0.008$.

RVIP task condition Hit rate on the RVIP task condition differed over the sessions (Friedman test: χ-square 37.3, df 3, $p < 0.001$), increasing with practice. *Post-hoc* analysis controlling for multiple comparisons revealed a significant difference between the first and last training sessions (67 ± 13 versus 78 ± 13; z −3.88, 23 ranks, $p < 0.001$), but no difference between the final training and the baseline fMRI session. False alarm rates were low and somewhat variable, the difference detected across the sessions (Friedman test: χ-square 14.3, df 3, $p = 0.003$) due to the contrast between practice two and 1A (0.84 ± 1.4 versus 0.32 ± 0.4; z −2.64, 23 ranks, $p = 0.008$), there being no change between the final practice and the first scan session. As expected, the increase in A' closely matched that of the hit rate (Friedman test: χ-square 36.1, df 3, $p < 0.001$; practice one versus three: 0.91 ± 0.04 versus 0.94 ± 0.04; z −3.89, 23 ranks, $p < 0.001$). The average median response latency reduced by approximately 20 ms with each practice; not significant per increment but highly significant overall (practice one to three: 398 ± 67 versus 358 ± 50; z −3.41, 23 ranks, $p = 0.001$). Again, there was no significant difference between the last practice and the first fMRI session.

Control task condition Stability of performance in the control task condition was anticipated; it was observed for median response latency (Friedman test: χ-square 4.1, df 3, $p = 0.26$), false alarm rates (Friedman test: χ-square 2.2, df 3, $p = 0.54$) and to a lesser degree for hit rates (Friedman test: χ-square 7.6, df 3, $p = 0.06$). For the sensitivity index, A', performance was equivalent in the first two trials only, differing between the sessions because of a relatively poor performance during practice three (Friedman test: χ-square 12.7, df 3, $p = 0.005$). This translated to an increase when the A' data from the baseline scan session was compared to that from the final practice run (0.96 ± 0.02 versus 0.98 ± 0.01; z −3.42, 23 ranks, $p < 0.001$).

BETWEEN-TASK COMPARISONS

Comparing the control and RVIP task conditions, the hit rate and A' scores were higher, with false alarm rates lower for the control task during practices one, two and the first fMRI session ($z < -3$, 23 ranks, $p < 0.005$ in all instances). The significance

was absent or diminished in the final training run (RVIP task compared to control condition: hit rate Z −1.56, 23 ranks, $p = 0.12$; false alarm rate Z −2.31, 23 ranks, $p = 0.02$; sensitivity index Z −1.57, 23 ranks, $p = 0.12$). The average median response latency was significantly longer in the control condition during practices two, three and the initial scan session, but not practice one (RVIP task condition versus control condition, practice one: 398 ± 67 versus 416 ± 35; Z −1.66, 23 ranks, $p = 0.097$).

4.6.2 Sustained attention and methamphetamine

WITHIN-GROUP COMPARISON

In order to gauge the effects of methamphetamine on sustained attention, subjects were analysed as a single group with performance on all parameters compared before and after methamphetamine for both the RVIP and control task conditions. The mean values and analysis outcomes are presented in table 4.3, on the page that follows. The most marked effect was on response times, the average median response latency for the group falling by approximately 30 ms after methamphetamine in both task conditions. False alarm rate increased after methamphetamine in the RVIP task condition but not in the control condition, whilst hit rate and A' were unaltered.

RESPONSE TIME THRESHOLD

The effects of methamphetamine were largely as expected but the consistency in the reduction of response times raised an important point: if subjects were reacting more swiftly, could the threshold for the acceptance of responses be inappropriate? A threshold for acceptable response times is applied because there is a limit to how fast an individual can actually process a stimulus (see §3.2.1), with very swift responses usually representing chance occurrences or pre-emptive strikes. During the RVIP task condition subjects may be tempted to guess at correct responses, anticipating the completion of sequences; not so for the control condition in which response latency is a purer test of reaction time and criterion checking. A threshold of 125 ms is commonly used, the assumption being that it is unrealistic to expect or believe that a subject could

	TASK PERFORMANCE		WILCOXON S-R TEST		
	1A	1B	ranks	Z	*p*
RVIP TASK CONDITION					
Hit rate (%)	82 ± 14	83 ± 12	24	− 1.11	.268
False alarm rate (%)	0.30 ± 0.4	0.52 ± 0.6	24	− 2.16	.030
Sensitivity index (A')	0.95 ± 0.04	0.96 ± 0.03	24	− 0.85	.394
Median response latency (ms)	347 ± 45	312 ± 32	24	− 3.97	.000
CONTROL CONDITION					
Hit rate (%)	89 ± 5	89 ± 8	24	− 0.21	.833
False alarm rate (%)	0.13 ± 0.2	0.12 ± 0.2	24	− 0.09	.928
Sensitivity index (A')	0.98 ± 0.01	0.97 ± 0.02	24	− 1.08	.281
Median response latency (ms)	427 ± 42	400 ± 36	24	− 3.76	.000

Table 4.3: Within-group analysis of all subjects (n = 24) using the Wilcoxon Signed Ranks test to compare task performance pre (1A) and post (1B) methamphetamine (before the course of either lithium or placebo). Methamphetamine hastens responses and increases false alarm rates.

detect and respond to a stimulus in that time. The finding that methamphetamine reduced the response latency across the RVIP task and control conditions cast a doubt, suggesting a genuine hastening of reaction times. If upheld, valuable data may be being disregarded through the application of the standard threshold.

Exploring this matter, the data was re-examined using a lower threshold of 100 ms. The pattern of differences between the pre- and post-methamphetamine conditions was largely maintained, but false alarm rates no longer differed. In the data from sessions 1A and 1B, setting the threshold at 125 and 100 ms excluded 33 and 18 responses respectively. Of the responses preserved by lowering the threshold, the majority were in the RVIP task condition and mostly after methamphetamine had been given (see table 4.4). Whilst this would support a lowering of the threshold to embrace the hastened response times, an alternative explanation requires consideration – that subjects became 'trigger happy'. In keeping with this interpretation, the more inclusive 100 ms threshold yielded a greater false alarm rate; subjects were guessing incorrectly as well as correctly responding. This occurrence could be due to the stimulant changing the subjects' response style, but the proportion of responses excluded from sessions 1A and 1B was similar for each threshold. Thus, lowering the

	125 ms threshold		100 ms threshold	
Excluded responses	1A	1B	1A	1B
RVIP task condition	4	26	2	14
Control task condition	1	2	1	1

Table 4.4: When analysing task data a threshold is applied in order to exclude responses which reflect the anticipation of the completion of a sequence. Lowering the threshold to 100 ms permitted the inclusion of more responses, but the proportions pre- and post-methamphetamine remain unchanged.

threshold to 100 ms permitted the inclusion of guessed responses without specifically gauging an anticipated effect of methamphetamine. It was concluded that the 100 ms threshold was inappropriate and all data was analysed with a 125 ms threshold.

4.6.3 Sustained attention and medication combinations

After establishing a stable level of performance that was open to manipulation with methamphetamine, the hypothesis that lithium would attenuate the effects of the stimulant on sustained attention was examined. The neuropsychological task data from all 24 subjects was suitable for analysis, divided *a priori* into groups. Six subjects received placebo and 18 took lithium, with equal numbers in the high and low dose groups. For all measures the group data from at least one session in the envisaged comparisons did not conform to a Gaussian distribution and so nonparametric tests were applied in all instances.

Within-group comparisons

In the first instance, a within-group analysis across sessions for each measure of task performance on the RVIP and control conditions was performed using the Friedman test, the results of which are presented in tables 4.5 and 4.6. Where indicated, *post-hoc* analysis was undertaken using the Wilcoxon signed-rank test (table 4.7), with the number of comparisons restricted to three: 1A versus 1B; 2A versus 2B; 1A versus 2A. The results are described below and depicted in figures 4.5 to 4.10 (pages 105–106). With three comparisons, Bonferroni correction maintaining an overall alpha level of 0.05 ascribes significance at $z \geqslant 2.39$ (2-sided), $p < 0.017$.

	RVIP TASK PERFORMANCE				FRIEDMAN		
	1A	1B	2A	2B	df	χ^2	p
MEDIAN RL							
Placebo	347 ± 25	306 ± 18	337 ± 26	307 ± 34	3	12.20	.007
Lithium · all	348 ± 51	315 ± 35	361 ± 42	338 ± 37	3	25.13	.000
· low	340 ± 34	318 ± 37	359 ± 46	335 ± 40	3	11.53	.009
· high	356 ± 65	311 ± 35	364 ± 41	342 ± 35	3	15.00	.002
HIT RATE							
Placebo	80 ± 17	85 ± 14	83 ± 13	89 ± 10	3	9.87	.020
Lithium · all	82 ± 13	83 ± 11	77 ± 16	81 ± 17	3	8.84	.032
· low	80 ± 16	81 ± 12	75 ± 19	79 ± 21	3	6.72	.081
· high	84 ± 8	85 ± 11	78 ± 14	83 ± 12	3	2.59	.460
FALSE ALARM RATE							
Placebo	0.33 ± 0.5	0.67 ± 1.0	0.17 ± 0.4	0.33 ± 0.5	3	5.40	.145
Lithium · all	0.29 ± 0.4	0.48 ± 0.3	0.29 ± 0.5	0.44 ± 0.6	3	5.08	.166
· low	0.42 ± 0.4	0.51 ± 0.3	0.46 ± 0.7	0.71 ± 0.7	3	2.23	.526
· high	0.17 ± 0.2	0.44 ± 0.4	0.12 ± 0.2	0.17 ± 0.4	3	4.93	.177
SENSITIVITY INDEX							
Placebo	0.95 ± 0.05	0.96 ± 0.04	0.96 ± 0.03	0.97 ± 0.07	3	6.52	.089
Lithium · all	0.95 ± 0.03	0.96 ± 0.03	0.94 ± 0.04	0.95 ± 0.04	3	7.16	.067
· low	0.95 ± 0.04	0.95 ± 0.03	0.93 ± 0.05	0.95 ± 0.05	3	5.53	.137
· high	0.96 ± 0.02	0.96 ± 0.03	0.95 ± 0.03	0.96 ± 0.03	3	2.06	.561

Table 4.5: Group analysis for performance in the RVIP task condition. Data presented as mean ± sd, arranged by fMRI session (defined in §4.4.4). Response latency in ms, hit rate and false alarm rate as percentage. The Friedman test being the nonparametric equivalent of an ANOVA, the *post-hoc* comparisons are presented in the text.

Placebo group (n = 6) In the RVIP task condition, the average median response latency was reduced by methamphetamine before (1A versus 1B: Z −2.20, $p = 0.028$) and after (2A versus 2B: Z −2.20, $p = 0.028$) the course of placebo tablets, but the difference was not considered significant after correction for multiple comparisons. With methamphetamine, hit rates did not change significantly on either day (1A versus 1B: Z −1.83, $p = 0.068$; 2A versus 2B: Z −1.89, $p = 0.058$), the trend level differences explaining the Friedman results which prompted the *post-hoc* comparison. Group mean response times and accuracy measures did not differ for the pre-methamphetamine RVIP task condition before and after placebo (1A versus 2A), indicating a return to a stable baseline performance between the assessment days. *Post-hoc* comparisons were not indicated for false alarm rates or A' in the RVIP task condition, nor any of the control task measures.

	CONTROL TASK PERFORMANCE				FRIEDMAN		
	1A	1B	2A	2B	df	χ^2	p
MEDIAN RL							
Placebo	405 ± 44	381 ± 36	402 ± 41	392 ± 38	3	4.20	.241
Lithium · all	434 ± 40	407 ± 35	438 ± 42	412 ± 43	3	31.27	.000
· low	436 ± 40	420 ± 34	445 ± 38	430 ± 46	3	10.73	.013
· high	433 ± 43	394 ± 32	432 ± 47	395 ± 33	3	22.47	.000
HIT RATE							
Placebo	91 ± 4	93 ± 4	92 ± 5	91 ± 9	3	1.02	.797
Lithium · all	89 ± 6	87 ± 9	88 ± 7	87 ± 9	3	0.19	.979
· low	88 ± 6	86 ± 9	86 ± 8	86 ± 9	3	0.38	.945
· high	90 ± 5	88 ± 8	91 ± 7	91 ± 9	3	0.45	.930
FALSE ALARM RATE							
Placebo	0.11 ± 0.2	0.15 ± 0.3	0.07 ± 0.1	0.15 ± 0.1	3	1.38	.711
Lithium · all	0.14 ± 0.2	0.11 ± 0.1	0.25 ± 0.4	0.22 ± 0.3	3	2.30	.513
· low	0.15 ± 0.3	0.07 ± 0.1	0.32 ± 0.5	0.20 ± 0.4	3	2.87	.413
· high	0.12 ± 0.1	0.15 ± 0.2	0.17 ± 0.3	0.24 ± 0.3	3	1.01	.797
SENSITIVITY INDEX							
Placebo	0.98 ± 0.01	0.98 ± 0.01	0.97 ± 0.02	0.98 ± 0.03	3	1.47	.690
Lithium · all	0.97 ± 0.02	0.97 ± 0.02	0.97 ± 0.02	0.97 ± 0.02	3	2.03	.567
· low	0.97 ± 0.02	0.97 ± 0.02	0.96 ± 0.02	0.97 ± 0.02	3	2.73	.435
· high	0.97 ± 0.01	0.97 ± 0.02	0.98 ± 0.02	0.98 ± 0.01	3	0.87	.833

Table 4.6: Group analysis for performance in the control task condition. Data presented as mean ± sd, arranged by fMRI session (defined in §4.4.4). Response latency in ms, hit rate and false alarm rate as percentage. The Friedman test being the nonparametric equivalent of an ANOVA, the *post-hoc* comparisons are presented in the text.

Combined lithium group (n = 18) The average mean response latency in the RVIP task and control conditions shortened with methamphetamine on the first test day (1A versus 1B: RVIP task Z −3.29, $p = 0.001$; control task Z −3.29, $p = 0.001$). After the course of lithium the reduction in response time induced by methamphetamine remained and although somewhat diminished, the difference withstood correction for multiple comparisons (2A versus 2B: RVIP task Z −2.77, $p = 0.006$; control task Z −2.72, $p = 0.006$). Mean hit rates in the RVIP task condition did not alter with methamphetamine before or after the administration of lithium (1A versus 1B: Z −0.60, $p = 0.550$; 2A versus 2B: Z −1.90, $p = 0.057$). Examining the effects of lithium itself on the RVIP task condition (1A versus 2A), the average median response latency was prolonged (Z −2.46, $p = 0.014$) and the hit rate lower (Z −2.59, $p = 0.009$) following the course of tablets.

			Wilcoxon signed-rank		
			1A vs 1B	2A vs 2B	1A vs 2A
Placebo group					
RVIP task	· median response latency	z	−2.20	−2.20	−0.73
		p	.028	.028	.463
	· hit rate	z	−1.83	−1.89	−1.23
		p	.068	.058	.221
Lithium group – all subjects					
RVIP task	· median response latency	z	−3.29	−2.77	−2.46
		p	.001	.006	.014
	· hit rate	z	−0.59	−1.90	−2.59
		p	.550	.057	.009
Control	· median response latency	z	−3.29	−2.72	−0.89
		p	.001	.006	.372
Lithium group – higher dose					
RVIP task	· median response latency	z	−2.55	−2.07	−1.48
		p	.011	.038	.139
Control	· median response latency	z	−2.67	−2.67	−0.18
		p	.008	.008	.859
Lithium group – lower dose					
RVIP task	· median response latency	z	−2.07	−1.72	−1.96
		p	.038	.086	.051
Control	· median response latency	z	−1.84	−1.24	−1.24
		p	.066	.214	.214

Table 4.7: *Post-hoc* analysis for the Friedman tests performed in tables 4.5 and 4.6.

High dose lithium group (n = 9) The average mean response latency in the RVIP task condition shortened with methamphetamine on the first test day (1A versus 1B: RVIP task z −2.55, $p = 0.011$). Controlling for multiple comparisons, the lesser reduction in subjects' response times following a high dose of lithium failed to reach significance (2A versus 2B: RVIP task z −2.07, $p = 0.038$). For the control task condition, the reduction in the group mean response latency was marked and comparable during both assessment days. In this smaller group of subjects, lithium alone was no longer seen to prolong RVIP task condition response times (1A versus 2A: z −1.48, $p = 0.139$).

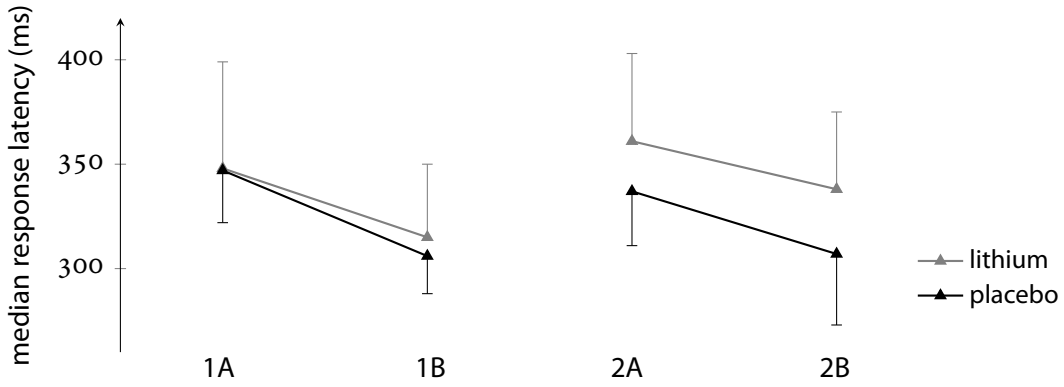

Figure 4.5: **Median response latency in the RVIP task condition**. Placebo versus combined lithium group values (mean ± sd) ordered by fMRI session (1A to 2B defined in section 4.4.4).

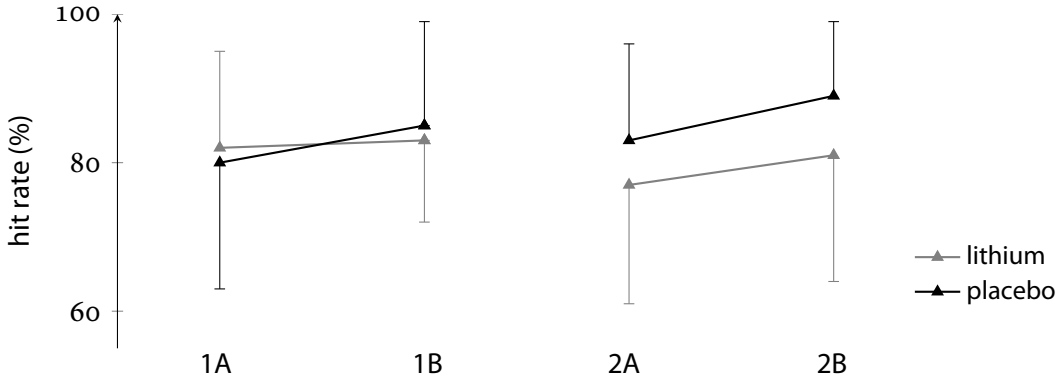

Figure 4.6: **Hit rates in the RVIP task condition**. Placebo versus combined lithium group values (mean ± sd) ordered by fMRI session (1A to 2B defined in section 4.4.4).

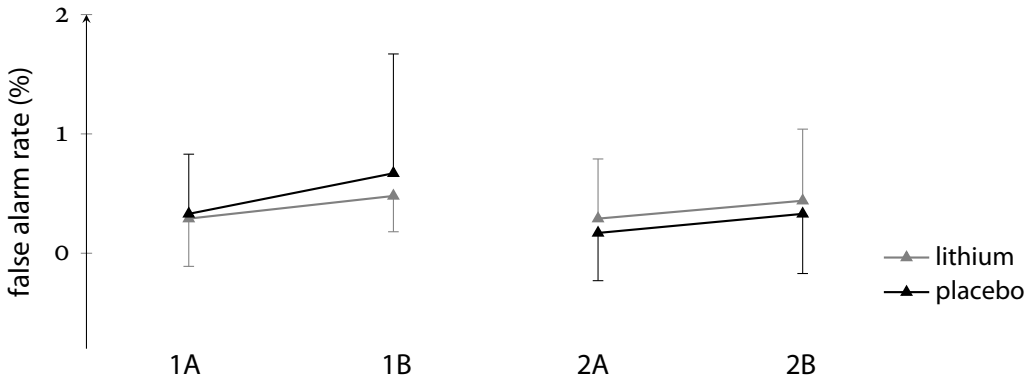

Figure 4.7: **False alarm rates in the RVIP task condition**. Placebo versus combined lithium group values (mean ± sd) ordered by fMRI session (1A to 2B defined in section 4.4.4).

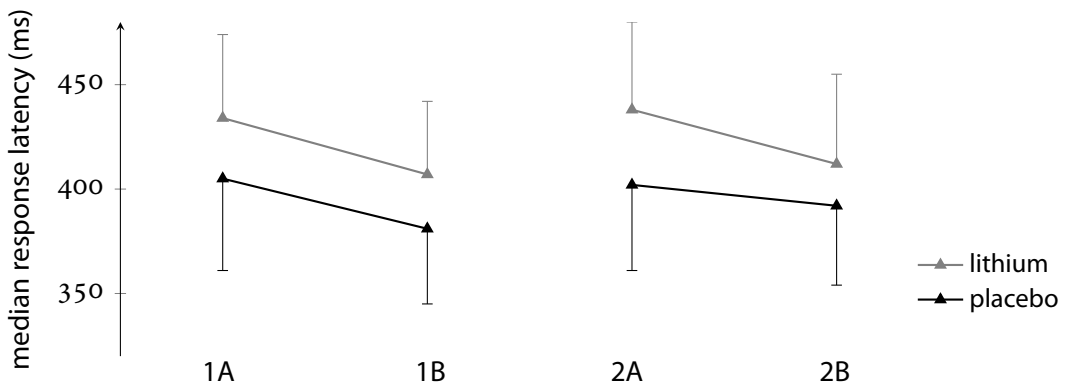

Figure 4.8: **Median response latency in the control task condition**. Placebo versus combined lithium group values (mean ± sd) ordered by fMRI session (1A to 2B defined in section 4.4.4).

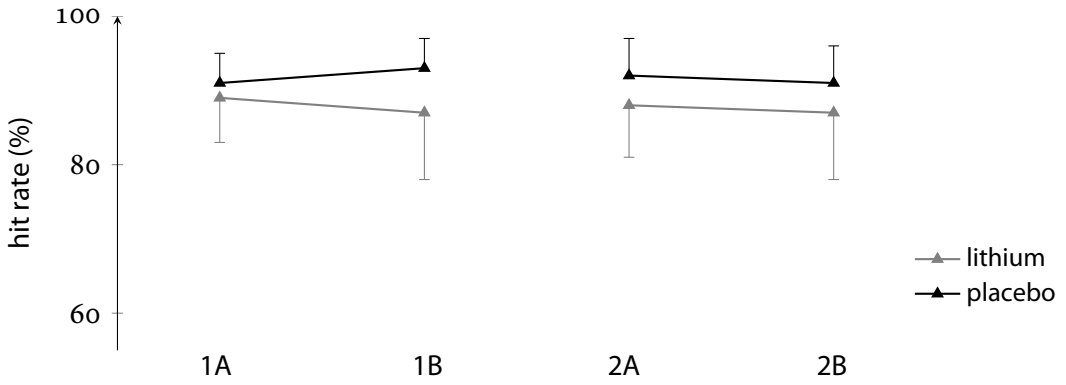

Figure 4.9: **Hit rates in the control task condition**. Placebo versus combined lithium group values (mean ± sd) ordered by fMRI session (1A to 2B defined in section 4.4.4).

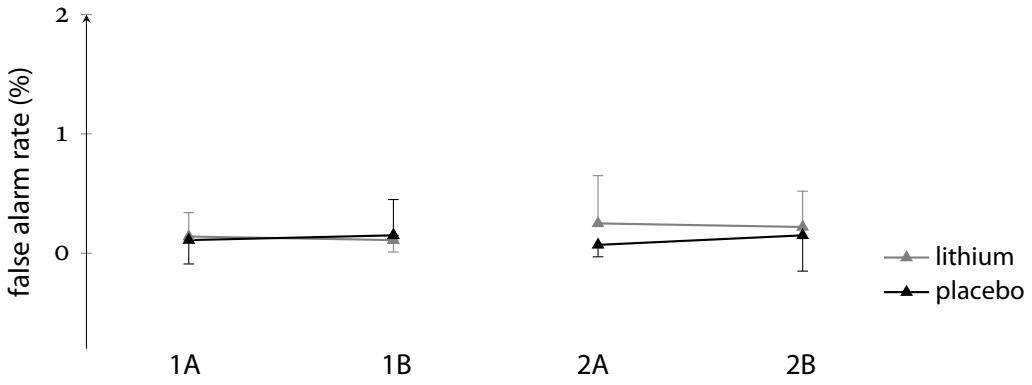

Figure 4.10: **False alarm rates in the control task condition**. Placebo versus combined lithium group values (mean ± sd) ordered by fMRI session (1A to 2B defined in section 4.4.4).

Low dose lithium group (n = 9) The results of the Friedman test showed that *post-hoc* analysis was indicated for mean response latency in the RVIP task and control conditions. Adjusting significance thresholds to control for multiple testing, no significant differences emerged in any of the comparisons.

INCREMENTAL CHANGE

A subsidiary analysis was undertaken comparing the percentage change in performance brought about by methamphetamine during the separate fMRI sessions for each group. The percentage change was calculated using equation 4.4.

$$\text{percentage change} = \frac{\text{value after} - \text{value before}}{\text{value before}} \times 100 \tag{4.4}$$

The percentage change in the median response latency was examined in the groups, separately for those randomised to receive placebo or lithium (subjects allocated to higher and lower doses were combined for this analysis). The methamphetamine-related reduction in median response latency was numerically smaller after subjects had taken the course of tablets, but not significantly so on within-group analysis (assessment day 1 versus assessment day 2: placebo group − 11.4% ± 5.9 versus − 9.0% ± 4.4, z −0.94, 6 ranks, $p = 0.345$; lithium group − 8.8% ± 8.0 versus − 6.1% ± 8.4, z −1.42, 18 ranks, $p = 0.157$). A between-group comparison (placebo versus lithium) showed no difference in the percentage change in median response latency on either occasion (assessment day 1: z −0.40, $p = 0.721$; assessment day 2: z −.867, $p = 0.415$).

When all the subjects who received lithium were analysed, the percentage change in hit rate induced by methamphetamine was greater after the course of lithium than before (assessment day 1 versus assessment day 2: 1.75% ± 10.7 versus 7.84% ± 18.5, z −2.37, 18 ranks, $p = 0.18$). Such a difference was not observed in the placebo group (assessment day 1 versus assessment day 2: 7.16% ± 11.7% versus 8.58 ± 12.3, z −2.37, 18 ranks, $p = 0.018$). Between-group comparisons showed no difference between those receiving lithium or placebo on either day.

4.7 RESULTS – SUBJECTIVE MEASURES

4.7.1 Subjective ratings

A complete set of results from the VAS ratings of mental state was available for 22 subjects, with two subjects excluded because of missing data on the second assessment day (both subjects received lithium). By way of clarification, the data collection points of 45, 90 and 135 minutes refer to the time after methamphetamine injection with the baseline assessment performed sometime during the hour before the scan began. The raw values grouped at these time points conformed to a Gaussian distribution and were analysed using a within-group comparison (ANOVA: VAS scores at baseline and 45, 90, and 135 minutes post-methamphetamine; separately for the lithium and placebo groups) followed by *post-hoc* testing controlling for multiple comparisons (Tukey's HSD test) with significance ascribed at $\alpha = 0.05$. When a difference between the baseline and a post-methamphetamine score emerged in *post-hoc* testing, the increment and the percentage change was calculated for each subjects. At the group level a comparison was made with the values between the same time points on the other study day using a paired *t*-test. If a difference to baseline was found at more than one time point, 45 and 90 minutes for example, a single comparison was made using the baseline to maxima.

Note that in terms of the anticipated effects of methamphetamine, the poles of the individual VAS domains can be considered as counterbalanced. After a stimulant, subjects are likely to place marks close to the anchors that convey a higher state of arousal. The relevant anchors fall at alternating poles of the score line so that subjects must consider each response rather than repeatedly placing marks on the same side of the page. To aid analysis and discussion, some VAS domains were reordered by inversion so that in all instances the pro-stimulant anchor represented the higher value. The order in which the domains are presented follows the arrangement of the VAS and not the magnitude of the findings. The VAS scores are expressed in millimetres (mm), with group data presented as the mean ± sd unless otherwise stated.

Raw scores equate to the distance from the left end of the line to the subject's mark. Consider the first two parameters, alert–drowsy and calm–excited. On the rating sheet, alert is on the left and excited on the right. A mark on alert–drowsy at 30 mm would become a score of 70, with the VAS domain description altered to drowsy–alert.

VAS measure (reordered)	Lithium group				Placebo group			
	Scan 1		Scan 2		Scan 1		Scan 2	
	F	*p*	F	*p*	F	*p*	F	*p*
Drowsy—Alert	7.81	.000	4.26	.009	0.41	.749	4.59	.013
Calm—Excited	3.46	.022	0.48	.693	0.31	.822	0.21	.889
Feeble—Strong	1.74	.168	2.42	.075	1.05	.392	2.77	.068
Muzzy—Clear headed	3.31	.026	1.58	.203	0.44	.724	2.05	.139
Clumsy—Well co-ordinated	0.63	.600	0.91	.440	1.82	.176	0.60	.626
Lethargic—Energetic	6.33	.001	2.06	.115	0.46	.715	3.30	.041
Discontented—Contented	0.34	.797	1.79	.160	0.57	.642	1.42	.268
Troubled—Tranquil	0.35	.787	0.23	.873	0.68	.575	0.27	.848
Mentally slow—Quick witted	6.97	.000	2.87	.044	2.12	.130	2.31	.107
Tense—Relaxed	0.97	.406	0.507	.679	0.48	.699	0.12	.945
Dreamy—Attentive	1.57	.207	1.02	.392	0.43	.733	1.88	.166
Incompetent—Proficient	5.21	.003	1.60	.200	0.35	.793	0.37	.777
Sad—Happy	0.53	.667	0.81	.494	0.85	.482	0.64	.600
Antagonistic—Amicable	0.48	.696	0.12	.950	0.27	.849	0.50	.688
Bored—Interested	0.64	.592	1.37	.262	0.18	.911	0.49	.693
Withdrawn—Gregarious	3.47	.022	1.57	.206	0.43	.732	0.34	.795

Table 4.8: Visual analogue scale scores spanning the period of methamphetamine administration submitted to ANOVA. Results are presented for placebo and lithium groups, before and after the period on medication.

Lithium group

Initially, seven VAS domains were sensitive to the effects of methamphetamine but after subjects received lithium, the difference in scores emerged for only two of these domains. The level of significance diminished for both measures and no new domains emerged as significant on the second assessment day (see table 4.8 above).

Drowsy—Alert On the first study day there was a difference between baseline and 45 minutes (61.3 ± 18.0 versus 85.9 ± 7.7, $p < 0.000$), 45 and 90 minutes (85.9 ± 7.7 versus 72 ± 13.7, $p = 0.050$), and 45 to 135 minutes (85.9 ± 7.7 versus 72.1 ± 16.1, $p = 0.042$). The findings were upheld on the second study day for baseline and 45 minutes (56.5 ± 24.5 versus 77.8 ± 15.2, $p = 0.008$) and baseline to 90 minutes only (56.5 ± 24.5 versus 73.6 ± 15.4, $p = 0.046$); see figure 4.11 on page 110. There was no significant difference in the baseline to 45 minute increment or percentage change in score, before and after lithium (increment in mm: 25.6 ± 19 versus 21.3 ± 22, t 0.91, 15 df, $p = 0.378$; percentage change: 57.7 ± 71 versus 61.3 ± 75, t −0.32, 15 df, $p = 0.754$).

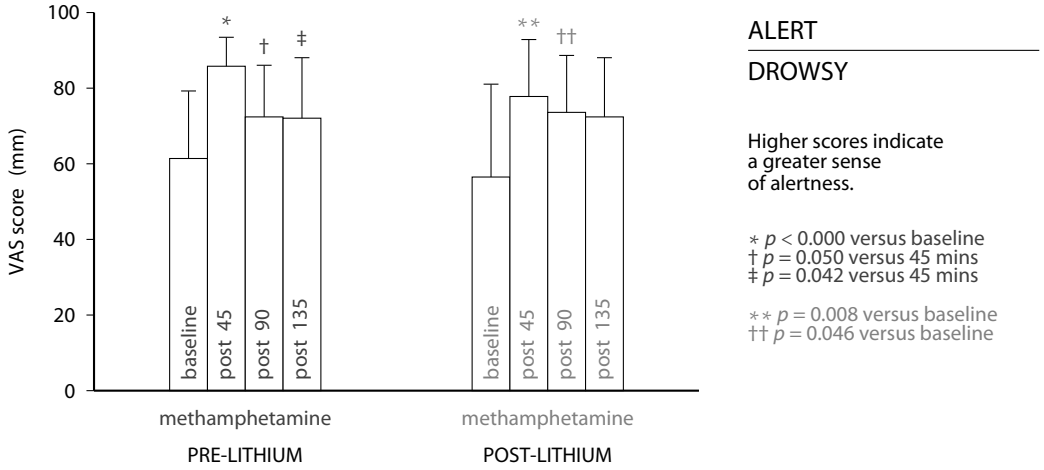

Figure 4.11: Visual analogue scale scores (mean ± sd) spanning methamphetamine administration for the alert–drowsy domain, before and after the course of lithium.

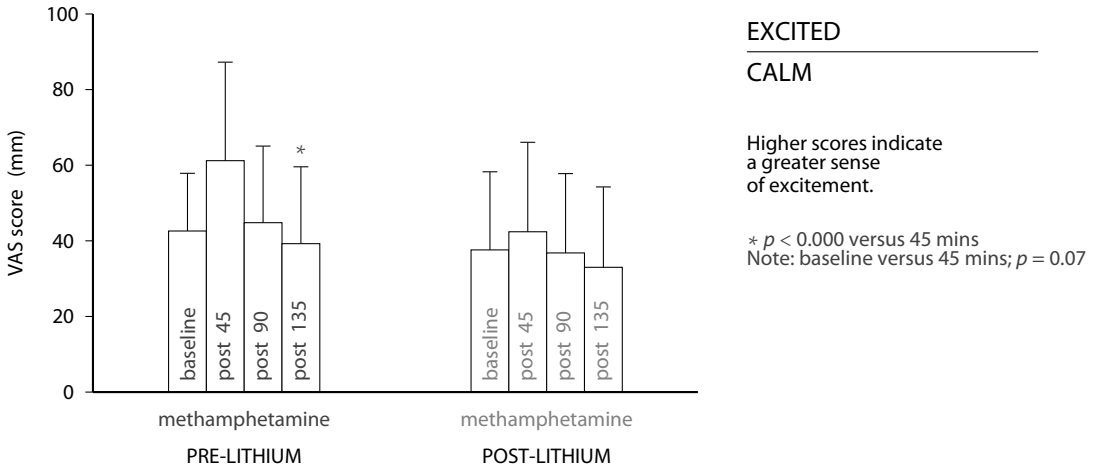

Figure 4.12: Visual analogue scale scores (mean ± sd) spanning methamphetamine administration for the calm–alert domain, before and after the course of lithium. This significant difference indicated by the asterisk pertains to the decrease in scores between the 45 and 135 minute time points.

Calm—Excited In the *post-hoc* analysis, the only comparison to emerge as significant on the first day was between 45 and 135 minutes (61.2 ± 26.1 versus 39.3 ± 20.5, p = 0.022), though a trend-level difference was observed between baseline and 45 minutes (42.7 ± 15.4 versus 61.2 ± 26.1, p = 0.070); see figure 4.12 on the previous page. There was a significant difference in the baseline to 45 minute increment before and after lithium (18.5 ± 26 versus 4.69 ± 24, t 2.31, 15 df, p = 0.036), consistent with lithium attenuating the effects of methamphetamine. This was not upheld when the percentage change in VAS score was examined, before and after lithium (54.0 ± 71 versus 31.2 ± 77, t 1.00, 15 df, p = 0.332).

Muzzy—Clear-headed Following methamphetamine, subjects reported feeling more clear-headed, with baseline scores differing to those at 90 minutes only (56.6 ± 18.7 versus 73.9 ± 16.3, p = 0.018). The difference was no longer present when methamphetamine was given after the course of lithium carbonate (see figure 4.13 on the following page). There was no significant difference in the baseline to 90 minute increment or percentage change in score, before and after lithium (increment in mm: 17.3 ± 18 versus 14.5 ± 20, t 0.55, 15 df, p = 0.593; percentage change: 42.6 ± 57 versus 53.2 ± 83, t −0.70, 15 df, p = 0.492).

Lethargic—Energetic Subjects felt energised after first receiving methamphetamine; compared to baseline scores, ratings were higher at 45 minutes (50 ± 19.7 versus 77.3 ± 17.2, p < 0.000) and 90 minutes (50 ± 19.7 versus 67.8 ± 21.0, p = 0.035), but not thereafter. This pattern apparently dampened post-lithium. There was a trend level difference in the baseline to 45 minute increment before and after lithium (27.3 ± 26 versus 14.8 ± 24, t 1.97, 15 df, p = 0.068), consistent with lithium attenuating the effects of methamphetamine (figure 4.14 on the following page). No difference was observed in the percentage change in VAS between these time points, before and after lithium (79.5 ± 83 versus 79.9 ± 152, t −0.02, 15 df, p = 0.988).

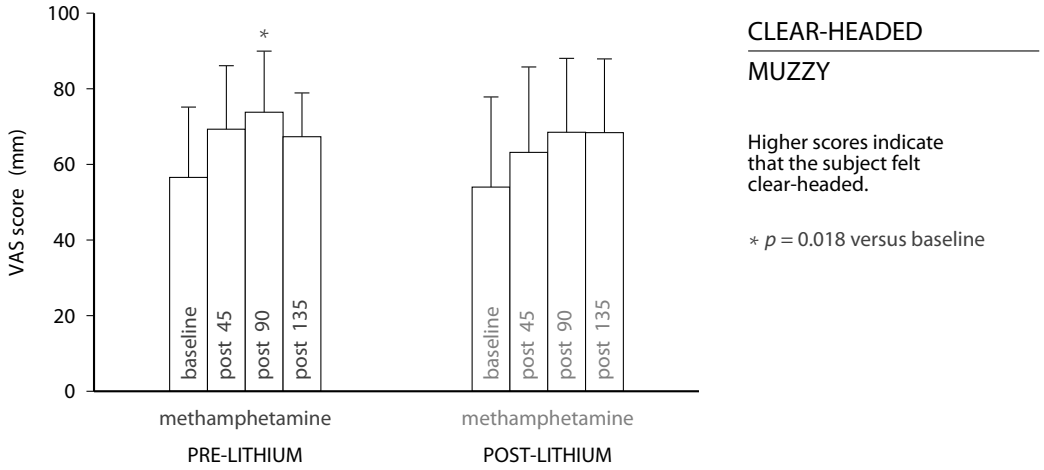

Figure 4.13: Visual analogue scale scores (mean ± sd) spanning methamphetamine administration for the muzzy–clear-headed domain, before and after the course of lithium.

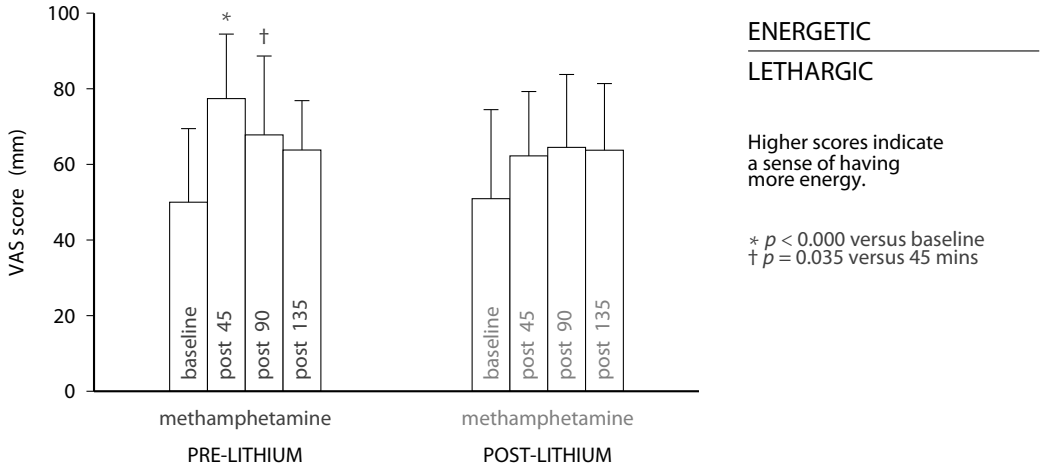

Figure 4.14: Visual analogue scale scores (mean ± sd) spanning methamphetamine administration for the lethargic–energetic domain, before and after the course of lithium.

Mentally slow—Quick-witted Compared to baseline on the first day, ratings swung toward the quick-witted anchor with methamphetamine, reaching significance at 45 minutes (57.6 ± 16.2 versus 81.5 ± 16.5, $p < 0.000$) and 90 minutes (57.6 ± 16.2 versus 72.4 ± 14.0, $p = 0.040$). The values during the final VAS rating approximated to baseline scores, resulting in a significant reduction when the 45 minute assessment was compared to 135 minutes (81.5 ± 16.5 versus 65.8 ± 14.7, $p = 0.026$). The ANOVA applied to the data from the second assessment day indicated a significant effect of methamphetamine, but *post-hoc* analysis revealed only trend-level differences between baseline and 45 minutes (55 ± 23.7 versus 71 ± 14.5, $p = 0.067$), and baseline to 135 minutes (55 ± 23.7 versus 71.1 ± 15.0, $p = 0.066$); see figure 4.15. There was no difference in the baseline to 45 minute increment or percentage change in score, before and after lithium (increment in mm: 24.9 ± 22 versus 15.8 ± 23, t 1.22, 15 df, $p = 0.240$; percentage change: 53.6 ± 60 versus 61.9 ± 102, t −0.37, 15 df, $p = 0.714$).

Incompetent—Proficient Following methamphetamine, subjects reported feeling more proficient; compared to baseline, ratings were significantly higher at 45 minutes (57.8 ± 19.7 versus 78.1 ± 16.1, $p = 0.002$) and 90 minutes (57.8 ± 19.7 versus 73.8 ± 11.8, $p = 0.023$), sustained to a trend-level at 135 minutes (57.8 ± 19.7 versus 71.6 ± 12.7, $p = 0.066$). No significant differences were found on day two (figure 4.16). There was no significant difference in the baseline to 45 minute increment or percentage change in score, before and after lithium (increment in mm: 20.1 ± 18 versus 13.0 ± 20, t 1.42, 15 df, $p = 0.175$; percentage change: 50.2 ± 58 versus 34.4 ± 54, t 0.97, 15 df, $p = 0.714$).

Withdrawn—Gregarious Comparing baseline scores to those following methamphetamine, subjects felt more outgoing at 45 minutes only (61.8 ± 13.5 versus 77.3 ± 15.5, $p = 0.016$). No difference was observed between any of the assessments performed after the course of lithium carbonate (figure 4.17 on page 115). There was no significant difference in the baseline to 45 minute increment or percentage change in score, before and after lithium (increment in mm: 15.4 ± 13 versus 10.7 ± 16, t 1.01, 15 df, $p = 0.329$; percentage change: 27.8 ± 27 versus 26.2 ± 43, t 0.13, 15 df, $p = 0.897$).

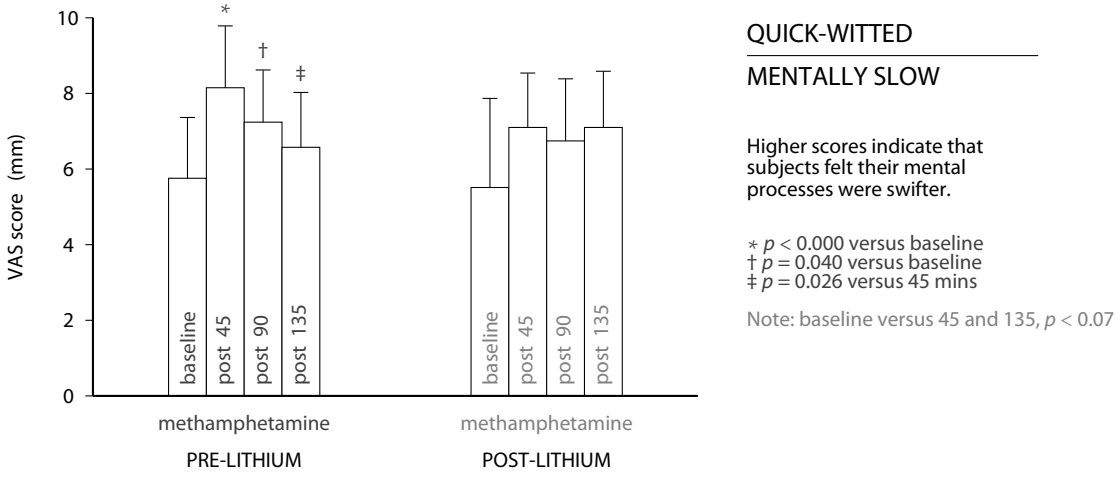

Figure 4.15: Visual analogue scale scores (mean ± sd) spanning methamphetamine administration for the quick-witted–mentally slow domain, before and after the course of lithium.

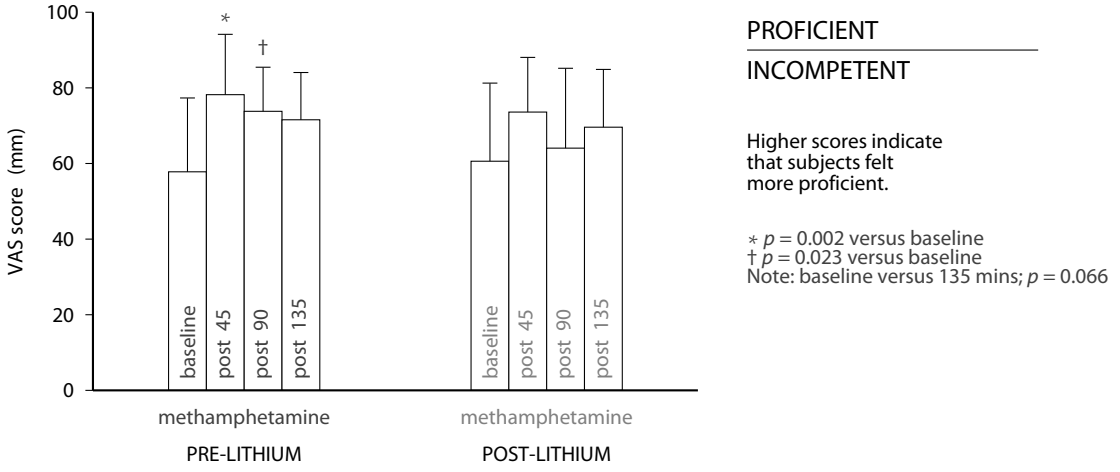

Figure 4.16: Visual analogue scale scores (mean ± sd) spanning methamphetamine administration for the proficient–incompetent domain, before and after the course of lithium.

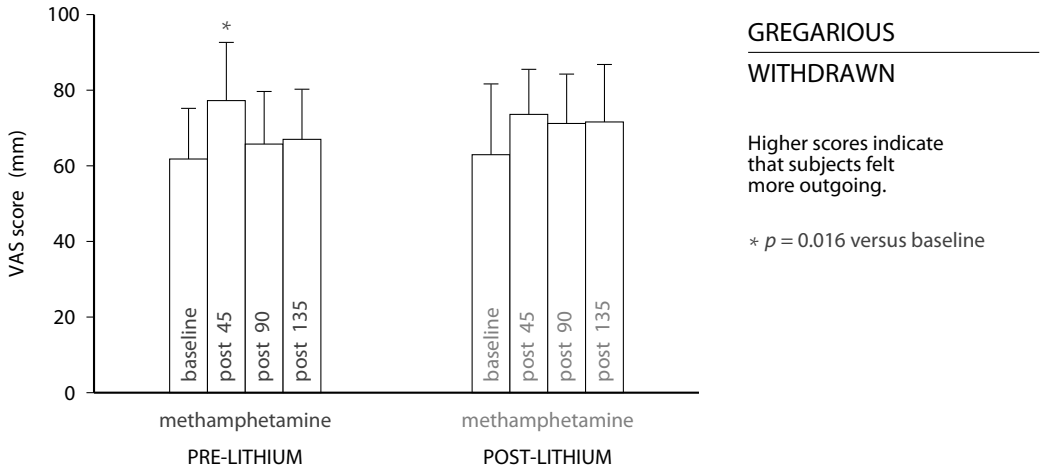

Figure 4.17: Visual analogue scale scores (mean ± sd) spanning methamphetamine administration for the gregarious–withdrawn domain, before and after the course of lithium.

PLACEBO GROUP

In the placebo group, differences in VAS scores attributable to methamphetamine were found only after the course of tablets, and for just two domains (table 4.8; page 109).

Drowsy—Alert On the second assessment only, methamphetamine increased feelings of alertness; compared to baseline, ratings were higher at 45 minutes (51.8 ± 22.7 versus 83.2 ± 10.6, $p = 0.012$), sustained to a trend-level at 90 minutes (51.8 ± 22.7 versus 76.2 ± 8.4, $p = 0.061$); see figure 4.18 on the next page. There was a trend-level increase in the baseline to 45 minute increment and percentage score change, before and after placebo (increment in mm: 4.50 ± 43 versus 31.5 ± 29, t −2.03, 5 df, $p = 0.098$; percentage change: 26.7 ± 92 versus 108.1 ± 133, t −2.08, 5 df, $p = 0.092$).

Lethargic—Energetic Subjects felt energised receiving methamphetamine on the second occasion; compared to baseline scores, ratings were higher at 45 minutes (52.4 ± 24.4 versus 78.4 ± 10.6, $p = 0.04$), but not thereafter (figure 4.19; page 116). There was no difference in the baseline to 45 minute increment or percentage change in score, before and after placebo (increment in mm: 0.17 ± 39 versus 25.7 ± 24, t −1.76, 5 df, $p = 0.138$; percentage change: 15.3 ± 77 versus 256.6 ± 560, t −1.07, 5 df, $p = 0.334$).

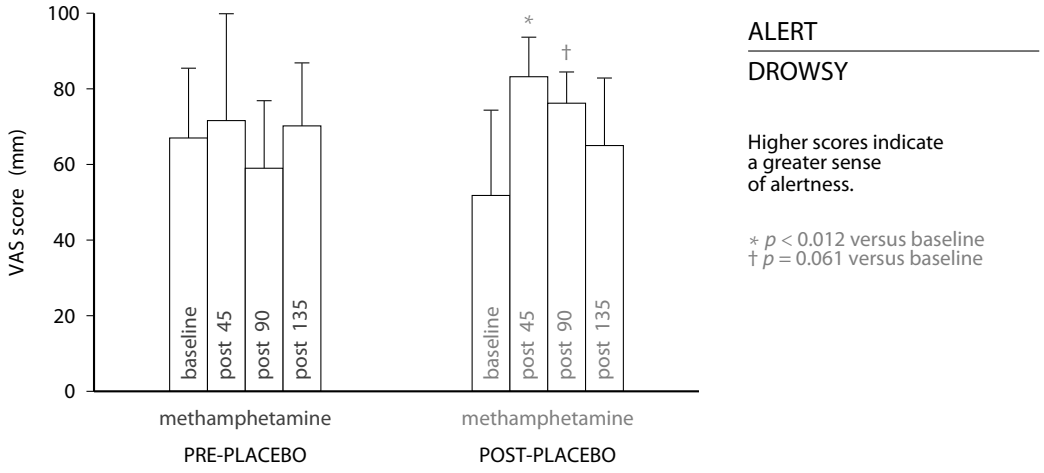

Figure 4.18: Visual analogue scale scores (mean ± sd) spanning methamphetamine administration for the alert–drowsy domain, before and after the course of placebo. Unlike the lithium group, significant differences emerged on the second assessment day, after the course of placebo.

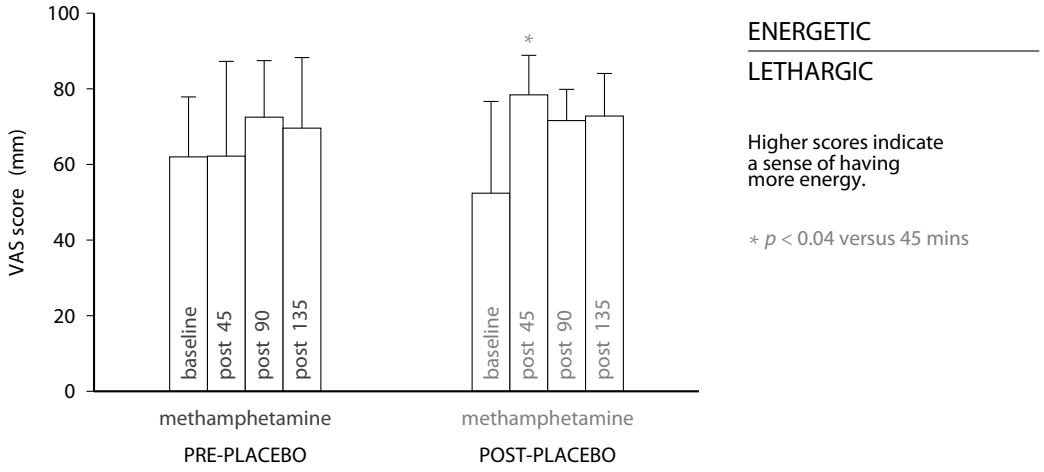

Figure 4.19: Visual analogue scale scores (mean ± sd) spanning methamphetamine administration for the energetic–lethargic domain, before and after the course of placebo. Unlike the lithium group, significant differences emerged on the second assessment day, after the course of placebo.

4.8 RESULTS – FUNCTIONAL IMAGING

4.8.1 Main effect of task

In order to establish the main areas of BOLD activation associated with the RVIP task, the RVIP-minus-control contrast data from session 1A for all subjects was submitted to analysis using a one-sample *t*-test. Deactivations were generated using the same first-level contrasts, but the second-level contrast was multiplied by −1 to create a control-minus-RVIP comparison.

ACTIVATIONS

Compared to the control task condition, performing the RVIP task resulted in regional activations in several brain areas, all of which demonstrated a bilateral distribution. The largest clusters were found in caudal brain regions, notably posterior parietal (right: 24 · −72 · 54) (left: −26 · −64 · 50) and temporal regions (right: 44 · −64 · 14) (left: −48 · −72 · 0). Smaller clusters of activation were observed in the dorsolateral frontal cortex (right: 48 · 2 · 36) (left: −50 · 10 · 30) and the medial aspect of the insula rostrally (right: 34 · 22 · −2) (left: −28 · 26 · 2). The results of this analysis are presented in their entirety in table 4.9 on the page that follows.

DEACTIVATIONS

Whilst performing the RVIP task condition, certain areas of the brain showed evidence of deactivation from their state in the control task condition. The most marked deactivation was in the left inferior parietal lobule (−52 · − 62 · 38), with a more diminutive cluster apparent on the right (52 · − 76 · 34). Deactivations occurring in the left hemisphere included the anterior (−8 · 54 · 0) and posterior (−8 · −46 · 34) regions of the cingulate cortex, and medial aspects of the prefrontal cortex (−8 · 58 · 34). Comparable changes on the right were not evident. The results of this analysis are presented in their entirety in table 4.10 on page 119.

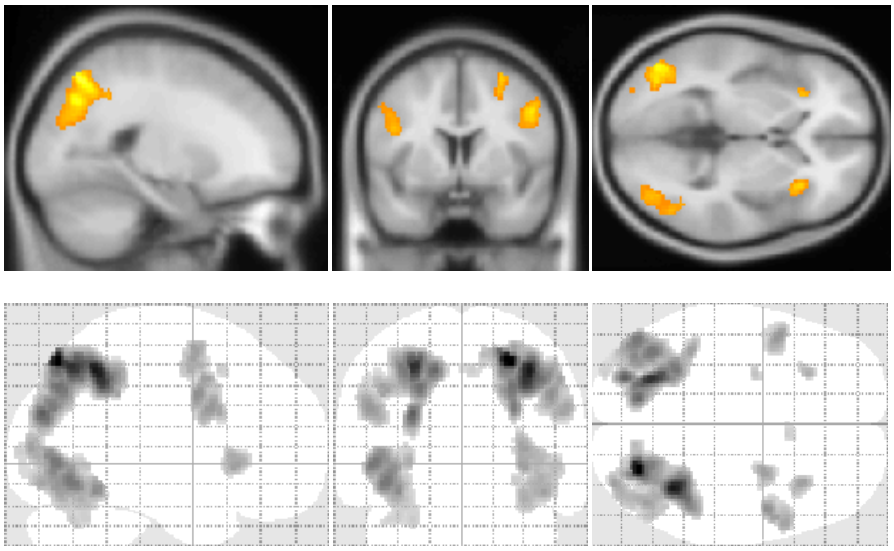

Table 4.9: **Main effect of RVIP task in all subjects: activations**; a random effects model one sample *t*-test, SPM{T_{23}}, was applied to all subjects using the *RVIP-minus-control contrast* from session 1A (family-wise-error correction $p < 0.05$). The images above depict the clusters rendered onto the ICBM152 T_1 template (sagittal view to the left of the midline), together with a glass brain projection.

CLUSTER-LEVEL				PEAK-LEVEL					LOCATION		
p_{FWE}	p_{FDR}	k_E	p_{UNC}	p_{FWE}	p_{FDR}	T	Z	p_{UNC}	x	y	z
.000	.000	1906	.000	.000	.001	13.40	7.01	.000	24	−72	54
				.000	.001	12.47	6.80	.000	36	−52	48
				.000	.016	9.55	6.01	.000	28	−70	40
.000	.000	1415	.000	.000	.002	11.64	6.60	.000	−26	−64	50
				.000	.012	10.16	6.20	.000	−26	−80	26
				.000	.012	10.14	6.19	.000	−22	−70	54
.000	.000	1473	.000	.000	.016	9.44	5.98	.000	−48	−72	0
				.000	.016	9.39	5.98	.000	−40	−64	−10
				.000	.032	8.87	5.79	.000	−38	−74	−4
.000	.000	408	.000	.001	.043	8.62	5.70	.000	48	2	36
				.001	.070	8.18	5.55	.000	52	6	44
				.002	.076	8.02	5.49	.000	56	12	28
.000	.000	274	.000	.001	.057	8.43	5.64	.000	−50	10	30
				.022	.440	6.66	4.92	.000	−52	6	40
.000	.000	171	.000	.001	.070	8.17	5.54	.000	28	2	58
				.003	.098	7.76	5.39	.000	24	−2	50
.000	.007	130	.000	.001	.070	8.15	5.53	.000	34	22	−2
.000	.000	1119	.000	.002	.070	8.10	5.52	.000	44	−68	−14
				.002	.070	8.10	5.52	.000	34	−86	8
				.003	.098	7.80	5.40	.000	34	−60	−18
.000	.004	44	.003	.003	.098	7.81	5.41	.000	−28	26	2
.000	.004	41	.004	.009	.220	7.16	5.14	.000	−28	−4	50
.001	.023	23	.023	.018	.392	6.77	4.97	.000	6	14	48

table shows 3 local maxima more than 8.0 mm apart

MAIN EFFECT OF TASK
ACTIVATIONS
ALL SUBJECTS
FWE_p: 6.210
FDR_p: 8.620
FWE_c: 23
FDR_c: 23

Height threshold: T = 6.21, p = 0.000 (0.050)
Extent threshold: k = 0 voxels, p = 1.000 (0.050)
Expected voxels per cluster, <k> = 4.170
Expected number of clusters, <c> = 0.05

Degrees of freedom = [1.0, 23.0]
FWHM = 13.1 12.9 13.3 mm; 6.6 6.4 6.7 voxel
Volume: 1319408 = 164926 vox = 540.9 resels
Voxel size: 2×2×2 mm; resel = 281.68 voxel

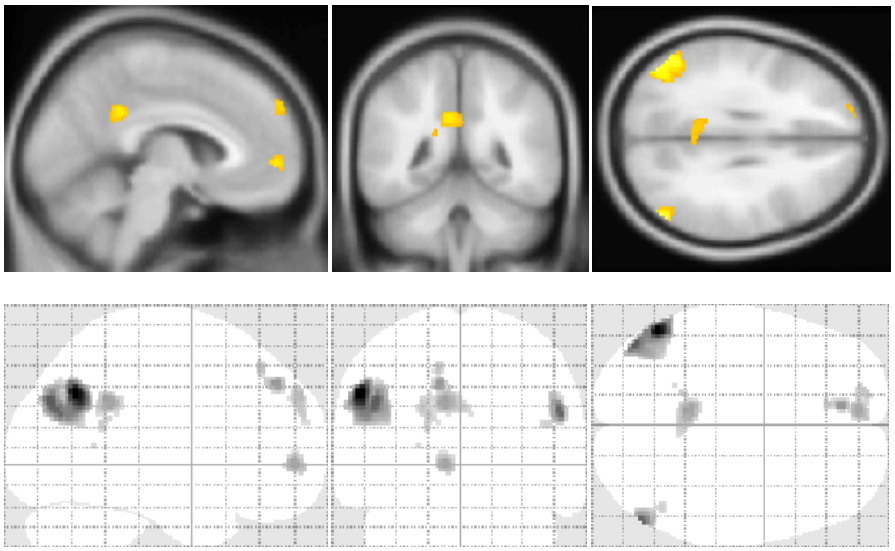

Table 4.10: **Main effect of RVIP task in all subjects: deactivations**; a random effects model one sample *t*-test, SPM{T_{23}}, was applied to all subjects using the *control-minus-RVIP contrast* from session 1A (family-wise-error correction $p < 0.05$). The images above depict the clusters rendered onto the ICBM152 T_1 template (sagittal view to the left of the midline), together with a glass brain projection.

CLUSTER-LEVEL				PEAK-LEVEL					LOCATION		
p_{FWE}	p_{FDR}	k_E	p_{UNC}	p_{FWE}	p_{FDR}	T	Z	p_{UNC}	x	y	z
.000	.000	549	.000	.000	.002	11.46	6.56	.000	−52	−62	38
				.000	.031	9.23	5.91	.000	−44	−76	34
.000	.000	96	.000	.000	.031	8.98	5.83	.000	52	−72	28
				.014	.457	6.90	5.03	.000	48	−72	36
.000	.001	57	.001	.003	.190	7.79	5.40	.000	−10	44	42
				.014	.457	6.88	5.02	.000	−12	38	50
.000	.000	166	.000	.004	.191	7.61	5.33	.000	−8	−46	34
.000	.001	70	.000	.004	.191	7.53	5.29	.000	−8	54	0
.000	.000	78	.000	.009	.361	7.12	5.12	.000	−8	58	34
				.017	.494	6.79	4.98	.000	−20	58	28
.009	.204	7	.181	.023	.550	6.62	4.90	.000	−18	−48	20
.005	.128	11	.099	.027	.593	6.55	4.87	.000	48	−60	22
.032	.627	1	.627	.042	.842	6.30	4.75	.000	−22	−52	10

table shows 3 local maxima more than 8.0 mm apart

MAIN EFFECT OF TASK
DEACTIVATIONS
ALL SUBJECTS
FWE_p: 6.210
FDR_p: 8.964
FWE_c: 1
FDR_c: 57

Height threshold: T = 6.21, p = 0.000 (0.050)
Extent threshold: k = 0 voxels, p = 1.000 (0.050)
Expected voxels per cluster, <k> = 4.170
Expected number of clusters, <c> = 0.05

Degrees of freedom = [1.0, 23.0]
FWHM = 13.1 12.9 13.3 mm; 6.6 6.4 6.7 voxel
Volume: 1319408 = 164926 vox = 540.9 resels
Voxel size: 2×2×2 mm; resel = 281.68 voxel

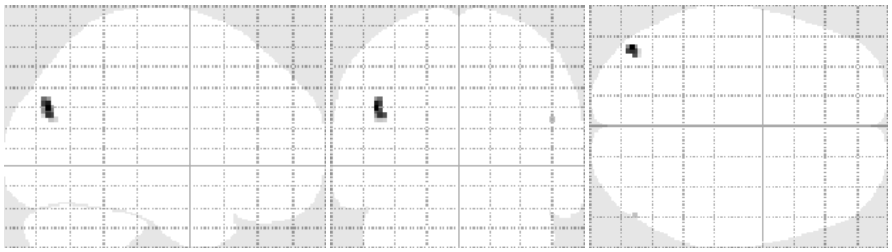

Table 4.11: **Effects of methamphetamine in all subjects – 'post-dose' minus 'pre-dose'** (1B − 1A); results of a random-effects paired *t*-test incorporating all subjects, SPM{T_{23}}, the *RVIP-minus-control contrasts* pre-methamphetamine subtracted from those post-methamphetamine (family-wise-error correction $p < 0.05$). The accompanying figure shows the clusters in the glass-brain projection.

CLUSTER-LEVEL				PEAK-LEVEL					LOCATION		
p FWE	p FDR	k_E	p UNC	p FWE	p FDR	T	Z	p UNC	x	y	z
.001	.021	27	.010	.021	.750	6.73	4.95	.000	−44	−76	30
.030	.602	1	.602	.044	.883	6.32	4.76	.000	50	−74	24

ALL SUBJECTS
SUBTRACTION
1B − 1A
FWE_p: 6.256
FDR_p: ∞
FWE_c: 1
FDR_c: 27

Height threshold: T = 6.26, p = 0.000 (0.050)
Extent threshold: k = 0 voxels, p = 1.000 (0.050)
Expected voxels per cluster, <k> = 3.672
Expected number of clusters, <c> = 0.05

Degrees of freedom = [1.0, 23.0]
FWHM = 12.5 12.6 12.8 mm; 6.3 6.3 6.4 voxel
Volume: 1304488 = 163061 vox = 593.4 resels
Voxel size: 2×2×2 mm; resel = 253.67 voxel

4.8.2 *Effects of methamphetamine*

The effects of methamphetamine on BOLD contrast were gauged by analysing the subjects as a single group. The RVIP-minus-control contrasts generated in the first level analysis of sessions 1A and 1B were submitted to a random effects analysis using a paired *t*-test. At the group level, the RVIP-minus-control contrasts before and after methamphetamine were compared by specifying two subtraction contrasts: session 1B–1A (post-minus-pre) and session 1A–1B (pre-minus-post). Thus, the regions of increased and decreased activation arising from methamphetamine were established.

SUBTRACTION ANALYSES

The 1B–1A comparison revealed two suprathreshold clusters; bilaterally in the inferior parietal lobules, the cluster on the left (−44 · −76 · 30) was larger than that on the right (50 · −74 · 24); see table 4.11 above. The 1A–1B comparison yielded no differences.

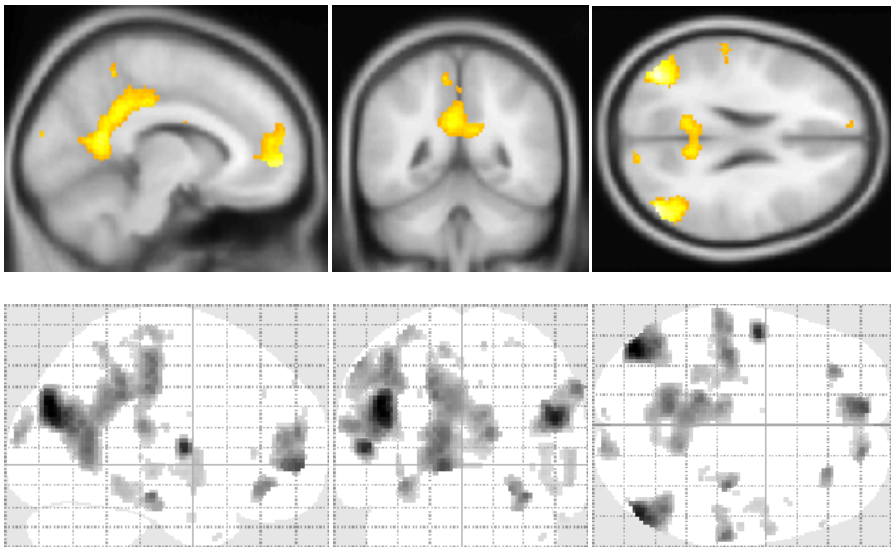

Table 4.12: **All subjects 'post' minus 'pre' methamphetamine in a lenient analysis** ($p < 0.001$ unc.); results of a random-effects paired *t*-test incorporating all subjects, SPM{T_{23}}, the *RVIP-minus-control contrasts* pre-methamphetamine subtracted from those post-methamphetamine ($p < 0.001$ unc.). The accompanying images depict the clusters rendered onto the ICBM152 T_1 template (sagittal view to the left of the midline), together with a glass brain projection.

CLUSTER-LEVEL				PEAK-LEVEL					LOCATION		
p FWE	p FDR	k_E	p UNC	p FWE	p FDR	T	Z	p UNC	x	y	z
.000	.000	773	.000	.021	.169	6.73	4.95	.000	−44	−76	30
				.259	.394	5.34	4.26	.000	−46	−68	20
.001	.001	489	.000	.044	.199	6.32	4.76	.000	50	−74	24
				.341	.394	5.16	4.17	.000	48	−60	22
.207	.100	113	.026	.074	.253	6.05	4.63	.000	−52	−4	8
.001	.001	473	.000	.178	.394	5.56	4.38	.000	−10	56	−2
				.369	.394	5.11	4.14	.000	−12	48	0
				.609	.401	4.74	3.92	.000	−12	50	12
.000	.000	1875	.000	.301	.394	5.24	4.21	.000	−12	−56	8
				.379	.394	5.10	4.13	.000	−14	−38	36
				.519	.401	4.87	4.00	.000	−14	−40	44
.500	.230	66	.079	.329	.394	5.19	4.18	.000	34	−22	−16
.000	.000	631	.000	.359	.394	5.13	4.15	.000	−38	−22	54
				.529	.401	4.85	3.99	.000	−36	−20	44
				.634	.401	4.70	3.90	.000	−54	−22	52
.091	.059	157	.011	.398	.394	5.06	4.11	.000	62	−24	40
				.935	.707	4.16	3.56	.000	54	−24	36
				.981	.834	3.95	3.42	.000	48	−24	30
.150	.078	130	.018	.492	.401	4.91	4.02	.000	14	56	16
				.987	.834	3.90	3.38	.000	8	56	10
.055	.041	185	.006	.580	.401	4.78	3.94	.000	−56	−26	20
				.998	.949	3.70	3.25	.001	−40	−22	16
.270	.124	99	.036	.778	.484	4.49	3.76	.000	12	−94	16
				.996	.945	3.76	3.29	.001	4	−94	12
.309	.133	92	.042	.956	.793	4.09	3.51	.000	−26	−40	−8
				.980	.834	3.96	3.42	.000	−28	−34	−14

table shows 3 local maxima more than 8.0 mm apart

ALL SUBJECTS SUBTRACTION 1B−1A
($p < 0.001$ UNC.)
FWE_p: 6.256
FDR_p: ∞
FWE_c: 473
FDR_c: 185

Height threshold: T = 3.48, p = 0.000 (0.050)
Extent threshold: k = 0 voxels, p = 1.000 (0.050)
Expected voxels per cluster, <k> = 21.666
Expected number of clusters, <c> = 8.80

Degrees of freedom = [1.0, 23.0]
FWHM = 12.5 12.6 12.8 mm; 6.3 6.3 6.4 voxel
Volume: 1304488 = 163061 vox = 593.4 resels
Voxel size: 2×2×2 mm; resel = 253.67 voxel

Subtracting the pre-methamphetamine from the post-methamphetamine data might be expected to yield areas of increased activation attributable to the stimulant. Considering the structure of the models and contrasts, such areas of apparent activation could actually represent a loss of deactivation. The clusters arising in the 1B–1A analysis performed with a family-wise-error correction threshold of $p < 0.05$ (presented in table 4.11) appeared to fall within the areas of deactivation seen in the main effect of the RVIP task analysis (table 4.10 on page 119). Lowering the threshold of the subtraction analysis ($p < 0.001$ uncorrected) demonstrated that this was the case (see table 4.12 on the previous page). Therefore, the RVIP-minus-control and control-minus-RVIP contrasts were examined in isolation for sessions 1A and 1B. This was achieved at the group-level in SPM8 by specifying a simple factorial second-level analysis using a single factor (RVIP-minus-control contrast) with two levels (before and after methamphetamine). This was a convenient way of performing what amounted to one-sample *t*-tests for the four conditions.

ACTIVATIONS

Submitting the RVIP-minus-control contrast to the factorial design, the areas of activation pre-methamphetamine matched those previously established for the main effect of the task (table 4.9); the comparison is essentially identical but the factorial model specifies potential comparisons, borne out as a greater number of degrees of freedom, smaller clusters and lower overall Z-scores (see table 4.13 on page 123). On visual inspection, the pattern of activation following methamphetamine appeared unchanged (see table 4.14 on page 124) – this excepting the appearance of a small cluster in the region of the left central sulcus ($-62 \cdot -16 \cdot 26$) and another in the right dorsolateral prefrontal cortex ($40 \cdot 40 \cdot 34$), neither of which survived comparison of sessions. Thus, the clusters emerging as significant in our paired *t*-test subtraction analysis (table 4.11) were not attributable to methamphetamine increasing BOLD contrast activations.

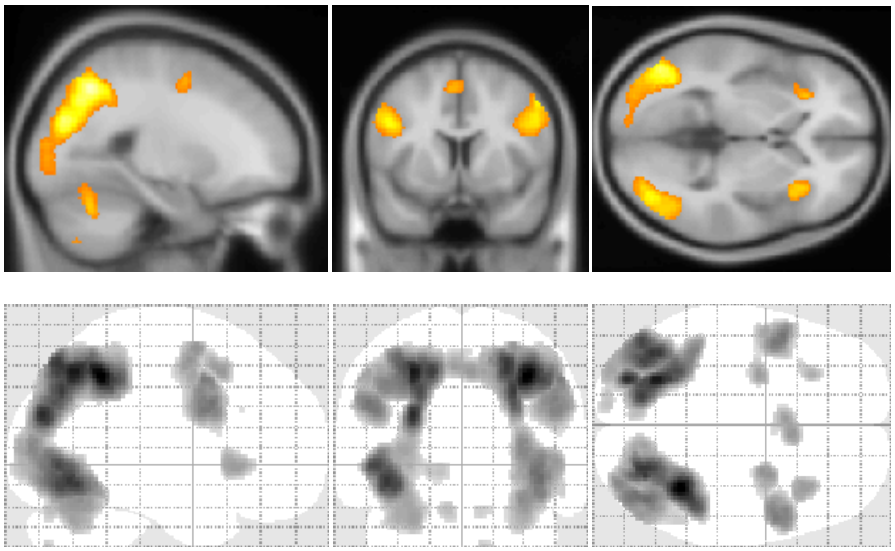

Table 4.13: **Task-related activations pre-methamphetamine** (all subjects, n = 24) — a group-wise analysis within a factorial design, SPM{T_{46}}, in a random effects model using the *RVIP-minus-control contrast* (1A activations, family-wise-error correction $p < 0.05$). The accompanying images depict the clusters rendered onto the ICBM152 T_1 template (sagittal view to the left of the midline), together with a glass brain projection.

CLUSTER-LEVEL				PEAK-LEVEL					LOCATION		
p FWE	p FDR	k_E	p UNC	p FWE	p FDR	T	Z	p UNC	x	y	z
.000	.000	5424	.000	.000	.000	11.99	∞	.000	36	−50	46
				.000	.000	10.21	7.34	.000	24	−70	50
				.000	.000	10.02	7.26	.000	28	−70	38
.000	.000	5210	.000	.000	.000	11.06	7.68	.000	−26	−64	48
				.000	.000	10.55	7.48	.000	−26	−80	26
				.000	.000	10.14	7.31	.000	−40	−66	−8
.000	.000	966	.000	.000	.000	8.32	6.47	.000	−50	10	32
				.000	.005	7.22	5.87	.000	−28	−4	52
				.000	.008	8.00	6.30	.000	50	0	46
.000	.000	728	.000	.000	.001	8.09	6.35	.000	52	6	44
				.000	.001	8.00	6.30	.000	50	6	34
				.000	.001	7.89	6.24	.000	50	12	28
.000	.000	277	.000	.000	.003	7.44	6.00	.000	28	2	60
.000	.000	272	.000	.000	.004	7.29	5.91	.000	6	14	48
				.000	.005	7.20	5.86	.000	−4	12	50
.000	.000	223	.000	.000	.005	7.20	5.86	.000	36	24	−2
.000	.002	83	.001	.001	.014	6.77	5.61	.000	−28	26	0
.000	.003	77	.002	.001	.026	6.54	5.47	.000	14	−76	−50
				.007	.155	5.92	5.08	.000	24	−76	−50
.000	.003	76	.002	.003	.066	6.23	5.28	.000	−8	−76	−22
.002	.052	27	.044	.010	.206	5.82	5.01	.000	10	−74	−24
.007	.158	13	.146	.010	.207	5.80	5.00	.000	−24	−72	−50
.036	.706	1	.706	.042	.835	5.31	4.67	.000	40	26	28

table shows 3 local maxima more than 8.0 mm apart

ALL SUBJECTS ACTIVATIONS 1A

FWE_p: 5.249
FDR_p: 6.545
FWE_c: 1
FDR_c: 73

Height threshold: T = 5.25, p = 0.000 (0.050)
Extent threshold: k = 0 voxels, p = 1.000 (0.050)
Expected voxels per cluster, <k> = 6.483
Expected number of clusters, <c> = 0.05

Degrees of freedom = [1.0, 46.0]
FWHM = 12.8 12.9 13.1 mm; 6.4 6.4 6.5 voxel
Volume: 1301856 = 162732 vox = 558.8 resels
Voxel size: 2×2×2 mm; resel = 268.79 voxel

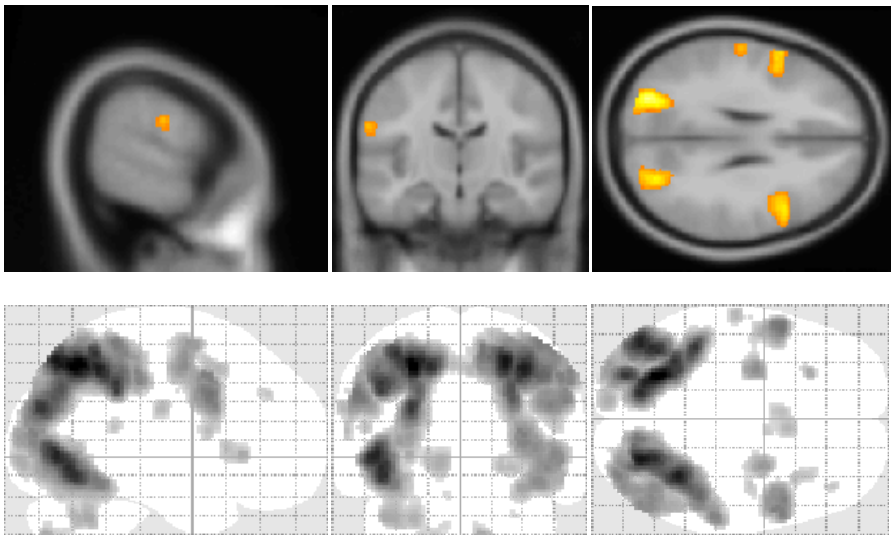

Table 4.14: **Task-related activations post-methamphetamine** (all subjects, n = 24) — a group-wise analysis within a factorial design, SPM{T_{46}}, in a random effects model using the *RVIP-minus-control contrast* (1B activations, family-wise-error correction $p < 0.05$). The accompanying images depict the clusters rendered onto the ICBM152 T_1 template (sagittal view to the left of the midline), together with a glass brain projection. Rendering emphasises the small cluster additional to the pattern seen in 1A on the previous page.

CLUSTER-LEVEL				PEAK-LEVEL					LOCATION		
p FWE	p FDR	k_E	p UNC	p FWE	p FDR	T	Z	p UNC	x	y	z
.000	.000	6723	.000	.000	.000	11.80	∞	.000	−26	−62	50
				.000	.000	10.64	7.52	.000	−46	−72	0
				.000	.000	10.36	7.40	.000	−16	−72	50
.000	.000	6520	.000	.000	.000	11.08	7.69	.000	24	−72	52
				.000	.000	10.78	7.57	.000	34	−50	48
				.000	.000	10.40	7.42	.000	24	−64	48
.000	.000	1027	.000	.000	.000	8.25	6.43	.000	−54	10	34
				.000	.002	7.58	6.08	.000	−30	−4	50
				.000	.058	6.30	5.32	.000	−60	8	14
.000	.000	787	.000	.000	.001	7.98	6.29	.000	54	10	42
				.000	.001	7.92	6.26	.000	48	12	28
				.000	.001	7.89	6.24	.000	56	10	30
.000	.001	112	.000	.000	.003	7.39	5.97	.000	12	−78	−46
.000	.000	254	.000	.000	.004	7.27	5.90	.000	28	−2	62
				.006	.122	6.01	5.14	.000	40	−8	52
.001	.016	47	.011	.001	.017	6.74	5.60	.000	−28	26	2
.000	.006	66	.003	.001	.034	6.50	5.45	.000	−62	−16	26
.000	.003	188	.000	.002	.045	6.40	5.38	.000	6	14	48
				.003	.076	6.19	5.26	.000	−4	10	50
				.009	.192	5.85	5.03	.000	8	2	56
.000	.001	114	.000	.003	.076	6.20	5.26	.000	36	18	4
.001	.038	33	.028	.005	.108	6.06	5.17	.000	−50	−42	16
.006	.151	15	.121	.005	.116	6.03	5.15	.000	40	40	34
.021	.480	4	.416	.034	.687	5.38	4.72	.000	−8	−72	−20
.025	.520	3	.485	.035	.687	5.38	4.71	.000	30	−64	−32
.036	.706	1	.706	.035	.687	5.38	4.71	.000	−60	−8	36

table shows 3 local maxima more than 8.0 mm apart

ALL SUBJECTS ACTIVATIONS 1B

FWE$_p$: 5.249
FDR$_p$: 6.397
FWE$_c$: 1
FDR$_c$: 33

Height threshold: T = 5.25, p = 0.000 (0.050)
Extent threshold: k = 0 voxels, p = 1.000 (0.050)
Expected voxels per cluster, <k> = 6.483
Expected number of clusters, <c> = 0.05

Degrees of freedom = [1.0, 46.0]
FWHM = 12.8 12.9 13.1 mm; 6.4 6.4 6.5 voxel
Volume: 1301856 = 162732 vox = 558.8 resels
Voxel size: 2×2×2 mm; resel = 268.79 voxel

DEACTIVATIONS

A striking difference was observed when the deactivations in sessions 1A and 1B were visualised, deactivations being the clusters emerging with the control-minus-RVIP contrast. The areas of deactivation emerging in session 1A within the factorial design (table 4.15 on page 126) largely matched those previously identified in the main effect of the RVIP task analysis (table 4.10). Following methamphetamine, suprathreshold deactivations all but disappeared (table 4.16; page 127). A single small cluster endured in the right posterior superior parietal region ($54 \cdot -70 \cdot 26$). It was concluded that subtracting the RVIP-minus-control contrasts in session 1A from those in 1B shows the brain regions in which methamphetamine has attenuated deactivation. The asymmetry of cluster volumes in emerging from that comparison most likely arose because of the persistence of deactivation in the right parietal region during session 1B.

CHARACTERISING THE DEACTIVATION CHANGE

The results thus far reported can, in the purest sense, be viewed as dichotomous: clusters either cross the determined threshold or they do not. With suprathreshold clusters, higher Z-scores are often taken as evidence of a greater degree of activation or deactivation, or at least a greater certainty that the activation or deactivation has occurred. When a previously activated or deactivated region falls below the threshold, nothing more can be said of it without conducting subsidiary analyses. The apparent abolition of deactivation following methamphetamine may be just that; it could also be a modest diminution to below threshold or a reversal to regional activation.

With the SPM MARSBAR toolbox, regions of interest were defined using the clusters of significance emerging as deactivations during in session 1A (left and right IPL, cingulate cortex and medial PFC). Statistical scores for each ROI were extracted from sessions 1A and 1B (essentially the first-level control-minus-RVIP contrasts pre- and post-methamphetamine, examined separately; table 4.17). The T-score deflection was reduced by methamphetamine in every ROI, but scores all remained negative. Methamphetamine thus diminished the deactivations to below the level of significance, but it did not abolish them or reverse the signal change to that of activation.

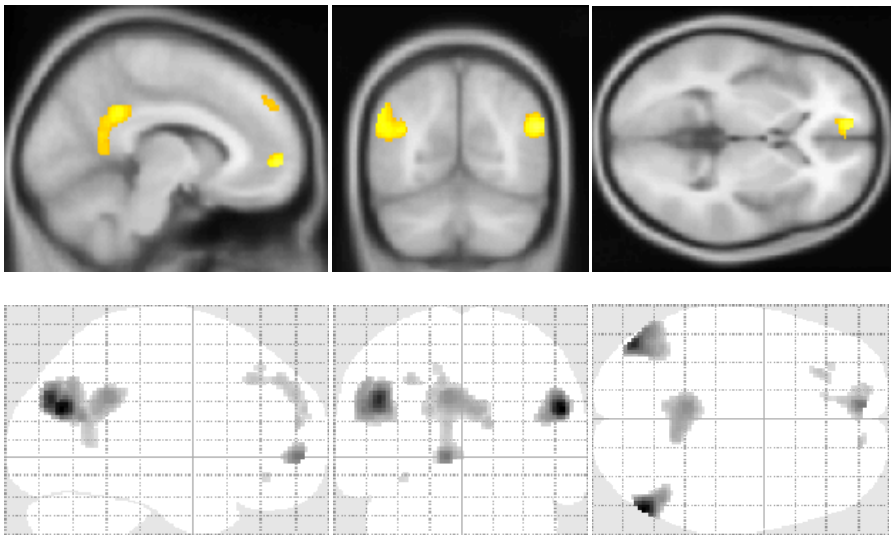

Table 4.15: **Task-related deactivations pre-methamphetamine** (all subjects, n = 24) — a group-wise analysis within a factorial design, SPM{T_{46}}, in a random effects model using the *control-minus-RVIP contrast* (1A deactivations, family-wise-error correction $p < 0.05$). The accompanying images depict the clusters rendered onto the ICBM152 T_1 template, together with a glass brain projection.

CLUSTER-LEVEL				PEAK-LEVEL					LOCATION		
p FWE	p FDR	k_E	p UNC	p FWE	p FDR	T	Z	p UNC	x	y	z
.000	.000	326	.000	.000	.000	9.48	7.02	.000	54	−70	26
				.001	.041	6.80	5.63	.000	48	−60	22
.000	.000	639	.000	.000	.000	8.64	6.63	.000	−44	−76	32
				.000	.018	7.14	5.83	.000	−52	−68	26
.000	.001	94	.001	.000	.018	7.18	5.85	.000	−8	56	0
.000	.000	618	.000	.001	.041	6.72	5.58	.000	−8	−44	30
				.002	.116	6.29	5.32	.000	6	−50	26
				.008	.292	5.87	5.04	.000	−8	−56	18
.007	.171	14	.133	.008	.292	5.89	5.06	.000	14	56	20
.000	.000	145	.000	.009	.292	5.85	5.03	.000	−12	54	34
				.010	.292	5.82	5.01	.000	−10	46	42
				.011	.296	5.77	4.98	.000	−16	60	26
.002	.061	28	.041	.011	.296	5.79	4.99	.000	−28	32	42
				.041	.822	5.32	4.67	.000	−22	38	40
.014	.315	7	.280	.029	.640	5.44	4.76	.000	−12	36	48
.018	.362	5	.362	.031	.642	5.42	4.74	.000	−32	38	−12

table shows 3 local maxima more than 8.0 mm apart

ALL SUBJECTS DEACTIVATIONS 1A

FWE_p: 5.249
FDR_p: 6.681
FWE_c: 5
FDR_c: 94

Height threshold: T = 5.25, p = 0.000 (0.050)
Extent threshold: k = 0 voxels, p = 1.000 (0.050)
Expected voxels per cluster, <k> = 6.483
Expected number of clusters, <c> = 0.05

Degrees of freedom = [1.0, 46.0]
FWHM = 12.8 12.9 13.1 mm; 6.4 6.4 6.5 voxel
Volume: 1301856 = 162732 vox = 558.8 resels
Voxel size: 2×2×2 mm; resel = 268.79 voxel

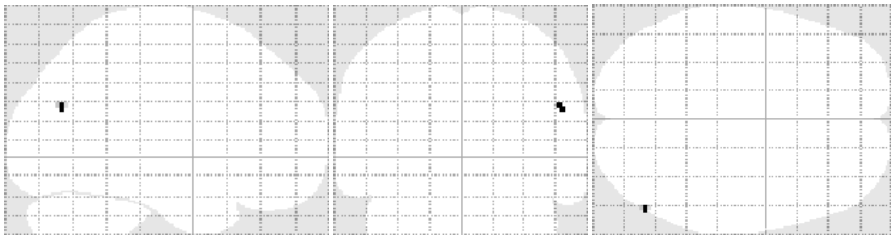

Table 4.16: **Task-related deactivations post-methamphetamine** (all subjects, n = 24) — a group-wise analysis within a factorial design, SPM{T_{46}}, in a random effects model using the *control-minus-RVIP contrast* (1B deactivations, family-wise-error correction $p < 0.05$). The accompanying figure shows the clusters in the glass-brain projection.

CLUSTER-LEVEL				PEAK-LEVEL					LOCATION		
p_{FWE}	p_{FDR}	k_E	p_{UNC}	p_{FWE}	p_{FDR}	T	Z	p_{UNC}	x	y	z
.021	.416	4	.416	.020	.386	5.58	4.85	.000	54	−70	26

ALL SUBJECTS
DEACTIVATIONS
1B

FWE_p: 5.249
FDR_p: ∞
FWE_c: 4
FDR_c: ∞

Height threshold: T = 5.25, p = 0.000 (0.050)
Extent threshold: k = 0 voxels, p = 1.000 (0.050)
Expected voxels per cluster, <k> = 6.483
Expected number of clusters, <c> = 0.05

Degrees of freedom = [1.0, 46.0]
FWHM = 12.8 12.9 13.1 mm; 6.4 6.4 6.5 voxel
Volume: 1301856 = 162732 vox = 558.8 resels
Voxel size: 2×2×2 mm; resel = 268.79 voxel

ALL SUBJECTS		REGIONS OF INTEREST VOXELS	x	y	z	T-SCORE 1A	1B
Inferior parietal lobule	right	326	54	−70	26	−7.95	−3.63
	left	639	−44	−76	33	−7.07	−4.15
Caudal PCC	—	618	−8	−44	30	−6.44	−3.10
Rostral ACC	left	94	−8	56	0	−6.95	−2.18
Superior medial PFC	left	145	−12	54	34	−6.82	−3.54

Table 4.17: **Group T-scores for the regions of interest extracted from the SPM factorial analysis** (all subjects, n = 24; control-minus-RVIP contrast, before and after methamphetamine on the first assessment day) using the MARSBAR toolbox. In all of the regions, methamphetamine reduced but did not abolish or reverse the T-score.

4.8.3 Within-group analysis – lithium and methamphetamine

The within-group analyses were performed using the full-factorial model (described in §4.4.6 on pages 93-94), into which the RVIP-minus-control contrasts from the first-level analyses were submitted and the appropriate comparisons specified.

DEACTIVATIONS

Subtracting the pre-methamphetamine from the post-methamphetamine data on day one (1B–1A), several suprathreshold clusters were observed (table 4.18; page 129). Given the distribution, these clusters were assumed to arise from a methamphetamine-induced reduction in deactivation as previously described. Following the course of lithium, the same comparison showed no clusters passing the designated threshold (not depicted). This finding may indicate that lithium attenuated the effect of methamphetamine on task-related deactivations.

Exploring this possibility, the clusters of deactivation for each condition (pre- and post-methamphetamine, before and after lithium) were visualised, generating four results tables (4.19 to 4.22 on pages 130–132). Prior to subjects taking the course of lithium, the patterns of deactivation before and after methamphetamine were as expected (those randomised to lithium did, after all, comprise the majority of the 'all-subject' group). The same comparisons after lithium were broadly similar, but with a notable difference. After methamphetamine administration on the first day, no suprathreshold deactivation clusters were observed but in the comparable analysis after lithium, significant deactivation was seen in one voxel (−18 · −50 · 14).

The visualisation of the deactivations was repeated with a less stringent threshold ($p < 0.001$ uncorrected); see figures 4.20 to 4.23. At this threshold, methamphetamine appeared to markedly reduce the extent of deactivation after it was first administered. Before the second dose of methamphetamine (session 2A), the task-related deactivations in those receiving lithium largely matched the pattern seen in session 1A, though their extent appeared slightly greater. Clusters of deactivation were, however, still in evidence with methamphetamine administration post-lithium.

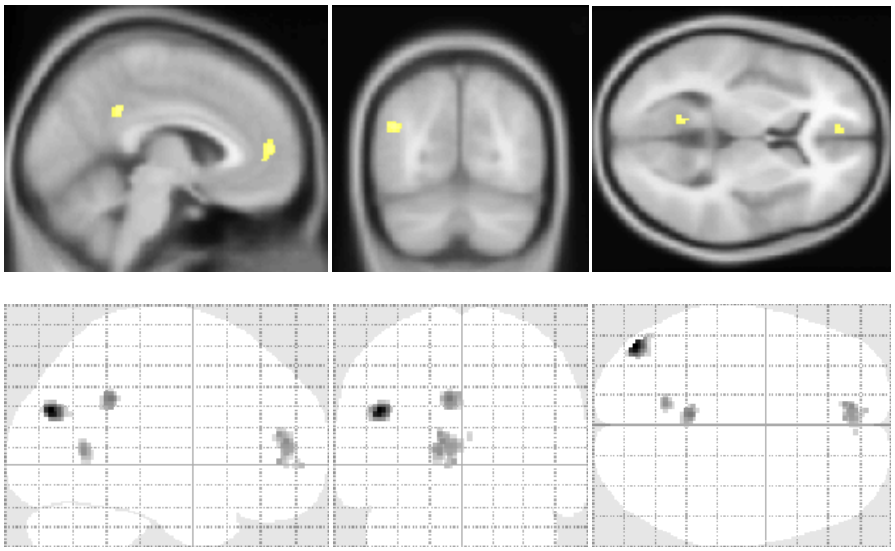

Table 4.18: **Effects of methamphetamine – 'post' minus 'pre' before lithium prescription** (1B−1A); results from the full factorial model, SPM{T_{88}}, in which the *RVIP-minus-control contrasts* pre-methamphetamine were subtracted from those post-methamphetamine, before lithium in those randomised to receive it (n = 18, family-wise-error correction $p < 0.05$). The accompanying images depict the clusters rendered onto the ICBM152 T_1 template (sagittal view to the left of the midline), together with a glass brain projection.

CLUSTER-LEVEL				PEAK-LEVEL					LOCATION		
p FWE	p FDR	k_E	p UNC	p FWE	p FDR	T	Z	p UNC	x	y	z
.000	.000	78	.003	.000	.054	6.25	5.67	.000	−44	−76	28
.000	.019	54	.010	.006	.390	5.51	5.09	.000	−6	−44	34
.000	.006	97	.001	.009	.390	5.38	4.99	.000	−10	50	12
				.016	.419	5.23	4.87	.000	−4	46	2
.001	.033	40	.022	.010	.390	5.36	4.97	.000	−12	−58	8
.020	4.63	5	.386	.025	.555	5.11	4.77	.000	−8	58	0
.030	.596	2	.596	.039	.767	4.98	4.66	.000	4	52	14

LITHIUM GROUP
RVIP-MINUS-CONTROL
1B−1A
FWE_p: 4.902
FDR_p: ∞
FWE_c: 2
FDR_c: 40

Height threshold: T = 4.90, p = 0.000 (0.050)
Extent threshold: k = 0 voxels, p = 1.000 (0.050)
Expected voxels per cluster, <k> = 7.151
Expected number of clusters, <c> = 0.05

Degrees of freedom = [1.0, 88.0]
FWHM = 12.4 12.5 12.6 mm; 6.2 6.2 6.3 voxel
Volume: 1260680 = 157585 vox = 597.0 resels
Voxel size: 2×2×2 mm; resel = 243.35 voxel

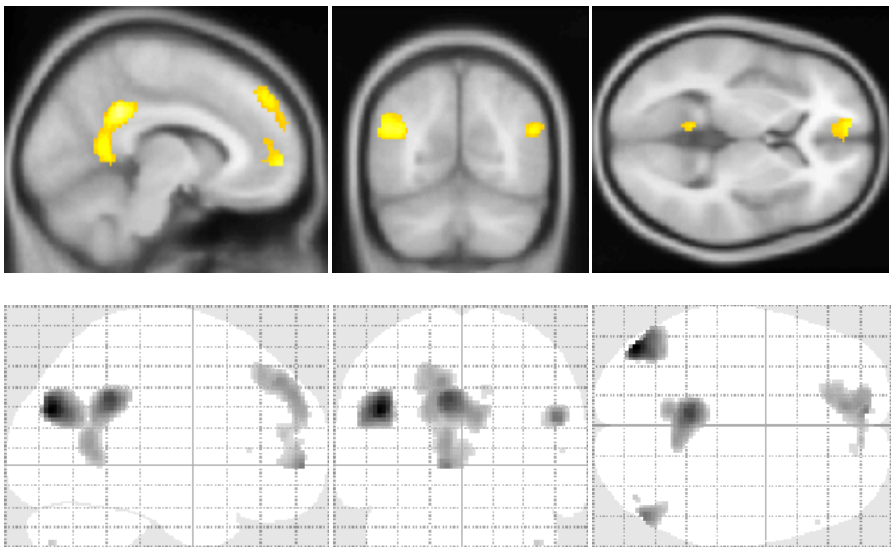

Table 4.19: **Task-related deactivations pre-methamphetamine and before lithium**; full-factorial random effects model, SPM{T_{88}}, demonstrating the *control-minus-RVIP contrast* in those randomised receive lithium (1A deactivations, n = 18, family-wise-error correction $p < 0.05$). The accompanying images depict the clusters rendered onto the ICBM152 T_1 template (sagittal view to the left of the midline), together with a glass brain projection.

CLUSTER-LEVEL				PEAK-LEVEL					LOCATION		
p FWE	p FDR	k_E	p UNC	p FWE	p FDR	T	Z	p UNC	x	y	z
.000	.000	498	.000	.000	.000	8.65	7.34	.000	−44	−76	28
.000	.000	900	.000	.000	.000	7.45	6.54	.000	−6	−44	34
				.001	.031	6.08	5.54	.000	8	−52	26
				.001	.040	5.98	5.46	.000	−8	−56	10
.000	.000	143	.000	.000	.010	6.61	5.94	.000	50	−70	24
.000	.000	200	.000	.000	.011	6.51	5.87	.000	−8	58	0
				.008	.220	5.42	5.02	.000	−12	48	16
.000	.000	516	.000	.000	.031	6.17	5.61	.000	−10	46	44
				.001	.031	6.09	5.55	.000	−12	54	36
				.002	.066	5.78	5.31	.000	−16	38	46
.003	.074	28	.050	.010	.239	5.37	4.98	.000	8	56	22
.030	.671	2	.596	.016	.380	5.23	4.86	.000	40	−76	−40
.015	.390	7	.304	.034	.752	5.02	4.69	.000	12	50	40
.036	.722	1	.722	.043	.864	4.94	4.63	.000	54	30	8

table shows 3 local maxima more than 8.0 mm apart

Height threshold: T = 4.90, p = 0.000 (0.050)
Extent threshold: k = 0 voxels, p = 1.000 (0.050)
Expected voxels per cluster, <k> = 7.151
Expected number of clusters, <c> = 0.05

Degrees of freedom = [1.0, 88.0]
FWHM = 12.4 12.5 12.6 mm; 6.2 6.2 6.3 voxel
Volume: 1260680 = 157585 vox = 597.0 resels
Voxel size: 2×2×2 mm; resel = 243.35 voxel

LITHIUM GROUP DEACTIVATIONS 1A

FWE_p: 4.902
FDR_p: 5.883
FWE_c: 1
FDR_c: 143

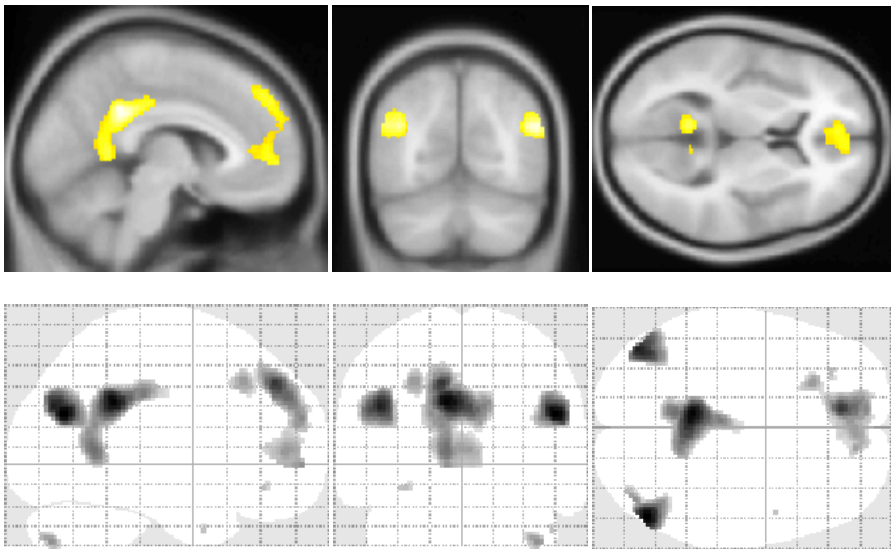

Table 4.20: **Task-related deactivations pre-methamphetamine and after lithium**; full-factorial random effects model, SPM{T_{88}}, demonstrating the *control-minus-RVIP contrast* in those who received lithium (2A deactivations, n = 18, family-wise-error correction $p < 0.05$). The accompanying images depict the clusters rendered onto the ICBM152 T_1 template (sagittal view to the left of the midline), together with a glass brain projection.

CLUSTER-LEVEL				PEAK-LEVEL					LOCATION		
p FWE	p FDR	k_E	p UNC	p FWE	p FDR	T	Z	p UNC	x	y	z
.000	.000	369	.000	.000	.000	8.03	6.93	.000	50	−68	26
.000	.000	1342	.000	.000	.000	7.88	6.83	.000	−8	−42	32
				.000	.017	6.38	5.77	.000	−8	−52	8
				.000	.024	6.24	5.66	.000	−4	−26	36
.000	.000	446	.000	.000	.000	7.49	6.57	.000	−44	−74	30
.000	.000	1225	.000	.000	.001	7.17	6.35	.000	−10	44	42
				.000	.012	6.51	5.87	.000	−12	50	34
				.001	.038	6.05	5.52	.000	−10	58	24
.003	.106	24	.067	.001	.038	5.98	5.46	.000	−40	−76	−40
.020	.441	5	.386	.009	.217	5.38	4.99	.000	−30	38	12
.007	.184	15	.138	.011	.250	5.33	4.95	.000	8	−52	8
.030	.596	2	.596	.012	.252	5.32	4.94	.000	48	6	−34

table shows 3 local maxima more than 8.0 mm apart

Height threshold: T = 4.90, p = 0.000 (0.050)
Extent threshold: k = 0 voxels, p = 1.000 (0.050)
Expected voxels per cluster, <k> = 7.151
Expected number of clusters, <c> = 0.05

Degrees of freedom = [1.0, 88.0]
FWHM = 12.4 12.5 12.6 mm; 6.2 6.2 6.3 voxel
Volume: 1260680 = 157585 vox = 597.0 resels
Voxel size: 2×2×2 mm; resel = 243.35 voxel

LITHIUM GROUP DEACTIVATIONS 2A

FWE_p: 4.902
FDR_p: 5.975
FWE_c: 2
FDR_c: 369

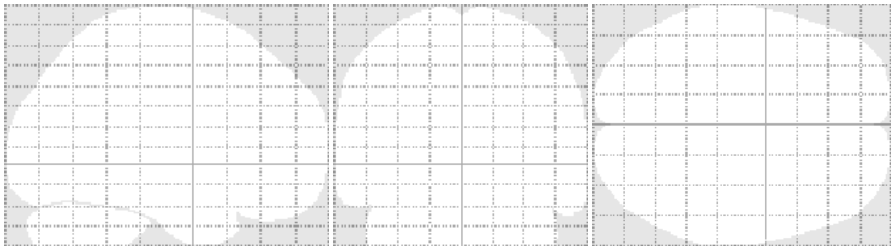

Table 4.21: **Task-related deactivations post-methamphetamine and before lithium**; full-factorial random effects model, SPM{T_{88}}, for the *control-minus-RVIP contrast* in those randomised receive lithium (1B deactivations, n = 18, family-wise-error correction $p < 0.05$), with a glass-brain projection.

CLUSTER-LEVEL				PEAK-LEVEL					LOCATION		
p_{FWE}	p_{FDR}	k_E	p_{UNC}	p_{FWE}	p_{FDR}	T	Z	p_{UNC}	x	y	z
no suprathreshold clusters											

LITHIUM GROUP DEACTIVATIONS 1B

FWE_p: 4.902

FDR_p, FWE_c, FDR_c: ∞

Height threshold: T = 4.90, p = 0.000 (0.050)
Extent threshold: k = 0 voxels, p = 1.000 (0.050)
Expected voxels per cluster, <k> = 7.151
Expected number of clusters, <c> = 0.05

Degrees of freedom = [1.0, 88.0]
FWHM = 12.4 12.5 12.6 mm; 6.2 6.2 6.3 voxel
Volume: 1260680 = 157585 vox = 597.0 resels
Voxel size: 2×2×2 mm; resel = 243.35 voxel

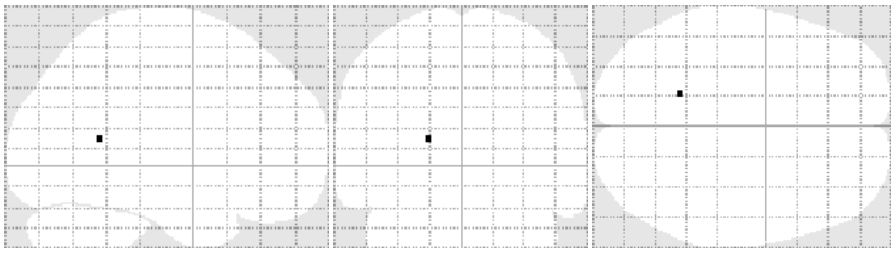

Table 4.22: **Task-related deactivations post-methamphetamine and after lithium**; full-factorial random effects model, SPM{T_{88}}, demonstrating the *control-minus-RVIP contrast* in those who received lithium (2B deactivations, n = 18, family-wise-error correction $p < 0.05$), with a glass-brain projection.

CLUSTER-LEVEL				PEAK-LEVEL					LOCATION		
p_{FWE}	p_{FDR}	k_E	p_{UNC}	p_{FWE}	p_{FDR}	T	Z	p_{UNC}	x	y	z
.036	.722	1	.722	.042	.843	4.95	4.64	.000	−18	−50	14

LITHIUM GROUP DEACTIVATIONS 2B

FWE_p: 4.902

FDR_p, FWE_c, FDR_c: ∞

Height threshold: T = 4.90, p = 0.000 (0.050)
Extent threshold: k = 0 voxels, p = 1.000 (0.050)
Expected voxels per cluster, <k> = 7.151
Expected number of clusters, <c> = 0.05

Degrees of freedom = [1.0, 88.0]
FWHM = 12.4 12.5 12.6 mm; 6.2 6.2 6.3 voxel
Volume: 1260680 = 157585 vox = 597.0 resels
Voxel size: 2×2×2 mm; resel = 243.35 voxel

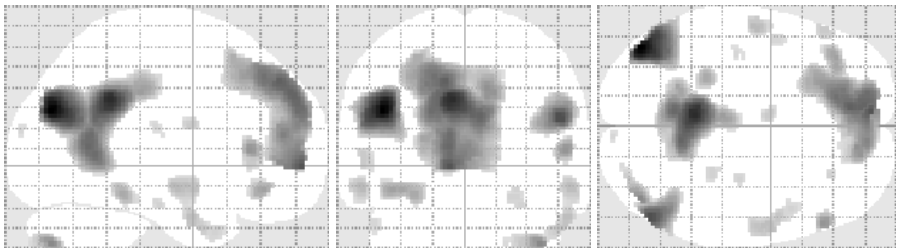

Figure 4.20: **Task-related deactivations pre-methamphetamine and before lithium** in all those due to receive it (session 1A; n = 18, $p < 0.001$ unc., height threshold T = 3.185,extent threshold $k = 0$ voxel).

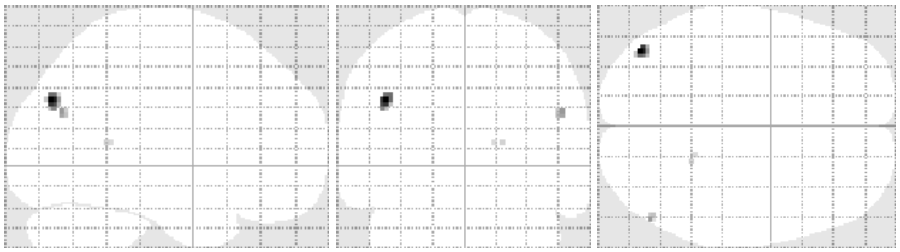

Figure 4.21: **Task-related deactivations post-methamphetamine and before lithium** in all those due to receive it (session 1B; n = 18, $p < 0.001$ unc., height threshold T = 3.185,extent threshold $k = 0$ voxel).

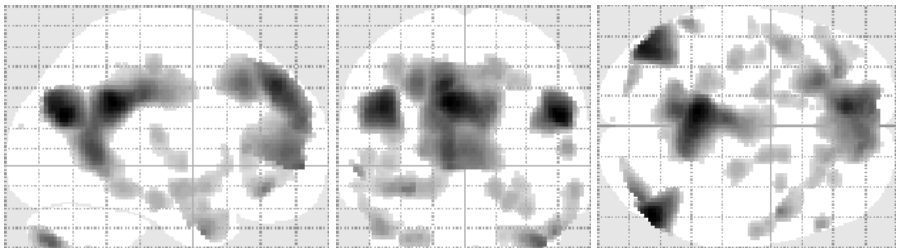

Figure 4.22: **Task-related deactivations pre-methamphetamine and after lithium** in all those who received it (session 2A; n = 18, $p < 0.001$ unc., height threshold T = 3.185,extent threshold $k = 0$ voxel).

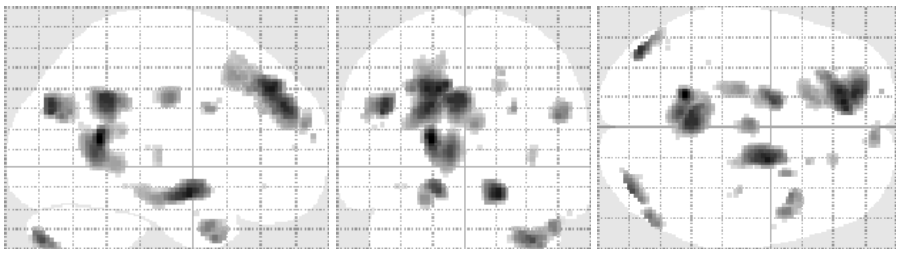

Figure 4.23: **Task-related deactivations post-methamphetamine and after lithium** in all those who received it (session 2B; n = 18, $p < 0.001$ unc., height threshold T = 3.185,extent threshold $k = 0$ voxel).

The magnitude of this difference was gauged in an ROI analysis, akin to the one described on page 125. The principal clusters of deactivation in session 1A served as the regions of interest (control-minus-RVIP contrast, family-wise-error corrected threshold $p < 0.05$). These were used to extract the T-scores from the group data pre- and post-methamphetamine in the sessions before and after lithium administration. The results of these explorations are presented in tables 4.23 and 4.24 on the next page. Methamphetamine reduced the T-scores in all regions before and after lithium, though the magnitude of the reduction appeared to be diminished after the course of lithium (not formally tested, for reasons discussed later in this thesis).

Returning to the full-factorial model and repeating the subtraction analyses (1B−1A; 2B−2A) at the lower threshold ($p < 0.001$ uncorrected), the influence of lithium on the methamphetamine-related reduction in deactivation could be visualised (see figures 4.24 and 4.25 below). Submitting the contrasts so derived to formal comparison, (1B−1A) minus (2B−2A), the difference was insufficient to reach significance.

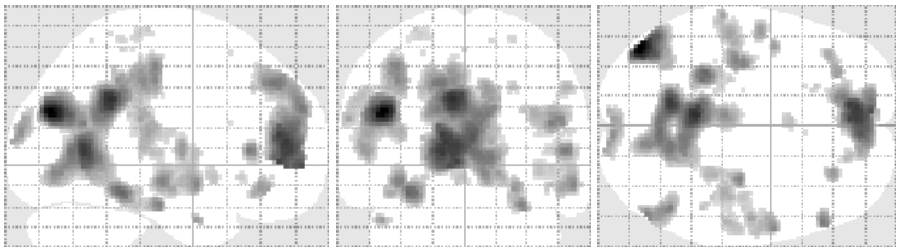

Figure 4.24: The difference in deactivations before and after methamphetamine in all those due to receive lithium (n = 18). Using the RVIP-minus-control contrast in the full factorial model, sessions were subtracted: 1B−1A ($p < 0.001$ uncorrected, height threshold T = 3.185,extent threshold $k = 0$ voxel).

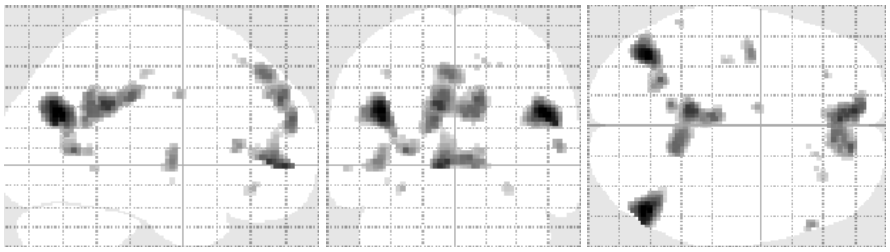

Figure 4.25: The difference in deactivations before and after methamphetamine in all those who received lithium (n = 18). Using the RVIP-minus-control contrast in the full factorial model, sessions were subtracted: 1B−1A ($p < 0.001$ uncorrected, height threshold T = 3.185,extent threshold $k = 0$ voxel).

PRE-LITHIUM		REGIONS OF INTEREST VOXELS	*x*	*y*	*z*	T SCORE 1A	1B
Inferior parietal lobule	right	143	50	−70	24	−6.12	−3.87
	left	498	−44	−76	28	−7.12	−2.73
Caudal PCC	—	900	−6	−44	34	−6.62	−2.02
Rostral ACC	left	200	−8	58	0	−6.39	−0.45
Superior medial PFC	left	516	−10	46	44	−6.75	−2.53

Table 4.23: **T-scores for the regions of interest extracted from the SPM factorial analysis** (lithium group, n = 18; control-minus-RVIP contrast, pre- and post-methamphetamine *prior to* lithium in those due to receive it) using the MARSBAR toolbox. Methamphetamine reduced the statistical score in all regions, clusters no longer passing the threshold for significance with family-wise error correction.

POST-LITHIUM		REGIONS OF INTEREST VOXELS	*x*	*y*	*z*	T SCORE 2A	2B
Inferior parietal lobule	right	143	50	−70	24	−6.83	−4.02
	left	498	−44	−76	28	−7.58	−3.79
Caudal PCC	—	900	−6	−44	34	−7.82	−5.05
Rostral ACC	left	200	−8	58	0	−5.48	−2.61
Superior medial PFC	left	516	−10	46	44	−7.47	−4.78

Table 4.24: **T-scores for the regions of interest extracted from the SPM factorial analysis** (lithium group, n = 18; control-minus-RVIP contrast, pre- and post-methamphetamine *after* lithium in those who received it) using the MARSBAR toolbox. Methamphetamine reduced the statistical score in all regions, clusters no longer passing the threshold for significance with family-wise error correction.

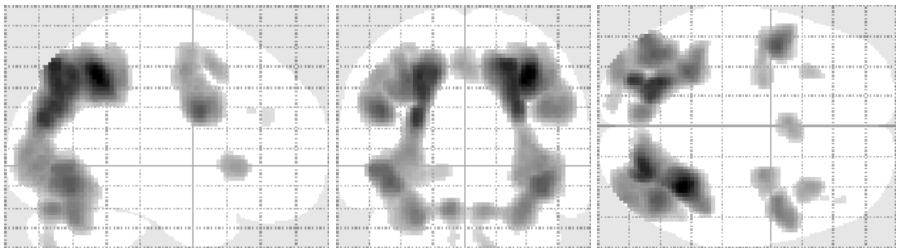

Figure 4.26: **Task-related activations pre-methamphetamine and before lithium**; full factorial random-effects model, SPM{T_{88}}, demonstrating the RVIP-minus-control contrast in all subjects due to receive lithium (session 1A, n = 18; $p < 0.05$ FWE, thresholds in table on the following page).

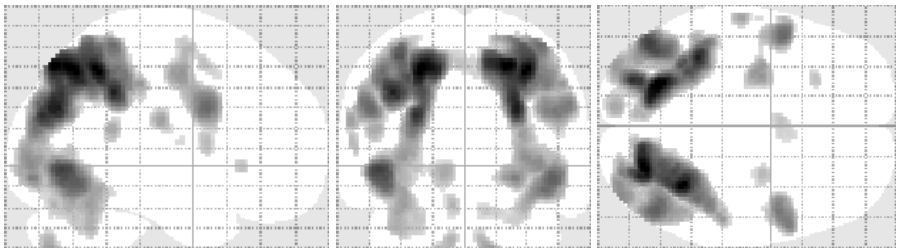

Figure 4.27: **Task-related activations post-methamphetamine and before lithium**; full factorial random-effects model, SPM{T_{88}}, demonstrating the RVIP-minus-control contrast in all subjects due to receive lithium (session 1B, n = 18; $p < 0.05$ FWE, thresholds in table on the following page).

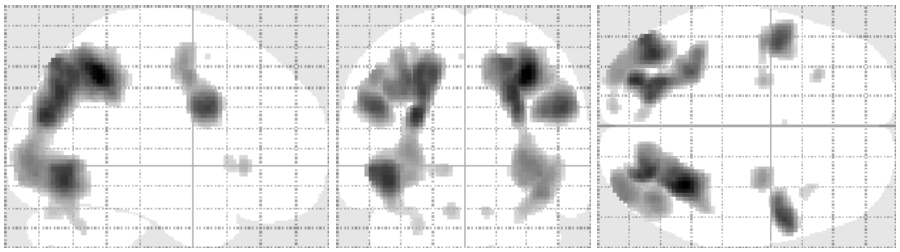

Figure 4.28: **Task-related activations pre-methamphetamine and after lithium**; full factorial random-effects model, SPM{T_{88}}, demonstrating the RVIP-minus-control contrast in all subjects who received lithium (session 2A, n = 18; $p < 0.05$ FWE, thresholds in table on the following page).

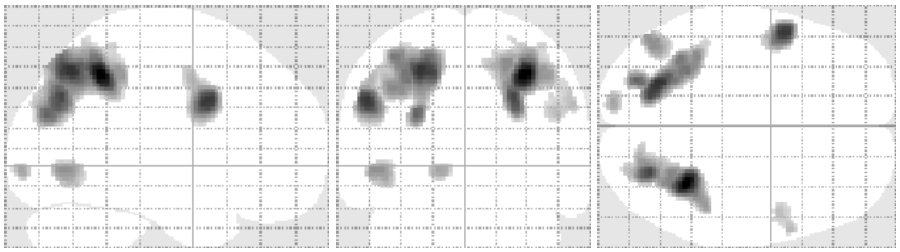

Figure 4.29: **Task-related activations post-methamphetamine and after lithium**; full factorial random-effects model, SPM{T_{88}}, demonstrating the RVIP-minus-control contrast in all subjects who received lithium (session 2B, n = 18; $p < 0.05$ FWE, thresholds in table on the following page).

CLUSTER-LEVEL				PEAK-LEVEL					LOCATION			
p FWE	p FDR	k_E	p UNC	p FWE	p FDR	T	Z	p UNC	x	y	z	
.000	.000	10133	.000	.000	.000	10.60	∞	.000	34	−52	46	LITHIUM GROUP ACTIVATIONS 1A
				.000	.000	9.58	∞	.000	24	−74	50	
				.000	.000	9.47	7.82	.000	26	−72	42	
.000	.000	1067	.000	.000	.000	8.32	7.13	.000	−44	4	28	FWE_p: 4.902
				.000	.003	6.55	5.90	.000	−46	−4	46	FDR_p: 5.800
				.000	.012	6.19	5.62	.000	−26	−4	50	FWE_c: 2
.000	.000	637	.000	.000	.000	7.39	6.50	.000	44	4	30	FDR_c: 44
				.000	.004	6.52	5.88	.000	48	2	40	
.000	.000	337	.000	.000	.001	6.82	6.09	.000	28	−4	50	
				.000	.009	6.26	5.68	.000	32	−2	58	
.000	.000	202	.000	.000	.003	6.58	5.91	.000	34	24	0	
.000	.000	197	.000	.000	.004	6.52	5.87	.000	−2	10	52	
.000	.000	5030	.000	.000	.000	9.28	7.72	.000	22	−74	52	LITHIUM GROUP ACTIVATIONS 1B
				.000	.000	9.27	7.81	.000	32	−50	48	
				.000	.000	8.61	7.31	.000	28	−72	30	
.000	.000	4836	.000	.000	.000	9.24	7.69	.000	−22	−66	50	FWE_p: 4.902
				.000	.000	8.58	7.29	.000	−38	−42	38	FDR_p: 5.837
				.000	.000	8.24	7.07	.000	−26	−80	26	FWE_c: 2
.000	.000	815	.000	.000	.001	7.17	6.35	.000	−50	8	30	FDR_c: 59
				.000	.013	6.30	5.70	.000	−28	−6	48	
				.003	.065	5.74	5.27	.000	−26	−4	56	
.000	.000	568	.000	.000	.002	6.87	6.13	.000	48	4	28	
				.000	.002	6.81	6.08	.000	54	10	30	
				.004	.101	5.60	5.17	.000	50	0	38	
.000	.000	149	.000	.000	.009	6.40	5.78	.000	14	−76	−46	
				.005	.127	5.53	5.11	.000	24	−72	−50	
.000	.000	144	.000	.000	.013	6.28	5.69	.000	−16	−74	−46	
				.002	.065	5.74	5.28	.000	−8	−76	−38	
.000	.000	144	.000	.001	.032	5.97	5.45	.000	−10	−90	−4	
				.031	.625	5.05	4.72	.000	−22	−88	−4	
.000	.001	126	.000	.004	.091	5.63	5.19	.000	28	−6	50	
				.010	.221	5.36	4.97	.000	26	−4	62	
.000	.000	3472	.000	.000	.000	9.56	∞	.000	34	−50	46	LITHIUM GROUP ACTIVATIONS 2A
				.000	.000	8.42	7.19	.000	26	−70	38	
				.000	.000	8.20	7.05	.000	28	−76	30	
.000	.000	3324	.000	.000	.000	8.54	7.27	.000	−26	−78	26	FWE_p: 4.902
				.000	.000	8.40	7.18	.000	−42	−68	−6	FDR_p: 5.923
				.000	.000	8.16	7.02	.000	−24	-64	46	FWE_c: 1
.000	.000	501	.000	.000	.000	8.15	7.01	.000	52	8	30	FDR_c: 85
.000	.000	631	.000	.000	.000	7.89	6.85	.000	−46	4	30	
				.000	.003	6.62	5.95	.000	−48	−2	46	
.000	.000	222	.000	.000	.008	6.37	5.76	.000	30	−4	54	
.000	.000	1690	.000	.000	.000	8.83	7.45	.000	32	−48	46	LITHIUM GROUP ACTIVATIONS 2B
				.000	.000	7.49	6.57	.000	26	−70	36	
				.000	.013	6.34	5.74	.000	24	−72	54	
.000	.000	1373	.000	.000	.000	7.84	6.81	.000	−24	−66	50	FWE_p: 4.902
				.000	.002	6.97	6.20	.000	−26	−78	26	FDR_p: 6.107
				.000	.004	6.71	6.01	.000	−32	−50	48	FWE_c: 59
.000	.000	430	.000	.000	.000	7.77	6.76	.000	−52	8	34	FDR_c: 59
				.004	.140	5.60	5.16	.000	−50	0	44	
				.019	.503	5.18	4.83	.000	−46	−4	50	
.000	.000	200	.000	.000	.017	6.22	5.64	.000	−48	−70	−2	
.000	.000	140	.000	.005	.149	5.56	5.69	.000	58	12	32	
				.006	.184	5.49	5.08	.000	48	4	28	
				.026	.556	5.10	4.76	.000	52	6	42	

Height threshold: T = 4.90, p = 0.000 (0.050)
Extent threshold: k = 0 voxels, p = 1.000 (0.050)
Expected voxels per cluster, <k> = 7.151
Expected number of clusters, <c> = 0.05

Degrees of freedom = [1.0, 88.0]
FWHM = 12.4 12.5 12.6 mm; 6.2 6.2 6.3 voxel
Volume: 1260680 = 157585 vox = 597.0 resels
Voxel size: 2×2×2 mm; resel = 243.35 voxel

Table 4.25: Statistical values supporting figures 4.25–4.29 on the previous page.

On formal comparison, methamphetamine was not associated with an increase in clusters of activation of the BOLD signal either before or after lithium (results not depicted). The pattern of activation in each session matched that expected from previous analyses (figures 4.26 to 4.29, together with the relevant statistical scores from SPM listed on page 137); the degree and extent of activation appeared somewhat diminished following lithium, but this did not emerge as significant on testing (not depicted).

4.8.4 Within-group analysis – placebo and methamphetamine

The analysis stages conducted for the lithium group were repeated for those allocated to the placebo group. No differences in activation or deactivation were observed when pre- and post-methamphetamine sessions were compared, before or after the course of placebo (results not depicted). Given the small size of the placebo group, it must be acknowledged that a voxel-wise examination of the whole brain may have been under powered. Scrutinising the contrasts generated in each session, clusters were small compared to those in of the lithium group, but essentially in the same brain regions (deactivations: table 4.26; activations: figures 4.30 to 4.33 and table 4.27).

4.8.5 Between-group analysis – lithium and placebo

Moving to a between-group analysis, the effects of methamphetamine on activations and deactivations before and after the course of either lithium or placebo were compared. No differences were seen between the placebo group and the lithium group on any comparison and at any threshold (results not depicted). Additional exploratory analyses were not performed.

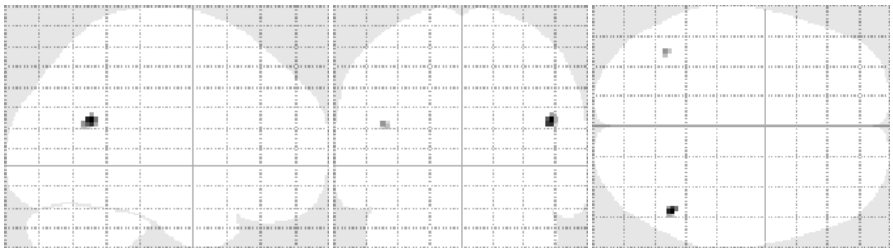

SESSION 1A

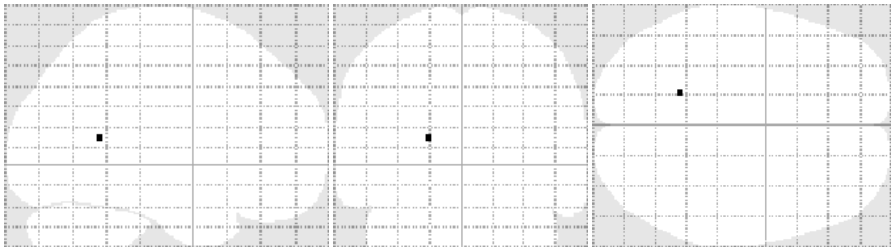

SESSION 2B

Table 4.26: **Task-related deactivations in the placebo group**; full-factorial random effects model, SPM{T_{88}}, listing the *control-minus-RVIP contrast* output for the various session (n = 6, family-wise-error correction $p < 0.05$).

CLUSTER-LEVEL				PEAK-LEVEL					LOCATION		
p_{FWE}	p_{FDR}	k_E	p_{UNC}	p_{FWE}	p_{FDR}	T	Z	p_{UNC}	x	y	z
.008	.302	14	.151	.010	.374	5.38	4.99	.000	48	−54	24
.017	.341	6	.341	.029	.564	5.07	4.73	.000	−42	−58	22

PLACEBO GROUP DEACTIVATIONS 1A
FWE_p: 4.902
FDR_p: ∞
FWE_c: 6
FDR_c: ∞

no suprathreshold clusters

PLACEBO GROUP DEACTIVATIONS 1B
FWE_p: 4.902
FDR_p: ∞
FWE_c: ∞
FDR_c: ∞

no suprathreshold clusters

PLACEBO GROUP DEACTIVATIONS 2A
FWE_p: 4.902
FDR_p: ∞
FWE_c: ∞
FDR_c: ∞

.009	.181	12	.181	.005	.090	5.57	5.14	.000	−36	−56	18

PLACEBO GROUP DEACTIVATIONS 2B
FWE_p: 4.902
FDR_p: ∞
FWE_c: 12
FDR_c: ∞

Height threshold: T = 4.90, p = 0.000 (0.050)
Extent threshold: k = 0 voxels, p = 1.000 (0.050)
Expected voxels per cluster, <k> = 7.151
Expected number of clusters, <c> = 0.05

Degrees of freedom = [1.0, 88.0]
FWHM = 12.4 12.5 12.6 mm; 6.2 6.2 6.3 voxel
Volume: 1260680 = 157585 vox = 597.0 resels
Voxel size: 2×2×2 mm; resel = 243.35 voxel

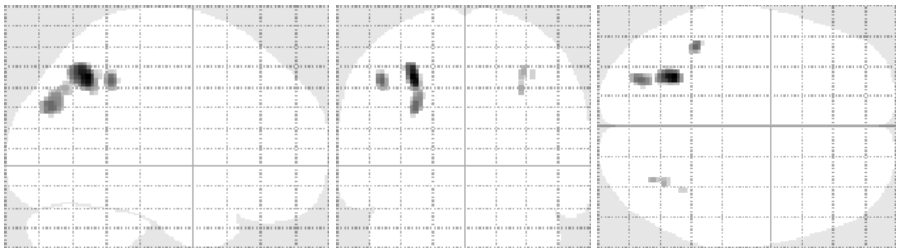

Figure 4.30: **Task-related activations pre-methamphetamine and before placebo**; full factorial random-effects model, SPM{T_{88}}, demonstrating the RVIP-minus-control contrast in all subjects due to receive placebo (session 1A, n = 6; $p < 0.05$ FWE, thresholds in table on the following page).

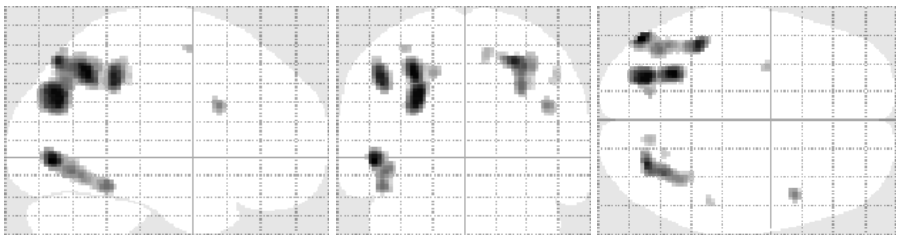

Figure 4.31: **Task-related activations post-methamphetamine and before placebo**; full factorial random-effects model, SPM{T_{88}}, demonstrating the RVIP-minus-control contrast in all subjects due to receive placebo (session 1B, n = 6; $p < 0.05$ FWE, thresholds in table on the following page).

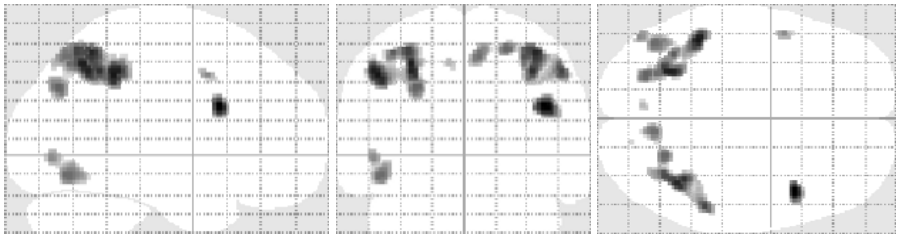

Figure 4.32: **Task-related activations pre-methamphetamine and after placebo**; full factorial random-effects model, SPM{T_{88}}, demonstrating the RVIP-minus-control contrast in all subjects who received placebo (session 2A, n = 6; $p < 0.05$ FWE, thresholds in table on the following page).

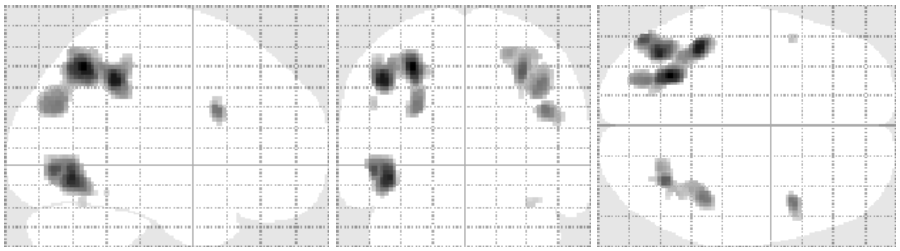

Figure 4.33: **Task-related activations post-methamphetamine and after placebo**; full factorial random-effects model, SPM{T_{88}}, demonstrating the RVIP-minus-control contrast in all subjects who received placebo (session 2B, n = 6; $p < 0.05$ FWE, thresholds in table on the following page).

CLUSTER-LEVEL				PEAK-LEVEL					LOCATION		
p FWE	p FDR	k_E	p UNC	p FWE	p FDR	T	Z	p UNC	x	y	z
.000	.003	110	.001	.001	.088	6.05	5.52	.000	−28	−56	46
.003	.099	28	.050	.006	.248	5.52	5.10	.000	−44	-44	44
.000	.013	68	.004	.006	.248	5.49	5.08	.000	−26	−76	32
.014	.326	8	.272	.020	.482	5.17	4.82	.000	30	−68	40
.012	.326	9	.244	.020	.482	5.16	4.81	.000	32	−62	48
.026	.508	3	.508	.039	.784	4.97	4.66	.000	36	−52	48
.000	.003	294	.000	.000	.006	6.81	6.09	.000	−48	−76	−2
				.002	.068	5.86	5.37	.000	−44	−46	−16
				.002	.068	5.85	5.36	.000	−42	−64	−8
.000	.000	541	.000	.000	.006	6.72	6.02	.000	−28	−56	46
				.000	.006	6.71	6.01	.000	−24	−72	34
				.007	.224	5.44	5.04	.000	−16	−70	46
.000	.000	134	.000	.000	.008	6.52	5.87	.000	−44	−42	44
.000	.000	346	.000	.000	.008	6.50	5.85	.000	26	−72	52
				.001	.038	6.07	5.54	.000	32	−62	50
				.001	.068	5.88	5.38	.000	30	−70	40
.002	.083	29	.046	.003	.108	5.67	5.22	.000	44	14	28
.003	.100	24	.067	.013	.353	5.29	4.92	.000	12	−70	58
.015	.304	7	.304	.013	.353	5.28	4.91	.000	−32	−2	60
.008	.194	14	.151	.021	.478	5.16	4.81	.000	48	−36	46
.015	.304	7	.304	.027	.556	5.08	4.75	.000	20	−62	56
.000	.003	91	.001	.000	.052	6.40	5.79	.000	42	14	28
.000	.000	519	.000	.000	.052	6.20	5.63	.000	−46	−42	44
				.000	.052	6.20	5.63	.000	−28	−58	50
				.001	.062	5.92	5.42	.000	−30	−62	58
.000	.000	410	.000	.001	.052	6.09	5.55	.000	38	−54	56
				.001	.058	6.02	5.49	.000	36	−50	46
				.001	.062	5.88	5.38	.000	52	−38	46
.000	.000	150	.000	.003	.094	5.65	5.21	.000	−44	−66	−10
				.007	.166	5.45	5.05	.000	−48	−76	−2
.000	.008	66	.005	.004	.097	5.63	5.19	.000	8	−68	54
.009	.242	12	.181	.007	.166	5.45	5.05	.000	−50	8	44
.017	.390	6	.341	.021	.425	5.16	4.81	.000	−8	−74	50
.036	.722	1	.722	.042	.835	4.95	4.64	.000	14	−80	−48
.000	.000	786	.000	.000	.001	7.37	6.49	.000	−28	−58	50
				.000	.002	7.04	6.25	.000	−44	−42	44
				.001	.040	6.00	5.48	.000	−26	−72	32
.000	.000	438	.000	.000	.003	6.92	6.49	.000	−40	−64	−6
				.000	.014	6.45	5.82	.000	−48	−74	−2
.000	.000	444	.000	.000	.019	6.32	5.73	.000	30	−62	−48
				.001	.040	6.04	5.51	.000	40	−40	42
				.004	.135	5.61	5.17	.000	24	−64	58
.000	.004	79	.002	.001	.040	6.07	5.53	.000	44	14	28
.011	.257	10	.220	.016	.376	5.23	4.87	.000	−48	12	32
.011	.257	10	.220	.025	.553	5.10	4.76	.000	34	−58	−20
.036	.722	1	.722	.050	.998	4.90	4.60	.000	−44	−46	−14

PLACEBO GROUP ACTIVATIONS 1A
FWE$_p$: 4.902
FDR$_p$: ∞
FWE$_c$: 3
FDR$_c$: 68

PLACEBO GROUP ACTIVATIONS 1B
FWE$_p$: 4.902
FDR$_p$: 6.074
FWE$_c$: 7
FDR$_c$: 134

PLACEBO GROUP ACTIVATIONS 2A
FWE$_p$: 4.902
FDR$_p$: ∞
FWE$_c$: 1
FDR$_c$: 66

PLACEBO GROUP ACTIVATIONS 2B
FWE$_p$: 4.902
FDR$_p$: 5.982
FWE$_c$: 1
FDR$_c$: 79

Height threshold: T = 4.90, p = 0.000 (0.050)
Extent threshold: k = 0 voxels, p = 1.000 (0.050)
Expected voxels per cluster, <k> = 7.151
Expected number of clusters, <c> = 0.05

Degrees of freedom = [1.0, 88.0]
FWHM = 12.4 12.5 12.6 mm; 6.2 6.2 6.3 voxel
Volume: 1260680 = 157585 vox = 597.0 resels
Voxel size: 2×2×2 mm; resel = 243.35 voxel

Table 4.27: **Task-related activations in the placebo group**; full-factorial random effects model, SPM{T_{88}}, listing the *control-minus-RVIP contrast* output for the various session (n = 6, family-wise-error correction $p < 0.05$).

4.8.6 Between-group analysis – lithium dose

As the high and low dose lithium groups each contained nine subjects, a voxel-wise comparison would likely have been inadequately powered. The effects of dose were therefore investigated by examining the regions in which methamphetamine reduced the task-related deactivations. It was hypothesised that in those randomised to receive a high dose of lithium, the methamphetamine-related reduction in deactivation would be attenuated more than in those allocated to a low dose of lithium.

Using the regions of interest previously defined (deactivations in session 1A for all subjects allocated to receive lithium, 18 subjects, 5 regions), T-scores and were extracted using the MARSBAR toolbox. The results are given in table 4.28 below; the pattern in T-scores is described rather than formally tested). Before the course of lithium, methamphetamine resulted in a reduction in the magnitude of the BOLD signal deactivation. Following lithium, T-scores fell to a similar degree in the low dose lithium group but in those allocated to receive high dose lithium, the T-scores demonstrated a degree of stability. That is to say, high dose lithium attenuated the effects of methamphetamine whilst low dose lithium failed to do so.

		T-SCORE BY SESSION			
REGION OF INTEREST	LITHIUM	1A	1B	2A	2B
Right inferior parietal lobule	higher dose	−5.96	−4.04	−3.60	−3.65
	lower dose	−4.76	−1.86	−6.78	−2.14
Left inferior parietal lobule	higher dose	−5.66	−2.68	−5.38	−4.61
	lower dose	−5.36	−1.46	−5.60	−2.43
Posterior cingulate cortex	higher dose	−3.46	−2.27	−5.50	−5.37
	lower dose	−7.42	−0.82	−5.94	−3.18
Left anterior cingulate cortex	higher dose	−4.97	−1.46	−3.26	−3.22
	lower dose	−4.55	0.22	−5.14	−1.18
Left superior medial PFC	higher dose	−4.71	−3.28	−4.40	−3.14
	lower dose	−6.10	−1.10	−7.94	−3.91

Table 4.28: **T-scores by region of interest according to lithium dose** (higher dose, n = 9; lower dose, n = 9), the regions of interest previously defined (see table 4.23). Lithium appeared to attenuate the methamphetamine-related reduction in deactivation, more so in the higher dose dose group.

4.8.7 Lithium and placebo prior to methamphetamine

LITHIUM

The effect of lithium itself was examined by comparing the contrasts generated from the first fMRI session (pre-methamphetamine and before lithium) with those derived from the equivalent session following the course of tablets (after lithium but before methamphetamine) within the full factoral model. Two analyses were conducted, namely 1A–2A and 2A–1A, into which the RVIP-minus-control contrast was entered. Clusters emerging from the 1A–2A represented areas of activation present with lithium but not before; those in the 2A–1A comparison were deactivations.

There were no differences in either analysis when multiple comparisons were corrected at the family-wise level of $p < 0.05$ (results not depicted). Lowering the threshold in an exploratory analysis, no areas of deactivation attributable to lithium emerged. Conversely, several points of activation emerged on formal comparison (RVIP-minus-control 1A–2A, $p < 0.001$ uncorrected). As demonstrated in table 4.29, these areas were small and barely passed the threshold for significance. The largest cluster of activation was located in the VTA ($-6 \cdot -18 \cdot -12$), tending towards significance at the cluster level ($p_{FWE} = 0.055$, $p_{UNC} = 0.008$). A smaller cluster was observed in the ventral striatum ($8 \cdot 0 \cdot 12$), but barely significant ($p_{FWE} = 0.291$, $p_{UNC} = 0.049$).

Using the MARSBAR toolbox, group T-scores for these two clusters were extracted, before and after lithium (combined group, n = 18). Initially, both regions showed deactivation (T-scores 1A: VTA = − 2.96; ventral striatum = − 1.19) but after lithium, activations were observed (T-scores 2A: VTA = 2.16; ventral striatum = 3.83).

PLACEBO

In a comparable analysis, placebo was not associated with the emergence of activations, but widespread deactivation was observed (RVIP-minus-control 2A–1A, $p < 0.001$ uncorrected). The areas showing deactivation were small, barely passing the threshold for significance (table 4.30; page 145). The largest area of deactivation was in the right IPL ($50 \cdot -72 \cdot 24$), significant at the cluster level ($p_{FWE} = 0.014$, $p_{UNC} = 0.002$).

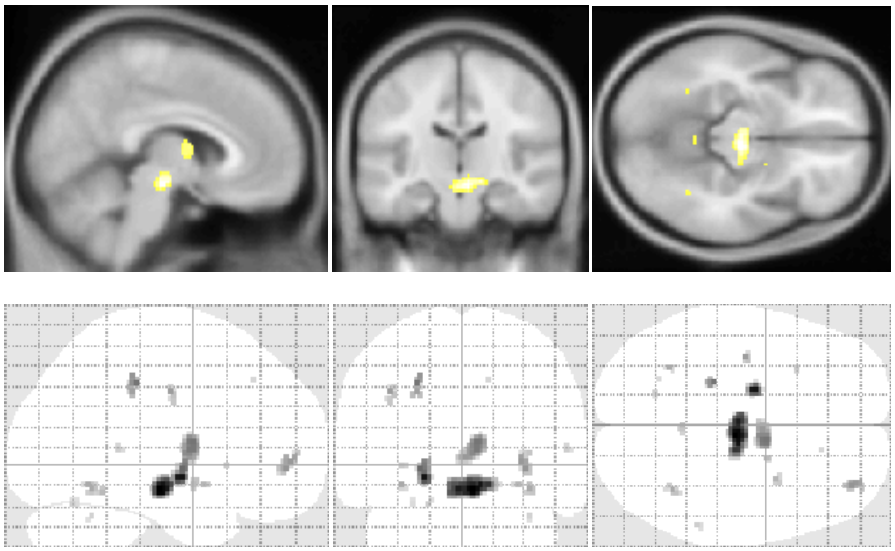

Table 4.29: **Activations arising after lithium, prior to methamphetamine**; full-factorial random effects model, SPM{T_{88}}, showing areas of activation present after lithium compared to before it, prior to methamphetamine (1A versus 2A; n = 18, $p < 0.001$ uncorrected). The accompanying images depict the clusters rendered onto the ICBM152 T_1 template, together with a glass brain projection.

CLUSTER-LEVEL				PEAK-LEVEL					LOCATION		
p FWE	p FDR	k_E	p UNC	p FWE	p FDR	T	Z	p UNC	x	y	z
.055	.144	212	.008	.299	.759	4.31	4.09	.000	−6	−18	−12
				.449	.759	4.13	3.94	.000	−2	−16	−12
				.570	.807	4.01	3.84	.000	14	−18	−10
.664	.873	51	.154	.405	.759	4.18	3.98	.000	−20	−6	−6
.955	.873	15	.438	.862	.948	3.71	3.56	.000	—24	−30	42
.291	.873	105	.049	.864	.948	3.70	3.56	.000	8	0	12
.875	.873	27	.295	.947	.948	3.55	3.43	.000	34	50	−2
				.995	.948	3.31	3.20	.001	36	56	6
.980	.873	9	.556	.961	.948	3.51	3.39	.000	−38	−12	38
.973	.873	11	.511	.979	.948	3.44	3.33	.000	36	−54	−12
.993	.873	4	.710	.979	.948	3.44	3.32	.000	−32	−56	−10
.986	.873	5	.672	.988	.948	3.39	3.27	.001	30	6	−10
.986	.873	7	.608	.989	.948	3.38	3.27	.001	0	−48	−14
.989	.873	6	.639	.990	.948	3.37	3.26	.001	18	0	−10
.997	.873	2	.806	.996	.948	3.30	3.19	.001	−32	18	0
.993	.873	4	.710	.990	.948	3.28	3.18	.001	56	−40	8
.997	.873	2	.806	.997	.948	3.27	3.17	.001	−18	−64	−20
.997	.873	2	.806	.998	.948	3.25	3.15	.001	36	−54	−26
.998	.873	1	.873	.998	.948	3.23	3.13	.001	14	32	44

table shows 3 local maxima more than 8.0 mm apart

BEFORE AND AFTER LITHIUM
1A−2A
($p < 0.001$ UNC.)
FWE_p: 4.902
FDR_p: ∞
FWE_c: ∞
FDR_c: ∞

Height threshold: T = 3.19, $p = 0.001$ (0.999)
Extent threshold: k = 0 voxels, $p = 1.000$ (0.999)
Expected voxels per cluster, <k> = 26.557
Expected number of clusters, <c> = 7.06

Degrees of freedom = [1.0, 88.0]
FWHM = 12.4 12.5 12.6 mm; 6.2 6.2 6.3 voxel
Volume: 1260680 = 157585 vox = 597.0 resels
Voxel size: 2×2×2 mm; resel = 243.36 voxel

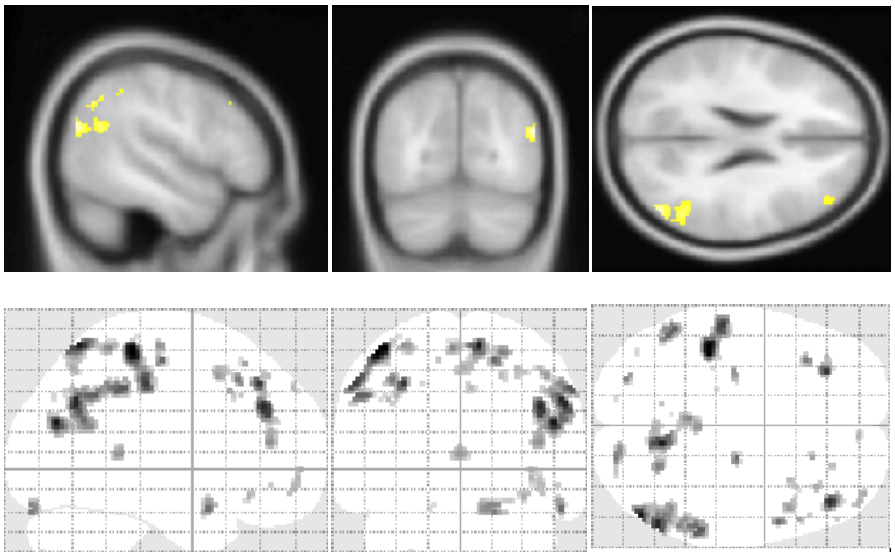

Table 4.30: **Deactivations arising after placebo, prior to methamphetamine**; full-factorial random effects model, SPM{T_{88}}, showing areas of activation present after placebo compared to before it, prior to methamphetamine (1A versus 2A; n = 6, $p < 0.001$ uncorrected). The accompanying images depict the clusters rendered onto the ICBM152 T_1 template (sagittal view to the right of the midline), together with a glass brain projection.

CLUSTER-LEVEL				PEAK-LEVEL					LOCATION		
p FWE	p FDR	k_E	p UNC	p FWE	p FDR	T	Z	p UNC	x	y	z
.125	.189	158	.019	.140	.584	4.58	4.32	.000	−44	−32	60
				.428	.623	4.16	3.96	.000	−56	−24	44
				.881	.678	3.68	3.54	.000	−50	−28	52
.014	.059	311	.002	.234	.584	4.40	4.17	.000	50	−72	24
				.305	.584	4.40	4.17	.000	56	−62	34
				.579	.678	4.01	3.83	.000	58	−38	42
.094	.189	176	.014	.247	.584	4.38	4.15	.000	10	−60	−64
				.829	.678	3.75	3.60	.000	22	−62	60
				.855	.678	3.72	3.57	.000	−4	−44	62
.325	.418	98	.056	.325	.584	4.27	4.09	.000	42	38	32
				.898	.682	3.65	3.51	.000	42	42	14
.859	.873	29	.277	.391	.623	4.20	4.00	.000	−30	36	−44
				.985	.764	3.41	3.30	.000	−38	36	36
.790	.873	37	.221	.635	.678	3.95	3.78	.000	−54	−52	38
.955	.873	15	.438	.681	.678	3.91	3.74	.000	18	−16	56
.912	.873	22	.344	.717	.678	3.87	3.71	.000	54	8	−20
.955	.873	15	.438	.798	.678	3.79	3.63	.000	−36	24	46
.799	.873	36	.277	.810	.678	3.77	3.62	.000	18	−86	−22
				.994	.827	3.33	3.23	.001	26	-86	−16

table shows 3 local maxima more than 8.0 mm apart

BEFORE AND AFTER PLACEBO
2A−1A
($p < 0.001$ UNC.)
FWE_p: 4.902
FDR_p: ∞
FWE_c: ∞
FDR_c: ∞

Height threshold: T = 3.19, $p = 0.001$ (0.999)
Extent threshold: k = 0 voxels, $p = 1.000$ (0.999)
Expected voxels per cluster, <k> = 26.557
Expected number of clusters, <c> = 7.06

Degrees of freedom = [1.0, 88.0]
FWHM = 12.4 12.5 12.6 mm; 6.2 6.2 6.3 voxel
Volume: 1260680 = 157585 vox = 597.0 resels
Voxel size: 2×2×2 mm; resel = 243.36 voxel

4.9 DISCUSSION

The study presented in this chapter investigated whether lithium could diminish the effects of methamphetamine and in doing so, demonstrate its ability to attenuate dopaminergic neurotransmission. In the strictest sense and by the most conservative criteria, the null hypothesis was not rejected. That is to say, no difference was observed on any measure when those taking lithium were compared to those taking placebo. A within-group analysis demonstrated no difference in the response to methamphetamine before and after the course of placebo tablets, other that a slight exaggeration of its subjective effects according to visual analogue scale ratings. In the within-group analysis of all subjects taking lithium, an attenuation of the effects of methamphetamine was observed – subjective effects were diminished and the deactivation in BOLD contrast that occurs when tasks are performed, which was reduced by methamphetamine, was partially restored. Examining the signal change in the key regions of interest, the effects of methamphetamine were most evidently modified in those randomised to receive a higher dose of lithium. Lithium itself slowed response times in the RVIP task condition and appeared to alter the BOLD signal contrast in striatal and midbrain areas, consistent with a modulation of the dopaminergic systems of the brain.

This discussion section first examines the effects of methampetamine in light of the work of others and as a reflection of manipulations in the dopaminergic systems. The effects on BOLD signal are summarised and the deactivations discussed in terms of the default-mode network theories. The mechanisms by which methamphetamine may bring about its effects on BOLD contrast are then appraised. Considering the various within-group analyses, it is argued that converging lines of evidence support the notion that lithium is able to attenuate the effects of the methamphetamine in man. Reflecting on the negative result for the null hypothesis, the design and power of the study – together with its strengths and weaknesses – requires discussion. This is reserved for the final chapter of this thesis, in which the additional analyses proposed for this data, together with potential directions for future work, are considered.

Methamphetamine model

Amphetamines have long been used to model psychiatric illness, mania in particular (Jacobs and Silverstone, 1986). By acting to increase synaptic levels of monoamines in the brain (Sulzer et al., 2005), various features of manic presentations can be replicated in healthy subjects. Whilst this thesis sought to examine the dopaminergic systems, amphetamines are known to increase activity in all monoaminergic pathways. To gain a degree of specificity for dopamine, certain strategies were employed and converging lines of evidence examined.

First, methamphetamine was employed as the pharmacological challenge. Akin to D-amphetamine, methamphetamine has actions on all three monoaminergic systems but the timing of its effects are more predictable. Second, as subjects performed a task requiring sustained attention, they likely recruited activity in the noradrenergic and dopaminergic systems of the brain (MacDonald et al., 2000); the control task condition required a degree of attention, but the RVIP task condition was harder and placed greater demands on executive function, arguably emphasising dopaminergic activity (McTavish et al., 2001). Third, fMRI was employed, its purpose being to localise the regions of the brain affected by the interventions – it was hypothesised that regions innervated by dopamine would demonstrate a change in activity, evidenced by an alteration in BOLD contrast.

SUBJECTIVE EFFECTS

Methamphetamine induced a change in the mental state of the subjects in this study. Established using standardised and validated visual analogue scales, administration resulted in subjects feeling more alert, excited, clear-headed, energetic, quick-witted, proficient and gregarious. This finding was not unexpected in the least, affirming the model, replicating the work of others and serving as a reminder as to why methamphetamine is a drug of abuse. Hearn et al. (2004) examined the subjective effects of methamphetamine on healthy subjects together with a pharmacological manipulation of the stress axis in a complicated, placebo-controlled study with a cross-over design.

The dose and administration of methamphetamine exactly matched the protocol used in this thesis, apart from the difference in environmental ambience (clinical laboratory compared to clinical scanner). Using an alternate set of VAS ratings, Hearn et al. (2004) reported increased scores on 'mind-race' and 'buzz' domains after methamphetamine was given; they observed no significant change on the scales employed in this thesis (those developed by Bond and Lader, 1974).

EFFECTS ON RVIP TASK PERFORMANCE

The effects of methamphetamine on the measures of task performance were largely as expected. Examining all subjects on the first day of assessment, before randomisation to receive either lithium or placebo, methamphetamine hastened response times and increased false alarm rates during the RVIP task condition. In the control task condition of the same session, the median response latency similarly fell but false alarm rates remained low, unchanged by the stimulant challenge. The hit rate and sensitivity index values in the RVIP and control task conditions were unaltered by the administration of methamphetamine.

Compared to the control condition, performing the RVIP task requires more attention and a degree of conflict resolution. Subjects may adopt the strategy of being vigilant for potential full sequences, responding if and when the correct third target digit appears. That is, if the numbers 2 and 4 are seen consecutively, a subject's attention becomes focussed on whether or not the next digit will be the number 6. The possibility of anticipating the completion of sequences explains why response times were swifter in the RVIP task condition compared to the control condition, in which targets appear without warning. The increase in false alarm rate in the face of stable accuracy suggests that the decision to respond was disturbed – after methamphetamine, subjects may have tended to respond in the affirmative whenever a potential sequence was identified, failing to inhibit responses to incorrect completions. A change in response patterns to a 'trigger-happy' style suggests that the processes of the executive network of the attentional systems has altered, so implicating dopamine (MacDonald et al., 2000; McTavish et al., 2001).

In a study conducted locally, methamphetamine was found to increase hit rates and sensitivity index scores on the RVIP task, reducing response latency but with no effect on response bias in healthy subjects (Hearn et al., 2004). The findings of the study conducted in this thesis more closely match those reported by Goodwin's group (McTavish et al., 2001), in which responses were hastened and B'' scores rose. It was not possible to calculate the response bias for subjects in the MRC-LAMP study, largely due to the use of a blocked design. Response bias cannot be derived if a subject returns a perfect score – all targets detected and no false responses made. In a continuous version of the RVIP, perfect performances are rare; divided into short blocks, a faultless performance in at least one of the blocks was not uncommon. Mean hit rates and false alarm rates were calculated for individual blocks, the values then averaged to determine performance for each task condition. Handled in a similar manner, if a subject's response bias could not be calculated for one of the blocks, then the mean for all of the blocks was undeterminable. Excluding the relevant blocks would have skewed the results; grouping scores into a single block would have misrepresented the manner in which the task was conducted.

FUNCTIONAL IMAGING FINDINGS

Compared to the control task condition, performing the RVIP task condition increased BOLD signal in posterior parietal and temporal regions, the dorsolateral frontal cortex and the medial aspect of the rostral insula bilaterally. Deactivations were observed bilaterally in the inferior parietal lobules and in the left hemisphere, posterior and anterior cingulate cortices together with medial aspects of the prefrontal cortex. These results directly replicate the findings of previous PET (Coull et al., 1996) and fMRI studies (Lawrence et al., 2003) investigating the RVIP task.

The physiological basis of BOLD signal activation is well characterised (see §2.5; pages 41–44), there being a consensus that increases in contrast represent presynaptic activity in the regions where they are present (Logothetis, 2002). Thus, performing the RVIP task can be said to engage the processes of all three attentional networks delineated by Fan et al. (2005). Deactivations are more poorly understood and until

recently were largely overlooked; this possibly as a consequence of interpreting the imaging findings within the paradigms of psychology (Morcom and Fletcher, 2007; Raichle and Snyder, 2007). In the clinical laboratory setting, experiments are usually designed such that a control condition is contrasted with a task condition in which greater demands are placed on the system under investigation. By extrapolation, subtracting the functional images acquired in a control task scenario from those gathered during the performance of a demanding task should demonstrate the areas in which brain activity increased – BOLD activations. Activity increases were expected and specifically sought; that certain brain functions might lessen or cease during the performance of a complex task was not on the agenda, though as it transpires this may be the case. Reverse subtractions (control task minus the demanding task) are thought to gauge that process (Raichle et al., 2001) – BOLD deactivations.

Deactivations in certain brain regions are consistently observed, falling mostly along the medial surface (precuneus, anterior and posterior cingulate, prefrontal) but also in the inferior parietal lobules (Raichle et al., 2001). The pattern is consistent with various tasks, its degree determined by the intensity of the task (Frankenstein et al., 2003; McKiernan et al., 2003). These brain areas are now described collectively as the *default mode regions*, the term implying that they are active at rest and become less active once a task is started. Deactivations in the default mode regions have attracted a great deal of debate and remain a contentious topic (Raichle and Snyder, 2007). What is accepted is that deactivations occur (Mazoyer et al., 2001); what is debated is whether the regions comprise a network, serve a purpose at rest and in a wider sense, what 'rest' can be said to represent (Morcom and Fletcher, 2007). It has been argued that the default regions actually form a neuronal network (Greicius et al., 2003), supporting evidence provided by fMRI studies of the resting state as well as electrophysiological investigations (van den Heuvel and Hulshoff Pol, 2010). Resting state studies rely on the detection of low frequency fluctuations in the BOLD signal which are thought to reflect communication within networks (Biswal et al., 1995), the idea being that areas with synchronous fluctuations are connected. Using probabilistic independent components analysis or seed region correlation techniques, the default

regions have been found to be linked (Fox and Raichle, 2007). The approaches are bewildering and it is not known if they can be trusted. Further, even if the regions are connected, the function of the network is unclear – the notion that it has something to do with day-dreaming holds a certain attraction (Raichle and Snyder, 2007).

Returning to the study in hand, methamphetamine did not alter the RVIP task-related activations but attenuated the deactivations in all regions. An exploratory region of interest analysis indicated that following administration of the stimulant, deactivations persisted but were of lesser magnitude, falling below the threshold of significance on whole-brain voxel wise comparison. This finding is a challenge to interpret, requiring an examination not only of the pharmacological actions of methamphetamine but also the manner by which BOLD contrast is generated.

It could be argued that methamphetamine acts directly on the default mode network, accepting it is a valid construct. Some regions of the proposed network, mostly the frontal components, are served by dopamine and the inter-relationship between activations, deactivations and dopaminergic activity has been investigated (Nagano-Saito et al., 2009; Tomasi et al., 2010; Delaveau et al., 2010). In the MRC-LAMP study, methamphetamine attenuated deactivation across the network, not just the frontal regions; this finding attracts at least three interpretations. First, dopamine is not constrained to the frontal regions, its neurones being widely distributed. Patients with Parkinson's disease fail to deactivate posterior midline and lateral default mode regions, but deactivation is restored after L-dopa administration (Delaveau et al., 2010). The effects of methampetamine may be similarly widespread. Second, networks being what they are, were methamphetamine to manipulate just the frontal components then it could reasonably be proposed that activity in the linked regions would follow suit. This may not actually be the case, the default mode network increasingly being considered as a fractionated system (Andrews-Hanna et al., 2010). Deactivations may be observed in isolation in each of the default mode regions, with the degree of deactivation in the medial prefrontal cortex proportional to the complexity of the task (Nagano-Saito et al., 2009). In healthy subjects, a greater degree of deactivation in the ventral ACC is associated with increased DAT availability in the striatum (Tomasi

et al., 2010) – lower synaptic dopamine equates to more deactivation, mirroring the findings of this thesis. Administration of apomorphine, a dopamine agonist, fosters deactivation in the ventral medial PFC in elderly subjects (Nagano-Saito et al., 2009). Dopamine depletion strategies, however, lessen the deactivation across anterior and posterior default mode regions (**?**). Clearly, the relationship between dopaminergic activity and the degree of deactivation, even within a single region, is complex. The third explanation invokes the mixed pharmacological properties of methamphetamine, positing that alterations in deactivations in posterior regions of the network have a basis in the manipulations of noradrenergic neurotransmission. Whilst tradition would have us avoid plurality, the complexity of the situation may necessitate it.

Adopting an alternative stance, it could be proposed that the actions of methamphetamine are removed from the default mode network, or at least that the network is not the primary site of its effects. Indeed, the existence of such a network need not be invoked, just that certain parts of the brain demonstrate a characteristic reduction in BOLD signal on embarking upon a task. The characteristics of the deactivations are paramount; crudely, they occur with any task and to an extent determined by the difficulty of the task. Consequently, musing over the specificity of the RVIP task for dopaminergic regions of the brain may be of little value in terms of understanding the deactivations. Methamphetamine may simply have acted to make the task easier to complete, thereby lessening the extent of the deactivations. It must be acknowledged that these actions could be subtle, diffuse and undetected by the analysis performed.

What can be said of methamphetamine is that it lessened the difference between the control task condition and the RVIP task condition, at least in terms of BOLD contrast generation. The generation of BOLD contrast is sensitive to the baseline state of the brain (Morcom and Fletcher, 2007), a concept pertinent to negative BOLD responses (deactivations). As discussed, negative deflections in BOLD signal compared to rest occur when tasks are performed; lowering activity in the brain to below rest and then embarking on the task results in a negative BOLD signal change of greater magnitude (Pasley et al., 2007) – the brain deactivates not by a fixed amount, but to a fixed point. Note that the experiment performed by Pasley et al. (2007) served to

demonstrate that negative BOLD signal deflections are most likely a consequence of neural deactivation rather than non-neural haemodynamic artefacts.

The effects of methamphetamine on the baseline condition are therefore of some importance. If, for argument's sake, the state of the brain during the control task condition is taken as being unchanged by methamphetamine, the lessening of the deactivation seen with the stimulant would imply that the subjects remained closer to the baseline state when engaging in the RVIP task – from a stable baseline, less BOLD signal deactivation equates to a smaller reduction in neuronal deactivation. Taken to the extreme, methamphetamine would be said to constrain subjects to the state of rest. This seems somewhat counterintuitive, contrary to the change in performance on the RVIP task and the subjective effects of the drug. It makes more sense to argue that the baseline state changed, that methamphetamine induced a degree of arousal that spanned that RVIP task and control conditions. In this state of arousal, attention may have been heightened and more closely approximated to the level required for the successful completion of the RVIP task condition. In effect, subjects deactivate from an already deactivated position.

The complexities of contrast comparison mean that reductions in deactivations may masquerade as activations in some analyses, possibly explaining the inconsistencies in the reported effects of amphetamines in BOLD fMRI studies (see §4.2.1; page 80). The finding that methamphetamine attenuates deactivation reaffirms its importance as a model of psychiatric illness. Recently, McKenna et al. (2010) argued that reports of 'hyperfrontality' in schizophrenia may actually represent failures of deactivation in the default mode network. Compared to healthy subjects, deactivations in those with chronic schizophrenia (n = 32) during a working memory task were of lesser magnitude, at least in the anterior midline node of the network. McKenna et al. (2010) also found that patients with bipolar disorder similarly failed to deactivate frontal regions, though to a lesser extent compared to schizophrenia. It is unclear whether the deactivation findings in these two illness reflects their contrasting pathologies or the effects of medication, lithium in particular.

4.9.1 Lithium and methamphetamine

FUNCTIONAL IMAGING FINDINGS

Having established that methamphetamine reduced the magnitude of deactivation in the default mode regions, the effects of lithium on that process were examined. In a within-group analysis, the reduction in deactivation attributable to methamphetamine was attenuated by lithium. The effect was partial, and likely greatest in those randomised to receive a higher dose of lithium.

Lithium has been previously been shown to modify the effects of amphetamine on the BOLD signal (Bell et al., 2005a). In a parallel design study, subjects were randomised to receive either placebo (n = 12) or lithium (n = 9) at a fixed dose of 900 mg per day for two weeks before undergoing investigation. Performing various neuropsychological tasks before and after 25 mg of D-amphetamine, lithium reportedly lessened the extent of activations associated with the stimulant more than placebo. The effect was observed during a spatial attention paradigm but not during a task that challenged working memory. Bell et al.'s (2005a) study may be compared to the investigation conducted in this chapter and so warrants further consideration.

The most obvious difference in the results of the studies was that Bell et al. (2005a) demonstrated a difference in BOLD signal change between lithium and placebo groups. In the MRC-LAMP study, the within-group analyses showed that lithium attenuated the effects of methamphetamine whilst placebo did not. The lack of a difference between the lithium and placebo interventions in the between-group analysis was most likely a type 2 error – with only six subjects in the placebo group, the study reported here was underpowered for such a comparison. Factors likely to lessen the power of the study, pure numbers aside, include the inter-subject variability in response to amphetamine, the nature of the fMRI analysis and the range of lithium doses used.

Bell et al. (2005a) found a difference between small groups (lithium n = 9, placebo n = 12) with a range of serum concentrations of lithium (0.39–0.77 mM) slightly lower than those achieved in this thesis. Their positive finding may be a reflection of the image analysis strategy employed. In the MRC-LAMP study, the entire brain was exam-

ined in a voxel-wise manner; the effects of methamphetamine were delineated and in the same subjects, the modification of these effects by lithium was examined. Bell et al. (2005a) applied regions of interest derived from a previous study to focus their analysis, but in doing so made the assumption that the effects of D-amphetamine were consistent across subjects and studies. Using these ROI, a small volume comparison was performed. Statistically more powerful at the level of analysis, the strategy is weakened by its circularity – one may see what one is looking for.

Ostensibly the reverse of the findings in this thesis, Bell et al. (2005a) reported that lithium reduced the extent of BOLD activations caused by D-amphetamine. It may be argued that the findings are comparable. Recall that in the initial subtraction analysis exploring the effects of methamphetamine on the BOLD signal, apparent activations were resolved as attenuations of deactivation. It is unclear from Bell et al.'s paper how the contrasts were specified, but it is conceivable that the 'activation' reported was actually a reduction in deactivation, with lithium lessening that reduction.

In terms of neurotransmitter systems, the BOLD signal is neither specific nor quantitative – implicating dopamine in the effects of lithium requires additional reasoning with empirical support. In regions innervated by dopamine, the BOLD signal varies with manipulations of the activity of the neurotransmitter. Following amphetamine administration to rodents, BOLD signal change matches microdialysis measures of dopamine release in the striatum, further correlating with PET regional cerebral blood flow assessments (Chen et al., 1997). In the nucleus accumbens of rodents, antagonism of D1-receptors prevents amphetamine-related increases in BOLD signal (Dixon et al., 2005) despite the ongoing release of dopamine (Choi et al., 2006); antagonism of D2-receptors has a lesser effect on BOLD activations (Dixon et al., 2005). As D1-receptors are not present on presynaptic membranes (Greengard, 2001b), dopaminergic firing may cause BOLD signal activation through postsynaptic mechanisms, in the striatum at least (Knutson and Gibbs, 2007). When amphetamines are given to rodents, the reduction in BOLD signal seen in cortical regions is attenuated by sulpiride (a D2-receptor antagonist), but less so with D1-receptor blockade (Dixon et al., 2005). Dopamine-driven deactivations may therefore have a presynaptic basis.

Lithium is known to have numerous effects on dopaminergic neurotransmission. Whilst not a receptor binder, a wealth of data supports the assertion that it modulates second messenger systems downstream of dopamine receptors, so modifying the functioning of postsynaptic neurones (see §1.4.2). The study reported in this chapter failed to replicate the findings of Dixon et al. (2005) – methamphetamine did not increase BOLD signal in the striatum. Consequently, the notion that lithium may attenuate the effects of amphetamines through postsynaptic modulation of D1-receptor functioning could not be explored. The absence of striatal activation may reflect the neuropsychological task employed, dopamine release in the nucleus accumbens classically associated with the anticipation of reward (Knutson and Gibbs, 2007).

Despite the findings of Dixon et al. (2005), there is a consensus that BOLD signal activation most likely reflects regional presynaptic activity in the brain (Logothetis, 2002). Whilst the situation is less clear for deactivations (Frankenstein et al., 2003), extrapolation may be justifiable since changes in neuronal activity appear to underpin reductions in BOLD signal (Pasley et al., 2007). Lithium has been shown to reduce the synthesis and release of dopamine in some (Rastogi and Singhal, 1977; Baptista et al., 1993), but not all (Reches et al., 1984; Berggren, 1985) preclinical studies. Clearance of dopamine from the synapse is increased (Ahluwalia and Singhal, 1981), the net effect presumably a reduction in dopaminergic signalling. In a recent series of placebo-controlled experiments using rodents, lithium was found to attenuate the behavioural effects of D-amphetamine and decrease the release of dopamine in the nucleus accumbens (McQuade, 2010); apomorphine, a postsynaptic dopamine receptor agonist, induced behaviours similar to those seen with amphetamine, but its effects were not altered by lithium. Thus, lithium may act presynaptically in reducing dopaminergic neurotransmission – a conclusion consistent with its attenuation of the effects of methamphetamine on BOLD signal deactivation.

NEUROPSYCHOLOGICAL MEASUREMENTS

Lithium diminished the subjective effects of amphetamine, according to VAS scores. This finding harks back to early observations of the effects of lithium in recreational

drug users (Flemenbaum, 1975). Strictly, in terms of neuropsychological task performance, lithium did not attenuate the effects of methamphetamine. That is, the reduction in median response latency caused by the stimulant was not diminished. It is of interest then to consider why a dissociation should be present between the neuropsychological and fMRI modalities of assessment.

Assuming, for the sake of argument, that RVIP task performance and BOLD signal are purely determined by dopaminergic system activity, they should change in concert. The generation of BOLD contrast is somewhat more complex, driven in large part by the effects of vasoactive substances released from neurones and astrocytes (Attwell and Iadecola, 2002). A major pathway leading to nitric oxide production, and so feed-forward vasodilatation in the capillary bed, involves the activation of glutamatergic receptors with a cascade of effects in calcium-dependent second messenger systems. By attenuating calcium release and influx, lithium dampens the effects of glutamate receptor stimulation (Sourial-Bassillious et al., 2009). Activation of various receptors including dopaminergic ones yields COX and AA, which in themselves have vasoactive properties. Chronic administration of lithium has been shown to selectively reduce AA turnover rates and COX-2 concentrations (Rapoport and Bosetti, 2002). Thus, whilst performance on the RVIP task may be sensitive to the effects of lithium on neuronal activity, generation of the BOLD signal may be targeted at several sites. Blocked fMRI experiments may, however, be relatively insensitive to decoupling of the neurovascular response, at least in temporal terms. Nevertheless, these concerns serve as a reminder that whilst a degree of reductionism may be laudable, fMRI and neuropsychological tasks are ultimately measuring different things.

4.9.2 Lithium and placebo prior to methamphetamine

Given the design of the study, it was possible to investigate the effects of lithium and placebo on performance during the task of sustained attention, within the context of functional imaging. In the group randomised to receive lithium, median response latency was greater after the course of tablets; placebo had no effect on any measure.

Lithium has consistently been associated with a sense of 'mental slowing' according to the subjective reports of patients (Joffe et al., 1988; Lenzer et al., 1989). These complaints have been borne out on formal testing, lithium impairing performance on tasks assessing psychomotor speed (Shaw et al., 1987; Kocsis et al., 1993; Jauhar et al., 1993). Attention, however, appears to be unaffected in patient groups and healthy subjects (Pachet and Wisniewski, 2003). The findings of the study reported in this chapter – accuracy scores and false alarm rates unaltered by lithium, but subjects responding more slowly – are therefore consistent with the field at large.

The fMRI findings of the effects of lithium and placebo in their own right are something of a challenge to interpret in the context of an examination of sustained attention. Comparing the pre-methamphetamine session after lithium with the pre-methamphetamine session prior to its administration, BOLD activations were evident in the VTA and ventral striatum without significant deactivations at the cluster level. The placebo group showed deactivations only, these being present in the default mode regions and most notably the inferior parietal lobules and precuneus. Activation in the VTA and ventral striatum has been linked to the anticipation of reward, rather than the receipt or pleasurable experience of the reward (Carter et al., 2009). One would expect them, therefore, to have no business appearing during the completion of the RVIP task. The analysis described is a complex one (comparing a contrast of contrasts) in which emerging clusters may have more to do with the difference between the assessment days than the tasks undertaken. The principal difference was of course the intervention with lithium or placebo, but it must also be recognised that the pre-methamphetamine sessions differed in other respects. On the second occasion, subjects were familiar with the scanner environment but more importantly, had previous experience of methamphetamine. It was highly likely that they were looking forward to their second dose during the first session of the second day, hence the activity in reward circuitry.

The question then is why should activation in the VTA and ventral striatum be present in the lithium group but not the placebo group. Exposure to stimuli that have become associated with the effects of a drug can induce the effects of the drug

itself, subjectively and objectively (Carter and Tiffany, 1999; Weiss, 2005). This cued-response has a neurobiological basis in the dopaminergic systems, demonstrated most pointedly in a recent PET study (Boileau et al., 2007). In healthy subjects, the repeated oral amphetamine administration reduced [^{11}C]raclopride binding potentials in the caudate and putamen compared to their baseline scan, indicative of increased dopamine release in these regions. When on one of the assessment days, unbeknown to the subjects, the amphetamine capsule actually contained a placebo compound, [^{11}C]raclopride bindings fell compared to baseline and did not differ from the reduction induced by amphetamine – the anticipation of amphetamine brought about its effects. It could be argued that in the MRC-LAMP study, the placebo group were anticipating the effects of methamphetamine and therefore, to some extent, experiencing its effects – hence the deactivation pattern emerging in the default mode regions. The attenuation of dopaminergic neurotransmission ascribed to lithium may have constrained this response, such that although subjects were expecting methamphetamine, the transition to the state of arousal seen in the placebo group was lacking – hence the activation in the VTA and ventral striatum.

4.10 CONCLUSION

The study presented in this chapter provides indirect evidence in support of the notion that lithium can attenuate over-activity in the dopaminergic pathways of the human brain. Used as a model of mania, methamphetamine induced subjective effects and changes in BOLD signal deactivation that were partially diminished by lithium. In a task requiring sustained attention, lithium itself slowed response times but did not lessen the effects of methamphetamine on that, or any other measure of performance. The implications of these findings – together with an appraisal of the strengths and weaknesses of the study – are discussed in the final chapter of this thesis.

5 LITHIUM & BRAIN STRUCTURE

Intriguingly, MRI studies indicate that lithium increases the volume of grey matter in the human brain – a finding widely interpreted as evidence that lithium may enhance neuroplasticity, engendering hope and reaffirming its importance as an illness modifying drug. Such optimism rather predicates an increase in grey matter being genuine and beneficial, but the actual mechanism underlying the imaging findings has not been established empirically in man. In this chapter an alternative to the neuroplasticity explanation is advanced, namely that the change in grey matter volume is artefactual, arising from an alteration in the characteristics of the MR signal. Specifically, it is hypothesised that lithium reduces the longitudinal relaxation time of protons, thereby changing the signal intensity of T_1-weighted images which in turn affects the classification of tissues during the analysis process. This assertion is tested through the analysis of structural and quantitative images, acquired in a longitudinal study of healthy men allocated to receive either lithium or placebo.

5.1 BACKGROUND

The first study in this field was a longitudinal investigation testing the hypothesis that lithium has neurotrophic effects *in vivo*, manifest by an increase in grey matter volume (Moore et al., 2000b). Ten subjects with bipolar disorder underwent MR investigation before and after treatment with lithium for a period of four weeks. Analysis comprised the use of a semi-automated technique in which the grey and white matter voxels were delineated from CSF, followed by the calculation of the segmented tissue volumes. An increase in grey matter volume of 3% was reported (approximating to 24 cm^3), with no change in white matter volume. The findings were linked to elevations in the brain metabolite NAA – a putative marker of neuronal integrity – which occurred to the greatest degree in the brain areas with highest grey matter densities (Moore et al., 2000a).

In subjects with bipolar disorder, the volumetric finding has been replicated in hypothesis-driven, cross-sectional studies (Sassi et al., 2002; Bearden et al., 2007, 2008; Yucel et al., 2008; Germaná et al., 2010) and prospective studies (Moore et al., 2005, 2009; Kim et al., 2008; Lyoo et al., 2010). Similar effects are observed when healthy subjects take lithium (Leow et al., 2005; Monkul et al., 2007), though the MRS findings have not been substantiated (Brambilla et al., 2004).

When grey matter is reportedly increased, the magnitude is typically between two and ten percent – the largest volume differences emerge from the cross-sectional investigations. The increase has been confirmed to arise with just one month of treatment, occurring in the hippocampus, amygdala, anterior cingulate and prefrontal cortex (Monkul et al., 2007; Bearden et al., 2008; Yucel et al., 2008; Moore et al., 2009; Germaná et al., 2010). A plateau seems to be reached after a few months (Lyoo et al., 2010) but in cross-sectional studies, the relationship between volume change, dose and treatment duration over greater periods is difficult to discern (Bearden et al., 2007). Some studies have found that increases in grey matter are associated with a favourable clinical response (Moore et al., 2005, 2009; Lyoo et al., 2010).

5.1.1 Interpretations of the volumetric findings

The imaging findings demand an explanation, but the polemic nature of the field has polarised the interpretations. Thus, two major theories currently vie for supremacy: cellular hydration versus neuroplasticity. That these explanations have been pitched as opposing is not clearly explained by their biological basis or plausibility – indeed the theories are not mutually exclusive and may actually be inseparable.

HYDRATION THEORIES

In essence this theory is simple – lithium as a salt affects water homeostasis, so the grey matter volume increase reflects elevated cellular water content. This explanation was briefly entertained by the authors of the index study (Moore et al., 2000b), but dismissed because they found no increase in their MRS estimates of brain water. It has not been systematically examined in man since this assertion.

Nevertheless, the proposal has empirical support from preclinical work. When compared to those receiving placebo, rats treated with lithium for five weeks have more water in the frontal grey matter (dissected wet brain weight 3% greater than dry brain weight; Phatak et al., 2006). Although this may be of insufficient magnitude to directly account for the volume changes in some studies (e.g., Bearden et al., 2007; Regenold et al., 2008), it does approximate to the changes seen in the longitudinal studies of man with a similar time scale (Moore et al., 2000b, 2009; Monkul et al., 2007; Kim et al., 2008; Lyoo et al., 2010). It should be noted, however, that the change in water content observed by Phatak et al. (2006) did not reach significance for other brain areas and an MRI assessment of brain volume change was lacking.

NEUROPLASTICITY THEORIES

By some margin, the majority of authors favour an interpretation invoking lithium's purported enhancement of neuroplasticity (see §1.4.4 on page 14). Neuroprotective theorists claim support from MRS work showing that lithium increases brain NAA concentration. Elevation of NAA levels following lithium treatment has been observed in subjects with bipolar disorder (Moore et al., 2000a), seemingly proportional to the amount of grey matter in the region examined. When combined with the substantial preclinical data, the argument in favour of neuroplasticity appears to be compelling.

Early reports used the descriptives neuroprotective and neurotrophic interchangeably. Latterly the term neuroplasticity has found favour.

Enthusiasm for this explanation may be tempered on empirical and theoretical grounds. First, the findings of Moore et al. (2000a) require replication as a comparable study healthy subjects showed neither volume increase nor NAA change with lithium (Brambilla et al., 2004). Second, chronic administration of lithium to rats has no effect on neocortical volume, density of neurons, total number of neurons or mean volume of neurons, and does not increase their brain volume (Licht et al., 1994, 2003). Third, the neuroplasticity conclusion is reached through inference, there being no direct evidence for lithium-driven neurogenesis in the human brain.

The interpretation of the NAA finding is challenging, as the neurobiological role of NAA is far from established (Moffett et al., 2007). Increased NAA concentration may favour neuroprotection over neurotoxicity, but it does not resolve the proposed

conflict between neuroprotection and hydration as NAA estimates are not independent of brain water. Functioning as an osmotic regulator, changes in NAA concentration could be a cause or consequence of altered hydration. Further, if MRS measurements of NAA concentration are normalised to estimates of brain water – as with the study of Moore et al. (2000a) – increasing the actual amount of water in the brain would reduce the estimated NAA concentration, water signal being the denominator.

NEUROTOXICITY THEORIES

The neuroprotective interpretation is refreshingly optimistic since an identical but opposing argument structure could be advanced – cellular swelling due to a neurotoxic effect of lithium. Whilst important to consider in theory, that subjects in the studies to date were either carefully titrated to the correct serum concentration or were already tolerating an established treatment regime makes a neurotoxic explanation unlikely. Fountoulakis et al. (2008) have recently weighed the evidence for and against the neuroprotective and neurotoxic effects of lithium, incorporating the imaging findings within a balanced review of a sizeable field.

ALTERED MRI CONTRAST

Several authors have recognised that in theory, the changes detected in grey matter could arise from an alteration in signal contrast secondary to an undefined effect of lithium (Moore et al., 2000b; Monkul et al., 2007). None have acceded the point and the concept has not been explored. This thesis proposes a mechanism for such a contrast change, asserting that a change in signal intensity secondary to a reduction in the longitudinal relaxation time of water may better explain the imaging findings.

5.1.2 Lithium and the magnetic resonance signal

To justify an experiment investigating this matter, two premises must be established. First, it should be possible for alterations in the contrast of an image to be misinterpreted as a volume increase during analysis. Second, lithium must be capable of altering the MRI signal such that this occurs.

TISSUE CHARACTERISATION

Magnetic resonance imaging utilises the specific behaviour of protons in a magnetic field following radiofrequency excitation, the principles of which were covered in *Chapter 2*. To recap the most salient points, structural images are usually T_1-weighted; the degree of contrast is inversely proportional to the T_1 time of protons. Such contrast is relative and based on the voxel intensities at a specific acquisition time, the absolute T_1 values not being determined. When algorithms such as VBM make a judgement on what sort of tissue a voxel is most likely to contain, they do so on the basis of its intensity profile, weighted by its position in the brain and the class allocated to the neighbouring voxels (see §2.3.3).

The output of classification may be considered as categorical data, the dominant tissue in a voxel taken to represent its whole for the purpose of volumetric estimation. For much of the time, classification is straightforward – regions of relatively pure tissue class are not uncommon and in such cases the voxels tend towards homogeneity. Although the intensity profiles of white and grey matter overlap, in most cases they are sufficiently distinct to permit accurate discrimination. The problems arise when partial volume effects are encountered, wherein the contents of a voxel are not wholly accounted for by a single tissue.

PARTIAL VOLUME EFFECTS

Partial volume effects can arise because of genuine tissue mixing in areas such as the thalamus, or because of inadequate image resolution when the voxel spans distinct tissues. The signal profile of such voxels may span the range of intensities common to more than one tissue class – allocation becomes a matter of probability. Voxels subject to partial volume effects must either be excluded from analysis or allocated to a tissue type even in cases of uncertainty. Critically, changes in image contrast resulting from alterations in T_1 relaxation could alter tissue allocation in marginal cases, resulting in a difference in apparent volume.

TISSUE MISCLASSIFICATION

Recall the first premise, that tissue misclassification must be a possibility. Discussing how confounding effects can affect the validity of segmentation, Ashburner and Friston (2000, page 808) observe that 'Subtle but systematic differences in image contrast or noise can easily become statistically significant when a large number of subjects are entered in a study.' Although in the example provided they cautioned against collectively analysing data acquired from different scanners, the concern equally applies to systematic changes brought about by drugs.

Salgado-Pineda et al. (2006) tested the hypothesis that a drug-related change in T_1 would affect the image intensity and thereby alter the number of voxels attributed to grey matter during VBM analysis. Comparing a single dose of L-dopa with placebo in a randomised cross-over study of healthy subjects, T_1-weighted images were acquired before and after drug administration (mean 105 minutes). More voxels were classified as grey matter after L-dopa administration, exclusively in the substantia nigra and the VTA – the sites of its actions. It is difficult to envisage a neurotrophic mechanism for true changes in grey matter volume secondary to L-dopa occurring in less than two hours. There was, however, a change in the intensity of the midbrain voxels which was thought to account for their altered classification; the signal change probably arose from the effects of L-dopa on the cellular milieu and functional status.

LITHIUM AND PROTON RELAXATION

In support of the second premise – that lithium could cause a change in the MRI signal without altering brain volume – there are two pieces of empirical work. First, Rangelguerra et al. (1983) conducted a longitudinal investigation of 20 patients with bipolar disorder, gauging proton relaxation times before and after treatment with lithium. In all cases, lithium shortened the T_1 of protons in the brain. Second, simply adding lithium chloride to water shortens the T_1 of its protons (Fabricand and Goldberg, 1967); the magnitude of this effect is small but linearly related to the concentration of lithium. Consequently, the situation is such that not only could the grey matter volume increase be illusory, it may also be driven by a non-biological process.

5.2 STUDY OBJECTIVES

The study that follows explores the idea that the increase in grey matter attributed to lithium arises not from an actual change in the volume of the brain, but from an alteration in the magnetic resonance relaxation time of protons in tissues exposed to the drug. In essence, it is proposed that the apparent volume change is an artefact of the signal acquisition and image analysis process.

The tools and techniques required to investigate this matter are readily available to the researcher. What is required is a comparison of assessments of grey matter volume measurement, taken before and after lithium, using two different image analysis strategies – one relying on voxel intensity to derive tissue volumes and another less dependent on such. Optimised VBM fulfils the first requirement, SIENA the second (see §2.3.3). If there is a discrepancy between the measured volume change using the two techniques, it should arise in the context of an alteration in image intensity. It is now possible to measure the relaxation times of tissues *in vivo* at the voxel-level using high resolution T_1-mapping techniques (the principles of relaxometry are described in §2.4). The necessary scan sequences – T_1-weighted imaging and quantitative assessments of longitudinal relaxation – may be implemented on a clinical scanner. With the concerns raised and the tools selected, the following hypothesis was proposed:

> *In analysing T_1-weighted images acquired before and after the administration of lithium to healthy subjects, increased grey matter volume will be reported by automated techniques that segment tissues on the basis of image intensity, but not with algorithms that primarily detect boundary shifts. Further, quantitative T_1–mapping techniques will show a reduction in the spin-lattice relaxation times of protons following lithium, with this effect sufficient to account for the volumetric imaging findings.*

5.3 STUDY METHODOLOGY

5.3.1 *Study design*

The study conducted was an open-label, longitudinal investigation during which healthy subjects received lithium tablets for eleven days, randomly allocated to a high or low dose regime. Hereafter referred to as the MRC-LITE study, subjects were scanned before and immediately after completing the course of tablets. The study protocol was approved by an LREC and funded by the MRC.

Akin to MRC-LAMP, the study spanned an equilibration period followed by one week at the target level.

The T_1-weighted images collected in the MRC-LAMP study were also included, increasing the power of the analysis and permitting a comparison against placebo. Quantitative T_1 sequences were acquired from six participants in the MRC-LAMP study.

5.3.2 *Subject recruitment*

Recruitment and screening procedures largely matched those of the MRC-LAMP study (§4.4.2–3), though the inclusion and exclusion criteria differed slightly. Subjects were able to enrol in the MRC-LITE study regardless of handedness or past history of stimulant use. As most of the volunteers contacting the team were interested in the fMRI study, subjects in the MRC-LITE study tended to be those deemed unsuitable for stimulant administration or those who, on reflection, were disinclined to take it.

5.3.3 *Lithium administration*

The dose of lithium carbonate was calculated as previously described (§4.4.5), with the necessary blood samples acquired during the screening visit. The dosing strategy, administration period and tablet preparation in the MRC-LITE study matched that of the MRC-LAMP study, differing only in the open-label nature of the intervention. All subjects were randomly allocated to receive either a high dose or a low dose of lithium, aiming for blood levels of 0.5 and 0.9 mM respectively. Subjects were asked to fill in a simple diary indicating whether or not they took their medication on each of the study days, and then completed the LISERS on returning for their second scan.

5.3.4 *Scan acquisition*

Data was acquired from all participants using the same 3T whole body Philips Achieva System using an 8-channel SENSE head coil. After the acquisition of a T_1-weighted image (3D T1_FFE sequence: TR = 9.6 ms, TE = 4.6 ms; flip angle = 8°, FOV = 240 × 180 × 240 mm, contiguous isometric voxel size 1 mm), a fast quantitative T_1 measurement was performed using a custom inversion recovery prepared EPI sequence (FEEPI sequence: TR = 15 s, TE = 24 ms, TIR = 0.25 to 2.5 s in 12 uniform steps, matrix 128 × 128, 72 slices, isotropic 2 mm resolution), followed by a low resolution B_0 field-map using a dual echo GRE (3D FFE sequence, TR = 27 ms, TE = 2.6, 6.1 ms).

5.3.5 *Analysis*

The characteristics of the subjects and their medication regimes, together with the serum lithium concentrations achieved and side effects experienced, were analysed using SPSS (*v.*17, SPSS inc., USA). Image analysis was performed on a personal computer running a Linux operating system (Ubuntu 8.04 LTS) – an admixture of proprietary, open-source and locally developed software packages were used (SPM, MRICRO, FSL, MRIGURU and MATLAB®). Group summary statistics are reported as mean values ± sd, unless otherwise stated.

VOXEL-BASED MORPHOMETRY

Preprocessing T_1-weighted anatomical images were segmented into three tissue compartments using the VBM mode of SPM8. In normalising the images to a standard template, the option of modulation was selected such that the intensity of each voxel represented a volume measure. Segmented, normalised images were smoothed with a Gaussian kernel of 12 mm FWHM prior to voxel-wise comparison.

Voxel-wise analysis The smoothed images of the subjects receiving lithium were submitted to a voxel-wise comparison by paired *t*-test in a random-effects model; likewise the placebo group. Regional volumetric differences thus detected were deemed

to be significant at $p < 0.05$ following FWE correction. Exploratory analyses employed a lower initial height threshold ($p < 0.001$ uncorrected), significance ascribed at a corrected cluster-level threshold of $p < 0.05$.

Tissue volumes Global volumes for grey matter, white matter and CSF were derived from the relevant segmented images using the 'get_totals' function in SPM, accessed through the MATLAB® command-line. The percentage volume change for each tissue compartment in every subject was calculated using equation 4.4 (page 107), and a group mean derived.

SIENA ALGORITHM

The percentage brain volume change between the two scan sessions was also estimated with the SIENA algorithm. This package relies on segmentation only in so much as to detect the edges of the brain tissues; to limit partial volume effects, a two-compartment model was selected (brain tissue and CSF), thus determining whether the brain as a whole enlarged following lithium. The automated procedure was initiated with the terminal command-line code: `siena <input_file> <output_file> −2`

QUANTITATIVE T_1 ANALYSIS

Regional T_1 histogram generation The following stages of analysis were performed using MRIGURU, a locally developed package that enables T_1-maps to be constructed and the relevant data extracted from specified brain regions. Separately, T_1-weighted and quantitative T_1 images in proprietary PAR-REC format were converted to ANALYSE format before brain extraction (MRIGURU implements the BET algorithm of FSL). The quantitative, brain-extracted T_1 image for each subject was then reordered and unwarped using their phase map. These images were divided into 16 regions of interest for each tissue class (grey matter, white matter and CSF; 48 in total).

The regions of interest were defined at the lobar level, eight for each hemisphere and classified as follows: frontal (superior and inferior), parietal, parietal-temporal, temporal, temporal-occipital, occipital, cerebellum. Regional division was performed

in native space, lessening the errors associated with partial volume effects compared to standard space operations (Aribisala and Blamire, 2009). The process used a standard space brain ROI template which was transformed into native space for each subject, based on a multi-step registration using their T_1-weighted, brain-extracted image. The same T_1-weighted image was then segmented to create three masks, one for each tissue compartment (grey matter, white matter and CSF). These masks were combined with the transformed brain template to generate tissue specific anatomical regions of interest, in turn applied to the processed T_1-map.

Quantitative T_1 times were calculated on a pixel by pixel basis, and an isotropic 3D relaxation map produced. For each ROI, the MRIGURU algorithm automatically determined the T_1 relaxation time for grey and white matter, yielding a regional histogram of values – those from the cerebellum were excluded as its mixed tissue produces a bimodal distribution. The subjects' mean T_1 values for each region were analysed according to group and medication status (before and after lithium or placebo) using *t*-tests.

Voxel-based relaxometry The low resolution fitted quantitative T_1 map of each subject was co-registered to their high resolution brain-extracted T_1-weighted counterpart before normalisation to a T_1 template. The SPM package proved unsuitable for this step as the images were brain-extracted and their orientations differed after preprocessing. Using the advanced options within the FSL linear registration package FLIRT, co-registration was achieved in all but one case. The 'incorrectly orientated' search parameters were applied (X, Y and Z axis search angles of −180° to +180°), with registration to the FSL standard brain-extracted template (MNI152_T1_2MM_brain.nii).

The co-registered images were then smoothed with a Gaussian kernel of 12 mm FWHM before being submitted to voxel-wise comparison by paired *t*-test using SPM. An initial height threshold of $p < 0.001$ was used, with a subsequent corrected cluster-level threshold of $p < 0.05$ to identify clusters passing correction for multiple comparisons.

5.4 RESULTS

5.4.1 Subject characteristics

Eight subjects enrolled directly into the MRC-LITE study and 24 into the MRC-LAMP study, of whom 18 received lithium carbonate. One of the subjects in the MRC-LITE study had a poor quality scan which left a total of 25 lithium-treated, and six placebo-treated subjects with images suitable for analysis. One of the quantitative T_1 images from the MRC-LAMP study could not be adequately coregistered, and this individual was excluded from relevant analyses.

All of the subjects were male and between 18–35 years of age; average alcohol consumption was within recommended limits (see table 5.1). The lithium and placebo groups did not differ in the characteristics of their subjects on formal comparison.

5.4.2 Medication regimes

By self-report, subjects took their tablets on the majority of days, with no individual missing more than one dose. The mean duration of the course of tablets was 10.4 ± 1.6 days (all subjects, n = 31), with no difference between the groups. In those who received lithium, this resulted in a mean serum level of 0.64 ± 0.3 mM (all subjects on lithium, n = 25). Those randomised to receive a higher dose of lithium had greater serum concentrations of lithium than the lower dose group (higher dose group 0.82 ± 0.30 versus low dose group 0.47 ± 0.16 mM ; 2-sample *t*-test : *t* 3.77, 23 df, $p < 0.001$).

Side effects arising from the lithium/placebo tablets were few, rarely greater than mild intensity on the LISERS. A one-way ANOVA of the LISERS scores showed a difference within the three groups (F 4.73, 2 df, $p = 0.017$). *Post-hoc* analysis revealed no difference between the lower dose lithium group and placebo, but the higher dose group reported more side effects than other subjects (Tukey's HSD: higher versus lower $p = 0.048$; higher versus placebo $p = 0.032$). On no occasion were side effects sufficient to prevent a subject from completing the course of tablets, and no serious adverse events were reported.

	PLACEBO GROUP	LITHIUM GROUPS	
		LOWER DOSE	HIGHER DOSE
CHARACTERISTICS			
Age (years)	25.4 ± 4.0	22.9 ± 5.0	21.8 ± 2.6
Body mass index (kg/m^2)	24.3 ± 2.1	24.2 ± 1.9	24.5 ± 3.2
Alcohol (units per week)	18.3 ± 9.1	18.0 ± 7.9	17.9 ± 13.8
TREATMENT DETAILS			
Duration of treatment (days)	10.2 ± 1.5	10.5 ± 1.7	10.4 ± 1.6
Side effects (LISERS score)	1.3 ± 1.5	2.5 ± 2.4	5.8 ± 4.5
Priadel™ dose (mg per day)	—	923 ± 192	1367 ± 317
Serum lithium level (mM)	—	0.47 ± 0.16	0.82 ± 0.30

Table 5.1: Descriptive statistics (mean ± sd) according to group for the MRC-LITE study. Lithium group: higher dose (n = 12), lower dose (n = 13); placebo group (n = 6).

5.4.3 Voxel-based morphometry volumes

LITHIUM GROUP

Grey matter volume increased after lithium (volume in cm^3: pre-lithium 749.6 ± 80.8, post-lithium 758.0 ± 83.3; t −3.63, 23 df, p = 0.001). This equated to a increase in grey matter volume of 1.11% when all those taking lithium were analysed. White matter was unchanged whilst the volume of the CSF compartment reduced (pre-lithium 273.1 ± 40.2, post-lithium 264.7 ± 41.5; t 3.24, 23 df, p = 0.003); see table 5.2 on page 173.

At a trend-level, percentage grey matter volume change correlated with the serum lithium level (r = 0.337; p = 0.099); the inverse was found for CSF (r = − 0.341; p = 0.096). The higher and lower dose groups did not differ in the percentage grey matter volume change (higher dose = 1.64 ± 1.71%, lower dose = 0.63 ± 1.28%; t −1.68, 23 df, p = 0.11). The sample was divided *post-hoc* into high (n = 12) and low (n = 13) serum concentration groups, above and below 0.7 mM respectively (higher concentration = 0.88 ± 0.19 mM; lower group = 0.41 ± 0.14 mM). A trend for the percentage change in grey matter volume to be greater in the high-concentration group was detected (high concentration = 1.71 ± 1.65%, low concentration = 0.57 ± 1.30%; t 1.93, 23 df, p = 0.066). Grey matter volume increased in the high-concentration group (pre-lithium 749.5 ± 74.3, post-lithium 762.5 ± 78.3; t −3.55, 11 df, p = 0.005), but not the low-concentration group (pre-lithium 749.6 ± 89.4, post-lithium 753.8 ± 90.6; t −1.67, 11 df, p = 0.12).

	GREY MATTER	WHITE MATTER	CEREBRAL FLUID
LITHIUM			
Pre-treatment	749.6 ± 80.8	552.6 ± 64.1	273.1 ± 40.2
Post-treatment	758.0 ± 83.3	554.1 ± 58.4	264.7 ± 41.5
PLACEBO			
Pre-treatment	707.6 ± 84.0	543.6 ± 77.6	279.5 ± 34.1
Post-treatment	699.7 ± 88.5	550.3 ± 80.1	277.1 ± 31.9

Table 5.2: Tissue volumes by VBM analysis, with volumes as mean ± sd in cm^3. The lithium group reported here includes all subjects (n = 25), placebo group (n = 6).

PLACEBO GROUP

In the placebo group, no significant difference was demonstrated for grey matter or CSF volumes, but an increase in white matter volume was found over the time period of the study (543.6 ± 77.6 versus 550.3 ± 80.1; t −4.14, 5 df, $p < 0.01$).

BETWEEN GROUPS

Percentage change tissue volumes were compared in those receiving lithium (n = 25) and placebo (n = 6). Percentage grey matter volume change differed between the two groups (lithium versus placebo; t 2.67, 29 df, $p = 0.012$), but white matter did not (lithium versus placebo; t −0.76, 29 df, $p = 0.455$).

5.4.4 Voxel-wise comparison using VBM

Submitting data from all subjects who received lithium to a voxel-wise comparison revealed no clusters representing volume increase at the FWE correction threshold of $p < 0.05$. Specifying a factorial design by dose in SPM, a comparable analysis was performed for the higher and lower dose lithium groups. Subtracting the pre-lithium from the post-lithium images in the higher dose group at the FWE correction threshold of $p < 0.05$, grey matter volume increase was seen in a solitary cluster (−6 · 0 ·20; voxels = 31, T = 5.41, $p = 0.015$). Those taking a lower dose of lithium also demonstrated a regional increase in grey matter volume on VBM, a single cluster passing the threshold for significance (−14 · −22 ·4; voxels = 10, T = 5.31, $p = 0.028$); see figure 5.1.

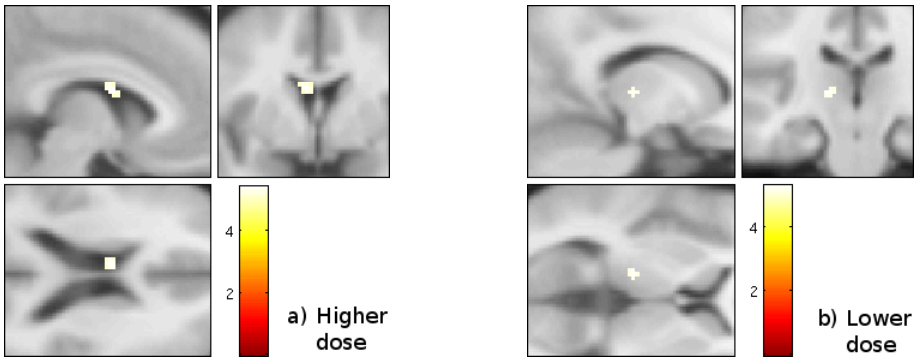

Figure 5.1: Regional grey matter change by voxel-based morphometry for the groups randomised to receive higher (n = 12) and lower (n = 13) doses of lithium (height threshold T = 4.95, extent threshold k = 0 voxels, $p < 0.05$ FWE). The scale represents the t-score for the rendered voxels.

5.4.5 *Volume change using the SIENA algorithm*

Percentage brain volume change over the course of the study was determined for each subject, and the group means compared – mean PBVC values were small, with no difference between the lithium and placebo groups (placebo group – 0.01% ± 0.17; lithium group 0.24 ± 0.48; t –1.23, 29 df, p = 0.23).

5.4.6 *Proton T_1 relaxation time*

Following lithium administration, there was a small but significant reduction in mean grey matter proton T_1 relaxation time when mean values derived from the histograms of all brain regions were compared (1474 ± 98 ms to 1466 ± 94 ms; z –2.65, 168 ranks, p = 0.008). Considering each lobar region in turn, before and after lithium, trend-level reductions in the mean grey matter proton T_1 were found in the temporal-occipital region on the left (1501 ± 56 ms versus 1482 ± 51 ms; z –1.83, 12 ranks, p = 0.060) and the occipital region on the right (1520 ± 69 ms versus 1503 ± 70 ms; z –1.73, 12 ranks, p = 0.084). White matter proton T_1 values were unchanged following lithium.

At a trend-level, percentage grey matter volume change correlated negatively with the change in grey matter T_1 values (r = – 0.500; p = 0.098); likewise serum lithium concentration and grey matter T_1 values (r = – 0.517; p = 0.085).

Submitting the grey and white matter T_1-maps separately to a voxel-wise paired t-test analysis, no significant regional differences emerged for either tissue class.

5.5 DISCUSSION

The results of this study could be interpreted as supporting the *a priori* hypothesis that lithium does not increase the actual volume of grey matter but rather reduces the proton longitudinal relaxation time, which emerges as an apparent structural change when the VBM technique is applied. In the following discussion the existing imaging data is appraised; the results of the MRC-LITE study presented in this chapter are considered in this context and the overall findings of the field summarised. The potential value of the VBM findings are highlighted, as are the shortcomings of the various other techniques applied. The proposed mechanisms by which lithium may bring about the observed findings are then explored, as are the reasons why a definitive conclusion may be elusive.

5.5.1 *Volumetric consequences of lithium administration*

In the MRC-LITE study, short-term administration of lithium to healthy men increased grey matter volume on VBM, leaving white matter volume unchanged. This finding replicates previous automated image analysis studies of the effects of lithium in healthy volunteers (Leow et al., 2005; Monkul et al., 2007) and patients with bipolar disorder (Moore et al., 2000b, 2005, 2009; Kim et al., 2008; Lyoo et al., 2010). The consistency of the observations suggests that the image analysis techniques are detecting a genuine difference in the MRI data before and after lithium. In the following discussion, that difference is not disputed but the interpretation of grey matter volume increasing as a result of enhanced neuroplasticity or altered cellular hydration is critically reviewed.

Clinical imaging studies to date have almost exclusively investigated either bipolar disorder or healthy subjects, despite there being a strong case for studying unipolar disorder.

First, a note on magnitude. Within the context of other studies, the mean increase in grey matter volume of 1.11% reported in this thesis is small. There are many reasons why this may be the case, notably the differences in the study designs, the duration of lithium administration and the specifics of the analyses undertaken. A powerful factor in the magnitude of the volume change is likely the choice of subjects – studies of healthy subjects yield smaller findings than those of patients with bipolar disorder. It must be recognised that the effects of lithium on a normal brain may differ substantially

from those occuring in illness states. Neuroprotective explanations, for example, are to be eschewed in the absence of a stressor and a cellular insult may be a requisite for the initiation of neurogenesis.

STUDY DESIGN

Prospective studies
· MOORE 2000
· LEOW 2005
· MONKUL 2007
· KIM 2008
· MOORE 2009
· LYOO 2010

Longitudinal studies The strongest design of study is the initiation of lithium with prospective follow-up. Subjects act as their own controls, selection bias is reduced and the accuracy of brain volume measurement is better than in cross-sectional studies. Moore et al. (2009) recently reported an extension to their original study of ten patients (2000b), adding 18 more subjects with bipolar disorder and finding that lithium increased total grey matter after one month, significantly so in the prefrontal cortex. Independently replicated in bipolar disorder (Kim et al., 2008) and healthy controls (Leow et al., 2005), a volume increase of 2–4% typifies the longitudinal studies, though the effect is sometimes seen only in frontal cortical regions (Monkul et al., 2007). Lyoo et al. (2010), in the only published prospective study examining a comparator intervention, found that lithium increased grey matter volume by approximately 3% over a period of several weeks. No change in volume was observed in patients treated with sodium valproate; healthy subjects not in receipt of an intervention acted as a control group, and demonstrated stable brain volumes. White matter volumes were unchanged in all groups.

Cross-sectional studies A greater number of cross-sectional studies than prospective ones have been conducted – the majority have demonstrated a lithium-related increase in grey matter, though some have not (Brambilla et al., 2002; Chen et al., 2007). When increases are reported, they are generally of a greater magnitude than those in the longitudinal investigations, substantially so in some studies. In terms of design, the principal weakness is that of selection bias towards, or against, lithium treatment in the patient groups. Such biases may exaggerate the magnitude of the findings. Cross-sectional comparisons of patients and healthy subjects are likely to be marred by true pathological differences unrelated to lithium.

A priori studies
· SASSI 2002
· BRAMBILLA 2002
· YUCEL 2008
· BEARDEN 2008
· GERMANIÁ 2010

The results of the *a priori* cross-sectional studies are mixed. Sassi et al. (2002) found that patients on lithium had much larger grey matter volumes than their untreated counterparts and healthy controls (748 versus 676 and 639 ml respectively). In a study of the hippocampus in bipolar disorder, Yucel et al. (2008) compared patients taking lithium with those receiving either sodium valproate/lamotrigine or no medication – the hippocampus (and its head) was larger in patients taking lithium compared to unmedicated subjects and healthy controls, intermediate volumes being found in the sodium valproate/lamotrigine group. Using surface-based anatomic mapping, Bearden et al. (2008) reported that the hippocampal volume of patients with bipolar disorder receiving lithium was 13.9% larger than that of unmedicated patients and 10.3% larger than healthy control subjects. Aiming to replicate diminished SGPFC volumes in bipolar disorder, Brambilla et al. (2002) hypothesised that subjects receiving lithium would not differ from healthy controls – as it happens, no abnormalities were detected and lithium had no bearing on the volumetric measures.

Post-hoc analyses
· BEYER 2004
· JAVADAPOUR2007
· BEARDEN 2007
· CHEN 2007
· SCHERK 2008

It is now routine to consider lithium when discussing structural imaging findings in the affective disorders – several authors have interrogated their data *post-hoc*. Beyer et al. (2004) reported that elderly subjects with bipolar disorder had larger left hippocampal volumes compared to age matched controls, attributing this difference to lithium. In a region of interest study, Javadapour et al. (2007) found that subjects with bipolar disorder had larger right ACC volumes compared to healthy controls, with a striking increase of 26% reported – the difference was significant in those taking lithium, but not with other medications. A recent optimized VBM study compared healthy subjects to those with bipolar disorder and found no difference in global grey matter volumes (Chen et al., 2007). When advanced techniques are used to map cortical grey matter, patients with bipolar disorder appear to have substantially greater tissue densities compared to controls (Bearden et al., 2007) – translating to a volume excess of about 9%, this difference was considered 'entirely attributable to patients treated with lithium'.

The volumetric findings of the MRC-LITE study here reported most closely approximate to those of the longitudinal studies, but the magnitude falls short of the reported

range. This indicates that other aspects of the interventions and assessments require scrutiny. In the sections that follow, the influence of the duration of treatment, the dose administered and the clinical effects of lithium are considered.

DURATION OF TREATMENT

The most obvious reason for the diminutive grey matter volume increase in the study reported here is the short period of lithium administration. Subjects in the MRC-LITE study took lithium for approximately 11 days, only the last week of which could be considered to be at a stable target serum level. Logically, regardless of the mechanism at play, volumetric increase on MRI must develop over time, eventually reaching a plateau. A simple linear correlation between duration of treatment and grey matter volume change is therefore unlikely, and in any case has not been found (Sassi et al., 2002). Bearden et al. (2007) reported a significant association between grey matter volume change and duration of treatment, finding a quadratic relationship between the two variables once the logarithm of the time on medication was plotted – something of a challenge to interpret.

The data from the study of Kim et al. (2008) supports an early effect as the increase in grey matter observed in the lithium group was evident at four weeks, unchanged at the end of the four month long study. In the studies of Moore et al., (2000b; 2005; 2009) scans were performed after one month on lithium, but the actual effective treatment duration may have been substantially less because of the titration schedule used. Lyoo et al. (2010) charted the course of grey matter volume change in patients with bipolar disorder and a healthy comparator group. Patients were randomly allocated to receive either lithium (n = 13) or valproate (n = 9), and were naïve to these medications prior to enrolment. Analysing 93 scans from 36 individuals, lithium but not valproate was associated with an increase in grey matter volume (2.56%, equivalent to 17.6 cm^3). Fitted to a quadratic mixed-effect regression model, the increase in grey matter volume peaked at 10-12 weeks. The fitted data of Lyoo et al. support the VBM findings of this thesis – subjects in the MRC-LITE study took lithium for a brief period it is possible that a greater volume change may have been observed over a longer course.

That the findings of this thesis largely match those of Lyoo et al. (2010) may also reflect the purity of the initiation of lithium. Importantly, patients in the studies of Moore et al., (2000b; 2005; 2009) were not necessarily lithium-naïve and those taking the drug at enrolment entered a two week washout period prior to the ostensible initiation of lithium treatment. This would be expected to have marked effects on mental state, theoretical effects on brain structure, probably generated a selection bias akin to the cross-sectional studies and in terms of wash-out and reversal of cellular effects, was of insufficient duration. The contribution of these effects to the magnitude and direction of brain volume change is too complicated to predict.

SERUM CONCENTRATION OF LITHIUM

Clinical studies have investigated patients either maintained at a therapeutic level or titrated to such a level as part of the protocol, the latter invariably the case for the healthy subject work. The range of serum levels in a given study is therefore quite narrow, with a target level of around 0.8 mM being common. No dose-effect studies have been conducted. As correlations across a limited range of values are unlikely to be meaningful, it is not surprising that few studies have included an analysis of the relationship between grey matter volume change and serum lithium level. By way of example, Moore et al. (2009) found no such correlation and the target level dictated by their protocol resulted in a restricted range of serum lithium levels (0.9 ± 0.2 mM).

In this thesis, no significant correlation between grey matter volume change and serum lithium concentration was observed, but an association at a trend-level was noted. The notion that greater concentrations of lithium induce more volume change on VBM was supported by the difference between the high and low serum level groups. In the group achieving a high serum concentration, the mean lithium level was 0.88 mM and their 1.73% grey matter volume increase using the values derived from VBM was closer to the changes reported in comparable longitudinal clinical studies (Moore et al., 2000b, 2005, 2009). It is important not to over emphasise this observation as the division of subjects was performed *post-hoc*, with no difference observed in the percentage grey matter volume change when the *a priori* groups were compared.

In the index study (Moore et al., 2000b), grey matter increases were observed in eight of the ten participants, and similar proportions have been reported in other studies. This begs the question of whether a subgroup can be defined in which the effects of lithium are manifest through imaging.

The therapeutic response to lithium is probably the most important of the variables to consider. In the longitudinal studies of bipolar disorder, most patients were depressed at the time of enrolment and response to lithium assessed with standard mood rating scales. Kim et al. (2008) found that grey matter volume increase was associated with clinical improvement. In a more detailed analysis, Moore et al. (2009) demonstrated an increase in grey matter volume in 20 of their 27 patients, comprising 9 of 10 lithium-responders and 11 of 17 non-responders. A trend-level correlation between response (HAM_D mood rating scale score) and grey matter increase was found ($p = 0.075$). For prefrontal cortical grey matter volumes, a main-effect of lithium and a trend towards a treatment-by-response interaction was shown ($p = 0.07$), in which lithium-responders had a significant volume increase ($p = 0.003$) but non-responders did not. In the longitudinal study of Lyoo et al. (2010), patients responded equally well to treatment with lithium or valproate, but only in those taking lithium did the improvements in depressive symptoms correlate with grey matter volume increase (Spearman $\rho = -0.59$, $p = 0.03$). In the cross-sectional studies, therapeutic response has not been formally gauged and so comparative analyses have not been possible.

Obviously therapeutic effects cannot inform the discussion of the results of this thesis, all the subjects being healthy volunteers. The closest approximation would be the LISERS scores and the RVIP task performance in those completing the MRC-LAMP study. These measures arguably focus on the detrimental effects of lithium, which may have little to do with its therapeutic potential. Further, arguing that the subjects with the greatest side effects are comparable to the patients who respond overlooks the fact that the true comparison should be with those patients who were less able to tolerate lithium. Such patients are unlikely to have completed the scanning studies.

5.5.2 *Summary of the reported findings*

The MRI studies describing a lithium-related increase in grey matter volume have a degree of consistency that suggests the observation is valid. To reiterate, that lithium has a detectable effect on grey matter is not disputed in this thesis, rather the assumption that the imaging findings represent a tangible increase in the physical volume of the brain. When discussing the potential mechanisms by which lithium may cause this effect, it may be of use to consider whether a pattern to the findings exists.

- The most important observation is that the change in grey matter can occur in those with bipolar disorder *and* in healthy subjects.
- The magnitude of the effect of lithium appears to be more marked in patients than in healthy subjects, and may be related to treatment response in the former.
- The grey matter difference occurs within in a time-scale consistent with the onset of the therapeutic effects of lithium, reaching a plateau within a few months.
- Serum levels in the therapeutic range appear to be necessary.
- The effect is seen across brain regions, the largest reported changes being in prefrontal and hippocampal areas.

5.5.3 *Synthesising the imaging findings*

All of the MRI studies investigating the the effect of lithium on brain structure have, by necessity, applied a processing step to distinguish grey matter from adjacent tissue classes. Various different automated and semi-automated image analysis packages have been used, but it would be reasonable to assert that all made use of the voxel intensity profile whilst segmenting the brain.

The VBM package relies heavily on intensity whilst segmenting the brain and in the study reported here, showed a lithium-related increase in grey matter volume. The SIENA algorithm uses voxel intensity to define the brain/CSF boundary, the volume change determined by analysing the boundary movement between scan sessions.

Using SIENA, no difference was detected in the mean percentage brain volume change for the placebo and lithium groups. No change in volume was observed in the placebo group and the mean change of 0.24% in the lithium subjects was barely above the 0.2% error range for this technique.

If the VBM findings represented a true change in brain structure, SIENA should have matched it in magnitude – as predicted, this was not the case. It was hypothesised that the VBM findings would be better explained by an alteration in voxel intensity, in turn due to lithium reducing the proton T_1 time. Analysis of the quantitative T_1 data revealed a reduction in proton T_1 when mean values for grey matter in all lobar regions of interest were compared (excluding cerebellum). Divided by regions, the reduction in T_1 values in the grey matter was significant in the superior frontal lobes, an area of apparent volume increase on VBM voxel-wise comparison. The mean T_1 reduction correlated with the VBM-derived percentage grey matter volume change at a trend-level. Collectively, these findings substantiate the *a priori* hypothesis and question the conclusions of the field at large.

5.5.4 Consequences of a reduced proton T_1

It has previously been established than an increase in voxel intensity can be misinterpreted as a regional increase in grey matter volume with VBM (Salgado-Pineda et al., 2006). With T_1-weighted imaging, reducing the proton T_1 increases the signal intensity and may reduce the contrast between tissue types; in grey matter, voxel intensity profiles would more closely approximate to those of white matter. Why then, if contrast is to blame, does lithium not cause an increase in white matter volume?

This is a difficult question to answer, and one clearly open to conjecture. It may be assumed that the categorisation of existing white matter voxels is unchanged by lithium as no change in their T_1 was observed. Likewise, an enormous change in signal would be required to confuse pure CSF with brain tissue. Grey matter voxels are inherently difficult to classify as their intensities overlap both CSF and white matter profiles, making them the likely site of segmentation errors in areas prone

to partial volume effects. In voxels containing a mixture of white and grey matter, reducing the T_1 should increase the likelihood of it being allocated to the white matter class. In voxels containing grey matter and CSF, one could argue that the increased signal intensity would exaggerate the contribution of the grey matter and swing the classification away from CSF. The grey matter/CSF boundary of the cortex is highly convoluted and the number of voxels prone to partial volume effects is large, greater than in the white matter and arguably greater than at the white matter/grey matter boundary (Rueda et al., 2010). A systematic reduction in grey matter T_1 may emerge as misclassification in these areas, explaining why the grey matter increase almost exactly matched the CSF reduction in this thesis. In support of this account, VBM localised the grey matter increase to the left lateral ventricle and thalamus (figure 5.1), the mixed tissue of this nucleus making it prone to partial volume effects.

It must be said that the reduction in proton T_1 observed, although significant, was small. Rangelguerra et al. (1983) reported a substantial reduction in the proton T_1 of patients with bipolar disorder (264 ± 88 ms before lithium, 208 ± 80 ms after; n = 20). In keeping with the reported volumetric findings, it may be that the magnitude of the effect of lithium in normal subjects is lesser, though the difference between the results presented here and those of Rangelguerra et al. (1983) are striking. Nevertheless, the change in relaxation time described in this thesis may be sufficient to bring about the required change in voxel intensity.

The absolute values for T_1 are shorter because the study was conducted at a lower field strength.

$$S = \frac{S_0 \left(1 - e^{-TR/T_1}\right) sin\alpha}{\left(1 - cos\alpha\right) e^{-TR/T_1}} \tag{5.1}$$

Signal intensity in T_1-weighted imaging can be calculated using equation 5.1 (above). In the MRC-LITE study, repetition time, echo time and flip angle were consistent across the sessions (TR = 9.6 ms, TE = 4.6 ms, $\alpha = 8°$) such that alterations in signal intensity must reflect a difference in the T_1 of protons. Submitting the mean T_1 values before and after lithium (1474 ms and 1466 ms respectively) to equation 5.1 and comparing the values, a 0.4% increase in grey matter signal intensity returned. The sensitivity of VBM to a systematic difference of this magnitude requires further investigation.

5.5.5 *Lithium-driven mechanisms of proton T_1 reduction*

Introduced as a premise (Rangelguerra et al., 1983) and confirmed by investigation, lithium appears to reduce the longitudinal relaxation time of protons in the brain of man. Whilst it is of interest that this occurrence could explain the volumetric findings from MRI studies, the mechanism by which proton relaxation is altered may arguably be of greater importance. That it could feasibly be related to the therapeutic effects of lithium may prove to be of some significance. A number of mechanisms could be proposed but, given the origins of the MRI signal, the interaction between lithium and water warrants the most attention.

KEY PROPERTIES OF WATER

'Water is H_2O, hydrogen two parts, oxygen one, but there is also a third thing that makes water and nobody knows what that is'. *D.H. Lawrence Pansies (1929)*

In isolation, a water molecule can be considered as a tiny v-shaped structure of the formula H_2O. In bulk, water may not simply be a random collection of these molecules but rather a complex network of hydrogen-bonded units which *en masse* give rise to anomalous liquid properties (Ball, 2008). It has been argued that in pure bulk water, the molecules have a propensity to cluster and transiently adopt various configurations, the nature of which is determined in large part by hydrogen bonding (Chaplin, 2000). The extent of the order in this *structuring* is influenced by various ambient factors such as temperature, pressure and applied electromagnetic radiation. Various models of the structure of bulk water have been proposed and contested, some more outlandish than others and none gaining universal acceptance(Wallqvist and Mountain, 1999). The main stumbling-block is the paucity of empirical data to support the existence of complex molecular configurations in bulk water – hydrogen bonds break and reform over picosecond time scales such that the proposed structures could exist only fleetingly (Eaves et al., 2005). Nevertheless, bulk water has been 'conceptualized as a mixture of two rapidly interconverting species: a less dense, more structured form, and a more dense, less structured arrangement' – Zhang and Cremer (2006, citing Chalikian (2001)).

Compared to the models of pure bulk water, evidence for the structuring of water in the presence of other ions has a stronger foundation. Water molecules are highly polarised and strongly attracted to ions, clustering around them to form an ordered primary hydration shell (Marcus, 2009). This shell may further alter the structuring of the neighbouring water molecules resulting in a larger, secondary hydration shell. The potency of various ions differs in this regard, as does their propensity to increase or decrease the structuring of water. Ions which bring order to the structure of water are termed *kosmotropes*, those diminishing the order are *chaotropes*; they are ranked in the *Hofmeister series*, the robustness of which is greater for anions than cations.

	KOSMOTROPIC	CHAOTROPIC
CATIONS	$Ca^{2+} > Mg^{2+} > Li^{+} > Na^{+}$	$K^{+} > Rb^{+} > Cs^{+} > NH_4^{+}$
ANIONS	$SO_4^{2-} > HPO_4^{2-}$	$Cl^{-} > NO_3^{-}$

Adding a kosmotrope to water can be thought of as making it more 'ice-like' (Ball, 2008) – its density is reduced and solutes are less likely to dissolve. A greater degree of structure equates to a more efficient spin-lattice energy transfer. It should be no surprise then, that the proton T_1 of an aqueous solution of lithium chloride is shorter than that of pure water (Fabricand and Goldberg, 1967). Indeed, the effects of ions on the T_1 of water closely follows the Hofmeister series (see figure 5.2). The question is whether this fundamental effect accounts for findings reported in this thesis.

Structuring water reduces its density, so the addition of lithium should cause an increase in the volume of water. This effect will be minuscule at the levels attained during treatment – this consequence of kosmotropy must not be confused with the proposed effects on MRI signal intensity and derived volumes.

LITHIUM & BULK WATER PROTON T_1

When lithium interacts with water molecules, its positive charge attracts the oxygen atom to create a primary hydration shell with outward facing hydrogen (Hermansson and Wojcik, 1998). Until recently, ions were thought to affect the structuring of water throughout its bulk by altering the strength of hydrogen bonds, kosmotropes such as lithium increasing the stability of clusters. This may not be the most suitable model to aid interpretation, as much of the effect of ions is restricted to the immediate

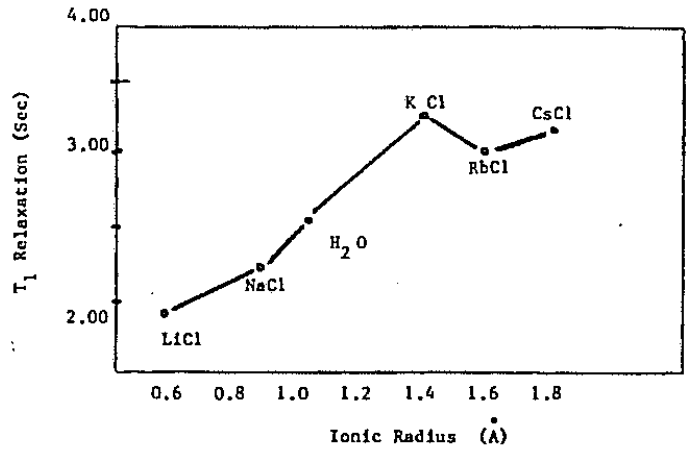

Figure 5.2: Plot of T_1 relaxation times of water protons versus crystal radii of alkali cations in aqueous solutions of alkali halides. Study performed at NMR frequency of 100 MHz on 4M solutions of alkali chlorides. (figure and caption reproduced from Rangelguerra et al. (1983))

hydration shell and the Hofmeister series pertains only to ions near a surface (Zhang and Cremer, 2006; Marcus, 2009). Water molecules beyond the hydration shell of the ion may remain randomly arranged, or at least not differently ordered than pure bulk water. Nevertheless, the small ionic radius and dense nuclear charge of lithium attracts more water molecules than sodium (Marcus, 2009), likely accounting for its more marked effects on proton T_1 (Rangelguerra et al., 1983). Presumably the localised effects of lithium on the relaxation of adjacent water molecules averages out as a T_1 reduction within the whole MR sampling volume.

In aqueous solution, proton T_1 is inversely related to lithium concentration (Fabricand and Goldberg, 1967). Extrapolated to therapeutic levels, with relaxation times adjusted to clinical field strengths, a very modest T_1 change would be envisaged. The effect of lithium on water structure is therefore unlikely to be of sufficient magnitude to explain findings in this thesis. The potency of a kosmotrope may, however, depend not just on its concentration but also on the presence of ambient factors. Application of a high magnetic field may have altered the water structuring potential of lithium, though there is no sound basis to favour a dramatic increase in structuring potency over a comparable decrease. Nevertheless, this fundamental physical effect in its purest form – no matter how minor – must be considered to contribute to the proton T_1 reduction and hence apparent grey matter volume change.

The Hofmeister series has empirical origins, the ions first being ranked in this way by their propensity to stabilise or destabilise solutions containing egg-white protein. As a diluent, water is not inert and in hydrating proteins it modifies their three-dimensional structure, an occurrence necessary for the protein to function (Ball, 2008). Water in close proximity to proteins is more structured than bulk water and factors which affect the ease with which this structuring is adopted may determine the conformational state of the protein, hence its functional status. Thus, kosmotropes foster the hydration, solubility, folding and stability of proteins; the converse is true of chaotropic ions.

The interaction between water, proteins and ions is potentially of great importance in understanding the effects of lithium on MR images. First, it serves as a reminder that the cellular environment is very different to that of a simple aqueous solution and that the number of sites where lithium can act may be substantially greater. In addition to the direct action of the ion on adjacent water molecules, its ability to alter the conformational state of proteins may widen the field of its effects – altering the structure of water across the entire protein may magnify the ionic reduction in proton T_1 of cellular water compared to aqueous solutions.

Second, it may explain the localisation of proton T_1 reduction to grey matter. The CSF can be considered as a relatively simple aqueous solution, immune to the postulated effects of proteins on relaxation parameters. White matter, with its high lipid content, may restrict the range of the effects of lithium as the ion's large hydration sphere (Marcus, 2009) will inhibit its mobility in such environments. Grey matter is laden with hydrophillic molecules, is the site of many of the effects of lithium and of the brain tissues, it is the most vulnerable to partial volume misclassification.

Third, it implies an association between the biological actions of lithium and the magnitude of MRI signal change. Lithium is thought to bring about a number of its effects through altering the functional status of key intracellular enzymes, potentially competing with the co-enzyme magnesium to alter calcium-dependent signalling

processes in the neuronal cell bodies (Birch, 1976). The hydrating effects of lithium more closely approximate to calcium and magnesium than to sodium and potassium, with the former ions being stronger kosmotropes than the latter. Localisation, signal distortion and therapeutic action may thus converge.

5.5.6 Signal change in complex systems

Thus far, the lithium ion has been considered the primary and direct cause of proton T_1 reduction, invoking its kosmotropic actions to explain this effect and as a possible parallel, its pharmacological properties. What if the direction of this argument were to be reversed? Could the proton T_1 reduction simply be a product of the myriad actions and effects of lithium, the consequence of diverse or disparate mechanisms rather than the agent of change? To do so would bring the argument full-circle, the neuroplasticity and hydration theories once more having currency in the debate – this time not through a tangible change in volume, but rather as modifiers of the cellular milieu and so the T_1 of protons in the brain.

Historically, unified theories which converge on a single action of lithium tend to fare poorly; sometimes the worth of an extreme view lies not in its validity, but in the clarity it may bring to the middle ground.

CELLULAR HYDRATION AND THE MR SIGNAL

Simply increasing the amount of water in brain tissue might be expected to increase its T_1 towards that of CSF. Whilst this is typically seen with oedema (Kato et al., 1986), the reverse can also occur (Yun et al., 2007). It may be inaccurate to conceptualise the tissue changes brought about by lithium as analogous to pathological oedema and so in terms of the MRI signal, the consequences of lithium increasing cellular hydration are open to speculation. Myoinositol is an osmoregulator and so it could be argued that the interaction between lithium and the components of the PI-cycle mediate the findings of the volumetric MRI studies. Free myoinositol levels are elevated in mania (Gani et al., 1993), so the effects of lithium on water homeostasis may be more marked in patients than in healthy subjects. Further, lobar variations in myoinositol concentration (Silverstone et al., 2005) may explain the regional differences in the MRI findings. However, the effects of lithium on hydration in the rat brain were not thought to be mediated through myoinositol (Phatak et al., 2006).

Neuroplasticity theories present less of a problem, but only in so much as there is no data to guide the debate. It is eminently possible that the T_1 characteristics of new or regenerating neurones differ from those of stable populations, something amenable to empirical testing should neurogenesis actually be established to occur in the adult human brain. It must also be recognised that the pathophysiological processes underpinning bipolar disorder may increase the T_1 of tissues, only for it to be normalised by lithium (Rangelguerra et al., 1983; Besson et al., 1987). Such observations also serve as a reminder that healthy subjects and patients may respond differently to the administration of lithium.

5.6 CONCLUSION

The data presented in this chapter gives credence to the theory that the lithium-related increase in grey matter observed using MRI arises not from a tangible change in brain volume, but from an alteration in relaxation properties of the tissues under investigation. In a longitudinal study of lithium administration to healthy subjects, grey matter volume increase was observed using VBM, but not with boundary-shift techniques; a small but significant reduction in grey matter proton T_1 accompanied these findings. A trend-level inverse relationship between grey matter volume change on VBM and grey matter T_1 time was observed; likewise grey matter T_1 reductions and serum lithium concentration. The implications, strengths and weaknesses of the study are discussed in the final chapter of this thesis.

6 LITHIUM SPECTROSCOPY

Whilst much is known of the pharmacokinetics of lithium in man, a complete account of its distribution in cells and tissues is lacking. Were this situation to be rectified, pharmacodynamic theories may be better modelled and important clinical questions addressed. It is the nature of lithium that has hindered progress – it cannot be usefully labelled, has no helpful particle-emitting isotopes and is not thought to displace receptor ligands; traditional spectroscopy techniques are only applicable *in vitro* and lithium may redistribute too rapidly for such methods to be of value in postmortem examination. Magnetic resonance spectroscopy – a technique proven in the natural sciences – has been applied in the biomedical field to good effect. In addition to possessing certain advantages as a method for determining the concentration of lithium *in vitro*, MRS has permitted the detection of lithium *in vivo*. The feasibility of determining the concentration of lithium in the human brain is well established, but the technique is restricted to a few specialist centres; progress has been slow and along somewhat divergent avenues.

This chapter describes a series of lithium MRS experiments which, building on existent approaches and expanding current knowledge, converge on an objective with novel elements: determining the absolute concentration of lithium in the human brain in a time scale suited to clinical use, in a manner that permits comment to be made on its level in different tissue classes.

6.1 BACKGROUND

6.1.1 The distribution of lithium in tissues

Following its administration, lithium distributes throughout the mammalian body (Birch and Hullin, 1972; Birch and Jenner, 1973; Ebadi et al., 1974; Stern et al., 1977). In doing so, its concentration remains within the same order of magnitude in almost all tissues (Birch, 1991) – table 6.1 on the following page. It is notable that with chronic

	Birch (1972)	Birch (1973)	Ebadi (1974)	Stern (1977)	
REGIME	Chronic	Chronic	Acute	Acute	Chronic
DURATION	18 month	28 day	—	—	12 day
ROUTE	po	po	iv	ip	ip
DAILY LITHIUM INTAKE (mmol Kg^{-1})	0.8	0.8	7.2	0.6	0.6
TIME AFTER LAST DOSE (hours)	12	12	24	12	12
TISSUE CONCENTRATION (mmol Kg^{-1})					
Brain	0.18	0.18	1.22		
Muscle	0.30	0.22	1.60		
Bone	1.38	1.15	1.59		
Liver	0.15		0.53		
Kidney	0.53		1.35		
Spleen			0.97		
Serum	0.17	0.14	1.22	0.08	0.21
Pituitary				0.26	0.39
Thyroid				0.31	0.43
Adrenal				0.15	0.24

Table 6.1: Concentration of lithium in different tissues following different treatment regimens in rats, administered orally (po), intravenously (iv) and via intraperitoneal (ip) routes (from Birch 1991).

administration, lithium appears to concentrate in bones, perhaps a consequence of the diagonal relationship with calcium (§1.1). Furthermore, endocrine glands attain higher concentrations than the serum, an observation of relevance to common side effects such as thyroid dysfunction. The distribution of lithium in the rat brain has been examined using atomic absorption techniques, in which small volumes of tissue are typically dissected and homogenised before submission to analysis. Reviewed by Ramaprasad (2005), post-mortem examination following chronic administration initially indicated an even distribution of lithium throughout the rat brain (Davenport, 1950). Subsequently, heterogeneous distributions were observed, lithium reaching higher concentrations in the hypothalamus, putamen and neocortex (Ozawa et al., 1976), and intermediate levels in the thalamus, septal nuclei, dentate gyrus and hippocampus (Nelson et al., 1980).

6.1.2 *Distribution of lithium in the human brain*

Few post-mortem studies examining the distribution of lithium in the human brain have been reported. Francis and Traill (1970) reported two cases, both patients having received lithium for only a few days prior to death. Concentrations of lithium were found to be highest in the basal ganglia and pituitary, and lowest in the spinal cord. In slight contrast, Spirtes (1976) observed higher concentrations in the hypothalamus and white matter than in the grey matter, thalamus and cerebellum – the patient examined suffered from bipolar disorder in life, and died from alcohol and opioid toxicity. Such studies are difficult to interpret, but with the advent of clinical MRS, and latterly the availability of high field strength scanners, it is now possible to explore the pharmacokinetics of lithium in man (Renshaw and Wicklund, 1988).

6.1.3 *Magnetic resonance properties of lithium*

In order to appraise the use of lithium MRS, a basic understanding of its magnetic resonance properties is required (the principles of magnetic resonance spectroscopy were outlined earlier in section 2.6). Naturally occurring lithium contains two isotopes and although both are visible using MRS, their respective properties differ. In the case of ^{6}Li (I = 1), the combination of its low abundance (7.42%) and slow relaxation (T_1 > 1000 s) means that it is poorly suited to clinical MRS. Conversely, the ^{7}Li nucleus is more abundant (92.58%), has a moderately low sensitivity compared to protons and an estimated T_1 time that makes experiments long but not impracticable (see tables 2.2 and 6.2).

That ^{7}Li yields a spectral singlet simplifies its delineation, but its nature precludes compartmental discrimination on the basis of tissue specific chemical shift. Its Larmor frequency at a given field strength can, however, be manipulated with shift-reagents. This property may be utilised during quantification and potentially exploited in the determination of intracellular concentrations, at least *in vitro* (Komoroski, 2000).

Akin to the other alkali metals, ^{7}Li (I = ⅜) is a quadrupolar species but in clinical and preclinical studies, these relaxation properties appear sufficiently weak for it

	TISSUE	SUBJECTS	B_0 FIELD (T)	REPORTED T_1 TIME (S)
RODENT STUDIES				
Ramaprasad (1992)	head		4.7	3–4
Ramaprasad (1998)	head		7	2.4
HUMAN STUDIES				
Renshaw (1988)	muscle	1	1.8	7.0
Komoroski (1993)	head	1	1.5	4.6
Gonzalez (1993)	head	2	1.5	4.2
Riedl (1997)	head	2	1.5	3.2–3.5
Girard (2001)	head	4	1.5	4.0–4.3
Kushnir (1993)	head	5	2.0	3.5 ± 0.25
Moore (2003)	head	1	4.0	4.7

Table 6.2: T_1 relaxation times for lithium in which the data fit a monoexponential decay.

to have been treated as a dipole (Komoroski, 2000). Single exponential modelling of its relaxation *in vivo* in man places the T_1 between three and five seconds, with shorter values closer to two seconds in the rat (Ramaprasad et al., 1992; Ramaprasad, 1998). There appears to be variability in the T_1 time between subjects, and differences according to field strength. In the rodent studies reviewed by Ramaprasad (2005), T_2 relaxation was found to have fast and slow components in the ranges 3–80 ms and 125–320 ms respectively. Little is known of the T_2 relaxation of lithium in man, but the ^{7}Li isotope yields a single narrow spectral line *in vivo*, suggesting a swift decay.

6.1.4 *Synopsis of the lithium MRS field*

The feasibility of detecting lithium in the human brain was demonstrated by Renshaw and Wicklund (1988), their experiment also being notable as the first to detect an exogenously administered substance of any kind using the MRS technique. In addition to the necessity of replication, early studies sought to establish the amount of ^{7}Li in large tissue regions, localised by surface coil placement (Komoroski et al., 1990, 1993; Gyulai et al., 1991; Kato et al., 1992, 1993, 1994, 1996; Kushnir et al., 1993). The concentration of ^{7}Li in the brain was almost invariably found to be lower than that in the serum, brain-to-serum ratios of 0.5–0.9 typifying the above studies.

Strictly speaking, the early studies with surface coils assayed lithium levels in the head, extracerebral structures being included in the sampling volumes.

From these and later studies, a simple or consistent correlation between brain and serum concentrations of ^{7}Li has not emerged, perhaps explained by its compartmental pharmacokinetics. It appears that ^{7}Li is rapidly absorbed into the serum, entering tissues fairly swiftly and crossing the blood-brain barrier within an hour (Renshaw and Wicklund, 1988). Tissue accumulation lags behind serum fluctuations, peaking earlier in muscle than in brain (Komoroski et al., 1990). Similarly, elimination from serum is more rapid than from muscle, in turn more rapid than from brain (Komoroski et al., 1993). The half-life of ^{7}Li in the brain is around 30 hours compared to an average of 20 hours for lithium in the serum; brain-to-serum ratios thus increase with time since last dose despite falling concentrations (Plenge et al., 1994).

Having established a framework and tissue-specific pharmacokinetics, ^{7}Li MRS studies moved to address the relationship between brain concentration and clinical parameters. Whilst some authors contested that brain concentrations more readily correlated with side-effect burden than serum levels (Kato et al., 1996), the value of ^{7}Li MRS as a predictor of therapeutic response is not universally upheld.

González et al. (1993) introduced the use of volume coils, overcame transmission and sensitivity constraints with adiabatic pulse sequences and B_1 field corrections, and selected their repetition times and reference methods to achieve absolute quantitation; admirable SNR within acceptable scan durations resulted. Their methods have since been replicated and adapted (Sachs et al., 1995; Soares et al., 2001; Moore et al., 2002).

A more recent goal of the field has been the charting of the distribution of ^{7}Li by spectroscopic imaging, favouring the use of volume coils (Komoroski, 2005). Based on post-mortem studies and the findings of rodent MRS studies in which very long scan times are possible (Komoroski and Pearce, 2004), regional differences in the distribution of ^{7}Li were anticipated in man. This appeared not to be the case, with uniformity of the ^{7}Li signal across brain regions reported (Girard et al., 2001). Realistically, spectroscopic imaging is unlikely to achieve anything other than a crude localisation, typical voxel resolutions being 4.3 × 4.3 × 6 cm. The ^{7}Li nucleus yields a singlet – much like protons in water – so it may be possible to visualise it with strategies akin to MRI. Early work supports this notion, with millimetre resolution

possible (Boada et al., 2010; Lee et al., 2010). Regrettably, the nature of the pulse sequences used in the reported imaging studies render the absolute quantitation of ^{7}Li an impracticality, relative differences in estimated concentrations being the reality. Thus to date, no human study has combined adequate resolution with an appropriate strategy to discern absolute ^{7}Li concentrations according to brain structure or tissue class.

6.2 EXPERIMENTAL OBJECTIVES & STRATEGIES

The principal aim of the work presented in this chapter was to develop a technique to measure the *in vivo* concentration of lithium in the human. Experiments were performed with a bespoke surface coil interfaced with a 3T clinical scanner. Secondary objectives at the outset were the acquisition of data in a time-scale suitable for potential application in a clinical setting and the determination of lithium concentration in different tissue classes, specifically comparing grey and white matter. It transpired that characterising the relaxation properties of lithium was paramount to achieving these aims. In preparing the techniques, the work of González et al. (1993) took a central position; their methods and strategies were adopted and adapted as follows:

- Combining a high field strength scanner with a surface coil to optimize the SNR.
- B_1 field modelling to correct for the inhomogeneous sensitivity of our coil, together with adiabatic RF pulses to address the comparable transmission profile.
- Minimising partial saturation effects by using repetition times informed by locally determined empirical estimates of the ^{7}Li T_1 in solution and *in vivo*.
- Quantitation of brain ^{7}Li by way of a coil-mounted external reference, calibrated against known concentrations of lithium chloride in aqueous solution.
- Estimation of the concentration of ^{7}Li in different brain tissues, using a morphometric segmentation analysis of T_1-weighted images to determine the proportion of grey and white matter in the volume sampled by MRS.

The experimental process was necessarily iterative, optimisation of the fundamental techniques only possible through pilot appraisal of the more advanced, yet ultimately contingent stages. In this account, a logical flow is taken in favour of an unabridged chronological narrative, at each stage summarising the key principles together with the techniques and findings of others.

6.3 INSTRUMENTATION & METHODOLOGY

6.3.1 Radiofrequency coil

An RF coil should be suited to requirements of the experiment at hand, in this case necessitating the construction of a new device. The first consideration in the development of an RF coil is its configuration and for ^{7}Li, various designs have been reported: principally surface coils; latterly volume coils; coil arrays to a lesser extent.

Surface coils Yielding high SNR by focusing on specific regions of interest, surface coils can localise signal by virtue of placement in addition to acquisition parameters. The transmission and reception profiles of surface coils are characteristically inhomogeneous, resulting in substantial variations in tip angles over the sample volume and reductions in the SNR with depth.

Volume coils Capable of covering the entire head, such coils may be used to sample large volumes and tissues at depth. Their principal disadvantage is a low SNR, a major limiting factor to resolution with low sensitivity nuclei. Bird-cage designs offer the advantage of homogeneous B_1 fields, but they are difficult to construct – proprietary phosphorous head-coils may be re-tuned to the frequency of ^{7}Li with relative ease.

Dual arrays Using a volume coil for pulse transmission and a surface coil for signal detection combines the benefits of homogeneous excitation with a favourable SNR. Such arrays present technical challenges which undermine this potential, notably phase incompatibility and field misalignment.

To achieve swift quantitation and tissue discrimination, a high SNR was deemed desirable and whole brain imaging unnecessary – the decision was made to perform the experiments with a *surface coil*. The shortcomings of a surface coil are not insurmountable and the strategies utilised are described at the appropriate junctures in the sections that follow. The salient points of the coil design are summarised below.

COIL DESIGN

A simple transceiver surface coil was constructed in-house, 8 cm in diameter, and tuned to 49.6 MHz using variable capacitors. The coil circuitry was housed in a locally manufactured polyurethane case of 8 mm thickness, with a central positional marker and an access port for the external standard reference. Tuning and matching rods extended from the housing, accessible at arm's length during scanning. The device, hereafter referred to as the ^{7}Li coil, was designed for placement over the frontoparietal regions of the head, combining biological relevance with ease of positioning against anatomical surface markers. The ^{7}Li coil was secured to a cushioned head restraint using Velcro™ attachments.

SCANNER-COIL INTERFACE

All experiments were performed on the same 3T Achieva whole body scanner (Philips Medical Systems, Best, The Netherlands) equipped with a second broadband channel for non-proton nuclei. The ^{7}Li coil interfaced with the scanner through a 'pig-tail' connector, the cable incorporating a $\frac{1}{4}\lambda$ sleeve balun. The cable was lightly secured in place to prevent movement during signal acquisition and subjects were shielded from direct contact with it.

6.3.2 Phantoms

VOLUME PHANTOMS

The phantoms for our studies were prepared in-house using plastic containers of various dimensions. In all instances the solute was analysis water, to which crystalline lithium chloride and sodium chloride was added as required.

A phantom is an artificial object with established characteristics, used to test and/or monitor the performance of an MR system.

EXTERNAL REFERENCE STANDARD

An external standard reference marker was mounted on the coil – directly above its centre and within the housing – comprising a hollow polyurethane sphere of uniform thickness, sealed after being filled with an aqueous solution containing lithium chloride and dysprosium chloride. Dysprosium acts as a shift reagent, displacing the ^{7}Li resonance to enable the discrimination of signals acquired concurrently from the subject and marker. The development and validation of the external reference is described in more detail later in this chapter.

Solutions were prepared by Dr Richard McQuade, Institute of Neuroscience, Newcastle University.

6.3.3 Subjects

DEVELOPMENTAL STAGES

To permit methodological developments, access to a pool of subjects with appreciable levels of ^{7}Li in their brains was required; namely the participants in the MRC-LAMP and MRC-LITE studies. Subjects were drawn from these studies as and when they were required, largely determined by the rate of experimental advances. Thus, recruitment in the development phase was not systematic, there being no guarantee of an even distribution of subjects on high and low dose lithium regimes. Application of the developmental ^{7}Li MRS techniques fell within the ethical approval granted for the MRC-LAMP and MRC-LITE studies.

MRC-LISP STUDY

The development process culminated in a pilot study (MRC-LISP) in which a small sample of subjects were invited to take lithium carbonate before returning to undergo MRS examination, specifically the discrimination of lithium level by tissue class. No baseline scans were required and the majority of subjects were investigated on the same day, minimising variations in scanner performance. Details of the subjects and the study design are provided in §6.8. Conducting a pilot investigation fell within the remit of the initial research proposal, approved by an LREC and funded by the MRC.

6.3.4 *Analysis*

All statistical analysis was performed using SPSS (*v.*17, SPSS inc., USA), with group data are reported as mean ± sd for each variable. Analysis of the spectroscopy data throughout this chapter was performed by Dr Fiona Smith.

6.4 PULSE DEVELOPMENT & CALIBRATION

At the outset of the experimental series, use of two pulse sequences was envisaged: a simple block pulse and a more sophisticated adiabatic pulse, the testing, calibration and application of which are described below. In all instances, the energy delivered to the subjects through the coil fell within specific absorption rate guidelines.

6.4.1 *Block pulses*

The form of a block pulse is simple – RF amplitude is constant when present and the transition between on and off states is abrupt, creating a squared profile. All things being equal, the tip angle is a product of the amplitude and duration of transmission. With block pulses, the tip angle can be easily varied and a range of frequencies excited. Block pulses were used in the initial exploratory stages of this project as well as during signal acquisition from the reference compound in the final quantitative protocol.

CALIBRATION

EXPERIMENT
· calibration run
· aqueous phantom
· 2 litre plastic tub
· 100 mM $LiCl{\cdot}H_2O$
· block pulse

For the calibration series a cuboid phantom was placed over the ^{7}Li coil, its dimensions covering the active volume of the coil. The container was filled with 2000 ml of an aqueous solution of lithium chloride, 100 mM in strength (this high concentration was chosen to ensure adequate coil loading and signal detection). Positioned in the scanner bore, tuning and matching was optimised before a pulse-acquisition series was run. A range of pulse durations were applied within a TR of 1000 ms, 60 unlocalised averages acquired on each occasion. Each FID underwent Fourier transformation, apodisation, line-width broadening of 20 Hz and phase shifting by visual inspection. The spectra were processed using the AMARES algorithm within the *j*MRUI software

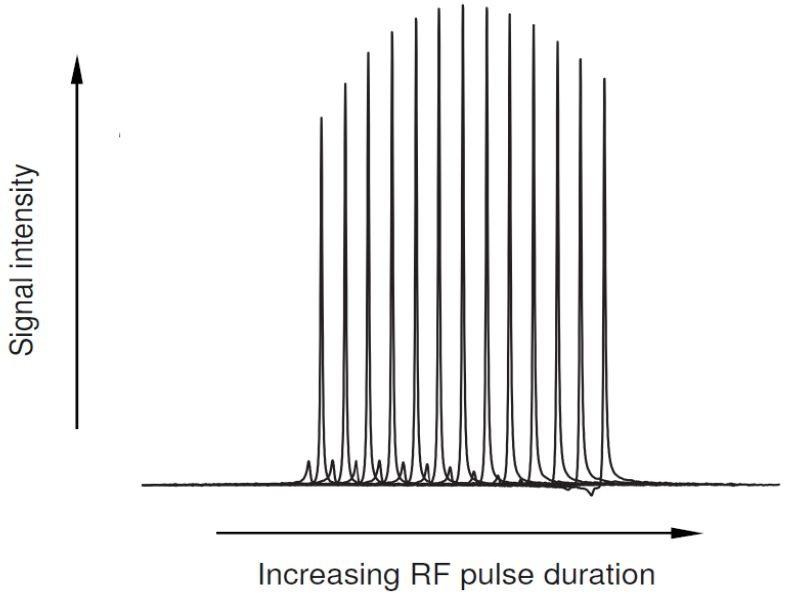

Figure 6.1: Pulse calibration series for the lithium coil using an aqueous phantom of 2000 ml volume, containing lithium chloride at a concentration of 100 mM. The parameters of the pulse giving rise to the largest signal were used to 'request' a 90° tip in future experiments.

package. Peak areas so derived were plotted against pulse duration; the parameters for a 90° pulse were taken as those which resulted in the maximum signal over the series (see figure 6.1 above). The process was repeated using a phantom containing lithium chloride at a concentration of 3 mM, the results of which demonstrated that the calibration was upheld at near-therapeutic levels.

LIMITATIONS

With surface coils, inhomogeneous B_1 fields principally occur when block pulse sequences are applied and are no small matter, intensity changing ten-fold within the sensitive volume of a coil. This is of course borne out as a variation in the tip angles induced, their magnitude falling with distance from the coil; the receive profile fits an identical pattern, sensitivity being lower at greater depths. Combining these properties means that adequate SNR can only be obtained for limited volume, roughly hemispherical with a depth approximately equalling the coil diameter. A 90° tip will be achieved in a fraction of this volume.

EXPERIMENT
· signal by depth
· aqueous phantom
· 1.5 ml glass vial
· 100 mM $LiCl{\cdot}H_2O$
· block pulse

To gauge the limitations of the ^{7}Li coil, signal was obtained from a small phantom placed at various distances from the coil. A 1.5 ml glass vial filled with an aqueous solution of lithium chloride (100 mM) was placed inside the central bore of an annulus-shaped, five litre aqueous phantom. This proprietary phantom was designed to ensure adequate coil loading whilst allowing small samples to be placed at various distances from the coil surface. After tuning and matching, pulse calibration was performed with the vial abutting the coil housing. A pulse-acquisition experiment was conducted, in which 40 averages were collected for several tip angles at a series of depths (TR = 1000 ms). The requested pulse angles (30 · 60 · 90 · 135 · 180 · 270°) were derived from the calibration run; the depth ranged from 15–140 mm in 5 mm increments, the offset due to the coil housing and vial base.

Consider the signal returned for each pulse angle requested in the region close to the coil (figure 6.2): requesting a 90° tip produces the maximum positive signal; applying a 270° pulse results in a comparable negative signal; the 180° pulse yields the null. Now consider the signal as a function of depth for each pulse, acknowledging that the B_1 field intensity reduces with distance from the coil. For a given pulse, moving away from the point of calibration results in a tip angle that is smaller than requested. With a calibrated 90° pulse, signal intensity progressively declines; the signal from stronger pulses shows a sinusoidal pattern in which the maximum positive deflection represents the depth at which the B_1 field has induced a 90° tip. The sinusoidal forms are damped – the maximum positive deflection from the 270° pulse is smaller than its counterpart from the 90° pulse. This is a consequence of the receive profile of the coil.

As expected, the combined inhomogeneities in transmission and reception precluded useful detection beyond 8 cm. Whilst these empirical findings are of interest, it is neither practical nor desirable to chart the complete profile of our surface coil. The receive profile can be corrected using the computer models described presently; transmission inhomogeneity effects can be overcome by using adiabatic pulses.

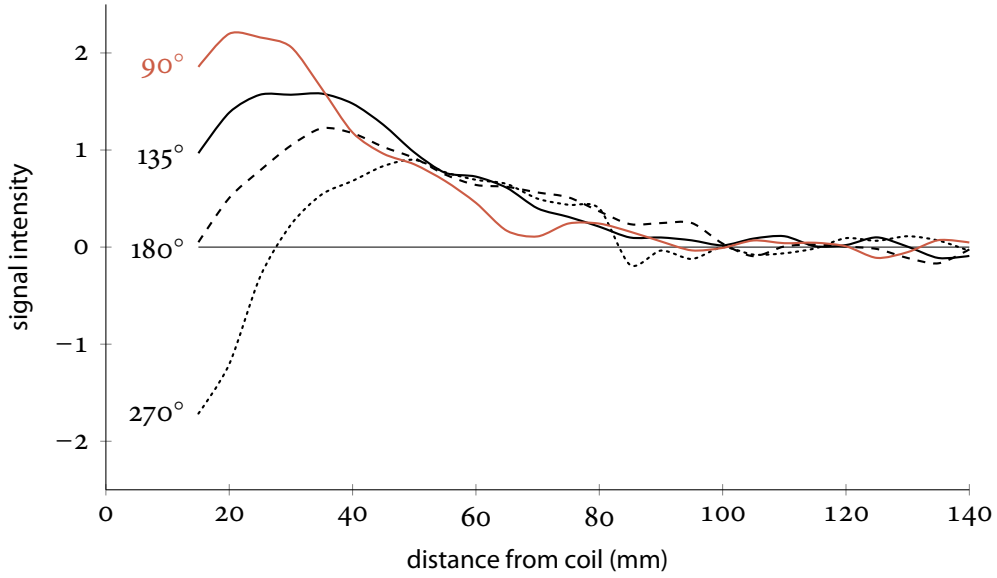

Figure 6.2: Profile of the lithium coil determined empirically. A small vial containing an aqueous solution of lithium (100 mm) was moved away from the coil in 5 mm increments. Signal was acquired at each depth, with various tip-angles requested. The 90° series (coloured line) shows diminishing signal with depth. Larger tip-angles returned their maximum signal intensities at greater depths, but their maximum intensities were smaller than that of the 90° tip series – this arose from the lowering of the receive sensitivity of the surface coil with distance.

6.4.2 *Adiabatic pulses*

Adiabatic pulses are fundamentally different to the transmission sequences thus far described. With a block pulse, the B_1 field is applied fully but intermittently and when present it excites the full range of selected frequencies simultaneously. In the case of adiabatic pulses the frequency of the excitation varies with time throughout the application of the RF waves. The RF frequency and amplitude are swept according to the adiabatic condition from off-resonance to on-resonance. When the adiabatic condition is satisfied, the tip angle of the net magnetisation vector is uniform and independent of B_1 amplitude, provided that a certain threshold has been crossed. Calibration need only be performed once, establishing the rate of sweep and B_1 threshold necessary to achieve the desired tip angle. Pulses resulting in a 90° tip are usually referred to as *adiabatic half-passage excitations*, full-passage denoting 180° conditions.

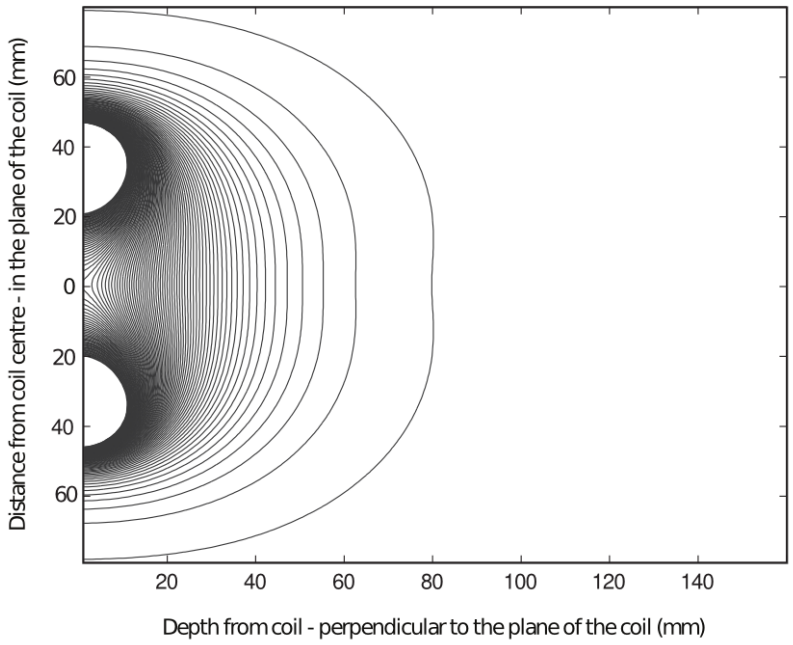

Figure 6.3: Modelled B_1 field for the lithium coil – this was used to derive the receive profile of the coil, enabling the correction of sensitivity loss with depth.

6.5 RECEIVE PROFILE

The receive profile of a surface coil matches that of its transmission – signal detection falls with depth but the problem cannot be overcome at the interface between the subject and the scanner. By characterising the receive profile, signal intensity can be systematically corrected during the analysis process. Replicating the work of Haase et al. (1984), the B_1 field of the ^{7}Li coil was modelled using MATLAB® functions. In block pulse transmission, the tip angle achieved is proportional to the B_1 field; in effect, the B_1 map also describes the sensitivity in detecting signals. This model was used to weight the signal received according to depth, its profile depicted in figure 6.3.

6.6 RELAXATION CHARACTERISTICS

For the reasons outlined in §2.6.4, it is desirable to understand the relaxation properties of the nucleus under investigation at the field strength used. In essence, to quantify a substance the degree of signal saturation must be known. Data on ^{7}Li T_1

in vivo is scarce and in man, limited to a few small studies or solitary reports, most of which involved subjects receiving lithium as treatment for an affective disorder. Consequently, normative group data is lacking. In the studies estimating the T_1 of ^{7}Li in man, data has generally been fitted to a monoexponential decay – when tested, biexponential models have not significantly improved the results. The notable exception, in preclinical studies, is the finding of Renshaw et al. (1986). Investigating the relaxation characteristics in a puppy head at 1.8T, a biexponential decay with fast and slow components of 3.5 and 6.6 seconds (30% and 70% respectively) was observed. This finding stimulated much debate, and it remains unclear if the findings are best explained by the contribution of different tissues to the relaxation data (such as muscle), or by genuine biexponential decay *in vivo*.

Monoexponential decays are found with dipolar spins, biexponential with quadrupolar. Biexponential decays are usually described as having fast and slow components.

6.6.1 Aqueous solution

The T_1 of lithium in aqueous solution is of interest and importance for a number of reasons. First, aqueous phantoms are easy to construct and a variety of compositions can tested – the relaxation of ^{7}Li should not alter with concentration, but estimates of the likely SNR *in vivo* can be made on aqueous phantoms without inconveniencing subjects. Second, in quantifying brain lithium concentration, use of an external reference was envisaged; this was most likely to be a solution containing lithium, the parameters of which had to be established. The methods used to determine the T_1 time of a sample are outlined in §2.6.5 on page 54.

BLOCK PULSE

Determination of the T_1 time of lithium in solution was performed using a saturation recovery technique (steady-state, spectral bandwidth = 8000 Hz, FOV = 350 mm, 2048 data points, 20 averages, 8 phase cycles, no volume selection; TR range: 5 to 75 s). The FID at each pulse duration underwent Fourier transformation, apodisation, line-width broadening of 20 Hz and phase shifting by visual inspection. The spectra were processed using the AMARES algorithm within the *j*MRUI software package. Peak areas were plotted against repetition time and the T_1 determined by finding the best

fit of the data to a curve given by the saturation expression below (equation 6.1, where S is the signal intensity). The experiment was repeated on three occasions over several days, from which the mean T_1 time was derived.

$$S_{(TR)} = S_{\infty}\left(1 - e^{-TR/T_1}\right) \tag{6.1}$$

In a 2000 ml cuboid phantom containing an aqueous solution of 50 mM lithium chloride, the mean T_1 of lithium was 13.5 ± 0.65 s. It was envisaged that block pulses would be used to acquire signal from the external standard during *in vivo* work; this scenario was simulated by placing a hollow polyurethane sphere containing the lithium solution (50 mM) in a cuboid phantom loaded with normal saline. Repeating the saturation recovery experiment with 40 averages yielded a T_1 of 17.1 ± 0.85 s.

The discrepancy between the T_1 values was thought to be due to the inhomogeneous B_1 field and receive profile of the coil. It was likely that a 90° tip angle would have been achieved over the entirety of the small sphere, but only part of the volume phantom – in other regions, the block pulse would have excited a greater range of tip angles. Spins tipped by degrees less than 90° attain equilibrium more swiftly, and in contributing the the sample as a whole, spuriously reduce the T_1 determined in the experiment. Consequently, the T_1 derived from the sphere was accepted.

The data from one of the saturation recovery experiments using the 2000 ml phantom is shown in figure 6.4 (on page 206). The decay curve was made to pass through zero as is usually the case, and it can be seen that the T_1 relaxation of lithium in aqueous solution may fit a single exponential decay. Intriguingly, signal intensity increased as repetition times approached zero – a finding that was consistent across experiments and phantom concentrations. The profile was not obviously biexponential and the occurrence was attributed to the phenomenon of *steady-state free precession*. When samples are re-excited too swiftly, dephasing of spins may be incomplete and a transverse component of the net magnetisation vector can persist; this is effectively incorporated into the longitudinal component that arises with the next excitation, adding to the signal subsequently detected.

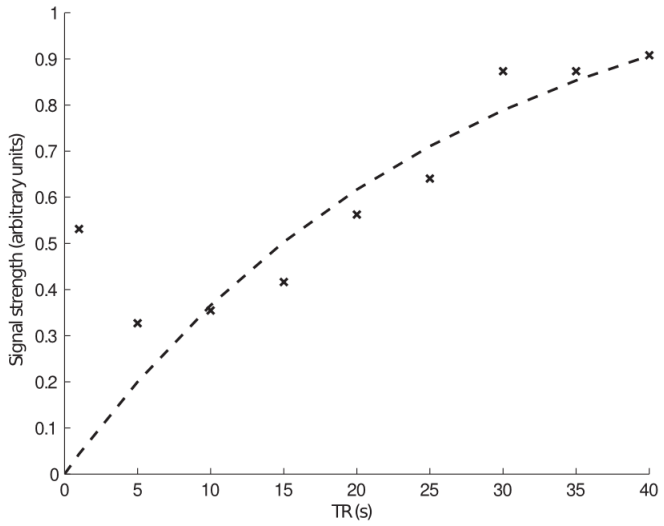

Figure 6.4: T_1 relaxation data for an aqueous solution of 50 mM lithium chloride in a 2000 ml volume phantom. The increase in signal intensity with the shortest TR is discussed in the text.

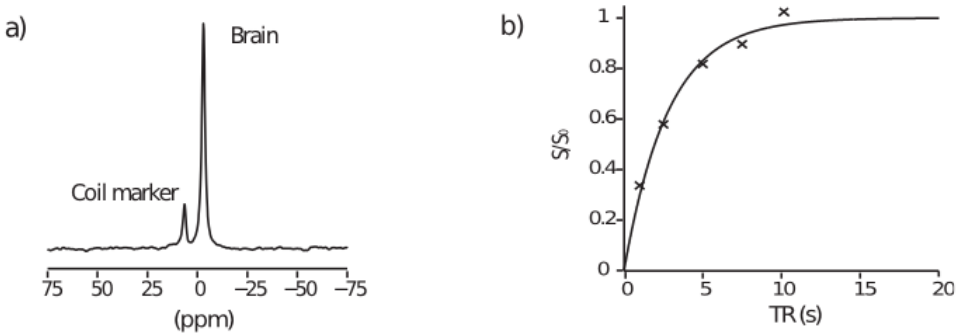

Figure 6.5: (a) Lithium MRS spectra *in vivo* in a healthy subject; the lithium in the reference sample (coil marker) is shifted by the addition of dysprosium chloride. (b) Estimation of the T_1 relaxation time in the healthy human brain; adiabatic pulse sequence and an 8 cm surface coil (2.4 ± 0.4 s).

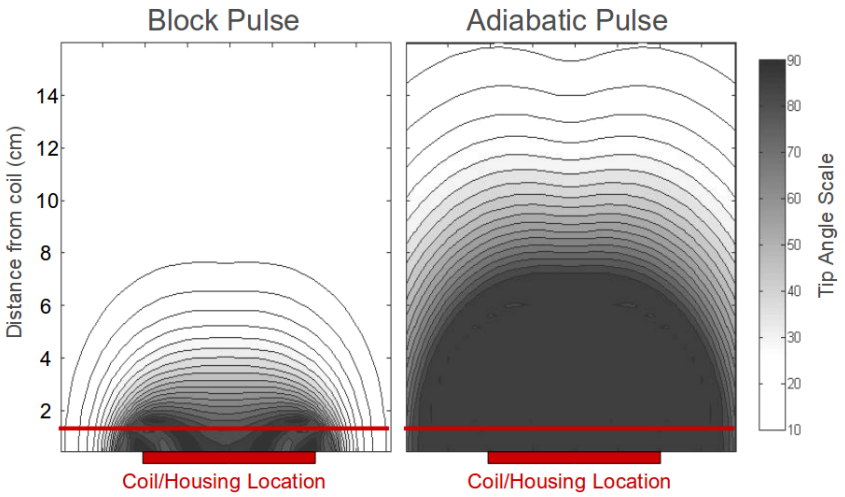

Figure 6.6: Bloch simulation of a block-pulse and adiabatic pulse sequence for the lithium coil.

6.6.2 *Human subjects*

T_1 measurements were made in the brains of healthy male subjects participating in the MRC-LITE study (n = 7, age 22 ± 4 years, duration of lithium administration 11 ± 1.6 days, serum lithium concentration 0.61 ± 0.3 mM). Data was acquired using a non-localised steady-state saturation sequence in which a 90° adiabatic half-passage excitation was applied over five repetition times (6 ms pulse duration, spectral width of 8000 Hz and 2048 data points). Forty averages were acquired at each TR (1000 · 2500 · 5000 · 7500 · 10000 ms), translating to a scan duration of just under 18 minutes. An example *in vivo* spectrum and T_1 fitting is provided in figure 6.5 on the previous page. Direct fitting of the saturation-recovery data yielded a T_1 of 2.0 ± 0.4 seconds.

The T_1 calculation assumed that a 90° uniform excitation was achieved across the whole volume. To justify this, the theoretical spatial B_1 distribution of the surface coil was used in a Bloch simulation of the complete adiabatic acquisition sequence (figure 6.6 above). The reliability of the saturation according to depth from the coil was determined, thereby estimating the potential error in the calculated T_1 value. This model was confirmed by 1D chemical shift imaging (CSI) in an extended aqueous phantom of known T_1 relaxation time. At most, the measured T_1 underestimated the true value by 5%.

6.7 QUANTIFICATION TECHNIQUES

The final stage of development was to establish the parameters which would allow the signal derived from a subject's brain to be quantified. This required the production and testing of solutions containing lithium and a shift reagent.

6.7.1 Reference compound

Various strategies exist to quantify signal from MRS investigations (see §2.6.4). As there are negligible amounts of lithium in the normal human brain, external reference compounds must be used. There are two fundamental approaches to the use of external references, at least in terms of timing: concurrent and consecutive data acquisition. With consecutive techniques the phantom is scanned at about the same time as the subject, and will usually be constructed in such a way that its characteristics match those of the subject in some way – doping the phantom to ensure similarity of T_1 values, normalising to water signals and so forth. This strategy can be time consuming. Concurrent data collection acquires signal from the reference at the time of scanning, usually with a small reference marker close to the coil. For ^{7}Li, the main problem is the small size of its chemical shift *in vivo* – unmodified, the data from the subject and reference would be indistinguishable other than by location.

AUTHOR	LITHIUM	VOLUME	SHIFT REAGENT	SHIFT
Renshaw (1988)	50 mM	10 ml	25 mM dysprosium tripolyphosphate	10–15 ppm
Komoroski (1990)	25 mM	–	12.5 mM dysprosium $(\text{tripolyphosphate})_2$	15.7 ppm
Gullapalli (1991)	50 mM	–	10 mM dysprosium tripolyphosphate	–
Kato (1992–1994)	15 mM	15 ml	25 mM dysprosium TTHA	–
Kushnir (1993)	0.4–0.8 mM	2000 ml	phosphoric acid	–
Gonzalez (1993)	500 mM	10 mm ⌀ tube	135 mM dysprosium chloride	15 ppm
Sachs (1995)	–	–	dysprosium tripolyphosphate	–
Riedl (1997)	–	20 ml	2.5 mM dysprosium TTHA	3 ppm
Komoroski (1997)	5 mM	25 mm ⌀ sphere	1 mM $[Na_3H_2Tm(DOTP)\cdot NaCl]$ in 15% D_2O	–
Komoroski (1998)	0.48 mM	30 ml	0.48 mM $[Na_3H_2Tm(DOTP)\cdot NaCl]$	–
Ramaprasad (1998)	–	–	dysprosium tripolyphosphate	–
Soares (2001)	20 mM	60 ml	25 mM dysprosium chloride	5 ppm

Table 6.3: Shift reagents in lithium MRS studies, arranged in approximately chronological order.

Shift reagents are powerful compounds which can alter the resonance frequency of spins. In the field of ^{7}Li MRS, by far the most commonly used shift reagent is dysprosium (see table 6.3), a heavy metal with toxic properties. Dysprosium is not suited for administration to humans and has limited value for *in vivo* work anyway, it not entering cells. It is, however, well suited to external phantom work. As a shift reagent it needs to be in close proximity to the lithium ion. This can be achieved either by using high concentrations or by combining chelating agents. Dysprosium is expensive and so the latter option is preferred as lower concentrations are required.

Following the comprehensive description of Renshaw and Wicklund (1988), a solution of 50 mM lithium chloride and 25 mM dysprosium tripolyphosphate was prepared. Chelating agents tend to deteriorate over time and the moieties no longer coordinate – in the studies in table 6.3, reference compounds were reportedly stable over a period of months. This was not the case in the series of developmental experiments conducted for this thesis. Apparent in the progressive loss of shift and a broadening of the spectral peak, deterioration rendered the reference standard unusable. A simple ionic solution of lithium and dysprosium chloride (albeit in high concentration) was favoured and found to be stable over time (LiCl 50 mM · $DyCl_3$ 135 mM) with an adequate down-field shift (figure 6.5 on page 206).

6.8 SPECTROSCOPIC IMAGING PILOT STUDY

6.8.1 Study design

The development process culminated in a pilot study (MRC-LISP) in which a small sample of subjects (n = 5) underwent MRS examination to determine lithium level by tissue class. Four subjects were recruited directly into this project, taking lithium for a period of time before having a single MR examination; spectroscopic data was also acquired from one subject in the MRC-LAMP study. In general, subject recruitment, screening and enrolment procedures matched those of the MRC-LITE study, as did the duration of lithium carbonate administration. For those entering the pilot study directly, the target serum concentration was set at 0.8 mM with open-label prescription,

ensuring detectable levels whilst limiting the risk of toxicity. For these individuals, CSI was collected on the same day, minimising variations in scanner performance – the duration between data acquisition and last dose varied but the interval between brain and serum level sampling was fixed at 30 minutes. The MRC-LAMP study subject underwent spectroscopic examination after completing the procedures of fMRI study, lengthening the time between last dose and data acquisition, but maintaining blindness for the purposes of post-methamphetamine rating scales.

The subjects (n = 5) were all men, with a mean age of 20.5 ± 1.0 years. Lithium was taken on average for 8.2 ± 0.45 days, resulting in a serum level of 0.96 ± 0.13 mM.

6.8.2 Acquisition

Spatially localised ^{7}Li data were acquired using a 1D-SI sequence with the spatial encoding place positioned parallel to the coil plane (adiabatic half-passage excitation, pulse duration 6 ms, TR = 6500 ms, 12 encode steps, FOV = 12 cm, spectral width 8000 Hz, 2048 data points, weighted k-space averaging, 3 averages, total scan time ≈ 4 minutes). Variation in coil performance between subjects was assessed by measuring the pulse width for non-selective 90° excitation of the external reference (fully relaxed hard pulse, TR = 60 s, 4 flip angles, single average).

6.8.3 Quantitation

The calculation of ^{7}Li concentration *in vivo* was made relative to calibration phantoms. The 1D-SI sequence was applied to eight extended volume aqueous phantoms, each containing one of four concentrations of lithium chloride (0.1, 0.3, 1.0 and 3.0 mM) at two different saline strengths (150 or 300 mM). Signal strength versus depth was determined for each concentration and normalised to the signal from the reference compound to create calibration curves. The *in vivo* spectra were again normalised to the external reference and the results compared with the calibration curves to determine uncorrected ^{7}Li concentration. Signal arising from blood was corrected for, the volume of brain vasculature assumed to be 5% (González et al., 1993).

6.8.4 *Localisation*

For each subject, the volume the tissues contributing to each spectral row was calculated as follows. Grey and white matter segmented images (native space) were prepared in SPM8, onto which a mask of the sampled volume was overlaid. This mask was derived from the receive profile of the coil – its correct orientation and position was determined by scrutinising the scout images acquired in preparation of the CSI sequence. The mask was then split into 1 cm thick slices, simulating the CSI acquisition. The relative proportions of each tissue in the sections of the mask were used to scale the MRS data in order to achieve the final corrected ^{7}Li concentration in each SI row.

6.8.5 *Statistical analysis*

Correlation between the serum lithium levels and the mean brain ^{7}Li concentration over all SI slices was assessed using bivariate analysis, taking a significance level of $p < 0.05$ (two tailed).

6.8.6 *Results*

Spectroscopic imaging data from four subjects was suitable for analysis, with an example from a single subject presented in figure 6.7 on page 212. Signal was easily discernible to a depth of 6 cm. The rapid reduction in signal intensity with distance from the coil reflects the sensitive profile, corrected using our B_1 model for the purposes of quantitation. The SNR at 3-4 cm was 20, with a total acquisition time of approximately 4 minutes.

The ^{7}Li concentrations by depth, including the mean of all subjects, are presented in figure 6.8. The calculated average brain ^{7}Li concentration for all subjects over all slices was 0.71 ± 0.19 mM. Contrasted with the serum level of 0.9 ± 0.16 mM, the mean brain-to-serum ratio was 0.78 ± 0.26. There was no significant correlation between serum lithium level and brain ^{7}Li concentration. No difference in ^{7}Li concentration was observed between white and grey matter (figure 6.9 on page 213).

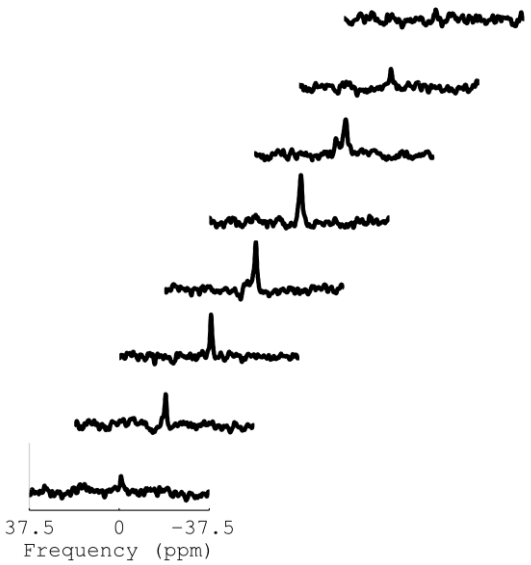

Figure 6.7: Single subject's CSI spectra with slice thickness equal to 1 cm (the slice nearest the axis label is closest to the coil surface) – signal can be easily discerned at a depth of 6 cm

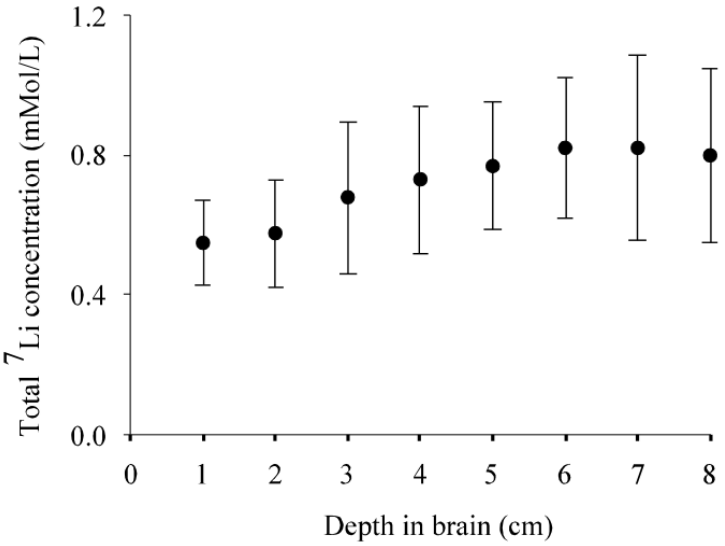

Figure 6.8: Lithium concentration by depth using one-dimensional spectroscopic imaging *in vivo*. Data points indicate mean values ± sd for the group of healthy subjects studied (n = 4), correcting for the sensitivity profile of the surface coil.

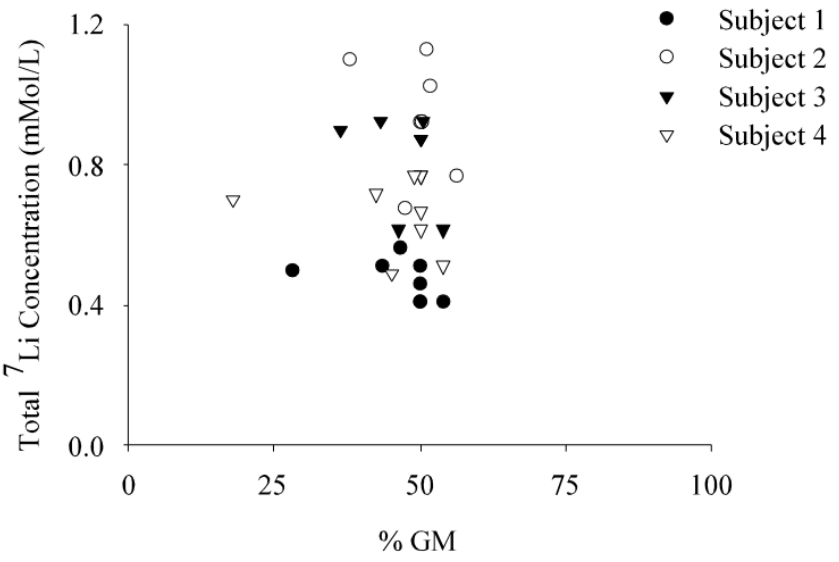

Figure 6.9: Lithium concentration according to percentage grey matter (% GM) in the SI slice. In the majority of subjects, SI slices contained fairly equal proportions of white an grey matter. Subjects 2 and 4 yielded data from slices containing a low percentage of grey matter, in which the concentration of lithium did not appear to deviate from the values returned from slices with a higher proportion of grey matter.

6.9 DISCUSSION

This chapter described the development and application of ^{7}Li magnetic resonance spectroscopy at 3T using a clinical scanner. It was demonstrated that adequate signal to noise ratio could be achieved at a depth of at least 6 cm using a surface coil, through the combination of adiabatic pulse sequences and receive-profile modelling. Acquisition times for the 1D CSI sequence remained under 5 minutes, with total scan times including calibration and T_1-weighted imaging approximating to 25 minutes. This discussion section places the key results in context, and highlights the most important contributions to the ^{7}Li MRS field.

6.9.1 Subject populations

Much of the ^{7}Li MRS research in human subjects has been restricted to measurements in patients prescribed lithium as part of their medication regime for bipolar disorder (Gyulai et al., 1991; Kato et al., 1992, 1993, 1994, 1996; González et al., 1993; Komoroski

et al., 1993; Kushnir et al., 1993; Riedl et al., 1997; Soares et al., 2000; Moore et al., 2002, 2003; Forester et al., 2008). The initial findings of these studies suggested that there is a correlation between the brain and serum lithium levels and also between brain to serum ratio and age (reviewed by Soares et al., 2000), although in a recent investigation this latter relationship was not upheld in older subjects (Forester et al., 2008). Other studies have also suggested that there is limited correlation between these measures (González et al., 1993; Kato et al., 1996). The extremely limited data in healthy subjects (Renshaw and Wicklund, 1988; Plenge et al., 1994) means that it is difficult to disentangle what may be specific effects in small patient cohorts from general effects of ageing. It is therefore important to define normative data for full interpretation of clinical studies. The findings of this thesis may be considered an initial step towards this goal – young, healthy men taking lithium were found to have a brain to serum lithium ratio of 0.78 ± 0.26. This ratio is consistent with data from patients of the same age (Moore et al., 2002). Understanding the relationship between administered dose, brain level and serum concentration is of some importance in this age group, it being close to the mean age of onset of the bipolar disorder, when medication is likely to be initiated for the first time. In the MRC-LISP study reported here, the lack of a significant correlation between brain and serum lithium concentration may have been due to the narrow range of serum levels achieved in the subjects.

6.9.2 Relaxation properties of lithium

The most important contribution of this thesis to the field of ^{7}Li MRS is arguably the determination of the T_1 time of lithium in a sizeable group of subjects. Knowledge of the relaxation characteristics of a nucleus *in vivo* is required for its concentration to be accurately determined. The most common approach in quantitative studies has been to adopt fully relaxed acquisition conditions, thus eliminating the need for any T_1 relaxation correction (González et al., 1993; Soares et al., 2000). This strategy is consistent with the use of signal differencing based localisation schemes such as image selected *in vivo* spectroscopy (ISIS) as well as with simple adiabatic 90° excitation with

surface coils. Previous studies have measured ^{7}Li T_1 in human brain at various field strengths (Komoroski et al., 1993; Kushnir et al., 1993; González et al., 1993; Riedl et al., 1997; Girard et al., 2001; Moore et al., 2003), but no data exist at 3T. This prompted Soares et al. (2000) to acquire data with a 15 s TR – the findings of this thesis suggest that a shorter TR may be applied whilst maintaining full saturation of signal.

In the largest group of subjects thus far investigated at any field strength, the T_1 of ^{7}Li *in vivo* at 3T was found to be 2.0 ± 0.4 seconds. It is of interest to consider why this value is relatively low compared to the published literature. From table 6.2 (page 193) it can be seen that most studies have reported the T_1 of ^{7}Li to be around three to four seconds, though a value of 2.4 seconds was found in the rat at 7T. This direction of this discrepancy is somewhat unexpected, as longitudinal relaxation times usually increase proportionally with the applied field strength.

The greatest potential source of error in the method applied in this chapter would be the failure to achieve 90° excitation, leading to lower saturation than expected. Validation of the method used was performed by combining a simulation of the RF coil performance with experimental validation – an aqueous phantom using a small point-source sample at coil isocentre where adiabatic excitation gave uniform 90° excitation. The model and studies indicated that the maximum error in calculated T_1 was 5%, suggesting that the T_1 value of ^{7}Li *in vivo* was no greater than 2.1 seconds. Greater T_1 times previously reported may be a consequence of the use of block pulses.

In this thesis, the T_1 of ^{7}Li was determined using a saturation recovery sequence; others have favoured inversion recovery techniques. Saturation recovery techniques are more time efficient, but potentially less accurate, possibly accounting for the difference in reported relaxation times. The standard deviation of the T_1 estimation reported here suggests that this was not the case. The positioning of the surface coil was such that contamination of signal from tissues other than the brain was unlikely – were muscle to be contributing to the T_1 estimate, it would most likely increase its value (Renshaw and Wicklund, 1988). It is conceivable that the short T_1 represented the detection of the fast component of a biexponential decay, though the pattern of the data would suggest otherwise, fitting to a single exponential function.

6.9.3 *Concentration of lithium in different brain tissues*

Spatial data on the distribution of lithium may inform theories of its action, as well as progressing the debate regarding its effects on the MR signal derived from grey matter. Ramaprasad et al. (1992) performed 2D spectroscopic cerebral imaging at high field in rats treated with lithium for a short period of time – distribution was uneven within the brain, though the resolution was poor. Similar findings have recently been demonstrated in man using ^{7}Li MR imaging (Boada et al., 2010; Lee et al., 2010), consistent with the post-mortem examinations reported decades previously (Francis and Traill, 1970; Spirtes, 1976). Such techniques were not, however, quantitative.

As with all non-proton MRS investigations, protocol design must balance localisation, spatial resolution and adequate SNR with a clinically acceptable examination length. Spatial information in clinical studies has varied from simple surface coil localisation (Kushnir et al., 1993; Kato et al., 1996), or slab localised 1D ISIS with examination times of minutes (González et al., 1993; Soares et al., 2001; Moore et al., 2002; Forester et al., 2008) through to 2D spectroscopic imaging requiring 55 minutes of data averaging (Girard et al., 2001). In the MRC-LISP study reported here, a combination of surface coil localisation with a 1D-SI adiabatic sequence was used, separating spectra from 10 mm thick planes parallel to the surface coil (essentially sagittal orientation). This protocol required a data collection time of 4 minutes and provided sufficient spatial resolution to examine differences with depth and the relationship between grey and white matter concentration. The coil was placed over the frontal region of the head, minimising the amount of skeletal muscle which may have contaminated data from the brain. Although any signal from muscle would be separated from brain signal by the SI encoding scheme, no such signal could be discerned.

Lithium concentration showed a trend to increase with depth into the brain, but a regression of local concentration against percentage grey matter contribution showed no significant difference according to tissue class. The 1D-SI measurement did not, however, provide complete localisation – an objective for future research.

7 DISCUSSION

The human brain can be conceptualised in many ways – developmentally by way of its genetic determinants, environmental influences and evolution; structurally through gross anatomy, regional connectivity, cellular morphology and molecular composition; functionally as neurochemical systems, metabolic processes and emergent behaviours; analytically in the construct of the psyche; spiritually and philosophically in terms that convey a different meaning. The experience and the effects of psychoactive substances can be interpreted across these realms, as can many of the techniques used to study this most fascinating organ.

The overarching aim of this thesis was to explore the interaction between lithium and the human brain using magnetic resonance techniques. The experimental work conducted was presented as three studies, each warranting its own chapter but overlapping for the purposes of some analyses. First, the effects of lithium on cerebral dopaminergic systems were examined in a randomised, placebo-controlled, BOLD fMRI study during which healthy subjects performed a task requiring their sustained attention, before and after receiving methamphetamine. Second, the notion that lithium could increase the volume of grey matter in the brain was explored and questioned through the application of quantitative structural imaging techniques. Finally, developmental work in the field of lithium MRS was undertaken with the goal of measuring the concentration of lithium in different brain tissues. In this concluding chapter, the implications of the results of these studies are discussed, their strengths and weaknesses considered, and suggestions for future research proffered.

7.1 LITHIUM & DOPAMINE

A great deal of evidence supports the notion that lithium can attenuate over-activity in the dopaminergic systems of the human brain. Much of this evidence was reviewed during the preparation of this thesis, at least that pertaining to bipolar disorder. Used as a model of mania in the MRC-LAMP study, methamphetamine reproduced some of

the features of the condition and lithium was found to lessen its subjective effects. The effects of methamphetamine on the BOLD signal required thoughtful interpretation, ultimately emerging as a reduction in the deactivation within the default mode regions observed when subjects embarked upon the RVIP task. Lithium attenuated these effects in a within-group analysis; placebo did not. This difference between lithium and placebo did not, however, emerge as significant in a between-group comparison. The most obvious effect of lithium itself was to slow the speed with which subjects responded to targets during the RVIP task, its effects on the BOLD signal before the second dose of methamphetamine being more difficult to interpret.

7.1.1 Strengths, weaknesses and future directions

The effects of lithium on amphetamine administration as a model of mania has previously been investigated using BOLD fMRI (Bell et al., 2005b); the study presented in this thesis is novel by way of its longitudinal design and the randomisation of subjects to high and low dose lithium regimes. The principal weakness of the MRC-LAMP study was that it was under-powered for a between-group comparison of lithium and placebo, this a consequence of the number of subjects enrolled and the analysis strategy applied.

Around the time of the inception of the MRC-LAMP study, the available data indicated that relatively small group sizes would be sufficient to detect a difference between lithium and placebo on the effects of amphetamines on the BOLD signal. Bell et al. (2005b) assessed the effect of pretreatment with lithium or valproate on D-amphetamine-induced changes in brain activity in healthy volunteers. Compared to placebo, lithium attenuated the effects of the stimulant on BOLD signal during a word-generation paradigm and the task involving spatial attention. These differences reached significance on a between-group analysis, with twelve subjects in the placebo group and nine taking lithium. The target sample-size of the MRC-LAMP study was therefore set as at least nine subjects in each of groups, aiming for a minimum of 27 subjects in total. It is a regretable short-coming of the study that only six subjects

were enrolled into the placebo group. Close to its planned ceasation the study was curtailed by an upgrade to the scanner software – data acquisition was not extended beyond this point for reasons of quality control and comparability.

Recruitment of subjects was more difficult than expected – finding young men who were willing to take methamphetamine but who had not taken it before (and who were also amenable to the idea of receiving lithium) proved something of a challenge. Most of the potential subjects declined to participate without giving reason, though the suspicion was that they were unwilling to admit to previous drug-use. Whilst more subjects may have been recruited had the exclusion criteria been less stringent, a larger heterogeneous sample does not necessarily translate to a more powerful study in terms of the interpretation of results. Designing a study-specific website (on which full details of the proposed research and criteria for participation were presented) streamlined subject selection. Future studies should capitalise on this – or whatever the most accessible media is at the time – early in the recruitment process.

Bell et al. (2005b) demonstrated a difference between lithium and placebo with range of serum levels similar, if not slightly lower than in the MRC-LAMP study; they administered medication for 14 days. The lack of a difference between placebo and lithium in this thesis could indicate that the study duration was too brief. Although lithium can be antimanic within several days, most of the clinical trials have gauged its effects over at least three weeks (Poolsup et al., 2000). Whilst ethical considerations constrain the duration of studies of healthy subjects, the case should be made for using longer courses of medication in future research.

The stategy adopted for the analysis of the data in the MRC-LAMP study requires consideration. Bell et al. (2005b) examined BOLD signal change in prespecified regions of interest derived from a previous study (Willson et al., 2004); the analysis in this thesis compared all voxels in the functional images. Whilst statistically more powerful, region of interest analyses are inherently restrictive. By scrutinising the entire brain, methamphetamine was shown to be associated not with BOLD activations, but with the lessening of deactivations – a new finding that would have otherwise have been missed.

Methodological strength is usually gained by adopting a longitudinal design. With stimulant administration, it appears to be a double-edged sword. There is substantial individual variation in the response to amphetamines, making a within-subject, or in this case a within-group comparison desirable. Repeated administration of stimulants, however, may lead to behavioural sensitisation and the consequences of anticipating their effects. It was argued in this thesis that subjects allocated to receive placebo self-replicated the effects of methamphetamine, attaining a state of arousal prior to the administration of the stimulant on the second occasion; lithium was thought to prevent this occurrence. This finding requires replication, for it may have consequences on the optimal design of future experiments.

Subjects in the MRC-LAMP study were randomly assigned to receive lithium in one of two regimes, aiming for high or low concentrations chosen to reflect those commonly advocated for the treatment of mania and the prevention of relapse. For each subject, the dose was calculated and initiated without titration. Estimating the dose in this way proved successful, ensuring a uniformity in the duration of administration that would have been precluded by a titration strategy. In an exploratory analysis, the effects of methamphetamine on BOLD deactivations appeared to be attenuated most in those receiving a higher dose of lithium. Formal comparison of the mean T-scores extracted in the region of interest analysis was not possible at the time of submission of this thesis. Future work with the data obtained in this study will include the extraction and comparison of signal contrast values from the regions of interest in each individual – whether the comparison should use data extracted from the whole cluster or a small element of the cluster (removed from the contaminating effects of CSF for example) is a matter to be addressed.

7.1.2 Implications of the findings

The MRC-LAMP study was confirmatory in nature, it being clear that lithium could act to attenuate dopaminergic system functioning. Indeed, such a study could not be conducted in good faith without a substantial body of supporting evidence. Observing

the subjective effects of methamphetamine affirmed its use as a model of mania; delineating its effects on deactivations within the default mode regions confirmed its validity as a manipulation of the brain regions most recently implicated in bipolar disorder (McKenna et al., 2010). Patients with mania commonly receive antipsychotic drugs as a first-line intervention, lithium being added to the treatment of those who fail to respond (Grunze et al., 2009). Antipsychotic medications are dopaminergic receptor antagonists, though their therapeutic action derives from a complex interplay of effects on neurotransmitter systems rather than solitary receptor blockade. The localisation of the effect of lithium to the presynaptic level, as suggested by the findings of this thesis, supports the combination of such drugs.

The use of lithium is not, and never has been, confined to the treatment of mania. Neuroplasticity theories have widened its indications to include various neurodegenerative conditions, not least the dementias. Patients with dementia commonly present with features of parkinsonism; a substantial minority Parkinson's disease plus dementia or Dementia with Lewy Bodies – archetypal hypodopaminergic states (Weisman and McKeith, 2007). Lithium is being investigated as a disease-modifier in the dementias by virtue of its purported neuroprotective effects (Hampel et al., 2009; Lauterbach et al., 2010). Were the conclusions of this thesis to be substantiated – that lithium reduces dopaminergic activity, most likely through presynaptic effects – the parkinsonian features in the dementia states may be worsened by its administration. Intervention with lithium may, on balance, prove to be detrimental.

7.2 LITHIUM & GREY MATTER

A decade has passed since it was first reported that lithium increases the volume of grey matter in the brain of man – at least, that is, when assessed by MRI techniques. The finding has been consistently replicated and although the underlying mechanism has not been established, it is widely accepted that the increase in volume has a basis in the established ability of lithium to enhance neuroplasticity.

The decision to investigate the relationship between lithium, grey matter volume and MR signal arose from approaching the field with a degree of cynicism. Viewed critically, though not without prejudice, the interpretations of the finding appeared flawed. If lithium acts to prevent neuronal damage, why does the volume of grey matter increase in studies of healthy individuals? Given the consistency of the finding, why was it not detected in early studies of patients with affective disorders – could this be a consequence of the analysis adopted rather than the state of the brain? Finally, should it not be a cause for alarm – or headache at least – that a drug intervention may increase brain tissue volume to such a degree as has been reported?

The MRC-LITE study sought to determine whether it was possible that the grey matter volume increase seen with lithium was actually a consequence of it altering the relaxation characteristics of protons, thereby altering signal contrast and volumetric assessments. Evidence was found in support of this notion – volume increase was observed using VBM but not SIENA, and a reduction in grey matter T_1 was detected.

7.2.1 Implications of the findings

The implications of these findings may be marked. If lithium substantially affects tissue classification, many recent MRI studies of bipolar disorder require reappraisal. If the cellular effects of lithium drive the T_1 change, a mechanism for charting the distribution of its action may have emerged – this may also explain why the volumetric finding proved so attractive, occurring as it did in brain regions pertinent to bipolar disorder and theories of action of lithium (ignoring the finding that the lithium-related NAA increase was most marked in the occipital regions (Moore et al., 2000a)).

7.2.2 Strengths, weaknesses and future directions

In the MRC-LITE study, established analysis techniques were applied in a simple longitudinal manner to well characterised, healthy subjects. The number of subjects studied was comparable to previous investigations in this area. The weakness of the study lies not so much in its construction or its power to detect volumetric differences, but in the nature of the phenomenon under investigation.

The grey matter T_1 reduction reported in this thesis was small, and it is debatable whether a change of this magnitude would be sufficient to disrupt the tissue classification process during VBM analysis. The determination of grey matter T_1 was at the mercy of the process it sought to investigate – mean values were extracted from lobar brain regions, but these regions were delineated using a process that required the segmentation of subjects' T_1-weighted images. Consequently, the T_1-maps may have been distorted by partial volume effects, with CSF voxels included in the grey matter regions diluting the lithium-related change in relaxation times. Estimation of the T_1 times therefore needs to be repeated using a different segmentation threshold, one with which it is certain that grey matter, and only grey matter, is extracted.

The rationale for using a short course of lithium requires scrutiny. Subjects who enrolled directly into the MRC-LITE study were given lithium to take for 11 days. This duration was chosen to match that of the MRC-LAMP study, allowing data to be combined for a more powerful analysis in statistical terms. It was also reasoned that the neurotrophic effects of lithium would be slow to manifest and that large increases in grey matter volume occurring acutely would attract a physical account based on the theorised change in MRI signal. During the writing of this thesis, Lyoo et al. (2010) demonstrated a progressive increase in grey matter volume with time, such that the results reported here could be interpreted as an early detection of a chronic process rather than a distinct, acute phenomenon. With hindsight, it would have been better to use the data from the MRC-LAMP study to investigate the acute effects of lithium and to recruit more subjects directly into the MRC-LITE study, administering lithium for several weeks to gauge the chronic effects of the medication.

Nevertheless, the difference in grey matter volume change determined using intensity-based and boundary-shift techniques requires replication – a relatively simple matter that could be performed using extant data. Given the potential implications of the relaxometry findings, replication in a future study would appear to be justified.

7.3 LOCATING LITHIUM

At the outset of this project as a whole, it was hoped that ^{7}Li MRS might be integrated into the MRC-LAMP and MRC-LITE protocols, combining assessments of the effects of lithium on brain structure and function with estimates of its regional concentration. Regrettably, that goal proved to be unrealistic in the time available. The developmental processes leading to the quantification of brain ^{7}Li concentration took longer than expected – the construction and testing of the coil was a relatively straightforward matter but establishing the T_1 time of lithium *in vivo* drained heavily on scan time.

As it transpires, the generation of normative group data for the T_1 relaxation time is probably the most important contribution of this thesis to the ^{7}Li MRS field. The mean value determined in healthy subjects using a surface coil with adiabatic excitation was lower than previous reports in man, but consistent with measures performed in the rat at high field strengths. Quantitative pulse sequence construction requires knowledge of the relaxation properties of the nucleus under investigation in order to avoid signal saturation. The values reported here should encourage the use shorter repetition times, reducing the overall scan duration or improving SNR should researcher elect to perform more acquisitions.

In the MRC-LISP study, no difference in the concentration of lithium in grey and white matter was found. The sequence applied permitted depth localisation only – the level of lithium in the different tissues was gauged using the segmented T_1-weighted images, providing relative proportions in each SI slice. Quantitative strategies are time consuming and as a consequence, resolution may be poor. Whilst the determination of absolute lithium concentration is a laudable goal, recent advances in lithium imaging may prove to be of greater value (Boada et al., 2010; Lee et al., 2010). Manipulating the lithium spectral singlet, as with water in MRI, may provide high resolution images relatively swiftly. In this thesis, a greater than expected signal intensity occurred as repetition times approached zero. Should this phenomenon prove to be consistent and predictable – as would be expected were it due to steady-state free precession – it could be harnessed to enable rapid lithium imaging using very short repetition times.

7.4 CONCLUDING REMARKS

Whilst lithium has a long history in medicine, and has been the focus of systematic research for decades, it is likely that there is much still to be learnt about this fascinating element. Indeed, much may yet be learned from lithium – the importance of illness-modification, the complexities of mental state, the idiosyncrasies of pharmacokinetics and the pitfalls and promises of imaging spring to mind.

Bibliography

Addington, J. and Addington, D. (1997). Attentional vulnerability indicators in schizophrenia and bipolar disorder. *Schizophrenia Research*, 23:197–204.

Adler, C. M., DelBello, M. P., and Strakowski, S. M. (2006). Brain network dysfunction in bipolar disorder. *CNS Spectrums*, 11:312–20.

Adli, M., Bschor, T., Canata, B., Dopfmer, S., and Bauer, M. (1998). Lithium in the treatment of acute depression. *Fortshritte der Neurologie-Psychiatrie*, 66:435–41.

Ahluwalia, P. and Singhal, R. (1981). Monoamine uptake into synaptosomes from various regions of rat brain following lithium administration and withdrawal. *Neuropharmacology*, 20:483–7.

Alda, M. (2006). *Lithium in neuropsychiatry: the comprehensive guide.*, chapter 28, pages 321–28. Informa Healthcare.

Anand, A., Verhoeff, P., Seneca, N., Zoghbi, S. S., Seibyl, J. P., Charney, D. S., and Innis, R. B. (2000). Brain SPECT imaging of amphetamine-induced dopamine release in euthymic bipolar disorder patients. *American Journal of Psychiatry*, 157:1108–14.

Andrews-Hanna, J., Reidler, J., Sepulcre, J., Poulin, R., and Buckner, R. (2010). Functional-anatomic fractionation of the brain's default network. *Neuron*, 65:550–62.

Aragon, M. C., Herrero, E., and Gimenez, C. (1987). Effects of systematically administered lithium on tryptophan transport and exchange in plasma-membrane vesicles isolated from rat-brain. *Neurochemical Research*, 12:439–44.

Aribisala, B. and Blamire, A. (2009). Comparison of analysis of brain relaxation times in standard space with analysis in individuals real space. *Proceedings ISMRM, 17*.

Arriaga, F., Dugovic, C., and Wauquier, A. (1988). Effects of lithium on dopamine behavioural supersensitivity induced by rapid eye movement sleep deprivation. *Neuropsychobiology*, 20:23–7.

Ashburner, J. and Friston, K. J. (2000). Voxel-based morphometry — the methods. *Neuroimage*, 11:805–21.

Attwell, D. and Iadecola, C. (2002). The neural basis of functional brain imaging signals. *Trends in Neuroscience*, 25:621–5.

Balanzá-Martínez, V., Selva, G., Martínez-Arán, A., Prickaerts, J., Salazar, J., González-Pinto, A., Vieta, E., and Tabarés-Seisdedos, R. (2010). Neurocognition in bipolar disorders — a closer look at comorbidities and medications. *European Journal of Pharmacology*, 626:87–96.

Baldessarini, R., Tondo, L., and Viguera, A. (1999). Discontinuing lithium maintenance treatment in bipolar disorders: risks and implications. *Bipolar Disorders*, 1:17–24.

Ball, P. (2008). Water as an active constituent in cell biology. *Chemical Reviews*, 108:74–108.

Baptista, T., Lacruz, A., de Mendoza, S., Guillén, M., Burguera, J., de Burguera, M., and Hernández, L. (2000). Endocrine effects of lithium carbonate in healthy premenopausal women: relationship with body weight regulation. *Progress in Neuropsychopharmacology and Biological Psychiatry*, 24:1–16.

Baptista, T., Teneúd, L., Contreras, Q., Burguera, J., Burguera, M., and Hernández, L. (1993). Effects of acute and chronic lithium treatment on amphetamine-induced dopamine increase in the nucleus accumbens and prefrontal cortex in rats as studied by microdialysis. *Journal of Neural Transmission General Section*, 94:75–89.

Baron, M., Gershon, E. S., Rudy, V., Jonas, W. Z., and Buchsbaum, M. (1975). Lithium-carbonate response in depression — prediction by unipolar bipolar illness, average-evoked response, catechol-*o*-methyl transferase, and family history. *Archives of General Psychiatry*, 32:1107–11.

Basturk, M., Karaaslan, F., Esel, E., Sofuoglu, S., Tutus, A., and Yabanoglu, I. (2001). Effects of short and long-term lithium treatment on serum prolactin levels in patients with bipolar affective disorder. *Progress in Neuro-Psychopharmacology and Biological Psychiatry*, 25:315–22.

Bauer, M., Adli, M., Baethge, C., Berghofer, A., Sasse, J., Heinz, A., and Bschor, T. (2003). Lithium augmentation therapy in refractory depression: clinical evidence and neurobiological mechanisms. *Canadian Journal of Psychiatry*, 48:440–8.

Bearden, C., Thompson, P., Dutton, R., Frey, B. N., Peluso, M., Nicoletti, M., Dierschke, N., Hayashi, K. M., Klunder, A. D., Glahn, D., Brambilla, P., Sassi, R., Mallinger, A. G., and Soares, J. (2008). Three-dimensional mapping of hippocampal anatomy in unmedicated and lithium-treated patients with bipolar disorder. *Neuropsychopharmacology*, 33:1229–38.

Bearden, C. E., Thompson, P. M., Dalwani, M., Hayashi, K. M., Lee, A. D., Nicoletti, M., Trakhtenbroit, M., Glahn, D. C., Brambilla, P., Sassi, R. B., Mallinger, A. G., Frank, E., Kupfer, D. J., and Soares, J. C. (2007). Greater cortical gray matter density in lithium-treated patients with bipolar disorder. *Biological Psychiatry*, 62:7–16.

Beaulieu, J. M. and Caron, M. G. (2008). Looking at lithium: Molecular moods and complex behaviour. *Molecular Interventions*, 8:230–41.

Beaulieu, J. M., Gainetdinov, R. R., and Caron, M. G. (2007). The Akt-GSK-3 signaling cascade in the actions of doparnine. *Trends in Pharmacological Sciences*, 28:166–72.

Beaulieu, J. M., Sotnikova, T. D., Yao, W. D., Kockeritz, L., Woodgett, J. R., Gainetdinov, R. R., and Caron, M. G. (2004). Lithium antagonizes dopamine-dependent behaviors mediated by an Akt/glycogen synthase kinase 3 signaling cascade. *Proceedings of the National Academy of Sciences of the United States of America*, 101:5099–5104.

Beckmann, H., St Laurent, J., and Goodwin, F. (1975). The effect of lithium on urinary MHPG in unipolar and bipolar depressed patients. *Psychopharmacologia*, 42:277–82.

Bell, E. C., Willson, M. C., Wilman, A. H., Dave, S., Asghar, S. J., and Silverstone, P. H. (2005a). Lithium and valproate attenuate dextroamphetamine-induced changes in brain activation. *Human Psychopharmacology*, 20:87–96.

Bell, E. C., Willson, M. C., Wilman, A. H., Dave, S., and Silverstone, P. H. (2005b). Differential effects of chronic lithium and valproate on brain activation in healthy volunteers. *Human Psychopharmacology*, 20:415–24.

Berggren, U. (1985). The effect of acute lithium administration on brain monoamine synthesis and the precursor amino acids tyrosine and tryptophan in brain and plasma in rats. *Journal of Neural Transmission*, 61:175–81.

Berggren, U., Engel, J., and Liljequist, S. (1981). The effect of lithium on the locomotor stimulation induced by dependence-producing drugs. *Journal of Neural Transmission*, 50:157–64.

Berggren, U., Tallstedt, L., Ahlenius, S., and Engel, J. (1978). The effect of lithium on amphetamine-induced locomotor stimulation. *Psychopharmacology*, 59:41–5.

Berghofer, A., Grof, P., and Muller-Oerlinghausen, B. (2006). *Lithium in neuropsychiatry: the comprehensive guide.*, chapter 37, pages 443–64. Informa Healthcare.

Berk, M., Dodd, S., Kauer-Sant'Anna, M., Malhi, G. S., Bourin, M., Kapczinski, F., and Norman, T. (2007). Dopamine dysregulation syndrome: implications for a dopamine hypothesis of bipolar disorder. *Acta Psychiatrica Scandinavica*, 116:41–9.

Berridge, M. J., Downes, C., and Hanley, M. (1989). Neural and developmental actions of lithium: a unifying hypothesis. *Cell*, 59:411–9.

Besson, J., Henderson, J., Foreman, E., and Smith, F. (1987). An NMR study of lithium responding manic depressive patients. *Magnetic Resonance Imaging*, 5:273–7.

Beyer, J. L., Kuchibhatla, M., Payne, M., Moo-Young, M., Cassidy, F., MacFall, J., and Krishnan, K. R. R. (2004). Caudate volume measurement in older adults with bipolar disorder. *International Journal of Geriatric Psychiatry*, 19:109–14.

Birch, N. J. (1976). Possible mechanism for biological action of lithium. *Nature*, 264:681.

Birch, N. J. (1991). *Lithium and the cell.*, chapter 9, pages 159–73. Academic Press.

Birch, N. J. and Hullin, R. (1972). The distribution and binding of lithium following its long-term administration. *Life Sciences*, 11:1095–9.

Birch, N. J. and Jenner, F. (1973). The distribution of lithium and its effects on the distribution and excretion of other ions in the rat. *British Journal of Psychology*, 47:586–94.

Biswal, B., Yetkin, F. Z., Haughton, V. M., and Hyde, J. S. (1995). Functional connectivity in the motor cortex of resting human brain using echo-planar MRI. *Magnetic Resonance in Medicine*, 34:537–41.

Blamire, A., Ogawa, S., Ugurbil, K., Rothman, D., McCarthy, G., Ellermann, J., Hyder, F., Rattner, Z., and Shulman, R. (1992). Dynamic mapping of the human visual cortex by high-speed magnetic resonance imaging. *Proceedings of the National Academy of Sciences of the United States of America*, 89:11069–73.

Bloom, F., Baetge, G., Deyo, S., Ettenberg, A., Koda, L., Magistretti, P., Shoemaker, W., and Staunton, D. (1983). Chemical and physiological aspects of the actions of lithium and antidepressant drugs. *Neuropharmacology*, 22:359–65.

Boada, F., Qian, Y., Gildengers, A., Phillips, M., and Kupfer, D. (2010). In vivo 3D lithium MRI of the human brain. In *The ISMRM-ESMRMB Joint Annual Meeting*.

Boileau, I., Dagher, A., Leyton, M., Welfeld, K., Booij, L., Diksic, M., and Benkelfat, C. (2007). Conditioned dopamine release in humans: A positron emission tomography [^{11}C]raclopride study with amphetamine. *Journal of Neuroscience*, 27:3998–4003.

Bond, A. and Lader, M. (1974). The use of analogue scales in rating subjective feelings. *British Journal of Medical Psychology*, 47:211–8.

Borison, R., Sabelli, H., Maple, P., Havdala, H., and Diamond, B. (1978). Lithium prevention of amphetamine-induced 'manic' excitement and of reserpine-induced 'depression' in mice: possible role of 2-phenylethylamine. *Psychopharmacology*, 59:259–62.

Botvinick, M., Nystrom, L., Fissell, K., Carter, C., and Cohen, J. (1999). Conflict monitoring versus selection-for-action in anterior cingulate cortex. *Nature*, 402:179–81.

Bowers, M. and Heninger, G. (1977). Lithium: clinical effects and cerebrospinal fluid acid monoamine metabolites. *Communications in Psychopharmacology*, 1:135–45.

Brambilla, F., Catalano, M., Lucca, A., and Smeraldi, E. (1988). Effect of lithium treatment on the GH-clonidine test in affective disorders. *European Journal of Clinical Pharmacology*, 35:601–5.

Brambilla, P., Nicoletti, M., Harenski, K., Sassi, R., Mallinger, A., Frank, E., Kupfer, D. J., Keshavan, M., and Soares, J. (2002). Anatomical MRI study of subgenual prefrontal cortex in bipolar and unipolar subjects. *Neuropsychopharmacology*, 27:792–9.

Brambilla, P., Stanley, J. A., Sassi, R. B., Nicoletti, M. A., Mallinger, A. G., Keshavan, M. S., and Soares, J. C. (2004). ^{1}H MRS study of dorsolateral prefrontal cortex in healthy individuals before and after lithium administration. *Neuropsychopharmacology*, 29:1918–24.

Brevard, C. (1981). *Handbook of high resolution multinuclear NMR.* Wiley.

Bright, P., Jaldow, E., and Kopelman, M. (2002). The national adult reading test as a measure of premorbid intelligence: a comparison with estimates derived from demographic variables. *Journal of the International Neuropsychological Society*, 8:847–54.

Brown, A. S., Mallinger, A. G., and Renbaum, L. C. (1993). Elevated platelet membrane phosphatidylinositol-4,5-bisphosphate in bipolar mania. *American Journal of Psychiatry*, 150:1252–4.

Brown, R & Jahanshahi, M. (1995). Depression in Parkinson's disease: a psychosocial viewpoint. *Advances in Neurology*, 65:61–84.

Bunney, W. J. and Garland, B. (1983). Possible receptor effects of chronic lithium administration. *Neuropharmacology*, 22:367–72.

Cade, J. F. J. (1949). Lithium salts in the treatment of psychotic excitement. *Medical Journal of Australia*, 36:349–52.

Cappeliez, P. and Moore, E. (1990). Effects of lithium on an amphetamine animal model of bipolar disorder. *Progress in Neuropsychopharmacology and Biological Psychiatry*, 14:347–58.

Carli, M., Morissette, M., Hébert, C., Di Paolo, T., and Reader, T. (1997). Effects of a chronic lithium treatment on central dopamine neurotransporters. *Biochemical Pharmacology*, 54:391–7.

Carter, B. and Tiffany, S. (1999). Meta-analysis of cue-reactivity in addiction research. *Addiction*, 94:327–40.

Carter, R., Macinnes, J., Huettel, S., and Adcock, R. (2009). Activation in the VTA and nucleus accumbens increases in anticipation of both gains and losses. *Frontiers in Behavioral Neuroscience*, 3:21.

Chalikian, T. (2001). Structural thermodynamics of hydration. *Journal of Physical Chemistry B*, 105:12566–78.

Chaplin, M. (2000). A proposal for the structure of water. *Biophysical Chemistry*, 83:211–21.

Chen, X. H., Wen, W., Malhi, G. S., Ivanovski, B., and Sachdev, P. S. (2007). Regional gray matter changes in bipolar disorder: a voxel-based morphometric study. *Australian and New Zealand Journal of Psychiatry*, 41:327–36.

Chen, Y. C. I., Galpern, W. R., Brownell, A. L., Matthews, R. T., Bogdanov, M., Isacson, O., Keltner, J. R., Beal, M. F., Rosen, B. R., and Jenkins, B. G. (1997). Detection of dopaminergic neurotransmitter activity using pharmacologic MRI: Correlation with PET, microdialysis, and behavioral data. *Magnetic Resonance in Medicine*, 38:389–98.

Chiu, C., Shen, W., Chen, K., and Lu, M. (2007). Application of the Cockcroft-Gault method to estimate lithium dosage requirement. *Psychiatry and Clinical Neurosciences*, 61:269–74.

Choi, J.-K., Chen, Y. I., Hamel, E., and Jenkins, B. G. (2006). Brain hemodynamic changes mediated by dopamine receptors: role of the cerebral microvasculature in dopamine-mediated neurovascular coupling. *Neuroimage*, 30:700–12.

Cipriani, A., Pretty, H., Hawton, K., and Geddes, J. (2005). Lithium in the prevention of suicidal behavior and all-cause mortality in patients with mood disorders: a systematic review of randomized trials. *American Journal of Psychiatry*, 162:1805–19.

Cipriani, A., Smith, K., Burgess, S., Carney, S., Goodwin, G., and Geddes, J. (2006). Lithium versus antidepressants in the long-term treatment of unipolar affective disorder. *Cochrane Database of Systematic Reviews*, 4:CD003492

Clark, L., Iversen, S. D., and Goodwin, G. M. (2001). A neuropsychological investigation of prefrontal cortex involvement in acute mania. *American Journal of Psychiatry*, 158:1605–11.

Clark, L., Iversen, S. D., and Goodwin, G. M. (2002). Sustained attention deficit in bipolar disorder. *British Journal of Psychiatry*, 180:313–9.

Clark, L., Kempton, M. J., Scarnà, A., Grasby, P. M., and Goodwin, G. M. (2005). Sustained attention-deficit confirmed in euthymic bipolar disorder but not in first-degree relatives of bipolar patients or euthymic unipolar depression. *Biological Psychiatry*, 57:183–7.

Corbetta, M., Kincade, J., Ollinger, J., McAvoy, M., and Shulman, G. (2000). Voluntary orienting is dissociated from target detection in human posterior parietal cortex. *Nature Neuroscience*, 3:292–7.

Corcoran, A. C., Taylor, R. D., and Page, I. H. (1949). Lithium poisoning from the use of salt substitutes. *Journal of the American Medical Association*, 139:685–8.

Coull, J., Frith, C., Buchel, C., and Nobre, A. (2000). Orienting attention in time: behavioural and neuroanatomical distinction between exogenous and endogenous shifts. *Neuropsychologia*, 38:808–19.

Coull, J., Nobre, A., and Frith, C. (2001). The noradrenergic alpha2 agonist clonidine modulates behavioural and neuroanatomical correlates of human attentional orienting and alerting. *Cerebral Cortex*, 11:73–84.

Coull, J. T., Frith, C. D., Frackowiak, R. S., and Grasby, P. M. (1996). A fronto-parietal network for rapid visual information processing: a PET study of sustained attention and working memory. *Neuropsychologia*, 34:1085–95.

Cousins, D., Butts, K., and Young, A. (2009). The role of dopamine in bipolar disorder. *Bipolar Disorders*, 11:787–806.

Cousins, D. A. and Young, A. H. (2007). The armamentarium of treatments for bipolar disorder: a review of the literature. *International Journal of Neuropsychopharmacology*, 10:411–31.

Crossley, N. A. and Bauer, M. (2007). Acceleration and augmentation of antidepressants with lithium for depressive disorders: two meta-analyses of randomized, placebo-controlled trials. *Journal of Clinical Psychiatry*, 68:935–40.

Davenport, V. (1950). Distribution of parenterally administered lithium in plasma, brain and muscle of rats. *American Journal of Physiology*, 163:633–41.

Davies, D. and Shepherd, M. (1955). Reserpine in the treatment of anxious and depressed patients. *Lancet*, 266:117–21.

Deakin, J. F. W., Pennell, I., Upadhyaya, A. J., and Lofthouse, R. (1990). A neuroendocrine study of 5-HT function in depression — evidence for biological mechanisms of endogenous and psychosocial causation. *Psychopharmacology*, 101:85–92.

Delaveau, P., Salgado-Pineda, P., Fossati, P., Witjas, T., Azulay, J., and Bin, O. (2010). Dopaminergic modulation of the default mode network in Parkinson's disease. *European Neuropsychopharmacology*, 20:784–92.

Devous, M. S., Trivedi, M., and Rush, A. (2001). Regional cerebral blood flow response to oral amphetamine challenge in healthy volunteers. *Journal of Nuclear Medicine*, 42:535–42.

Dixon, A. L., Prior, M., Morris, P. M., Shah, Y. B., Joseph, M. H., and Young, A. M. J. (2005). Dopamine antagonist modulation of amphetamine response as detected using pharmacological MRI. *Neuropharmacology*, 48:236–45.

Drevets, W., Gautier, C., Price, J., Kupfer, D., Kinahan, P., Grace, A., Price, J., and Mathis, C. (2001). Amphetamine-induced dopamine release in human ventral striatum correlates with euphoria. *Biological Psychiatry*, 49:81–96.

Duhm, J. (1992). *Lithium kinetics.*, chapter Pathways of lithium transport across the human erythrocyte membrane., pages 27–53. Marius Press.

Dunigan, C. and Shamoo, A. (1995). Lithium stimulates ATP-regulated dopamine uptake in PC12 cells. *Neuroscience*, 65:1–4.

Eaves, J., Loparo, J., Fecko, C., Roberst, S., Tokmakoff, A., and Geissler, P. (2005). Hydrogen bonds in liquid water are broken only fleetingly. *Proceedings of the National Academy of Sciences*, 102:13019–22.

Ebadi, M., Simmons, V., Hendricksen, M., and Lacy, P. (1974). Pharmacokinetics of lithium and its regional distribtuion in rat brain. *European Journal of Pharmacology*, 27:324–9.

Ebstein, R. P., Eliashar, S., Belmaker, R. H., Benuriah, Y., and Yehuda, S. (1980). Chronic lithium treatment and dopamine-mediated behavior. *Biological Psychiatry*, 15:459–67.

El-Badri, S. M., Ashton, C. H., Moore, P. B., Marsh, V. R., and Ferrier, I. N. (2001). Electrophysiological and cognitive function in young euthymic patients with bipolar affective disorder. *Bipolar Disorders*, 3:79–87.

Fabricand, B. and Goldberg, S. (1967). Proton relaxation times in ^{7}LiCL and ^{6}LiCl solutions. *Molecular Physics*, 13:323–30.

Fan, J., McCandliss, B. D., Fossella, J., Flombaum, J. I., and Posner, M. I. (2005). The activation of attentional networks. *Neuroimage*, 26:471–9.

Ferrier, I. N., Stanton, B. R., Kelly, T. P., and Scott, J. (1999). Neuropsychological function in euthymic patients with bipolar disorder. *British Journal of Psychiatry*, 175:246–51.

Fessler, R. G., Sturgeon, R. D., London, S. F., and Meltzer, H. Y. (1982). Effects of lithium on behavior induced by phencyclidine and amphetamine in rats. *Psychopharmacology*, 78:373–6.

Flemenbaum, A. (1975). Lithium and amphetamine hyperactivity in rats. differential effect on D and L isomers? *Neuropsychobiology*, 1:325–34.

Forester, B., Berlow, Y. A., Finn, C. T., Wardrop, M., Renshaw, P. F., and Moore, C. M. (2008). Brain lithium, N-acetyl aspartate (NAA) and myo-inositol (M-INO) levels in older adults with bipolar disorder treated with lithium: a lithium^{7} and proton magnetic resonance spectroscopy (MRS) study. *Biological Psychiatry*, 63:25S.

Fountoulakis, K. N., Vieta, E., Bouras, C., Notaridis, G., Giannakopoulos, P., Kaprinis, G., and Akiskal, H. (2008). A systematic review of existing data on long-term lithium therapy: neuroprotective or neurotoxic? *International Journal of Neuropsychopharmacology*, 11:269–87.

Fox, M. and Raichle, M. (2007). Spontaneous fluctuations in brain activity observed with functional magnetic resonance imaging. *Nature Review Neuroscience*, 8:700–11.

Francis, R. I. and Traill, M. A. (1970). Lithium distribution in brains of 2 manic patients. *Lancet*, 2(7671):523–4.

Frankenstein, U., Wennerberg, A., Richter, W., Bernstein, C., Morden, D., Rémy, F., and McIntyre, M. (2003). Activation and deactivation in blood oxygen level dependent functional magnetic resonance imaging. *Concepts in Magnetic Resonance Part A*, 16A:63–70.

Gani, D., Downes, C., Batty, I., and Bramhan, J. (1993). Lithium and myo-inositol homeostasis. *Biochimica et Biophysica Acta*, 1177:253–69.

Gao, K. M., Kemp, D. E., Ganocy, S. J., Gajwani, P., Xia, G. H., and Calabrese, J. R. (2008). Anti psychotic-induced extrapyramidal side effects in bipolar disorder and schizophrenia — a systematic review. *Journal of Clinical Psychopharmacology*, 28:203–9.

Garrod, A. B. (1859). *The nature and treatment of gout and rheumatic gout.* Walton and Maberly.

Geddes, J., Burgess, S., Hawton, K., Jamison, K., and Goodwin, G. (2004). Long-term lithium therapy for bipolar disorder: systematic review and meta-analysis of randomized controlled trials. *American Journal of Psychiatry*, 161:217–22.

Germaná, C., Kempton, M., Sarnicola, A., Christodoulou, T., Haldane, M., Hadjulis, M., Girardi, P., Tatarelli, R., and Frangou, S. (2010). The effects of lithium and anticonvulsants on brain structure in bipolar disorder. *Acta Psychiatrica Scandinavica*, 122:481–7.

Gerner, R. H., Fairbanks, L., Anderson, G. M., Young, J. G., Scheinin, M., Linnoila, M., Hare, T. A., Shaywitz, B. A., and Cohen, D. J. 1984. CSF neurochemistry in depressed, manic, and schizophrenic patients compared with that of normal controls. *American Journal of Psychiatry*, 141:1533–40.

Gerner, R. H., Post, R. M., and Bunney, W. E. (1976). Dopaminergic mechanism in mania. *American Journal of Psychiatry*, 133:1177–80.

Girard, F., Suhara, T., Sassa, T., Okubo, Y., Obata, T., Ikehira, H., Sudo, Y., Koga, M., Yoshioka, H., and Yoshida, K.(2001). Li^7 2D CSI of human brain on a clinical scanner. *Magnetic Resonance Materials in Physics Biology and Medicine*, 13:1–7.

González, R. G., Guimaraes, A. R., Sachs, G. S., Rosenbaum, J. F., Garwood, M., and Renshaw, P. F. (1993). Measurement of human brain lithium *in vivo* by MR spectroscopy. *American Journal of Neuroradiology*, 14:1027–37.

Goodwin, G. M. (1994). Recurrence of mania after lithium withdrawal — implications for the use of lithium in the treatment of bipolar affective-disorder. *British Journal of Psychiatry*, 164:149–52.

Goswami, U., Sharma, A., Khastigir, U., Ferrier, I. N., Young, A. H., Gallagher, P., Thompson, J. M., and Moore, P. B. (2006). Neuropsychological dysfunction, soft neurological signs and social disability in euthymic patients with bipolar disorder. *British Journal of Psychiatry*, 188:366–373.

Goswami, U., Sharma, A., Varma, A., Gulrajani, C., Ferrier, I., Young, A., Gallagher, P., Thompson, J., and Moore, P. (2009). The neurocognitive performance of drug-free and medicated euthymic bipolar patients do not differ. *Acta Psychiatrica Scandinavica*, 120:456–63.

Gotham, A. M., Brown, R. G., and Marsden, C. D. (1986). Depression in Parkinson's disease — a quantitative and qualitative-analysis. *Journal of Neurology Neurosurgery and Psychiatry*, 49:381–9.

Gottberg, E., Grondin, L., and Reader, T. A. (1989). Acute effects of lithium on catecholamines, serotonin, and their major metabolites in discrete brain-regions. *Neurochemical Research*,22:338–45.

Gottberg, E., Montreuil, B., and Reader, T. A. (1988). Acute effects of lithium on dopaminergic responses: iontophoretic studies in the rat visual cortex. *Synapse*, 2:442–9.

Gould, T., Keith, R., and Bhat, R. (2001). Differential sensitivity to lithium's reversal of amphetamine-induced open-field activity in two inbred strains of mice. *Behavioural Brain Research*, 118:95–105.

Gray, P., Solomon, J., Dunphy, M., Carr, F., and Hession, M. (1976). Effects of lithium on open field behavior in 'stressed' and 'unstressed' rats. *Psychopharmacology*, 48:277–81.

Greengard, P. (2001a). The neurobiology of dopamine signaling. *Bioscience Reports*, 21:247–69.

Greengard, P. (2001b). Neuroscience - the neurobiology of slow synaptic transmission. *Science*, 294:1024–30.

Greenspan, K., Schildkraut, J., Gordon, E., Baer, L., Aronoff, M., and Durell, J. (1970). Catecholamine metabolism in affective disorders. 3. MHPG and other catecholamine metabolites in patients treated with lithium carbonate. *Journal of Psychiatric Research*, 7:171–83.

Greicius, M. D., Krasnow, B., Reiss, A. L., and Menon, V. (2003). Functional connectivity in the resting brain: a network analysis of the default mode hypothesis. *Proceedings of the National Academy of Sciences of the United States of America*, 100:253–8.

Grier, J. (1971). Nonparametric indexes for sensitivity and bias: computing formulas. *Psychological Bulletin*, 75:424–9.

Grof, E., Brown, G., Grof, P., and Van Loon, G. (1986). Effects of lithium administration on plasma catecholamines. *Psychiatry Research*, 18:87–92.

Grof, P. (2006). *Lithium in Neuropsychiatry: The Comprehensive Guide.*, chapter 14, pages 157–78. Informa Healthcare.

Grunze, H., Kasper, S., Goodwin, G., Bowden, C., Möller, H., and WFSBP Task Force on Treatment Guidelines for Bipolar Disorders. (2004). The World Federation of Societies of Biological Psychiatry (WFSBP) guidelines for the biological treatment of bipolar disorders, part III: maintenance treatment. *World Journal of Biological Psychiatry.*, 5:120–35.

Grunze, H., Vieta, E., Goodwin, G., Bowden, C., Licht, R., Möller, H., and Kasper, S. (2009). The World Federation of Societies of Biological Psychiatry (WFSBP) guidelines for the biological treatment of bipolar disorders: update 2009 on the treatment of acute mania. *World Journal of Biological Psychiatry*, 10:255.

Grunze, H., Vieta, E., Goodwin, G., Bowden, C., Licht, R., Möller, H., Kasper, S., WFSBP Task Force on Treatment Guidelines for Bipolar Disorders. (2010). The World Federation of Societies of Biological Psychiatry (WFSBP) guidelines for the biological treatment of bipolar disorders: Update 2010 on the treatment of acute bipolar depression. *World Journal of Biological Psychiatry*, 11:81–109.

Gyulai, L., Wicklund, S. W., Greenstein, R., Bauer, M. S., Ciccione, P., Whybrow, P. C., Zimmerman, J., Kovachich, G., and Alves, W. (1991). Measurement of tissue lithium concentration by lithium magnetic-resonance spectroscopy in patients with bipolar disorder. *Biological Psychiatry*, 29(12):1161–70.

Haase, A., Hanicke, W., and Frahm, J. (1984). The influence of experimental parameters in surface-coil NMR. *Journal of Magnetic Resonance*, 56:401–12.

Hampel, H., Ewers, M., Bürger, K., Annas, P., Mörtberg, A., Bogstedt, A., Frölich, L., Schröder, J., Schönknecht, P., Riepe, M., Kraft, I., Gasser, T., Leyhe, T., Möller, H., Kurz, A., and Basun, H. (2009). Lithium trial in Alzheimer's disease: a randomized, single-blind, placebo-controlled, multicenter 10-week study. *Journal of Clinical Psychiatry*, 70:922–31.

Hamra, B. J., Nasrallah, H. A., Clancy, J., and Finn, R. (1983). Psychiatric-diagnosis and risk for tardive-dyskinesia. *Archives of General Psychiatry*, 40:346–7.

Harmer, C. J., Clark, L., Grayson, L., and Goodwin, G. M. (2002). Sustained attention deficit in bipolar disorder is not a working memory impairment in disguise. *Neuropsychologia*, 40:1586–90.

Hearn, A. J., Gallagher, P., Owen, B. M., Smith, M. S., Watson, S., and Young, A. H. (2004). Effect of sub-chronic hydrocortisone on responses to amphetamine in normal male volunteers. *Psychopharmacology*, 171:458–64.

Hermansson, K. and Wojcik, M. (1998). Water exchange around Li^+ and Na^+ in $LiCl_{(aq)}$ and $NaCl_{(aq)}$ from MD simulations. *Journal of Physical Chemistry B*, 102:6089–97.

Hesketh, J., Nicolaou, N., Arbuthnott, G., and Wright, A. (1978). The effect of chronic lithium administration on dopamine metabolism in rat striatum. *Psychopharmacology*, 56:163–6.

Hines, G. and Poling, T. (1984). Lithium effects on active and passive avoidance behavior in the rat. *Psychopharmacology*, 82:78–82.

Howard, R., Ellis, C., Bullmore, E., Brammer, M., Mellers, J., Woodruff, P., David, A., Simmons, A., Williams, S., and Parkes, J. (1996). Functional echoplanar brain imaging correlates of amphetamine administration to normal subjects and subjects with the narcoleptic syndrome. *Magnetic Resonance Imaging*, 14:1013–6.

Hughes, J. H., Dunne, F., and Young, A. H. (2000). Effects of acute tryptophan depletion on mood and suicidal ideation in bipolar patients symptomatically stable on lithium. *British Journal of Psychiatry*, 177:447–51.

Jacobs, D. and Silverstone, T. (1986). Dextroamphetamine-induced arousal in human-subjects as a model for mania. *Psychological Medicine*, 16:323–9.

Jauhar, P., McClure, I., Hillary, C., and Watson, A. (1993). Psychomotor performance of patients on maintenance lithium t8herapy. *Human Psychopharmacology*, 8:141–3.

Javadapour, A., Malhi, G. S., Ivanovski, B., Chen, X. H., Wen, W., and Sachdev, P. (2007). Increased anterior cingulate cortex volume in bipolar i disorder. *Australian and New Zealand Journal of Psychiatry*, 41:910–6.

Joffe, R., MacDonald, C., and Kutcher, S. (1988). Lack of differential cognitive effects of lithium and carbemazepine in bipolar affective disorder. *Journal of Clinical Psychopharmacology*, 8:425–8.

Joffe, R., Post, R., Ballenger, J., Rebar, R., and Gold, P. (1986). The effects of lithium on neuroendocrine function in affectively ill patients. *Acta Psychiatrica Scandinavica*, 73:524–8.

Johnson, F. N. (1984). *The history of lithium therapy.* Macmillan.

Johnson, L., El-Khoury, A., Aberg-Wistedt, A., Stain-Malmgren, R., and Mathé, A. (2001). Tryptophan depletion in lithium-stabilized patients with affective disorder. *International Journal of Neuropsychopharmacology*, 4:329–36.

Juckel, G. and Mavrogiorgou, P. (2006). *Lithium in neuropsychiatry: the comprehensive guide.*, chapter 29, pages 329–40. Informa Healthcare.

Kahn, D., Prohovnik, I., Lucas, L., and Sackeim, H. (1989). Dissociated effects of amphetamine on arousal and cortical blood flow in humans. *Biological Psychiatry*, 25:755–67.

Kato, H., Kogure, K., Ohtomo, H., Izumiyama, M., Tobita, M., Matsui, S., Yamamoto, E., Kohno, H., Ikebe, Y., and Watanabe, T. (1986). Characterization of experimental ischemic brain edema utilizing proton nuclear magnetic resonance imaging. *Journal of Cerebral Blood Flow and Metabolism*, 6:212–21.

8 Kato, T., Fujii, K., Shioiri, T., Inubushi, T., and Takahashi, S. (1996). Lithium side effects in relation to brain lithium concentration measured by lithium^{7} magnetic resonance spectroscopy. *Progress in Neuro-Psychopharmacology and Biological Psychiatry*, 20:87–97.

Kato, T., Inubushi, T., and Takahashi, S. (1994). Relationship of lithium concentrations in the brain measured by lithium^{7} magnetic resonance spectroscopy to treatment response in mania. *Journal of Clinical Psychopharmacology*, 15:330–42.

Kato, T., Shioiri, T., Inubushi, T., and Takahashi, S. (1993). Brain lithium concentrations measured with ^{7}Li magnetic resonance spectroscopy in patients with affective disorders — relationship to erythrocyte and serum concentrations. *Biological Psychiatry*, 33:147–52.

8 Kato, T., Takahashi, S., and Inubushi, T. (1992). Brain lithium concentration by ^{7}Li magnetic and ^{1}H magnetic resonance spectroscopy in bipolar disorder. *Psychiatry Research-Neuroimaging*, 45:53–63.

Kebabian, J. and Calne, D. (1979). Multiple receptors for dopamine. *Nature*, 277:93–6.

Kempton, M. J. (2006). *MRI and neuropsychological investigations in euthymic patients with bipolar disorder.* PhD thesis, Imperial College London (University of London).

Kim, J. E., Lyoo, I. K., Friedman, S. D., Dunner, D. L., Dager, S. R., and Renshaw, P. F. (2008). Brain gray matter increase in drug-naïve bipolar disorder patients with lithium treatment but not with valproate treatment: a long-term longitudinal follow-up brain imaging study. *Journal of Affective Disorders*, 107:s61–s62.

Knutson, B. and Gibbs, S. E. B. (2007). Linking nucleus accumbens dopamine and blood oxygenation.8 *Psychopharmacology*, 191:813–22.

Kocsis, J., Shaw, E., Stokes, P., Wilner, P., Elliot, A., Sikes, C., Myers, B., Manevitz, A., and Parides, M. (1993). Neuropsychologic effects of lithium discontinuation. *Journal of Clinical Psychopharmacology*, 13:268–76.

Komoroski, R. A. (2000). Applications of ^{7}Li NMR in biomedicine. *Magnetic Resonance Imaging*, 18:103–16.

Komoroski, R. A. (2005). Biomedical applications of ^{7}Li NMR. *NMR in Biomedicine*, 18:67–73.

Komoroski, R. A., Newton, J. E. O., Sprigg, J. R., Cardwell, D., Mohanakrishnan, P., and Karson, C. N. (1993). *In vivo* ^{7}Li nuclear-magnetic-resonance study of lithium pharmacokinetics and chemical-shift imaging in psychiatric-patients. *Psychiatry Research-Neuroimaging*, 50:67–76.

Komoroski, R. A., Newton, J. E. O., Walker, E., Cardwell, D., Jagannathan, N. R., Ramaprasad, S., and Sprigg, J. (1990). *In vivo* NMR-spectroscopy of ^{7}Li in humans. *Magnetic Resonance in Medicine*, 15:347–56.8

Komoroski, R. A. and Pearce, J. M. (2004). Localized ^{7}Li MR spectroscopy and spin relaxation in rat brain *in vivo*. *Magnetic Resonance in Medicine*, 52:164–8.

Koslow, S. H., Maas, J. W., Bowden, C. L., Davis, J. M., Hanin, I., and Javaid, J. (1983). CSF and urinary biogenic-amines and metabolites in depression and mania — a controlled, univariate analysis. *Archives of General Psychiatry*, 40:999–1010.

Kovacs, P. and Hernadi, I. (2002). Iontophoresis of lithium antagonises noradrenergic action on prefrontal neuron of the rat. *Brain Research.*, 947:150–6.

Kurtz, M. and Gerraty, R. (2009). A meta-analytic investigation of neurocognitive deficits in bipolar illness: profile and effects of clinical state. *Neuropsychology*, 23:551–62.

Kushnir, T., Itzchak, Y., Valevski, A., Lask, M., Modai, I., and Navon, G. 1993. Relaxation times and concentrations of ^{7}Li in the brain of patients receiving lithium therapy. *NMR in Biomedicine*, 6:39–42.

Lanng Nielsen, J., Amdisen, A., Darling, S., and Pedersen, E. (1977). Plasma prolactin during lithium treatment. *Neuropsychobiology*, 3:30–4.

Lauterbach, E., Victoroff, J., Coburn, K., Shillcutt, S., Doonan, S., and Mendez, M. (2010). Psychopharmacological neuroprotection in neurodegenerative disease: assessing the preclinical data. *Journal of Neuropsychiatry and Clinical Neurosciences*, 22:1–18.

Lawrence, N. S., Ross, T. J., Hoffmann, R., Garavan, H., and Stein, E. A. (2003). Multiple neuronal networks mediate sustained attention. *Journal of Cognitive Neuroscience*, 15:1028–38.

Lee, J., Norris, M., Adler, C., Macaluso, E., Chu, W., Komoroski, R. A., and Strakowski, S. M. (2010). 4T ^{7}Li MRSI in the brains of bipolar disorder subjects. In *The ISMRM-ESMRMB Joint Annual Meeting*.

Lenox, R. H., McNamara, R. K., Papke, R. L., and Manji, H. K. (1998). Neurobiology of lithium: an update. *Journal of Clinical Psychiatry*, 59 s6:37–47.

Lenzer, I., Eastwood, D., and Street, P. (1989). Reinterpreting memory complaints through neuropsychological assessment. *Clinical Gerontology*, 8:57–60.

Leow, A. D., Thompson, P. M., Hayashi, K. M., Bearden, C., Nicoletti, M. A., Monkul, S. E., Sassi, R. B., Brambilla, P., Mallinger, A. G., and Soares, J. (2005). Effects of lithium treatment on human brain structure mapped using longitudinal MRI. *Neuropsychopharmacology*, 30:s227.

Lerer, B., Globus, M., Brik, E., Hamburger, R., and Belmaker, R. (1984). Effect of treatment and withdrawal from chronic lithium in rats on stimulant-induced responses. *Neuropsychopharmacology*, 11:28–32.

Licht, R., Larsen, J., Smith, D., and Braendgaard, H. (1994). Effect of chronic lithium treatment with or without haloperidol on number and sizes of neurons in rat neocortex. *Psychopharmacology*, 115:371–4.

Licht, R., Larsen, J., Smith, D., and Braendgaard, H. (2003). Chronic lithium treatment with or without haloperidol fails to affect the morphology of the rat cerebellum. *European Neuropsychopharmacology*, 13:173–6.

Lieberman, A. (2006). Depression in Parkinson's disease — a review. *Acta Neurologica Scandinavica*, 113:1–8.

Lindskog, M., Kim, M., Wikström, M., Blackwell, K., and Kotaleski, J. (2006). Transient calcium and dopamine increase PKA activity and DARPP-32 phosphorylation. *PLoS Computational Biology*, 9:e119.

Liu, S., Chiu, C., Chang, C., Hwang, T., Hwu, H., and Chen, W. (2002)8. Deficits in sustained attention in schizophrenia and affective disorders: stable versus state-dependent markers. *American Journal of Psychiatry*, 159:975–82.

Logothetis, N. (2002). The neural basis of the blood-oxygen-level-dependent functional magnetic resonance imaging signal. *Philosophical Transactions of the Royal Society of London. Series B, Biological Sciences*, 357:1003–37.

Lopez, A., Mathers, C., Ezzati, M., Jamison, D., and Murray, C. (2006). Global and regional burden of disease and risk factors, 2001: systematic analysis of population health data. *Lancet*, 367:1747–57.

Lyoo, I., Dager, S., Kim, J., Yoon, S., Friedman, S., and Dunner, D. R. P. (2010). Lithium-induced gray matter volume increase as a neural correlate of treatment response in bipolar disorder: a longitudinal brain imaging study. *Neuropsychopharmacology*, 35:1743–50.

MacDonald, A., Cohen, J., Stenger, V., and Carter, C. (2000). Dissociating the role of the dorsolateral prefrontal and anterior cingulate cortex in cognitive control. *Science*, 288:1835–8.

Maj, M. (1992). Clinical prediction of response to lithium prophylaxis in bipolar disorder: a critical update. *Lithium*, 3:15–21.

Maj, M., Pirozzi, R., Magliano, L., and Bartoli, L. (1998). Long-term outcome of lithium prophylaxis in bipolar disorder: a 5-year prospective study of 402 patients at a lithium clinic. *American Journal of Psychiatry*, 155:30–5.

Manji, H., Hsiao, J., Risby, E., Oliver, J., Rudorfer, M., and Potter, W. (1991). The mechanisms of action of lithium. I. effects on serotoninergic and noradrenergic systems in normal subjects. *Archives of General Psychiatry*, 48:505–12.

Marcus, Y. (2009). Effects of ions on the structure of water: structure making and breaking. *Chemical Reviews*, 109:1346–70.

Marrocco, R. and Davidson, M. (1998). *The attentive brain.*, chapter 3, pages 33–50. MIT Press.

Mathew, R. and Wilson, W. (1985). Dextroamphetamine-induced changes in regional cerebral blood flow. *Psychopharmacology*, 87:298–302.

Mattay, V. S., Callicott, J. H., Bertolino, A., Heaton, I., Frank, J. A., Coppola, R., Berman, K. F., Goldberg, T. E., and Weinberger, D. R. (2000). Effects of dextroamphetamine on cognitive performance and cortical activation. *Neuroimage*, 12:268–75.8

Mazoyer, B., Zago, L., Mellet, E., Bricogne, S., Etard, O., Houdé, O., Crivello, F., Joliot, M., Petit, L., and Tzourio-Mazoyer, N. (2001). Cortical networks for working memory and executive functions sustain the conscious resting state in man. *Brain Research Bulletin*, 54:287–98.

McKenna, P., Salvador, R., Fernandez-Corcura, P., Moro, N., Sarro, S., Goikolea, J., Sans-Sansa, B., Gomar, J., Ortiz, J., Amann, B., Vieta, E., and Pomarol-Clotet, E. (2010). Default mode network dysfunction: a potentially significant abnormality in schizophrenia. *Schizophrenia Bulletin*, 35:190–1.

McKiernan, K., Kaufman, J., Kucera-Thompson, J., and Binder, J. (2003). A parametric manipulation of factors affecting task-induced deactivation in functional neuroimaging. *Journal of Cognitive Neuroscience*, 15:394–408.

McQuade, R. (2010). Targeting networks, Akt/GSK3 signalling in the actions of mood stabilisers. *Journal of Psychopharmacology*, 24(s3):A12(s34).

McTavish, S. F., McPherson, M. H., Harmer, C. J., Clark, L., Sharp, T., Goodwin, G. M., and Cowen, P. J. (2001). Antidopaminergic effects of dietary tyrosine depletion in healthy subjects and patients with manic illness. *British Journal of Psychiatry*, 179:356–60.

McTavish, S. F. B., McPherson, M. H., Sharp, T., and Cowen, P. J. (1999). Attenuation of some subjective effects of amphetamine following tyrosine depletion. *Journal of Psychopharmacology*, 13:144–7.

Miller, E. and Cohen, J. (2001). An integrative theory of prefrontal cortex function. *Annual Review of Neuroscience*, 24:167–202.

Moffett, J. R., Ross, B., Arun, P., Madhavarao, C. N., and Namboodiri, A. M. A. (2007). N-acetylaspartate in the CNS: from neurodiagnostics to neurobiology. *Progress in Neurobiology*, 81:89–131.

Monkul, E. S., Matsuo, K., Nicoletti, M. A., Dierschke, N., Hatch, J. P., Dalwani, M., Brambilla, P., Caetano, S., Sassi, R. B., Mallinger, A. G., and Soares, J. C. (2007). Prefrontal gray matter increases in healthy individuals after lithium treatment: a voxel-based morphometry study. *Neuroscience Letters*, 429:7–11.

Moore, C., Frederick, B., Henry, M., Streeter, C., Cohen, B. M., and Renshaw, P. F. (2003). Human *in vivo* lithium magnetic resonance spectroscopy at 4.0 Tesla: initial findings. *Biological Psychiatry*, 53:202S.

Moore, C. M., Demopulos, C. M., Henry, M. E., Steingard, R. J., Zamvil, L., Katic, A., Breeze, J. L., Moore, J. C., Cohen, B. M., and Renshaw, P. F. (2002). Brain-to-serum lithium ratio and age: An *in vivo* magnetic resonance spectroscopy study. *American Journal of Psychiatry*, 159:1240–2.

Moore, G. J., Bebchuk, J. M., Hasanat, K., Chen, G., Seraji-Bozorgzad, N., Wilds, I. B., Faulk, M. W., Koch, S., Glitz, D. A., Jolkovsky, L., and Manji, H. K. (2000a). Lithium increases N-acetyl-aspartate in the human brain: *in vivo* evidence in support of *bcl-2*'s neurotrophic effects? *Biological Psychiatry*, 48:1–8.

Moore, G. J., Bebchuk, J. M., Wilds, I. B., Chen, G., and Menji, H. K. (2000b). Lithium-induced increase in human brain grey matter. *Lancet*, 356:1241–2.

Moore, G. J., Cortese, B. M., Glitz, D. A., Zajac-Benitez, C., Quiroz, J. A., Uhde, T. W., Drevets, W. C., and Manji, H. (2005). Lithium increases gray matter in the prefrontal and subgenual prefrontal cortices in treatment responsive bipolar disorder patients. *Neuropsychopharmacology*, 30:S179–S180.

Moore, G. J., Cortese, B. M., Glitz, D. A., Zajac-Benitez, C., Quiroz, J. A., Uhde, T. W., Drevets, W. C., and Manji, H. K. (2009). A longitudinal study of the effects of lithium treatment on prefrontal and subgenual prefrontal gray matter volume in treatment-responsive bipolar disorder patients. *Journal of Clinical Psychiatry*, 70:699–705.

Morcom, A. and Fletcher, P. C. (2007). Does the brain have a baseline? why we should be resisting a rest. *Neuroimage*, 37:1073–82.

Mulholland, C. and Cooper, S. (2000). The symptom of depression in schizophrenia and its management. *Advances in Psychiatric Treatment*, 6:169–77.

Nagano-Saito, A., Liu, J., Doydon, J., and Dagher, A. (2009). Dopamine modulates default mode network deactivation in elderly individuals during the Tower of London task. *Neuroscience Letters*, 458:1–5.

Nelson, S. C., Herman, M. M., Bensch, K. G., and Barchas, J. D. (1980). Localization and quantitation of lithium in rat-tissue following intra-peritoneal injections of lithium-chloride. 2: Brain. *Journal of Pharmacology and Experimental Therapeutics*, 212:11–5.

Nivoli, A., Murru, A., and Vieta, E. (2010). Lithium: still a cornerstone in the long-term treatment in bipolar disorder? *Neuropsychobiology*, 62:27–35.

Nolen, W. A. and Bloemkolk, D. (2000). Treatment of bipolar depression, a review of the literature and a suggestion for an algorithm. *Neuropsychobiology*, 42(s1):11–7.

Oldfield, R. (1971). The assessment and analysis of handedness: the Edinburgh inventory. *Neuropsychologia*, 9:97–113.

Otero Losada, M. and Rubio, M. (1992). Effects of i.c.v. lithium chloride administration on monoamine concentration in rat mediobasal hypothalamus. *European Journal of Pharmacology*, 215:185–9.

Ozawa, H., Nozu, T., and Aihara, H. (1976). Distribution of lithium and its effects on electrolyte and norepinephrine metabolism in discrete areas of the rat brain. *Nippon Yakurigaku Zassi*, 72:851–60.

Pachet, A. K. and Wisniewski, A. M. (2003). The effects of lithium on cognition: an updated review. *Psychopharmacology (Berl)*, 170:225–34.

Palaniyappan, L. and Cousins, D. A. (2010). Brain networks: foundations and futures in bipolar disorder. *Journal of Mental Health*, 19:157–67.

Pasley, B., Inglis, B., and Freeman, R. (2007). Analysis of oxygen metabolism implies a neural origin for the negative bold response in human visual cortex. *Neuroimage*, 36:269–76.

Pearlson, G. D., Wong, D. F., Tune, L. E., Ross, C. A., Chase, G. A., Links, J. M., Dannals, R. F., Wilson, A. A., Ravert, H. T., Wagner, H. N., J., and et al. (1995). *In vivo* D2 dopamine receptor density in psychotic and nonpsychotic patients with bipolar disorder. *Archives of General Psychiatry*, 52:471–7.

Phatak, P., Shaldivin, A., King, L. S., Shapiro, P., and Regenold, W. T. (2006). Lithium and inositol: effects on brain water homeostasis in the rat. *Psychopharmacology*, 186:41–7.

Pittman, K., Jakubovic, A., and Fibiger, H. (1984). The effects of chronic lithium on behavioral and biochemical indices of dopamine receptor supersensitivity in the rat. *Psychopharmacology*, 82:371–7.

Plenge, P., Stensgaard, A., Jensen, H. V., Thomsen, C., Mellerup, E. T., and Henriksen, O. (1994). 24-hour lithium concentration in human brain studied by ^{7}Li magnetic-resonance spectroscopy. *Biological Psychiatry*, 36:511–6.

Poolsup, N., Li Wan Po, A., and de Oliveira, I. (2000). Systematic overview of lithium treatment in acute mania. *Journal of Clinical Pharmacy and Therapuetics*, 25:139–56.

Price, L. H., Charney, D. S., Delgado, P. L., Goodman, W. K., Krystal, J. H., Woods, S. W., and Heninger, G. R. (1990). Clinical-studies of 5-HT function using IV L-tryptophan. *Progress in Neuropsychopharmacology and Biological Psychiatry*, 14:459–72.

Price, L. H., Charney, D. S., Delgado, P. L., and Heninger, G. R. (1989). Lithium treatment and serotoninergic function — neuroendocrine and behavioral-responses to intravenous tryptophan in affective-disorder. *Archives of General Psychiatry*, 46:13–9.

Price, L. H., Charney, D. S., and Heninger, G. R. (1986). Variability of response to lithium augmentation in refractory depression. *American Journal of Psychiatry*, 143:1387–92.

Quiroz, J., Machado-Vieira, R., Zarate, C. J., and Manji, H. (2010). Novel insights into lithium's mechanism of action: neurotrophic and neuroprotective effects. *Neuropsychobiology*, 62:50–60.

Quraishi, S. and Frangou, S. (2002). Neuropsychology of bipolar disorder: a review. *Journal of Affective Disorders*, 72:209–26.

Rahman, S., Li, P. P., Young, L. T., Kofman, O., Kish, S. J., and Warsh, J. J. (1997). Reduced [H^3]cyclic AMP binding in postmortem brain from subjects with bipolar affective disorder. *Journal of Neurochemistry*, 68:297–304.

Raichle, M., MacLeod, A., Snyder, A., Powers, W., Gusnard, D., and Shulman, G. (2001). A default mode of brain function. *Proceedings of the National Academy of Sciences*, 98:676–82.

Raichle, M. and Snyder, A. (2007). A default mode of brain function: a brief history of an evolving idea. *Neuroimage*, 37:1083–90.

Ramaprasad, S. (1998). Lithium spectroscopic imaging of rat brain at therapeutic doses. *Magnetic Resonance Imaging*, 22:727–34.

Ramaprasad, S. (2005). Magnetic resonance spectroscopic imaging studies of lithium. *Progress in Nuclear Magnetic Resonance Spectroscopy*, 47:111–21.

Ramaprasad, S., Newton, J. E. O., Cardwell, D., Fowler, A. H., and Komoroski, R. A. (1992). *In vivo* ^{7}Li NMR imaging and localized spectroscopy of rat-brain. *Magnetic Resonance in Medicine*, 25:308–18.

Rangelguerra, R. A., Perezpayan, H., Minkoff, L., and Todd, L. E. (1983). Nuclear magnetic resonance in bipolar affective disorders. *American Journal of Neuroradiology*, 4:229–31.

Rapoport, S. I. and Bosetti, F. (2002). Do lithium and anticonvulsants target the brain arachidonic acid cascade in bipolar disorder? *Archives of General Psychiatry*, 59:592–6.

Rastogi, R. and Singhal, R. (1977). Lithium suppresses elevated behavioural activity and brain catecholamines in developing hyperthyroid rats. *Canadian Journal of Physiology and Pharmacology*, 55:490–5.

Reches, A., Jackson-Lewis, V., and Fahn, S. (1984). Lithium does not interact with haloperidol in the dopaminergic pathways of the rat brain. *Psychopharmacology*, 82:330–4.

Regenold, W. T., Hisley, K. C., Phatak, P., Marano, C. M., Obuchowski, A., Lefkowitz, D. M., Sassan, A., Ohri, S., Phillips, T. L., Dosanjh, N., Conley, R. R., and Gullapalli, R. (2008). Relationship of cerebrospinal fluid glucose metabolites to MRI deep white matter hyperintensities and treatment resistance in bipolar disorder patients. *Bipolar Disorders*, 10:753–64.

Renshaw, P. F., Haselgrove, J., Bolinger, L., Chance, B., and Leigh, J. (1986). Relaxation and imaging of lithium *in vivo*. *Magnetic Resonance Imaging*, 4:193-8.

Renshaw, P. F. and Wicklund, S. W. (1988). *In vivo* measurment of lithium in humans by nuclear magnetic resonance spectroscopy. *Biological Psychiatry*, 23:465–75.

Riddell, F., Patel, A., and Hughes, M. S. (1990). Lithium uptake rate and lithium: lithium exchange rate in human erythocytes at a nearly pharmacologically normal level monitored by ^{7}Li NMR. *Journal of Inorganic Biochemistry*, 39:187–92.

Riedl, U., Barocka, A., Kolem, H., Demling, J., Kaschka, W. P., Schelp, R., Stemmler, M., and Ebert, D. (1997). Duration of lithium treatment and brain lithium concentration in patients with unipolar and schizoaffective disorder — a study with magnetic resonance spectroscopy. *Biological Psychiatry*, 41:844–50.

Risby, E., Hsiao, J., Manji, H., Bitran, J., Moses, F., Zhou, D., and Potter, W. (1991). The mechanisms of action of lithium. II. effects on adenylate cyclase activity and beta-adrenergic receptor binding in normal subjects. *Archives of General Psychiatry*, 48:513–24.

Robinson, L. J. and Ferrier, I. N. (2006). Evolution of cognitive impairment in bipolar disorder: a systematic review of cross-sectional evidence. *Bipolar Disorders*, 8:103–16.

Robinson, L. J., Thompson, J. M., Gallagher, P., Goswami, U., Young, A. H., Ferrier, I. N., and Moore, P. B. (2006). A meta-analysis of cognitive deficits in euthymic patients with bipolar disorder. *Journal of Affective Disorders*, 93:105–15.

Rudorfer, M., Karoum, F., Ross, R., Potter, W., and Linnoila, M. (1985). Differences in lithium effects in depressed and healthy subjects. *Clinical Pharmacology and Therapeutics*, 37:66–71.

Rueda, A., Acosta, O., Couprie, M., Bourgeat, P., Fripp, J., Dowson, N., Romero, E., and Salvado, O. (2010). Topology-corrected segmentation and local intensity estimates for improved partial volume classification of brain cortex in MRI. *Journal of Neuroscience Methods*, 188:305–15.

Sachs, G. S., Renshaw, P. F., Lafer, B., Stoll, A. L., Guimaraes, A. R., Rosenbaum, J. F., and González, R. G. (1995). Variability of brain lithium levels during maintenance treatment — a MRS study. *Biological Psychiatry*, 38:422–8.

Salgado-Pineda, P., Delaveau, P., Falcon, C., and Blin, O. (2006). Brain T_1 intensity changes after levodopa administration in healthy subjects: a voxel-based morphometry study. *British Journal of Clinical Pharmacology*, 62:546–51.

Sassi, R. B., Nicoletti, M., Brambilla, P., Mallinger, A. G., Frank, E., Kupfer, D. J., Keshavan, M. S., and Soares, J. C. (2002). Increased gray matter volume in lithium-treated bipolar disorder patients. *Neuroscience Letters*, 329:243–5.

Sax, K. W., Strakowski, S. M., Zimmerman, M. E., DelBello, M. P., Keck, P. E., and Hawkins, J. M. (1999). Frontosubcortical neuroanatomy and the continuous performance test in mania. *American Journal of Psychiatry*, 156:139–41.

Scarnà, A., Gijsman, H. J., McTavish, S. F., Harmer, C. J., Cowen, P. J., and Goodwin, G. M. (2003). Effects of a branched-chain amino acid drink in mania. *British Journal of Psychiatry*, 182:210–3.

Schatzberg, A. F. and Nemeroff, C. B. (1998). *Textbook of Psychopharmacology*, American Psychiatric Press, Washington DC.

Schou, M., Juel-Nielsen, N., Stromgren, E., and Voldby, H. (1954). The treatment of manic psychoses by the administration of lithium salts. *Journal of Neurology, Neurosurgery and Psychiatry*, 17:250–60.

Seamans, J. K. and Yang, C. R. (2004). The principal features and mechanisms of dopamine modulation in the prefrontal cortex. *Progress in Neurobiology*, 74:1–57.

Sevak, R., Stoops, W., Hays, L., and Rush, C. (2009). Discriminative stimulus and subject-rated effects of methamphetamine, D-amphetamine, methylphenidate, and triazolam in methamphetamine-trained humans. *Journal of Pharmacologu and Experimental Therapeutics*, 328:1007–18.

Shalmi, M. and Thomsen, K. (1991). *Lithium and the cell.*, chapter 14, pages 249–72. Academic Press.

Shaw, E., Stokes, P., Mann, J., and Manevitz, Z. (1987). Effects of lithium carbonate on the memory and speed of bipolar outpatients. *Journal of Abnormal Psychology*, 96:64–9.

Shoblock, J., Maisonneuve, I., and Glick, S. (2003a). Differences between D-methamphetamine and D-amphetamine in rats: working memory, tolerance, and extinction. *Psychopharmacology*, 170:150–6.

Shoblock, J., Sullivan, E., Maisonneuve, I., and Glick, S. (2003b). Neurochemical and behavioral differences between D-methamphetamine and D-amphetamine in rats. *Psychopharmacology*, 165:359–69.

Shorter, E. (2009). The history of lithium therapy. *Bipolar Disorders*, 11:4–9.

Silverstone, P. H., Asghar, S. J., O'Donnell, T., Ulrich, M., and Hanstock, C. C. (2004). Lithium and valproate protect against dextro-amphetamine induced brain choline concentration changes in bipolar disorder patients. *World Journal of Biological Psychiatry*, 5:38–44.

Silverstone, P. H., McGrath, B. M., and Kim, H. (2005). Bipolar disorder and myo-inositol: a review of the magnetic resonance spectroscopy findings. *Bipolar Disorders*, 7:1–10.

Silverstone, T. (1984). Response to bromocriptine distinguishes bipolar from unipolar depression. *Lancet*, 8382:903–4.

Silverstone, T. (1985). Dopamine in manic depressive illness. a pharmacological synthesis. *Journal of Affective Disorders*, 8:225–31.

Soares, J. C., Boada, F., and Keshavan, M. S. (2000). Brain lithium measurements with ^{7}Li magnetic resonance spectroscopy (MRS): a literature review. *European Neuropsychopharmacology*, 10:151–8.

Soares, J. C., Boada, F., Spencer, S., Mallinger, A. G., Dippold, C. S., Wells, K. F., Frank, E., Keshavan, M. S., Gershon, S., and Kupfer, D. J. (2001). Brain lithium concentrations in bipolar disorder patients: preliminary ^{7}Li magnetic resonance studies at 3T. *Biological Psychiatry*, 49:437–43.

Sourial-Bassillious, N., Rydelius, P., Aperia, A., and Aizman, O. (2009). Glutamate-mediated calcium signaling: a potential target for lithium action. *Neuroscience*, 161:1126–34.

Spirtes, M. (1976). Lithium levels in monkey and human brain after chronic, therapeutic, oral dosage. *Pharmacology Biochemistry and Behavior*, 5:143–7.

Stein, D. and Stahl, S. (2000). Serotonin and anxiety: current models. *International Clinical Psychopharmacology*, s2:1–6.

Stern, K. H. and Amis, E. S. (1959). Ionic size, a comprehensive review on radii in crystals. *Chemical Reviews*, 59:1.

Stern, S., Frazer, A., Mendels, J., and Frustaci, C. (1977). Distribution of the lithium ion in endocrine organs of the rat. *Life Sciences*, 20:1669–74.

Subhash, M. N., Vinod, K. Y., and Srinivas, B. N. (1999). Differential effect of lithium on 5-HT$_1$ receptor-linked system in regions of rat brain. *Neurochemistry International*, 35:337–43.

Subrahmanyam, S. (1975). Role of biogenic-amines in certain pathological conditions. *Brain Research*, 87:355–62.

Suhara, T., Nakayama, K., Inoue, O., Fukuda, H., Shimizu, M., Mori, A., and Tateno, Y. (1992). D1 dopamine receptor binding in mood disorders measured by positron emission tomography. *Psychopharmacology*, 106:14–8.

Sulzer, D., Sonders, M., Poulsen, N., and Galli, A. (2005). Mechanisms of neurotransmitter release by amphetamines: a review. *Progress in Neurobiology*, 75:406–33.

Swann, A., Bowden, C., Morris, D., Calabrese, J., Petty, F., Small, J., Dilsaver, S., and Davis, J. (1997). Depression during mania. treatment response to lithium or divalproex. *Archives of General Psychiatry*, 54:37–42.

Thellier, M., Stelz, T., and Wissocq, J. C. (1976). Detection of stable isotopes of lithium or boron with the help of a (n, α) nuclear reaction. Application to the use of lithium as a tracer for unidirectional flux measurements and to the microlocalization of lithium in animal histologic preparations. *Biochimica et Biophysica Acta*, 437:604–27.

Thornhill, D. and Field, S. (1982). Distribution of lithium elimination rates in a selected population of psychiatric patients. *European Journal of Clinical Pharmacology*, 21:351–4.

Tomasi, D., Volkow, N. D., Wang, R., Telang, F., Wang, G., Chang, L., Ernst, T., and Fowler, J. (2010). Dopamine transporter in the striatum correlate with deactivation in the default mode network during visuospatial attention. *PLoS ONE*, 4:*e*6102.

Torack, R. M. and Morris, J. C. (1988). The association of ventral tegmental area histopathology with adult dementia. *Archives of Neurology*, 45:497–501.

Treiser, S. L., Cascio, C. S., Odonohue, T. L., Thoa, N. B., Jacobowitz, D. M., and Kellar, K. J. (1981). Lithium increases serotonin release and decreases serotonin receptors in the hippocampus. 213:1529–31.

Tunbridge, E., Burnet, P. W. J., Sodhi, M. S., and Harrison, P. J. (2004). Catechol-o-methyltransferase (COMT) and proline dehydrogenase (PRODH) mRNAs in the dorsolateral prefrontal cortex in schizophrenia, bipolar disorder, and major depression. *Synapse*, 51:112–8.

Uftring, S. J., Wachtel, S. R., Chu, D., McCandless, C., Levin, D. N., and de Wit, H. (2001). An fMRI study of the effect of amphetamine on brain activity. *Neuropsychopharmacology*, 25:925–35.

Ure, A. (1860). Calculus in the bladder, treated by litholysis. *Lancet*, 76:185–6.

van den Heuvel, M. and Hulshoff Pol, H. (2010). Exploring the brain network: a review on resting-state fMRI functional connectivity. *European Neuropsychopharmacology*, 20:519–34.

Vanderborght, T. M., Kilbourn, M. R., Koeppe, R. A., Dasilva, J. N., Carey, J. E., Kuhl, D. E., and Frey, K. A. (1995). *In vivo* imaging of the brain vesicular monoamine transporter. *Journal of Nuclear Medicine*, 36:2252–60.

VanKammen, D. P. and Murphy, D. L. (1975). Attenuation of euphoriant and activating effects of D-amphetamine and L-amphetamine by lithium carbonate treatment. *Psychopharmacologia*, 44:215–24.

van Praag, H. M. and Korf, J. (1975). Central monoamine deficiency in depressions — causative or secondary phenomenon. *Pharmakopsychiatrie Neuro-Psychopharmakologie*, 8:322–6.

Vollenweider, F., Maguire, R., Leenders, K., Mathys, K., and Angst, J. (1998). Effects of high amphetamine dose on mood and cerebral glucose metabolism in normal volunteers using positron emission tomography (PET). *Psychiatry Research*, 83:149–62.

Wada, A. (2009). Lithium and neuropsychiatric therapeutics: neuroplasticity via glycogen synthase kinase-3 beta, beta-catenin, and neurotrophin cascades. *Journal of Pharmacological Sciences*, 110:14–28.

Wallqvist, A. and Mountain, R. (1999). Molecular models of water: derivation and description. *Reviews in Computational Chemistry.*, 13:183–247.

Walsh, A. E., Ware, C. J., and Cowen, P. J. (1991). Lithium and 5-HT_{1A} receptor sensitivity — a neuroendocrine study in healthy volunteers. 105:568–572.

Wang, H. Y. and Friedman, E. (1996). Enhanced protein kinase C activity and translocation in bipolar affective disorder brains. *Biological Psychiatry*, 40:568–75.

Weisman, D. and McKeith, I. (2007). Dementia with Lewy bodies. *Seminars in Neurology*, 27:42–7.

Weiss, F. (2005). Neurobiology of craving, conditioned reward and relapse. *Current Opinion in Pharmacology*, 5:9–19.

Wesnes, K. and Warburton, D. (1983a). Effects of scopolamine on stimulus sensitivity and response bias in a visual vigilance task. *Neuropsychobiology*, 9:154–7.

Wesnes, K. and Warburton, D. (1983b). Effects of smoking on rapid information processing performance. *Neuropsychobiology*, 9:223–9.

Westerink, B. (1985). Sequence and significance of dopamine metabolism in the rat brain. *Neurochemistry International*, 7:221–7.

Westerink, B. (2006). Targeting exocytosis: ins and outs of the modulation of quantal dopamine release. *CNS and Neurological Disorders Drug Targets*, 5:57–77.

Wilder-Willis, K., Sax, K., Rosenberg, H., FÃűleck, D., Shear, P., and Strakowski, S. (2001). Persistent attentional dysfunction in remitted bipolar disorder. *Bipolar Disorders*, 3:58–62.

Willner, P. (1983). Dopamine and depression — a review of recent-evidence. 3: The effects of antidepressant treatments. *Brain Research Reviews*, 6:237–46.

Willson, M. C., Wilman, A. H., Bell, E. C., Asghar, S. J., and Silverstone, P. H. (2004). Dextroamphetamine causes a change in regional brain activity *in vivo* during cognitive tasks: a functional magnetic resonance imaging study of blood oxygen level-dependent response. *Biological Psychiatry*, 56:284–91.

Wingo, A., Wingo, T., Harvey, P., and BaldesÃűsarini, R. (2009). Effects of lithium on cognitive performance: a meta-analysis. *Journal of Clinical Psychiatry*, 70:1588–97.

Wolkin, A., Angrist, B., Wolf, A., Brodie, J., Wolkin, B., Jaeger, J., Cancro, R., and Rotrosen, J. (1987). Effects of amphetamine on local cerebral metabolism in normal and schizophrenic subjects as determined by positron emission tomography. *Psychopharmacology*, 92:241–6.

Yatham, L. N., Liddle, P. F., Lam, R. W., Shiah, I. S., Lane, C., Stoessl, A. J., Sossi, V., and Ruth, T. J. (2002a). PET study of the effects of valproate on dopamine D2-receptors in neuroleptic- and mood-stabilizer-naïve patients with nonpsychotic mania. *American Journal of Psychiatry*, 159:1718–23.

Yatham, L. N., Liddle, P. F., Shiah, I. S., Lam, R. W., Ngan, E., Scarrow, G., Imperial, M., Stoessl, J., Sossi, V., and Ruth, T. J. (2002b). PET study of [^{18}F]6-fluoro-L-dopa uptake in neuroleptic- and mood-stabilizer-naïve first-episode nonpsychotic mania: effects of treatment with divalproex sodium. *American Journal of Psychiatry*, 159:768–74.

Yucel, K., Taylor, V. H., McKinnon, M. C., MacDonald, K., Alda, M., Young, L. T., and MacQueen, G. M. (2008). Bilateral hippocampal volume increase in patients with bipolar disorder and short-term lithium treatment. *Neuropsychopharmacology*, 33:361–7.

Yun, T., Na, D., Kwon, B., Rho, H., Park, S., and Suh, Y.L. Chang, K. (2007). A T_1 hyperintense perilesional signal aids in the differentiation of a cavernous angioma from other hemorrhagic masses. *American Journal of Neuroradiology*, 29:494–500.

Zhang, Y. and Cremer, P. (2006). Interactions between macromolecules and ions: the Hofmeister series. *Current Opinion in Chemical Biology.*, 10:658–63.

Zonta, M. and Carmignoto, G. (2003). Calcium oscillations encoding neuron-to-astrocyte communication. *Journal of Physiology, Paris.*, 96:193–8.

Zubieta, J. K., Taylor, S. F., Huguelet, P., Koeppe, R. A., Kilbourn, M. R., and Frey, K. A. (2001). Vesicular monoamine transporter concentrations in bipolar disorder type 1, schizophrenia, and healthy subjects. *Biological Psychiatry*, 49:110–6.